Charles University in Prague

Faculty of Science

Department of Genetics and Microbiology

Mgr. Lucie Cuchalová

Characterization of the two smallest core subunits of eIF3 and their roles in translation

Charakterizace dvou nejmenších podjednotek iniciačního faktoru eIF3 a jejich role v translaci

Ph. D. Thesis

Supervisor: Leoš Shivaya Valášek, Ph.D.

Prague, 2013

Declaration:

I declare that I have worked on this thesis under the guidance of my supervisor and that all sources of the previous knowledge are properly cited. No part of this work was used and will not be used for obtaining any other academic degree, than PhD from Charles University in Prague.

Prague …… ……

Acknowledgement

I would like to express my deep and sincere gratitude to my supervisor, Leoš Shivaya Valášek Ph.D., head of Laboratory of Regulation of Gene Expression, Institute of Microbiology AS CR, v.v.i., Prague. His wide knowledge together with encouraging and personal guidance have provided a good basis for the present thesis.

I wish to express my warm and sincere thanks to all my colleagues, members of LRGE laboratory. I appreciate the collaboration with them and thank them for their enthusiasm and friendship.

I am deeply grateful to Dr Tobias von der Haar, Claudia Solscheid and other members of School of Biosciences, University of Kent, UK for their kind driving me into the "termination" world and backing me during my intership at their University.

I owe my most sincere gratitude to all members of laboratories of: Libor Krásný Ph.D., Laboratory of Molecular Genetics of Bacteria, Institute of Microbiology AS CR, v.v.i., Prague and David Staněk Ph.D., Laboratory of RNA Biology, Institute of Molecular Genetics of the ASCR, v. v. i., Prague for the possibility to discuss my work with them, their constructive criticism and excellent advice during the preparation of our papers

My warm thanks are due to Susan Wagner and Anna Herrmannova for their valuable advice and friendly help. Their extensive discussions around my work and interesting explorations in operations have been very helpful for these studies.

I owe my loving thanks to my husband Karel Cuchal for his never ending patience.

During this work I have collaborated with many colleagues for whom I have great regard, and I wish to extend my warmest thanks to all those who have helped me with my work

Last but not least, I am grateful to: the Wellcome Trusts Grant, the Howard Hughes Medical Institute, NIH Research Grant funded by the Fogarty International Center, the Fellowship of Jan E. Purkyne from the Academy of Sciences of the Czech Republic, the Institute Research Concept, and the Intramural Research Program of the National Institutes of Health for their financial support of our work.

"Dedicated to men who always kept the faith and trust in me: my grandfather Zdeněk Šváb and my supervisor Leoš Shivaya Valášek"

Contents

List of Abbreviations

ABCE	encoding ATP-binding cassette
ATP	adenosine triphosphate
CTD	C-terminal domain
CTT	C-terminal tail
Met-tRNA$_i^{Met}$	methionyl initiator tRNA
mRNA	messenger RNA
eIFs	eukaryotic initiation factor
EF	elongation factors
GAP	GTPase accelerating factor
GTP	guanosine triphosphate
IC	initiation komplex
MFC	multifactor complex
NMD	nonsense - mediated decay
NMR	nuclear magnetic resonance
NTD	N-terminal domain
ORF	open reading frame
PIC	pre-initiation complex
PCI	proteasome component
PTC	peptidyl transferase center
rRNA	ribosomal RNA
REI	reinitiation
RFs	release factors
RLI	RNase L inhibitor

RPEs	REI-promoting elements
RPS	ribosomal protein (small subunit)
RRF	ribosome recycling factor
RS	responsive site
RRM	RNA recognition motif
SD	Shine-Dalgarno
tRNA	transfer RNA
TC	ternary complex
UTR	untranslated region
wt	wild-type

Abstracts in English and Czech

Abstract

Protein synthesis or mRNA translation is a complex and highly conserved process. Translation consists of initiation, elongation, termination, and ribosome recycling stages. Since most regulation occurs during initiation, its mechanism is being studied intensively to elucidate the molecular basis of every potential control point. The initiation factor eIF3, which in yeast consists of five essential core subunits (eIF3a/TIF32, b/PRT1, c/NIP1, g/TIF35, and i/TIF34) and one transiently associated, non-essential subunit (j/HCR1), is undisputedly one of the key promoters of initiation. In addition, it has also been implicated in playing a critical role during ribosomal recycling, reinitiation, signal transduction, NMD etc.

We have focused on determining the molecular mechanism of the roles of eIF3 and its associated eIFs not only in translation initiation but also in termination and in reinitiation. This included the biochemical and genetic mapping of yeast eIF3 binding site on the small ribosomal subunit, among others.

We showed that the interaction between the residues 200–400 of a/TIF32-NTD and flexible C-terminal tail RPS0A significantly stimulates attachment of eIF3 and its associated eIFs to small ribosomal subunits *in vivo*, thus a/TIF32-NTD together with the recently published PCI (proteasome component) domain in c/NIP1-CTD form important intermolecular bridges between eIF3 and the 40S. Moreover, we demonstrated that the partial deletion of the RPS0A-binding domain of a/TIF32 also severely blocks the induction of *GCN4* translation that occurs via reinitiation. Genetic analysis reveals a functional interaction between 5´ *cis*-acting sequences of the *GCN4* mRNA and a/TIF32-NTD. This interaction facilitates stabilizing post-termination 40S subunits on upstream ORF1 of the *GCN4* mRNA and resuming of scanning downstream.

Furthermore, another part of my Ph.D. thesis reveals functional characterization of two essential eIF3 subunits, g/TIF35 and i/TIF34, previously suggested to be dispensable for formation of the 48S preinitiation complexes (PICs) *in vitro*, hallmark function of eIF3. We

showed that both subunits are involved in promoting the rate and processivity of scanning in living cells. Moreover, we demonstrated that g/TIF35 specifically interacts with ribosomal proteins RPS3 and RPS20 located near the ribosomal mRNA entry channel and its RRM domain plays role in reinitiation by stabilizing uORF1 post-termination 40S ribosomes on *GCN4*, although by different molecular mechanism than a/TIF32-NTD. Besides, we reported the 2.2A˚ resolution crystal structure of i/TIF34 subunit in complex with the minimal CTD of b/PRT1 (654–700), the boundaries of which were defined by solution NMR spectroscopy

In my last part of this thesis we identified and defined a role for eIF3 in the stop codon selection process in vivo and uncovered its active roles in translation termination, defining a communication bridge between initiation and termination/recycling phases of protein synthesis.

Abstrakt

Syntéza bílkovin, neboli translace mRNA, je komplexní a velmi konzervovaný proces. Translace probíhá v několika na sebe navazujících fázích: iniciaci, elongaci, terminaci a recyklaci ribozomu. Vzhledem k tomu, že většina regulačních procesů probíhá v iniciační fázi, již po několik desetiletí je právě k ní upírán vědecký zrak se snahou objasnit molekulární mechanismus všech jejich kontrolních bodů. Iniciační faktor eIF3, který se v kvasinkách skládá z pěti esenciálních podjednotek tvořících jeho jádro (eIF3a/TIF32, b/PRT1, c/NIP1, g/TIF35, a i/TIF34) a jedné přidružené neesenciální podjednotky (j/HCR1), patří neoddiskutovatelně ke klíčovým hráčům iniciace. Kromě této úlohy hraje rovněž důležitou roli v recyklaci ribozomu, reiniciaci, signálních drahách buněčné signalizace, kontrolních a regulačních mechanismech, jakým je kupříkladu degradace mRNA s předčasným stop kodonem (nonsense-mediated mRNA decay - NMD) atp.

Zaměřili jsme se na objasnění molekulárního mechanismu, kterým eIF3 spolu s ostatními iniciačními faktory vykonávající svou funkci nejen v iniciaci translace, ale i její terminaci a reiniciaci. To zahrnovalo mimo jiné i genetické mapování vazebných míst eIF3 na malou ribozomální podjednotku.

Ukázali jsme, že vazba mezi 200-400-tým aminokyselinovým zbytkem N-konce a/eIF3 a flexibilním chvostem C-konce RPS0A významně stimuluje navázání eIF3 a s ní asociovaných faktorů na malou ribozomální podjednotku *in vivo*, a tak a/TIF32-NTD, spolu s nedávno publikovanou PCI (proteasome component) doménou C-konce c/NIP1, tvoří důležitý mezimolekulární most mezi eIF3 a 40S. Dále jsme předvedli, že částečná delece domény vázající RPS0A v a/TIF32 blokuje znovu zahájení translace genu *GCN4*, který probíhá prostřednictvím reiniciaci. Genetická analýza odhalila funkční vazbu mezi 5´*cis*-působících sekvencí mRNA genu *GCN4* a N-koncem a/TIF32. Tato interakce se podílí na stabilizování post-terminačních 40S ribozomálních podjednotek na uORF1 (čtecím rámci v protisměru) mRNA genu *GCN4* a obnovení skenování.

Další část mé dizertační práce odhaluje funkční charakteristiku dvou esenciálních podjednotek eIF3: g/TIF5 and i/TIF34, u kterých bylo dříve *in vitro* prokázáno, že jsou postradatelné pro vytvoření 48S neiniciačních komplexů, jedné ze základních rolí eIF3. Ukázali jsme, že oba proteiny ovlivňují rychlost a procesivitu skeninku v živých buňkách.

Dále jsme ukázali, že g/TIF35 se specificky váže na ribozomální proteiny RPS3 a RPS20, které se nalézají v blízkosti vstupního kanálu mRNA do ribozomu a její RRM (RNA recognition motif) doména hraje roli v reiniciaci již zmiňovaným stabilizování uORF1 post-terminačních 40S ribozomů na mRNA genu *GCN4*, ačkoliv jiným molekulárním mechanismem než a/TIF32-NTD. Mimo to jsme uveřejnili krystalovou strukturu, v rozlišení 2.2A˚, i/TIF34 podjednotky v komplexu s malou částí C-konce b/PRT1 (654-700-tým zbytkem).

V poslední části mé dizertační práce jsme identifikovali a definovali roli eIF3 v procesu rozpoznání stop kodonu a odhalili její aktivní roli v terminaci translace.

Introduction

Protein synthesis or mRNA translation is a complex and highly conserved process. Translational control critically contributes to the overall regulation of gene expression, development, stress responses, memory formation and aging. Compared to transcriptional regulation, translational control of existing mRNAs allows for more rapid changes in cellular concentrations of the encoded proteins and, thus, can be used for maintaining homeostasis, in addition to modulating more permanent changes in cell physiology or fate. Indeed, there are numerous examples demonstrating that deregulation of translational control either directly causes various diseases or significantly contributes to their rapid development (for example neurodegenerative conditions, diabetes, cancer, etc.).The process of translation can be divided into initiation, elongation, termination and ribosome recycling phases.

Translation initiation

There has been enormous progress over the last decade in dissecting the molecular mechanism of eukaryotic translation initiation, fueled by advances in several areas. The initiation phase of protein synthesis is promoted by numerous proteins or protein complexes called eukaryotic initiation factors (eIFs). The beginning of a translational cycle involves a series of steps that culminate in the assembly of the 80S initiation complex (IC) on the AUG start codon (Valášek 2012). The mechanism of start codon selection differs fundamentally between bacteria and eukaryotes. In bacteria, base-pairing of the Shine-Dalgarno (SD) sequences ensures a direct placement of the start codon into the ribosomal P-site. In eukaryotes, the start codon is generally identified by a scanning mechanism (Kozak and Shatkin 1978). A small subset of eukaryotic mRNAs but mainly the viral mRNAs can circumvent the scanning process using specialized sequences, called internal ribosome entry sites (IRESs), to recruit the 40S subunit more directly to the mRNA initiation region (Mokrejs, Masek et al. 2010). This mechanism may seems analogous to the use of SD sequences is, used by bacteria, however, but it is much more complicated. Despite the recent

progress in this particular field, the mechanism of the recruitment of IRES-driven mRNAs these elements to the 40S ribosomes remains unclear (Komar, Mazumder et al.).

In my work presented in this Ph.D. thesis I focused on the canonical translation initiation pathway, which consists of several sequential steps. In the first step of a new translational cycle, Met-tRNA$_i^{Met}$ is bound by eukaryotic initiation factor 2 (eIF2) in its GTP form to produce the Met-tRNA$_i^{Met}$ ·eIF2·GTP ternary complex (TC). The TC is subsequently recruited to the small ribosomal subunit with help of eIF3, eIF1, eIF5, and eIF1A, forming the 43S pre-initiation complex (PIC) (Hinnebusch, Dever et al. 2007; Pestova, Lorsch et al. 2007; Jackson, Hellen et al. 2010; Valášek 2012). In the next step, the 43S PIC interacts with the 5´end of mRNA in a reaction stimulated by eIF4F, eIF4B, PABP, and eIF3. The 48S PIC thus formed scans the mRNA leader until the AUG start codon is recognized (Hinnebusch 2011). Scanning is promoted by eIF1, eIF1A, and eIF4F in a mammalian reconstituted system (Pestova and Kolupaeva 2002), whereas yeast genetic data indicate that eIF3 and eIF5 also participate in vivo (Nielsen, Szamecz et al. 2004; Yamamoto, Singh et al. 2005; Cuchalová, Kouba et al. 2010). In the open conformation of the 40S ribosome that is induced by eIFs 1 and 1A, and that is conducive for scanning, the anticodon of Met-tRNA$_i^{Met}$ is not fully engaged in the ribosomal P-site in order to prevent premature engagement with putative start codons. eIF2 partially hydrolyzes its GTP with help of the GTPase accelerating factor (GAP) eIF5; however, prior to start codon recognition, the "gate-keeping" function of eIF1 prevents the release of the resultant phosphate ion producing GTP- and GDP•Pi-bound two states of the factor, possibly in equilibrium. In fact, Pi is not released from the scanning complex until AUG initiation codon–anticodon base-pairing induces dissociation or displacement of eIF1 (Algire, Maag et al. 2005; Cheung, Maag et al. 2007). Recognition of the AUG start codon in an optimal Kozak context (Kozak 1986; Algire, Maag et al. 2005) also induces a reciprocal conformational switch of the 48S PIC to the closed/scanning arrested form (Cheung, Maag et al. 2007). The scanning arrested 40S-mRNA- Met-tRNA$_i^{Met}$ PIC then joins the 60S subunit in a reaction stimulated by GTP-bound eIF5B (Pestova, Lomakin et al. 2000; Lee, Pestova et al. 2002). Subunit joining is thought to facilitate ejection of all eIFs but eIF1A and most likely also eIF3 and eIF4 (Pöyry, Kaminski et al. 2004; Szamecz, Rutkai et al. 2008; Munzarová, Pánek et al. 2011). Finally, GTP hydrolysis on eIF5B triggers its own dissociation, producing an active 80S ribosome poised for elongation. The translation initiation factor eIF3, which in

yeast consists of five essential core subunits (eIF3a/TIF32, b/PRT1, c/NIP1, g/TIF35, and i/TIF34) and one transiently associated, non-essential subunit (j/HCR1), is actively involved in regulation of the first three of these steps: 1) Met-tRNA$_i^{Met}$ recruitment to the 40S subunit to form the 43S pre-initiation complex (PIC), 2) mRNA recruitment to the 43S PIC to form the 48S PIC, 3) scanning of the 48S PIC to the first recognized start codon (Valášek, Nielsen et al. 2002; Valášek, Mathew et al. 2003; Szamecz, Rutkai et al. 2008; Chiu, Wagner et al. 2010; Cuchalová, Kouba et al. 2010; ElAntak, Wagner et al. 2010; Herrmannová, Daujotyte et al. 2012; Kouba, Danyi et al. 2012). In the PIC assembly steps, the action of eIF3 is further stimulated by one of its interacting partners, the highly conserved and essential ATP-binding cassette protein RLI1 (ABCE1 in mammals), by an unknown mechanism (Dong, Lai et al. 2004). In contrast to most eIFs, eIF3 interacts with the exposed side of the small ribosomal subunit and as such, it is thought to remain bound at this position during the first elongation cycles (see also discussion).

Initiation is followed by elongation, when amino acids are added to the nascent polypeptide chain.

Termination

Termination occurs when the ribosome reaches the end of the coding region and a stop codon enters the ribosomal A-site (UAA, UAG, and UGA). The termination process consists of stop-codon recognition and hydrolysis of the ester bond of the peptidyl-tRNA located in the ribosomal P-site, which releases the nascent polypeptide (Jackson, Hellen et al. 2012). Peptidyl-tRNA is hydrolyzed following nucleophilic attack of a water molecule on the ester carbonyl group of peptidyl-tRNA in the peptidyl transferase center (PTC) of the large ribosomal subunit. In bacteria and eukaryotes, termination is mediated by two classes of release factors (RFs): class I release factors (eRF1 in eukaryotes and RF1 or 2 in bacteria) recognize stop codons in the A site and catalyze peptidyl–tRNA hydrolysis via the conserved GGQ-motif present in all class I release factors (Klaholz 2011). Class II release factors (eRF3 in eukaryotes and RF3 in bacteria, both ribosome-dependent GTPases with limited homology restricted to their GTP-binding (G) domains) are homologues of the canonical translation factors EF-G and EF-Tu, respectively (Kong, Ito et al. 2004), and coordinate the ribosome binding and activity of the class I RFs (Jackson, Hellen et al. 2012).

According to recent models (Shoemaker and Green 2011; Becker, Franckenberg et al. 2012), eRF1 enters the ribosomal A-site in complex with a second release factor, eRF3, in its GTP bound form. Recognition of a stop codon triggers GTPase activity of eRF3, which leads to its dissociation from the complex in its GDP bound form. eRF1 is then free to activate the ribosomal peptidyl transferase centre (PTC), which hydrolyses the bond between the P-site tRNA and the nascent polypeptide. Importantly, these steps are promoted by ABCE1/RLI1 in an ATP-independent manner; i.e. by the same factor that also stimulates eIF3 functions in the initiation phase. Molecular details of this RLI1 role in termination are not known, nevertheless, the proposed active role of RLI1 in stop codon recognition is consistent with observations that conditional downregulation of RLI1 protein levels increases stop codon read-through in yeast (Khoshnevis, Gross et al. 2010). Based on the most recent structural model, RLI1 binds to the same site on the terminating ribosome as eRF3 (thus their binding is mutually exclusive), and its 4Fe-4S domain interacts with the C-terminal domain of eRF1 to push the conserved GGQ motif in the middle domain of eRF1 to the PTC next to the acceptor stem of the P-site tRNA to trigger polypeptide release (Becker, Franckenberg et al. 2012).

Ribosome recycling

To begin a new translational cycle, first a pool of separated ribosomal subunits has to be generated from those that have just finished (terminated) translation of a given mRNA in the „previous“ cycle. After termination has occurred, the post-termination complexes (post-TCs) consisting of an 80S couple still bound to mRNA, P-site deacylated tRNA and eukaryotic release factors 1 and 3 (or at least eRF1) need to be recycled. In bacteria, ribosome recycling factor (RRF) and elongation factor EF-G act together to induce splitting of the 70S ribosome into 30S and 50S subunits (Zavialov, Hauryliuk et al. 2005; Gao, Zavialov et al. 2007). In eukaryotes, besides the known termination factors, ABCE1/RLI1 has recently been shown to play an essential role in ribosome recycling (Pisarev, Skabkin et al. 2010). It mediates recycling of eRF1-associated post-TCs, this time, however, in an ATP-dependent manner (Pisarev, Skabkin et al. 2010; Shoemaker and Green 2011). It was hypothesized that RLI1, upon binding and hydrolysing ATP, switches its conformation into a closed state, and the mechanochemical work generated by this switch splits post-TCs into free 60S subunits and deacylated tRNA- and mRNA-bound 40S subunits (40S-post-TC) (Becker, Franckenberg et al. 2012). Finally, Pisarev et al. showed that the release of tRNA and mRNA from the 40S-post-TCs is, at least in vitro, ensured by the bona fide initiation factors eIF1, eIF1A and eIF3 (Pisarev, Hellen et al. 2007; Pisarev, Skabkin et al. 2010). eIF3, and in particular its j/HCR1, were suggested to play the key role specifically in mRNA dissociation. Hence, it appears that the role of ABCE1/ RLI1 and several canonical initiation factors as “terminators” of the translational cycle is conserved among eukaryotes. It should be noted that the molecular mechanism by with eRFs 1 and 3 are ejected from post-TCs is still unclear.

Fig. 1

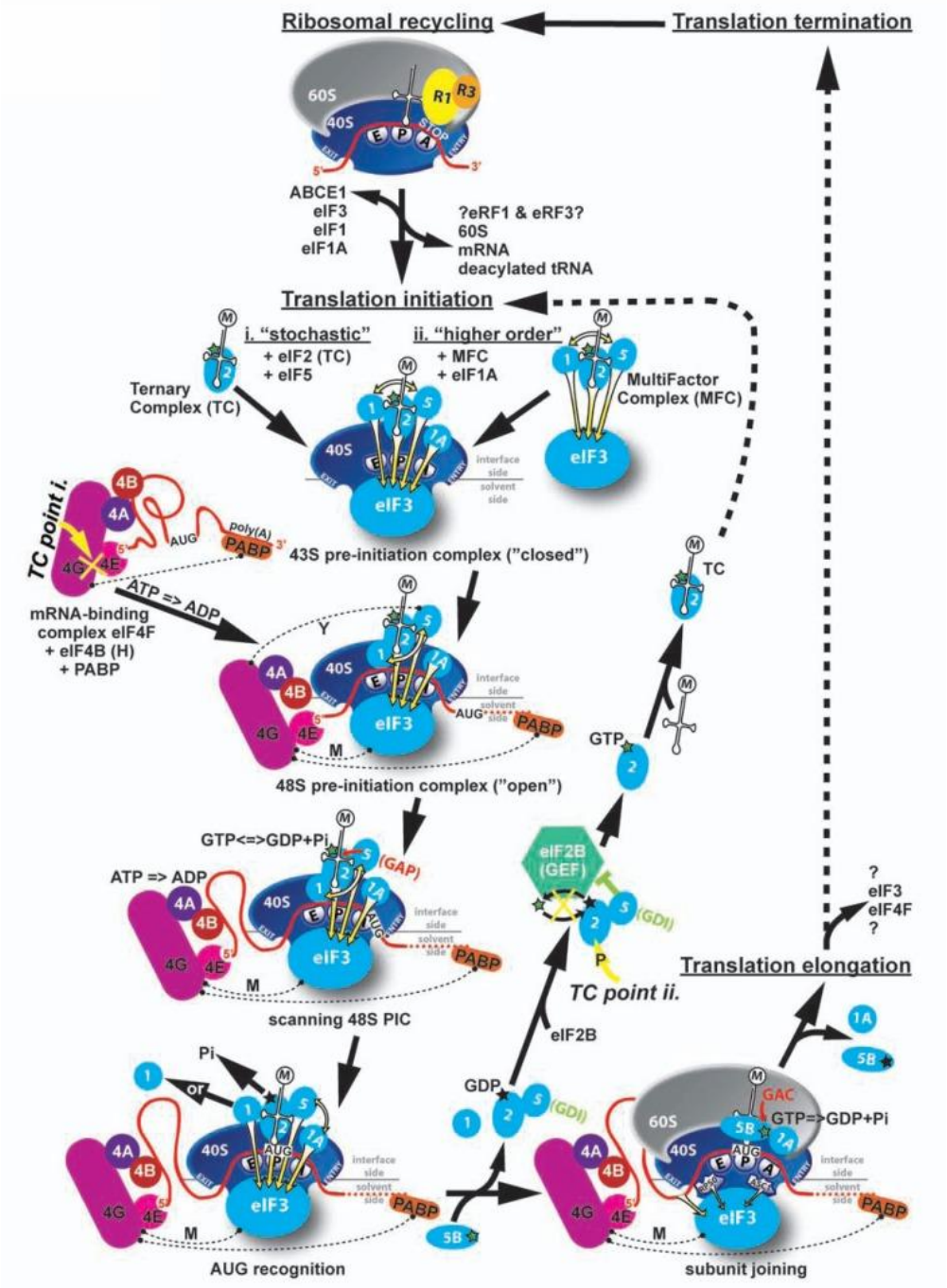

Schematic of the canonical translation pathway in eukaryotes with the ribosomal recycling and initiation phases shown in detail (Valášek 2012).

Reinitiation

Various alternative mechanisms to the canonical translation initiation pathway exist that are mostly utilized by viruses or function in gene-specific translational control. They rely on *cis*-acting mRNA features and exhibit distinct factor requirements. Reinitiation (REI) is one such mechanism utilized to down- or up-regulate translation of regulatory proteins such as transcription factors and proto-oncogenes in response to various environmental stimuli (Kozak 2005). Most eukaryotic mRNAs contain only a single translatable gene (ORF - open reading frame); however, in approximately 13% of yeast and 50% of human transcripts the main ORF is preceded by one or more short upstream ORFs (uORFs) (Calvo, Pagliarini et al. 2009), consisting of the AUG start codon and at least one additional coding triplet. Ribosomes initiate in the normal way at the first AUG codon; however, at the termination codon, the 40S subunit (40S) remains bound to the mRNA, resumes scanning, and initiates again at a downstream start site. Since its discovery (Kozak 1987), many factors were identified that influence efficiency of the reinitiation process. It is reduced for example by slower rate of elongation (Kozak 2001; Pöyry, Kaminski et al. 2004), increasing length of the short uORF (Luukkonen, Tan et al. 1995), *cis*-acting sequences that may precede and/or immediately follow uORFs, etc. (Grant, Miller et al. 1994; Grant, Miller et al. 1995; Kozak 2005; Valášek 2012). However, except for a few specific mRNA features (see also below), we know very little about the molecular mechanisms underlying REI.

As aforementioned, there are a few examples where uORFs bear special characteristics that render them highly permissive for REI (REI-permissive), such as the mRNAs encoding the yeast transcription factors *YAP1* (Vilela, Linz et al. 1998), *GCN4* (Hinnebusch 2005) and its mammalian ortholog *ATF4* (Vattem and Wek 2004), and bZIP transcriptional regulator *ATF5* (Zhou, Pallam et al. 2008).The best-studied example of the REI mechanism is the translational control of yeast *GCN4*, a transcriptional activator of a large number of biosynthetic genes (Hinnebusch 2005). Although *GCN4* mRNA is synthesized constitutively, its translation is repressed under nutrient-rich conditions through a REI mechanism involving four upstream open reading frames (uORFs 1–4) that is very sensitive to the TC levels in cells. After translating the first and only REI-permissive uORF1, small ribosomal subunit remains attached to the mRNA, resumes scanning, and reinitiates

downstream. Under non-starvation conditions, characterized by high levels of the TC, nearly all of the rescanning 40S ribosomes will rebind the TC before reaching REI-nonpermissive uORFs 3 and 4, translate one of them, and dissociate from the mRNA. Amino acid starvation leads to phosphorylation of eIF2 by kinase GCN2, converting eIF2.GDP from a substrate to a competitive inhibitor of its GEF, eIF2B, thus reducing the concentration of TC. Low TC levels derepress *GCN4* translation by allowing ~50% of rescanning 40S ribosomes to rebind TC after bypassing uORF4 and reinitiate at *GCN4* instead. Failure to induce expression of *GCN4* in response to a shortage of amino acids in various mutant cells confers increased sensitivity to inhibitors of amino acid biosynthetic enzymes, and is designated the Gcn$^-$ phenotype. Conversely, constitutive expression of *GCN4* independent of amino acid levels due to a defect in TC assembly or recruitment overcomes sensitivity to the latter inhibitors in *gcn2*Δ cells. A crucial but vaguely understood feature of *GCN4* translational control has been for a long time the highly disparate capacities of uORF1 and uORF4 to permit efficient resumption of scanning following translation termination. Original mutational analyses suggested that AU-rich sequences surrounding the stop codon of uORF1 favor resumption of scanning and REI, whereas GC-rich sequences flanking the uORF4 stop codon likely trigger ribosome release (Grant and Hinnebusch 1994). However, recent findings in our laboratory argue strongly against the importance of the specific nucleotide content (Munzarová, Pánek et al. 2011). Besides the sequences surrounding the stop codon of uORF1, sequences 5´of uORF1 were also shown to be critical for efficient REI (Grant, Miller et al. 1995). Our recent work even revealed the molecular mechanism of their action (Munzarová, Pánek et al. 2011), (see Fig.2 and also discussion)

Fig. 2

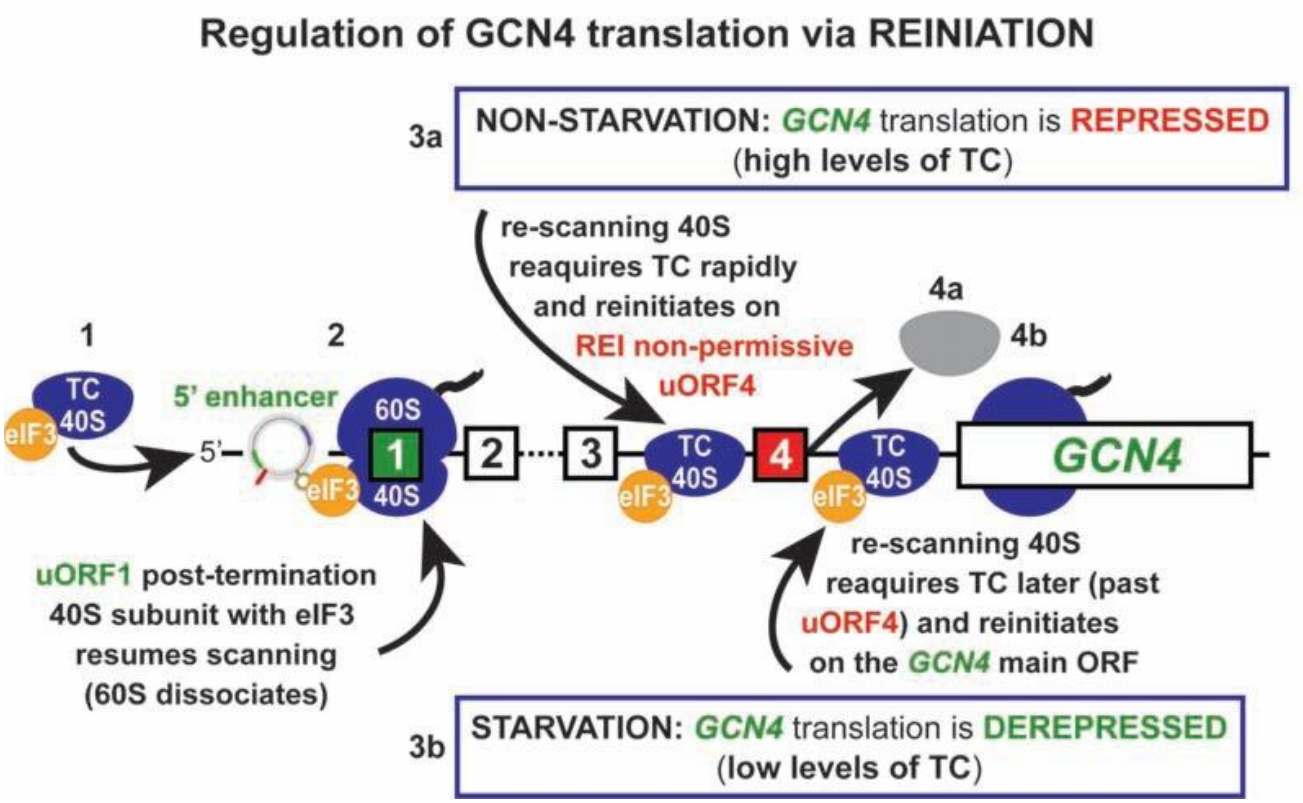

Schematic of the *GCN4* mRNA leader showing distribution of all four short uORFs (REI-permissive uORF1 is labeled green; REI-non-permissive uORF4 is labeled red), the predicted structure of the uORF1's 5' *cis*-acting sequences (5' enhancer), 40S- and 80S-bound eIF3, and the description of the mechanism of the *GCN4* translation control. The 3a and 4a "*GCN4*-expression repressed" steps take places under non-starvation conditions with abundant TC levels, whereas the 3b and 4b "*GCN4*-expression derepressed" steps occur under starvation condition with limited supply of the TC (Munzarová, Pánek et al. 2011; Valášek 2012).

Aims of the study

The aim of the study was to understand and describe the molecular mechanism of the roles of eIF3 and its associated eIFs not only in translation initiation but also in termination and in reinitiation.

1. We addressed the longstanding question of what endows uORF1 from the *GCN4* mRNA leader with its unique ability to allow highly efficient REI.
2. We focused on functional characterization of two small subunits of eIF3, g/TIF35 and i/TIF34, the cellular roles of which have remained highly elusive even though these subunits are essential for the viability of yeast cells
3. We have concerted our effort to the role of eIF3 in translation termination

Material and methods

Experiments were carried out with the model system of budding yeast *Saccharomyces cerevisiae.*

List of methods

Polysome profile analysis

1% or 2% HCHO-cross-linking, WCE preparation, and fractionation of extracts for analysis of preinitiation complexes

β-galactosidase assays

Glutathione S-transferase (GST) pulldown experiments

Western blot analysis

mRNA binding assay

Ni^{2+} chelation chromatography

NMR spectroscopy

40S-binding assay

Preparation of antibodies

Read-through assay

Polysomal gradient analysis

Coimmunoprecipitations and affinity tag pull downs

Results

List of publications:

eIF3a cooperates with sequences 5' of uORF1 to promote resumption of scanning by post-termination ribosomes for reinitiation on GCN4 mRNA.

Szamecz B, Rutkai E, Cuchalová L, Munzarová V, Herrmannová A, Nielsen KH, Burela L, Hinnebusch AG, Valásek L.

Genes Dev. 2008 Sep 1;22(17):2414-25. doi: 10.1101/gad.480508.

The RNA recognition motif of eukaryotic translation initiation factor 3g (eIF3g) is required for resumption of scanning of posttermination ribosomes for reinitiation on GCN4 and together with eIF3i stimulates linear scanning.

Cuchalová L, Kouba T, Herrmannová A, Dányi I, Chiu WL, Valásek L.

Mol Cell Biol. 2010 Oct;30(19):4671-86. doi: 10.1128/MCB.00430-10. Epub 2010 Aug 2.

Structural analysis of an eIF3 subcomplex reveals conserved interactions required for a stable and proper translation pre-initiation complex assembly.

Herrmannová A, Daujotyte D, Yang JC, Cuchalová L, Gorrec F, Wagner S, Dányi I, Lukavsky PJ, Valásek LS.

Nucleic Acids Res. 2012 Mar;40(5):2294-311. doi: 10.1093/nar/gkr765. Epub 2011 Nov 15.

Small ribosomal protein RPS0 stimulates translation initiation by mediating 40S-binding of eIF3 via its direct contact with the eIF3a/TIF32 subunit.

Kouba T, Dányi I, Gunišová S, Munzarová V, Vlčková V, Cuchalová L, Neueder A, Milkereit P, Valášek LS.

PLoS One. 2012;7(7):e40464. doi: 10.1371/journal.pone.0040464. Epub 2012 Jul 5.

Translation in Yeast Cells Begins and Ends with Translation Initiation Factor 3 (eIF3)

Lucie Cuchalová and Petra Beznosková, Christopher J. Shoemaker, Stanislava Gunišová, Tobias von der Haar, and Leoš Shivaya Valášek

Under the review in PLoS Biol.

eIF3a cooperates with sequences 5' of uORF1 to promote resumption of scanning by post-termination ribosomes for reinitiation on GCN4 mRNA.

Szamecz B, Rutkai E, Cuchalová L, Munzarová V, Herrmannová A, Nielsen KH, Burela L, Hinnebusch AG, Valásek L.

Genes Dev. 2008 Sep 1;22(17):2414-25. doi: 10.1101/gad.480508.

In this study, we focused on the role of the NTD of a/TIF32 in promoting association of eIF3 and other MFC components with the 40S. We found that a partial deletion of the RPS0A-binding site in the a/TIF32-NTD is not lethal but reduces the amounts of 40S-bound MFC components in vivo, consistent with the idea that the a/TIF32-NTD forms a crucial intermolecular bridge between eIF3 and the 40S.

Then we reveal that the TIF32-NTD also plays a crucial role in the gene-specific regulatory mechanism called reinitiation. The best-studied example of the REI mechanism is the translational control of yeast GCN4, a transcriptional activator of a large number of biosynthetic genes, which must be repressed under nutrient rich conditions and derepressed during nutrient starvation. The *GCN4* mRNA contains four short upstream ORFs. Only the first uORF allows efficient reinitition after its translation, which is the basis of the GCN4 translational control.

We showed that eIF3 stays ribosome-bound even after subunit joining and travels with the 80S ribosome for several elongating cycles during which it progressively dissociates. This quality of eIF3 is then the key for reinitiation-permissiveness of the 3-codon long uORF1. We demonstrated that the a/TIF32-NTD interacts with sequences upstream of uORF1 when the 80S ribosome terminates its translation and thus selectively stabilizes the small subunit on the mRNA, so that it can subsequently resume scanning for reinitiation downstream.

eIF3a cooperates with sequences 5′ of uORF1 to promote resumption of scanning by post-termination ribosomes for reinitiation on *GCN4* mRNA

Béla Szamecz,[1] Edit Rutkai,[1] Lucie Cuchalová,[1] Vanda Munzarová,[1] Anna Herrmannová,[1] Klaus H. Nielsen,[2] Laxminarayana Burela,[3] Alan G. Hinnebusch,[3] and Leoš Valášek[1,4]

[1]Laboratory of Regulation of Gene Expression, Institute of Microbiology AVCR, Prague, Videnska 1083, 142 20, The Czech Republic; [2]Centre for mRNP Biogenesis and Metabolism, Department of Molecular Biology, University of Aarhus, 8000 Århus C, Denmark; [3]Laboratory of Gene Regulation and Development, National Institute of Child Health and Human Development, Bethesda, Maryland 20892, USA

Yeast initiation factor eIF3 (eukaryotic initiation factor 3) has been implicated in multiple steps of translation initiation. Previously, we showed that the N-terminal domain (NTD) of eIF3a interacts with the small ribosomal protein RPS0A located near the mRNA exit channel, where eIF3 is proposed to reside. Here, we demonstrate that a partial deletion of the RPS0A-binding domain of eIF3a impairs translation initiation and reduces binding of eIF3 and associated eIFs to native preinitiation complexes in vivo. Strikingly, it also severely blocks the induction of *GCN4* translation that occurs via reinitiation. Detailed examination unveiled a novel reinitiation defect resulting from an inability of 40S ribosomes to resume scanning after terminating at the first upstream ORF (uORF1). Genetic analysis reveals a functional interaction between the eIF3a-NTD and sequences 5′ of uORF1 that is critically required to enhance reinitiation. We further demonstrate that these stimulatory sequences must be positioned precisely relative to the uORF1 stop codon and that reinitiation efficiency after uORF1 declines with its increasing length. Together, our results suggest that eIF3 is retained on ribosomes throughout uORF1 translation and, upon termination, interacts with its 5′ enhancer at the mRNA exit channel to stabilize mRNA association with post-termination 40S subunits and enable resumption of scanning for reinitiation downstream.

[*Keywords*: Translation initiation; reinitiation; eIF3; 40S ribosomal subunit; *GCN4*; short uORF]

Supplemental material is available at http://www.genesdev.org.

Received March 20, 2008; revised version accepted July 8, 2008.

General translation initiation (GTI) in eukaryotes consists of several steps that ultimately lead to formation of the 80S ribosome with the anti-codon of methionyl initiator tRNA (Met-tRNA$_i^{Met}$) base-paired to the AUG start codon in the ribosomal P-site. In the first step, Met-tRNA$_i^{Met}$ is bound by eukaryotic initiation factor 2 (eIF2) in its GTP form to produce the ternary complex (TC). The TC is subsequently recruited to the small ribosomal subunit with the help of eIF3, eIF1, eIF5, and eIF1A, forming the 43S preinitiation complex (PIC). The 43S PIC then interacts with the 5′ end of mRNA in a reaction stimulated by eIF4F, eIF4B, PABP, and eIF3. The 48S PIC thus formed scans the mRNA leader until the AUG start codon is recognized (for review, see Marintchev and Wagner 2005). Scanning is promoted by eIF1, eIF1A, and eIF4F in a mammalian reconstituted system (Pestova and Kolupaeva 2002), whereas yeast genetic data indicate that eIF3 and eIF5 also participate in vivo (Nielsen et al. 2004; Yamamoto et al. 2005). The GTP bound to eIF2 is partially hydrolyzed to GDP and P_i, dependent on the GAP eIF5, but the P_i is not released from the scanning complex until initiation codon–anticodon base-pairing induces dissociation or displacement of eIF1 (Algire et al. 2005; Cheung et al. 2007). Met-tRNA$_i^{Met}$ is then released into the P-site, and the 60S subunit can join the 40S-mRNA-Met-tRNA$_i^{Met}$ PIC in a reaction stimulated by GTP-bound eIF5B (Pestova et al. 2000). Subunit joining is thought to facilitate ejection of all eIFs but eIF1A (Unbehaun et al. 2004). Finally, GTP-hydrolysis on eIF5B triggers its dissociation, producing an active 80S ribosome poised for elongation (summarized in Fig. 6, below).

Various alternative mechanisms to the GTI pathway exist that are mostly utilized by viruses or function in

[4]Corresponding author.
E-MAIL valasekl@biomed.cas.cz; FAX 420-241-062-665.
Article is online at http://www.genesdev.org/cgi/doi/10.1101/gad.480508.

gene-specific translational control. They rely on *cis*-acting mRNA features and exhibit distinct factor requirements. Reinitiation (REI) is one such mechanism utilized to down- or up-regulate translation of regulatory proteins such as transcription factors and proto-oncogenes in response to various environmental stimuli (Kozak 2005). Ribosomes initiate in the normal way at the first AUG codon; however, at the termination codon, the 40S subunit (40S) remains bound to the mRNA, resumes scanning, and initiates again at a downstream start site. REI depends on de novo recruitment of the TC that is required to recognize the next AUG codon; therefore, it can be delicately regulated by manipulating the eIF2·GTP levels (for review, see Hinnebusch 2005).

Except for a few features in mRNA structure, we know very little about the molecular mechanisms underlying REI. It was shown that the ability of the 40S to reinitiate is limited by the size of the upstream ORF (uORF); however, the critical parameter that determines whether the 40S resumes scanning seems to be the time taken to translate the uORF, rather than its length (Kozak 2001; Rajkowitsch et al. 2004). REI is usually inefficient owing to excessive length or other features of the uORF that prevent retention of post-termination 40S ribosomes on mRNA. Hence, short uORFs generally serve to reduce protein production from a major ORF downstream (Kozak 2005). There are, however, a few examples where uORFs bear special characteristics that render them highly permissive for REI (REI-permissive), such as the mRNAs encoding the yeast transcription factors *YAP1* (Vilela et al. 1998), *GCN4* (Hinnebusch 2005) and its mammalian ortholog *ATF4* (Vattem and Wek 2004), and bZIP transcriptional regulator *ATF5* (Zhou et al. 2008).

GCN4 is a transcriptional activator of a large number of biosynthetic genes (Hinnebusch 2005). Although *GCN4* mRNA is synthesized constitutively, its translation is repressed under nutrient-rich conditions through a REI mechanism involving four upstream open reading frames (uORFs 1–4) that is very sensitive to the TC levels in cells. After translating the first and only REI-permissive uORF1, small ribosomal subunits remain attached to the mRNA, resume scanning, and reinitiate downstream. Under nonstarvation conditions, characterized by high levels of the TC, nearly all of the rescanning 40S ribosomes will rebind the TC before reaching uORFs 2–4, translate one of them, and dissociate from the mRNA. Amino acid starvation leads to phosphorylation of eIF2α by kinase GCN2, converting eIF2.GDP from a substrate to a competitive inhibitor of its GEF, eIF2B, thus reducing the concentration of TC. Low TC levels derepress *GCN4* translation by allowing ~50% of rescanning 40S ribosomes to rebind TC after bypassing uORF4 and reinitiate at *GCN4* instead. Failure to induce expression of *GCN4* in response to a shortage of amino acids in various mutant cells confers increased sensitivity to inhibitors of amino acid biosynthetic enzymes, and is designated the Gcn$^-$ phenotype. Conversely, constitutive expression of *GCN4* independent of amino acid levels due to a defect in TC assembly or recruitment overcomes sensitivity to the latter inhibitors in *gcn2*Δ cells and is called the Gcd$^-$ phenotype. A related but not identical mechanism has been shown to govern translation of the mammalian *ATF4* and *ATF5* transcription factors, indicating that at least basic principles of this regulatory system have been evolutionarily conserved (Vattem and Wek 2004).

A crucial but vaguely understood feature of *GCN4* translational control is the highly disparate capacities of uORF1 and uORF4 to permit efficient resumption of scanning following translation termination. Mutational analyses revealed that AU-rich sequences surrounding the stop codon of uORF1 favor resumption of scanning and REI, whereas GC-rich sequences flanking the uORF4 stop codon likely trigger ribosome release (Grant and Hinnebusch 1994). Sequences 5′ of uORF1 were also shown to be critical for efficient REI (Grant et al. 1995). Virtually nothing is known about what *trans*-acting factors, if any, function in concert with these mRNA features to promote REI. Mutations in eIF3 subunits b and c, and in eIF1, eIF5, eIF1A, and eIF5B, respectively, were shown to deregulate translational control of *GCN4* through their defects in TC recruitment, scanning, AUG selection, or subunit joining (for review, see Hinnebusch 2005); however, no mutations have been isolated that impair retention of post-termination ribosomes at the uORF1 stop codon and the resumption of scanning that is required for REI.

Our previous studies of yeast *Saccharomyces cerevisiae* eIF3 demonstrated that it plays a stimulatory role in nearly all steps of GTI (for review, see Hinnebusch 2006). It is composed of six subunits (a, b, c, i, g, and j), all of which have corresponding orthologs in mammalian eIF3 (meIF3). In *S. cerevisiae*, the TC and eIF1, eIF3, and eIF5 can be found in the higher-order ribosome-free assembly called the Multifactor Complex (MFC), and we and others previously demonstrated that there is a substantial cooperation among the eIFs assembled in the MFC in their binding to the 40S as well as their ribosome-associated functions in scanning and AUG recognition (Valášek et al. 2002, 2004; Nielsen et al. 2004, 2006; Yamamoto et al. 2005; Jivotovskaya et al. 2006). An important task is to elucidate the molecular mechanism underlying this extensive cooperation within the MFC.

We began addressing this issue by mapping the positions of individual components of the MFC on the 40S (Valášek et al. 2003). We found that deleting the N- and C-terminal domains (NTD and CTD) of eIF3c or the NTD of eIF3a impaired association of otherwise intact eIF3 complexes with the 40S, and, in addition, deleting the eIF3a-CTD reduced 40S association of the MFC when the connection between eIF3 and eIF5/TIF5 in the MFC was impaired by the *tif5-7A* mutation. In a separate study, the RNA recognition motif (RRM) of the eIF3b-NTD that mediates its interactions with eIF3j and eIF3a was implicated in the ability of eIF3j to stimulate 40S binding by eIF3 (Nielsen et al. 2006). This RRM-eIF3j network is conserved in mammals (ElAntak et al. 2007). Importantly, our findings that the eIF3a-CTD interacts with helices 16–18 of 18S rRNA and that eIF3a-NTD binds to ribosomal proteins RPS0A and RPS10A (Valášek

et al. 2003) suggested that yeast eIF3 associates with the solvent-exposed side of the 40S (Fig. 1A), as suggested by others for meIF3 (Srivastava et al. 1992; Siridechadilok et al. 2005).

In this study, we focused on the role of the NTD of eIF3a, known as *TIF32* in yeast, in promoting association of eIF3 and other MFC components with the 40S. We found that a partial deletion of the RPS0A-binding site in the a/*tif32-NTD* (Δ8) is not lethal but reduces the amounts of 40S-bound MFC components in vivo, consistent with the idea that the eIF3a-NTD forms a crucial intermolecular bridge between eIF3 and the 40S. Strikingly, the *a/tif32-Δ8* truncation imparted a severe Gcn$^-$ phenotype with novel characteristics, providing the first in vivo evidence that eIF3 is required for post-termination retention of 40S ribosomes at the uORF1 stop codon. Genetic epistasis interactions between mutations in the stimulatory sequences upstream of uORF1 and *a/tif32-Δ8* strongly indicate that eIF3a interacts with this REI-enhancing element that we named eIF3a-NTD-responsive site (eIF3a-RS). Thus, we propose that establishment of the interaction between eIF3a-NTD and the specific eIF3a-RS 5′ of uORF1 at or near the mRNA exit channel of the post-termination 40S subunit stabilizes its association with mRNA and promotes the resumption of scanning for efficient REI at the downstream ORF.

Results

The eIF3a-NTD constitutes a critical link between eIF3 and the 40S subunit

We recently identified several important domains of eIF3 subunits and eIF5 mediating interaction of the MFC with the 40S that allowed us to predict certain aspects of the organization of the 43S PIC (Fig. 1A; Valášek et al. 2003). Among them, the eIF3a-NTD was found to interact in vivo and in vitro with the CTD of small ribosomal protein RPS0A, which has been located beneath the mRNA exit channel on the solvent side of the 40S (Spahn et al. 2001). Consistently, a partial deletion of the RPS0A-binding domain (R0BD) in *a/tif32-Δ8* (Fig. 1B) that did not interfere with the integrity of the MFC (Valášek et al. 2002) completely eliminated binding of the mutant form of the complex (MFC-Δ8) to the 40S in vivo when competing with the wild-type MFC (Valášek et al. 2003). Our previous finding that *a/tif32-Δ8* partially complemented the temperature sensitive (Ts$^-$) phenotype of the *a/tif32-R731I/rpg1-1* mutant strain (Valášek et al. 2002) prompted us to inquire whether *a/tif32-Δ8* can support viability in cells lacking wild-type *a/TIF32*. If so, we could eliminate the effect of competition and examine the phenotypes of *a/tif32-Δ8* in cells lacking wild-type *a/TIF32*. Thus, we constructed a YAH01 strain in which wild-type *a/TIF32* is expressed under control of the *MET3* promoter that can be turned off by addition of methionine to the medium. Indeed, plasmid-borne *a/tif32-Δ8* supported growth of YAH01 cells in the presence of methionine, albeit producing a slow-growth phenotype (Slg$^-$) with a doubling time (dt) of 2.8 h compared with 1.6 h for the wild-type strain (Fig. 1C, row 3 vs. 2). By contrast, *a/tif32-Δ7*, with a nearly complete deletion of the R0BD (Fig. 1B), did not complement depletion of wild-type eIF3a (Fig. 1C, row 4), even when expressed from a high-copy plasmid (data not shown).

We next wished to confirm that Slg$^-$ of the *a/tif32-Δ8* cells is associated with a defect in GTI. To that end, we analyzed the polysome content in *a/tif32-Δ8* cells pre-

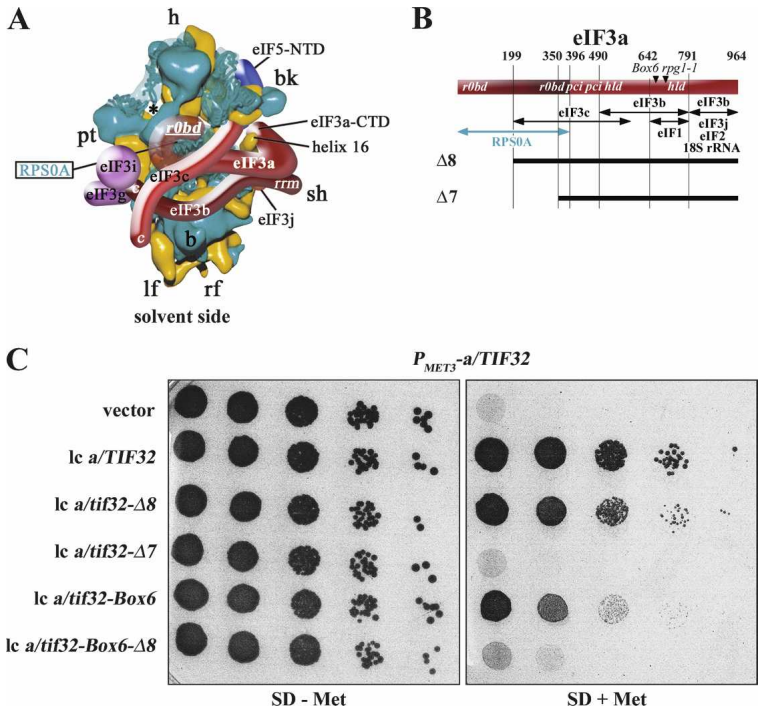

Figure 1. Genetic evidence that a partial deletion of the RPS0A-binding domain in the eIF3a-NTD affects cell growth. (*A*) Hypothetical location of the eIF3 complex on the *S. cerevisiae* 40S subunit based on Cryo-EM reconstruction adapted from Valášek et al. (2003). The 40S subunit is shown from the solvent side, with RNA segments in yellow and proteins in green. Positions of RPS0A and the RPS0A-binding domain (R0BD) of eIF3a are indicated. The mRNA exit channel is designated by an asterisk. (*B*) Schematic of eIF3a with arrows delimiting the minimal binding domains for the indicated proteins identified previously. The lines beneath the schematic depict two N-terminally truncated eIF3a-His proteins that were analyzed in this study. The locations of the RPS0A-binding domain (*r0bd*), the PCI homology domain (*pci*), the eIF3j/HCR1-like domain (*hld*), and two mutations are indicated in the colored rectangle. (*C*) Partial deletion of the R0BD in the eIF3a-NTD (*a/tif32-Δ8*) produces the Slg$^-$ phenotype. Transformants of strain YAH01 bearing the *a/TIF32* wild-type allele under control of the *MET3* promoter containing empty vector; lc pRSeIF3a-His; lc pRSeIF3a-Δ8-His; lc pRSeIF3a-Δ7-His; lc pRSeIF3a-Box6; and lc pRSeIF3a-Δ8-Box6-His, respectively, were spotted in five serial dilutions on SD medium in the absence (*left* panel) or presence (*right* panel) of 2 mM methionine and incubated for 2 d at 30°C.

treated with formaldehyde to cross-link ribosomes on mRNA, by resolving whole-cell extracts (WCEs) by velocity sedimentation through 5%–45% sucrose gradients (Valášek et al. 2007). The *a/tif32-Δ8* extracts showed polysomal run-off and an increased amount of 80S monosomes, leading to a ~2.5-fold decrease in the polysome to monosome (P/M) ratio, which indicates a reduced rate of GTI (Fig. 2A).

To provide evidence that the eIF3a-NTD represents an important link between the MFC and the 40S, we measured binding of eIF3 subunits and other MFC components to 40S subunits in WCEs of mutant *a/tif32-Δ8* cells treated with 1% formaldehyde. This treatment cross-links eIFs to 40S ribosomes in vivo, minimizing dissociation of PICs during sedimentation and thus provides the best available approximation of the native 43S/48S PICs composition in vivo (Valášek et al. 2007). As shown in Figure 2, B and C, we observed ~40% decreases in the amounts of selected eIF3 subunits sedimenting in the 40S-containing fractions (10–12) with commensurate increases in their levels in fractions 4–7 containing free MFC in the *a/tif32-Δ8* cells versus the wild-type control. Similar, but less pronounced, reductions in 40S binding (~25%) were also observed for eIF5 and the TC component eIF2γ. These results demonstrate that partial deletion of the R0BD of eIF3a reduces stable association of eIF3 and, to a lesser extent, eIF2 and eIF5 with the 40S in vivo.

Further support for the role of the eIF3a-NTD in anchoring eIF3 to the 40S arose from combining *a/tif32-Δ8* with a 10-alanine substitution of amino acids 692–701 in the eIF3j/HCR1-like domain (HLD) of eIF3a designated *a/tif32-Box6*. The *a/tif32-Box6* mutation also imparts a Slg$^-$ phenotype (dt ~3.6 h) and reduces association of eIF3 and other MFC constituents with the 40S, suggesting that the HLD also promotes 40S binding of the MFC (L. Burela, L. Valášek, and A.G. Hinnebusch, unpubl.). As shown in Figure 1C, rows 5 and 6, combining the *Δ8* and *Box6* mutations in the same *a/TIF32* allele results in synthetic lethality, consistent with the idea that these mutations disrupt independent contacts of eIF3 with the 40S.

Evidence that a/tif32-Δ8 severely interferes with reinitiation by preventing retention of post-termination ribosomes on mRNA at uORF1

We next wished to confirm our observation that *a/tif32-Δ8* reduces association of the TC with the 40S by examining translational regulation of *GCN4* expression, which is very sensitive to decreases in the rate of TC loading on 40S subunits in living cells. Based on our biochemical data, we expected that the *a/tif32-Δ8* mutation would impart a Gcd$^-$ phenotype and allow *gcn2Δ* cells to grow on 3-aminotriazole (3-AT), an inhibitor of histidine biosynthetic genes. However, this was not observed (data not shown), suggesting that the derepression of *GCN4* translation expected from a defect in TC recruitment is being suppressed by another stronger defect in the REI process in this mutant.

In fact, we found that *a/tif32-Δ8 GCN2*$^+$ cells exhibit a severe Gcn$^-$ phenotype, displaying sensitivity to 3-AT nearly as strong as that of the *a/TIF32*$^+$ *gcn2Δ* strain where eIF2α cannot be phosphorylated (Fig. 3A). Consistently, derepression of the *GCN4-lacZ* reporter contain-

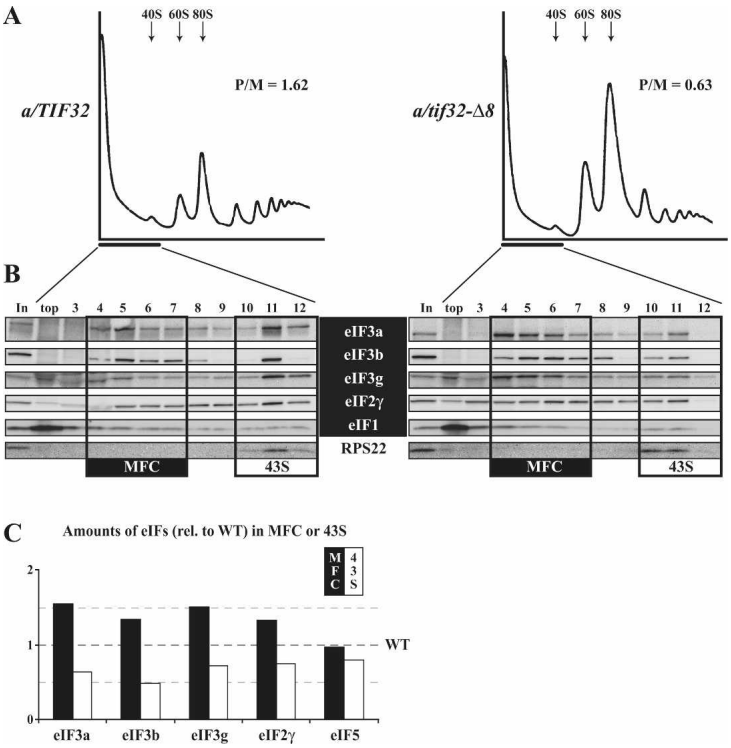

Figure 2. The eIF3a-NTD constitutes a critical link between eIF3 and the 40S ribosome. (*A*) Isogenic strains YBS47 (*GCN2 a/tif32*Δ pRSeIF3a-His) and YBS53 (*GCN2 a/tif32*Δ pRSeIF3a-Δ8-His) were grown in YPD medium at 30°C to an OD_{600} of ~1.5 and cross-linked with 1% HCHO prior to harvesting. WCEs were prepared and subsequently separated on a 5%–45% sucrose gradient by centrifugation at 39,000 rpm for 2.5 h. The gradients were collected and scanned at 254 nm to visualize the ribosomal species. Positions of 40S, 60S and 80S species are indicated by arrows and P/M ratios are given above the profiles. (*B*) The same as in *A*, except that WCEs were separated on a 7.5%–30% sucrose gradient by centrifugation at 41,000 rpm for 5 h. Proteins from the collected fractions were subjected to Western analysis using antibodies against the proteins listed between the blots. An aliquot of each WCE was analyzed in parallel (In, input), and the first two fractions were combined (top). Rectangles indicate fractions where the Multifactor complex (MFC) constituents (highlighted in black) or the 43S PICs (43S), respectively, sediment. (*C*) Amounts of the each individual factor in all fractions from three independent experiments were quantified by fluorescence imaging, combined, and the percentage representation of the signal corresponding to the MFC (4–7) or 43S (10–12) fractions was calculated. Values obtained for the *a/TIF32* wild-type strain were set to 100%, and relative distribution of individual factors in the MFC and 43S fractions in the *a/tif32-Δ8* mutant cells was plotted.

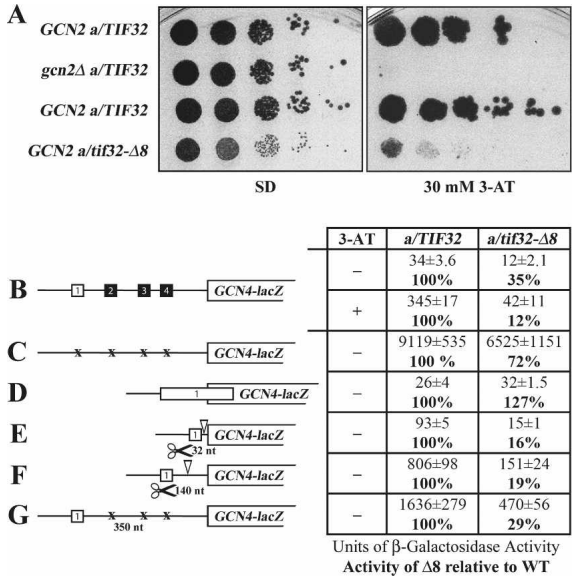

3-AT	a/TIF32	a/tif32-Δ8
–	34±3.6 **100%**	12±2.1 **35%**
+	345±17 **100%**	42±11 **12%**
–	9119±535 **100 %**	6525±1151 **72%**
–	26±4 **100%**	32±1.5 **127%**
–	93±5 **100%**	15±1 **16%**
–	806±98 **100%**	151±24 **19%**
–	1636±279 **100%**	470±56 **29%**

Units of β-Galactosidase Activity
Activity of Δ8 relative to WT

Figure 3. Evidence that *a/tif32-Δ8* severely interferes with the reinitiation process by preventing post-termination retention of the 40S ribosome on mRNA. (*A*) *a/tif32-Δ8* imparts a severe Gcn⁻ phenotype implicating eIF3 in regulation of translational control of *GCN4* expression that occurs via REI. Isogenic strains H2880 (*GCN2 a/TIF32*; row 1), and H2881 (*gcn2Δ a/TIF32*; row 2), YBS47 (*GCN2 a/tif32Δ* pRSeIF3a-His; row 3), YBS53 (*GCN2 a/tif32Δ* pRSeIF3a-Δ8-His; row 4), respectively, were spotted in five serial dilutions on SD (*left* panel) or SD containing 30 mM 3-AT (*right* panel) and then incubated for 3 and 7 d at 30°C, respectively. (*B*) *a/tif32-Δ8* reduces basal expression of *GCN4-lacZ* and prevents its full derepression upon starvation. Isogenic strains YBS47 (*a/TIF32*) and YBS53 (*a/tif32-Δ8*) were transformed with p180, grown in minimal media for 6 and 8 h, respectively, and the β-galactosidase activities were measured in the WCEs and expressed in units of nanomoles of o-nitrophenyl-b-D-galactopyranoside hydrolyzed per minute per milligram of protein. To induce *GCN4-lacZ* expression, *a/TIF32* and *a/tif32-Δ8* transformants grown at the minimal media for 2 h were treated with 10 mM 3-AT for 6 or 16 h, respectively. The mean values and standard deviations obtained from at least six independent measurements with three independent transformants, and activity in *a/tif32-Δ8* relative to wild type, respectively, are given in the table to the *left* of schematics. (*C*,*D*) The failure of *a/tif32-Δ8* to derepress *GCN4-lacZ* is not caused by leaky scanning. YBS47 and YBS53 were transformed with p227 (*C*) and pM226 (*D*), respectively, and analyzed as in *B*, except that they were not treated with 3-AT. (*E–G*) The failure of *a/tif32-Δ8* to derepress *GCN4-lacZ* is not caused by slow or defective scanning. YBS47 and YBS53 were transformed with pG67 (*E*), pM199 (*F*), or p209 (*G*), respectively, and analyzed as in *C* and *D*.

ing all four uORFs in response to 3-AT was reduced by a factor of about nine compared with the wild-type *a/TIF32* strain (Fig. 3B, "+"), fully accounting for the severe 3-AT^S phenotype of the *a/tif32-Δ8* mutant. This derepression defect resulted partly from a decrease in the induction ratio by a factor of about three and partly from a decrease in the basal level of *GCN4-lacZ* expression by a factor of about three (Fig. 3B, "–"). The fact that expression from the uORF-less *GCN4-lacZ* construct was reduced only by a factor of ~1.3 in *a/tif32-Δ8* cells (Fig. 3C) suggests that neither decreased *GCN4-lacZ* mRNA production nor a general decrease in translation efficiency owing to the 40S binding defect of *a/tif32-Δ8* can account for its severe derepression defect. In addition, phosphorylation of eIF2α by GCN2 upon starvation was found to be unaffected in *a/tif32-Δ8* cells (data not shown), ruling out this possible mechanism for the Gcn⁻ phenotype. Thus, these results strongly indicate that the eIF3a-NTD plays a critical role in the REI mechanism on *GCN4* mRNA, however, by a mechanism distinct from a simple reduction in TC recruitment to the rescanning ribosomes.

The reinitiation process can be divided into two phases: the initial REI-specific phase and the following GTI-like phase. The REI-specific steps occur following translation of uORF1 and include (1) 80S ribosome recycling after polypeptide termination, (2) post-termination retention of the 40S subunit, and (3) recruitment of factors required for resumption of scanning. The GTI-like phase is represented by (1) scanning, (2) TC recruitment, (3) GTP-hydrolysis by TC, (4) AUG recognition, and (5) subunit joining. To determine what step is perturbed by *a/tif32-Δ8* and leads to impairment of *GCN4* derepression, we analyzed a series of *GCN4-lacZ* reporters varying in their *GCN4* mRNA leader sequences. It should be noted here that the *GCN4-lacZ* mRNA levels for all constructs used throughout this study were found to be indistinguishable between the wild-type and *a/tif32-Δ8* cells (Supplemental Fig. 1). Defects in recognition of the AUG start codon or subunit joining could result in the bypass of uORF1 by scanning PICs (leaky scanning) with initiation at REI-nonpermissive uORFs 2–4 instead. To examine this possibility, the β-galactosidase activity was measured in WCEs from wild-type and mutant cells bearing a reporter plasmid in which uORF1 is elongated and overlaps the beginning of *GCN4*. The *a/tif32-Δ8* mutation produced only a small increase in expression from this construct (Fig. 3D), which cannot account for the strong derepression of wild-type *GCN4-lacZ* for the following reason: By comparing the results in panels C and D, it can be deduced that only a negligible amount of 40S ribosomes (<1%) that scan from the 5′ end leaky scan the uORF1 AUG, in both mutant and wild-type cells.

Another way to explain the derepression defect in *a/tif32-Δ8* cells is to propose that rescanning ribosomes progress more slowly from uORF1 to uORF4 in the mutant cells. This slower rate of scanning would compensate for the reduction in TC recruitment that we observed by providing the scanning 40Ss sufficient time to rebind TC before reaching uORF4. To test that, we analyzed constructs carrying only uORF1 at three different positions relative to *GCN4-lacZ* (Fig. 3E–G). As observed previously for *prt1-1* (eIF3b) (Nielsen et al. 2004), slow scanning would be expected to increase *GCN4-lacZ* expression from these constructs, particularly those in which uORF1 is closer than normal to the *GCN4* AUG start codon (Fig. 3E,F). Importantly, *a/tif32-Δ8* strongly decreases, not increases, expression from all three constructs (Fig. 3E–G), arguing against the slow scanning mechanism. It is noteworthy that *a/tif32-Δ8* reduces ex-

pression from all three constructs by nearly the same factor (71%–84%), despite the fact that the uORF1–*GCN4* interval varies dramatically from 32 nucleotides (nt) to 350 nt. This phenotype is also inconsistent with less processive scanning, leading to dissociation of 40S reinitiation complexes (RICs) as they travel downstream from uORF1. Reduced processivity would elicit a much greater reduction in REI efficiency for the construct with the 350-nt spacer (Fig. 3G) versus that with the 32-nt spacer (Fig. 3E), which is not the case.

Hence, we propose that *a/tif32-Δ8* impairs the ability of the 40S to either remain attached to *GCN4* mRNA following peptide termination at uORF1 or to acquire factors, such as eIF1 and eIF1A, which promote scanning. Either defect would reduce the number of 40Ss that resume scanning and reinitiate at *GCN4*. This model readily explains why the REI efficiency is reduced by nearly the same factor for the constructs in Figure 3, E–G, in *a/tif32-Δ8* mutant cells. The implication of this model is that the specialized ability of uORF1 to promote efficient REI depends on the eIF3a-NTD and, hence, on the presence of eIF3 on the terminating ribosome at the uORF1 stop codon. The *a/tif32-Δ8* mutation thus establishes a novel class of Gcn$^-$ mutants affecting translational control of *GCN4* by impairing the initial specific steps of REI.

A functional interaction between the eIF3a-NTD and sequences 5′ of uORF1 promotes resumption of scanning by post-termination 40S subunits

It was shown previously that the high propensity of uORF1 for REI requires sequences upstream of its start codon as well as its last codon and 6 nt following the stop codon (Grant and Hinnebusch 1994; Grant et al. 1995); however, the molecular mechanism of their function(s) is unknown. Having established that the eIF3a-NTD promotes association of eIF3 with the 40S and is critical for REI, we wished to examine whether the eIF3a-NTD acts together with specialized sequences that impart the high REI potential of uORF1. Based on its interaction with RPS0A, the eIF3a-NTD is expected to bind in the vicinity of the mRNA exit channel on the solvent side of the 40S (Spahn et al. 2001; Valášek et al. 2003). Whereas the 3′ 12-nt sequence feature surrounding the stop codon of uORF1 should be buried in the mRNA-binding cleft of the terminating 80S ribosome, sequences beginning at nucleotide –10 upstream of the uORF1 AUG would most likely have emerged from the mRNA exit channel and be accessible to the eIF3a-NTD (Fig. 4A; Wang and Sachs 1997). Hence, it is conceivable that interaction of the eIF3a-NTD with sequences upstream of –9 would stabilize binding of the 40S to the mRNA following termination at uORF1 and thereby promote its ability to resume scanning.

It was demonstrated that deletion of 40 nt from nucleotide –21 upstream of the 5′ sequences of uORF1 (*Δ40*) dramatically reduced (by ~65%) the induction of *GCN4-lacZ* expression in wild-type cells (Fig. 4D), whereas replacing the –15 to –1 region 5′ of ORF1 ("linker" and "buried" sequences in Fig. 4A) with the corresponding region upstream of uORF4 had no effect (Miller and Hinnebusch 1989; Grant et al. 1995). Nearly complete elimination of the 5′ sequences in *Δ160* then further diminished *GCN4-lacZ* expression, showing only 15% of the wild-type activity derived most probably from the intact 3′ feature (Fig. 4F; Grant et al. 1995). We found, in addition, that replacement of the –21 AAAATT –16 stretch with CCCCGG [$(C)_4GG$] also significantly reduced β-galactosidase activity by ~40% in wild-type cells (Fig. 4C). Combining the latter mutation with *Δ40* in the *Δ46* construct carrying deletion of 46 nt from nucleotide –61 to –15 resulted in an additive effect (~75% reduction; Fig. 4E). Thus, we reasoned that if the region upstream of nucleotide –15 contains the eIF3a-NTD-binding site, then all these mutations should have a smaller to no effect on REI in *a/tif32-Δ8* versus wild-type cells because the interaction would be already disrupted by *a/tif32-Δ8*. Accordingly, $(C)_4GG$, *Δ40*, and *Δ46* mutations conferred significantly smaller reductions of

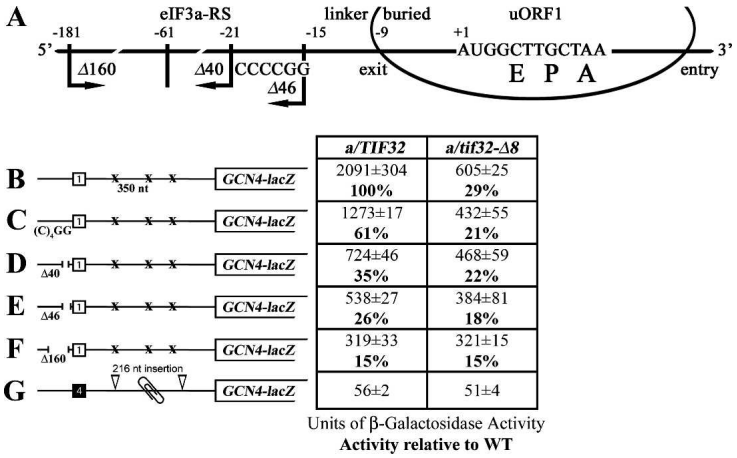

Figure 4. The eIF3a-NTD functionally interacts with the 5′ sequences of uORF1 to ensure efficient resumption of scanning. (*A*) Schematic showing predicted position of the 40S ribosome terminating at the stop codon of uORF1 from the *GCN4* mRNA leader (data adapted from Wang and Sachs 1997). E, P, and A sites of the 40S ribosomes are aligned with the last two coding triplets and the TAA stop codon. Location of the eIF3a-NTD-responsive site (eIF3a-RS), linker, and buried parts of the sequences upstream of uORF1 are indicated at the *top*; 3′ boundary of the *Δ40* deletion (identical to *Δ160*), *Δ46* deletion, and the $(C)_4GG$ multiple substitution are shown *below* the line depicting mRNA. (*B–F*) Same as in Figure 3B, except that YBS47 and YBS53 were transformed with p209, pBS64, pBS62, pVM11, and pBS63, respectively, and analyzed without 3-AT treatment. Activities relative to wild type are given in bold in the table to the *left* of schematics. (*G*) *a/tif32-Δ8* does not affect *GCN4-lacZ* expression after translating the REI-nonpermissive uORF4. YBS47 and YBS53 were transformed with pA80z and analyzed as in Figure 3B.

GCN4-lacZ expression in *a/tif32-Δ8* cells, whereas the most destructive *Δ160* mutation completely eliminated the negative impact of *a/tif32-Δ8* on REI efficiency, producing identical residual activities in both wild-type and *a/tif32-Δ8* cells (Fig. 4C–F). These findings of genetic epistasis strongly suggest that the 5′ sequences from nucleotides –181 to –16 constitute an eIF3a-NTD-responsive site (eIF3a-RS), perhaps a direct binding domain, which is required for efficient REI.

To further underscore this point, we analyzed a construct containing solitary uORF4 with its 5′ and 3′ flanking sequences that was placed precisely at the normal position of uORF1 (Fig. 4G). Since it was previously shown that sequences functionally equivalent to the eIF3a-RS of uORF1 are lacking upstream of uORF4, and thus this short uORF allows only a negligible level of REI (Grant and Hinnebusch 1994), we predicted that *a/tif32-Δ8* should not affect *GCN4-lacZ* expression from the latter construct when compared with wild type. Indeed, Figure 4G clearly demonstrates that the deletion of eIF3a-NTD has no impact on REI in the absence of the eIF3a-RS of uORF1.

Proper placement of the eIF3a-RS of uORF1 relative to the 40S mRNA exit channel is critical for efficient reinitiation

Reinitiation was found to decrease as the uORF was lengthened up to 35 codons, or the rate of translation elongation was slowed down (Kozak 2001; Rajkowitsch et al. 2004). To explain this phenomenon, it was proposed that REI depends on retention of certain initiation factors that gradually dissociate from 80S ribosomes during the course of elongation, thereby reducing the efficiency of REI (Kozak 2005). The results presented so far allow us to propose that eIF3 is a factor that stays bound temporarily to the elongating ribosome, owing to its strategic position on the solvent-exposed "back" side of the 40S subunit. Furthermore, our finding of the specific eIF3a-RS 5′ of uORF1 that promotes REI suggested to us that lengthening uORF1 could decrease REI efficiency by a combination of two effects: (1) displacing this potential eIF3a-NTD-binding site from the mRNA exit channel when the ribosome reaches the stop codon, and (2) by progressive reduction of the eIF3 occupancy on elongating ribosomes.

Since the effect of progressive lengthening of uORF1 has not been investigated before, we analyzed the effect of adding an increasing number of alanine codons to uORF1 on *GCN4-lacZ* expression in wild-type *a/TIF32* cells. As expected, extending the MAC coding sequence of uORF1 with additional Ala codons led to a gradual decrease in β-galactosidase activity (Fig. 5E–I, left column). Addition of two Ala codons [Fig. 5B,G, MA(A)$_2$C] reduced activity by 14%, whereas addition of 10 Ala codons resulted in a ~72% reduction (Fig. 5I; MA(A)$_{10}$C). Assuming that spacing between the eIF3a-RS of uORF1 and its stop codon affects REI efficiency and that the two-Ala extension will reduce eIF3 occupancy on the elongating ribosomes only by a small margin, we should

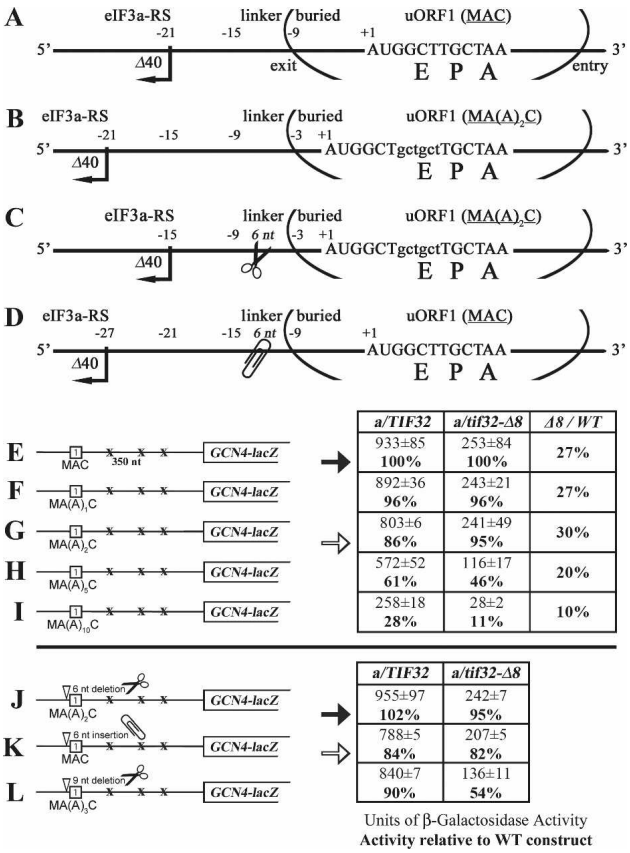

Figure 5. Proper placement of the eIF3a-NTD-responsive site (eIF3a-RS) in 5′ of ORF1 relative to the mRNA exit channel is a critical requirement for efficient REI. (*A–D*) Schematics as in Figure 4A except that the change in a position of the 40S ribosome on the mRNA of uORF1 extended by two codons (*B*), extended by two codons and at the same time shortened by 6 nt in the linker region (*C*), and shortened by 6 nt in the linker only (*D*) are shown. (*E–I*) Progressive extension of the uORF1 reading frame results in a gradual decrease in the *GCN4-lacZ* expression in the wild-type but not in *a/tif32-Δ8* strains. Same as in Figure 4, B–F, except that YBS47 and YBS53 transformed with pM128 or pBS71 through pBS74, respectively, were examined. In addition, activities in *a/tif32-Δ8* relative to wild type, respectively, are given in the *right* column of the table. (*J–L*) Spacing between the eIF3a-RS and the uORF1 stop codon is a critical determinant of REI. Same as above, except that the strains were transformed with pBS75, pBS77, and pBS94, respectively. Closed and open arrows highlight β-galactosidase activities obtained with constructs with the eIF3a-RS in its native position or shifted by 6 nt upstream, respectively.

be able to restore the REI activity of the MA(A)$_2$C construct at least partially by shortening the linker sequence by 6 nt (Fig. 5C). Indeed, the 6-nt linker deletion in MA(A)$_2$C produced 102% of wild-type activity (Fig. 5, J vs. E, closed arrows). Consistently, moving the eIF3a-RS further upstream by extending the linker by 6 nt in the MAC construct (Fig. 5D) decreased *GCN4-lacZ* expression to a level comparable with the MA(A$_2$)C construct (Fig. 5, K vs. G, open arrows). In contrast, correcting the spacing in MA(A)$_3$C by the deletion of 9 nt no longer

restored the wild-type activity (Fig. 5L), most probably due to the more pronounced reduction in eIF3 occupancy on the elongating 80S as judged from a more dramatic impact on REI activity in *a/tif32-Δ8* cells (see also below). The fact that similar results were obtained by testing some of these uORF1 extensions and deletions in a construct containing uORF1 and uORF4 that suffice for wild-type regulation of *GCN4* expression (Supplemental Fig. 2) further support our aforementioned suggestion of the compound effect of lengthening of uORF1 on efficiency of REI.

Addition of two Ala codons to uORF1 did not reduce *GCN4-lacZ* expression as much in *a/tif32-Δ8* cells as in the wild type; however, the longer extensions of five or 10 Ala codons produced a larger decrease in β-galactosidase activity in the mutant versus wild-type strains (Fig. 5E–I; middle and far right columns). This ostensibly paradoxical result can be understood by recalling that *a/tif32-Δ8* is expected to reduce REI by two distinct mechanisms: (1) impairing functional interaction of eIF3 with the eIF3a-RS 5′ of uORF1 and (2) decreasing retention of eIF3 by elongating ribosomes translating uORF1 by reducing the binding of eIF3 to 40S subunits. We observed that addition of five Ala codons was required to detect a marked decrease in *GCN4-lacZ* activity from a construct containing REI-nonpermissive uORF4 only (B. Szamecz and L. Valášek, unpubl.). Hence, we can stipulate that the retention of eIF3 is not significantly reduced by increasing the length of uORF1 by only one or two Ala codons. This would mean that the attenuation in *GCN4-lacZ* expression from the $MA(A)_1C$ and $MA(A)_2C$ constructs in wild-type cells results primarily from displacement of the 5′ sequence feature away from the mRNA exit site of a post-termination ribosome. We showed above that the *a/tif32-Δ8* mutation diminishes the effect of disrupting the 5′ eIF3a-RS by the $(C)_4GG$, *Δ40*, and *Δ46* mutations; hence, *a/tif32-Δ8* should likewise blunt the effects of the $MA(A)_1C$ and $MA(A)_2C$ mutations on REI, as we observed in Figure 5G. We further stipulate that the larger increases in uORF1 length of five or 10 codons lead to a significant reduction in eIF3 occupancy by post-termination 40S subunits. Because *a/tif32-Δ8* weakens binding of eIF3 to the 40S subunit, it can be expected that this mutation would exacerbate the effect of lengthening uORF1, as observed in Figure 5, H and I, for the $MA(A)_5C$ and $MA(A)_{10}C$ mutations. Taken together, these findings strongly support the idea that, at least for REI-permissive uORF1, it is not only the length of the coding region but also a proper placement of the 5′ eIF3a-RS relative to the mRNA exit channel on the post-termination 40S ribosome that represent two critical parameters for efficient REI.

Discussion

The major part of this study was driven by our efforts to address the longstanding question of what endows uORF1 from the *GCN4* mRNA leader with its unique ability to allow highly efficient REI. We began by demonstrating that the N-terminal domain of eIF3a forms an important intermolecular bridge between eIF3 and the 40S ribosomal subunit, most probably by its previously reported interaction with RPS0A (Valášek et al. 2003). The *a/tif32-Δ8* mutation also reduced 40S association of TC and eIF5, consistent with the role of eIF3 in stimulating 40S binding of other MFC components. We observed a mild defect in 40S biogenesis in *a/tif32-Δ8* cells, evident from the increased ratio of free 60S to 40S subunits (Fig. 2A; B. Szamecz and L. Valášek, unpubl.), which might contribute to the Slg^- phenotype. However, the fact that combining *a/tif32-Δ8* with *a/tif32-Box6*, which is known to affect 40S binding of eIF3 but not ribosome biogenesis (L. Burela, L. Valášek, and A.G. Hinnebusch, unpubl.), resulted in synthetic lethality supports our conclusion that the eIF3a-NTD is required primarily for an important contact between eIF3 and the 40S. Previously, mutations in eIF3b and eIF3c were shown to affect binding of eIF3 to the 40S (Valášek et al. 2001, 2004; Nielsen et al. 2006). Unlike *a/tif32-Δ8*, however, these mutations destabilized the MFC and thus might impair 40S binding indirectly. Hence, our results provide the first in vivo evidence implicating a particular domain of a core subunit of eIF3 in its 40S-binding activity.

Although *a/tif32-Δ8* decreases the efficiency of TC recruitment to 40S subunits in vivo, it does not constitutively derepress *GCN4* translation manifested by the Gcd^- phenotype. Rather, *a/tif32-Δ8* strongly impairs derepression of *GCN4* translation in starved cells. Our genetic analysis ruled out several mechanisms to explain this Gcn^- phenotype that were established previously for mutations in other eIFs, including leaky scanning of uORF1, a slow rate of scanning, and less processive scanning (Fig. 3). The simplest explanation of our results is that *a/tif32-Δ8* reduces the ability of 40S subunits to resume scanning after terminating at uORF1, neutralizing the specialized features that optimize uORF1 for this key first step in REI and that are lacking at uORF4. These are the first results directly implicating eIF3 in this critical aspect of the canonical REI mechanism involving short uORFs.

There is previous evidence that REI diminishes with increasing uORF length or in response to other perturbations that increase the time required to translate the uORF (Kozak 2001; Rajkowitsch et al. 2004). Accordingly, Kozak (2001) proposed that contacts between one or more eIFs and the 40S established in the PIC are not disrupted at subunit joining and, instead, decay stochastically during elongation. This would allow persistence of an eIF in association with post-termination 40S subunits following translation of a short uORF and thereby facilitate the resumption of scanning and REI. We found that elongating uORF1 by one or two Ala codons has only a small effect, whereas addition of five or 10 Ala codons produces a marked reduction in REI efficiency. Importantly, *a/tif32-Δ8* exacerbates the reduction in REI produced by lengthening uORF1 by five or 10 codons. Considering that *a/tif32-Δ8* impairs 40S binding of eIF3, these last data provide strong genetic evidence that eIF3 is a factor that remains bound to the 40S subunits of elongating 80S ribosomes as they translate uORF1, and

that this interaction is crucial for REI by post-termination ribosomes.

Based on structural (Srivastava et al. 1992; Siridechadilok et al. 2005) and biochemical data (Valášek et al. 2003), it appears that both mammalian and yeast eIF3 bind primarily to the solvent-exposed side of the 40S (Figs. 1A, 6A). Hence, it is plausible to suggest that eIF3 remains associated with the 40S, at least temporarily, after subunit joining (Fig. 6B–D). The interaction should be relatively weak, however, owing to the absence of supporting contacts that eIF3 makes with several eIFs that are ejected at subunit joining (summarized in Hinnebusch 2006). Presumably, eIF3 relies on direct interactions with 40S components—e.g., the eIF3a-NTD binding to RPS0A—and possibly also on contacts with mRNA residues near the entry and exit sites on the solvent side of the 40S subunit. Indeed, meIF3 and mRNA were shown to mutually stabilize their 40S interactions in vitro (Kolupaeva et al. 2005). Moreover, UV-cross-linking of 48S complexes revealed that human eIF3a specifically interacted with mRNA positions –14 and –17 and eIF3d cross-linked to positions –8 through –17, sug-

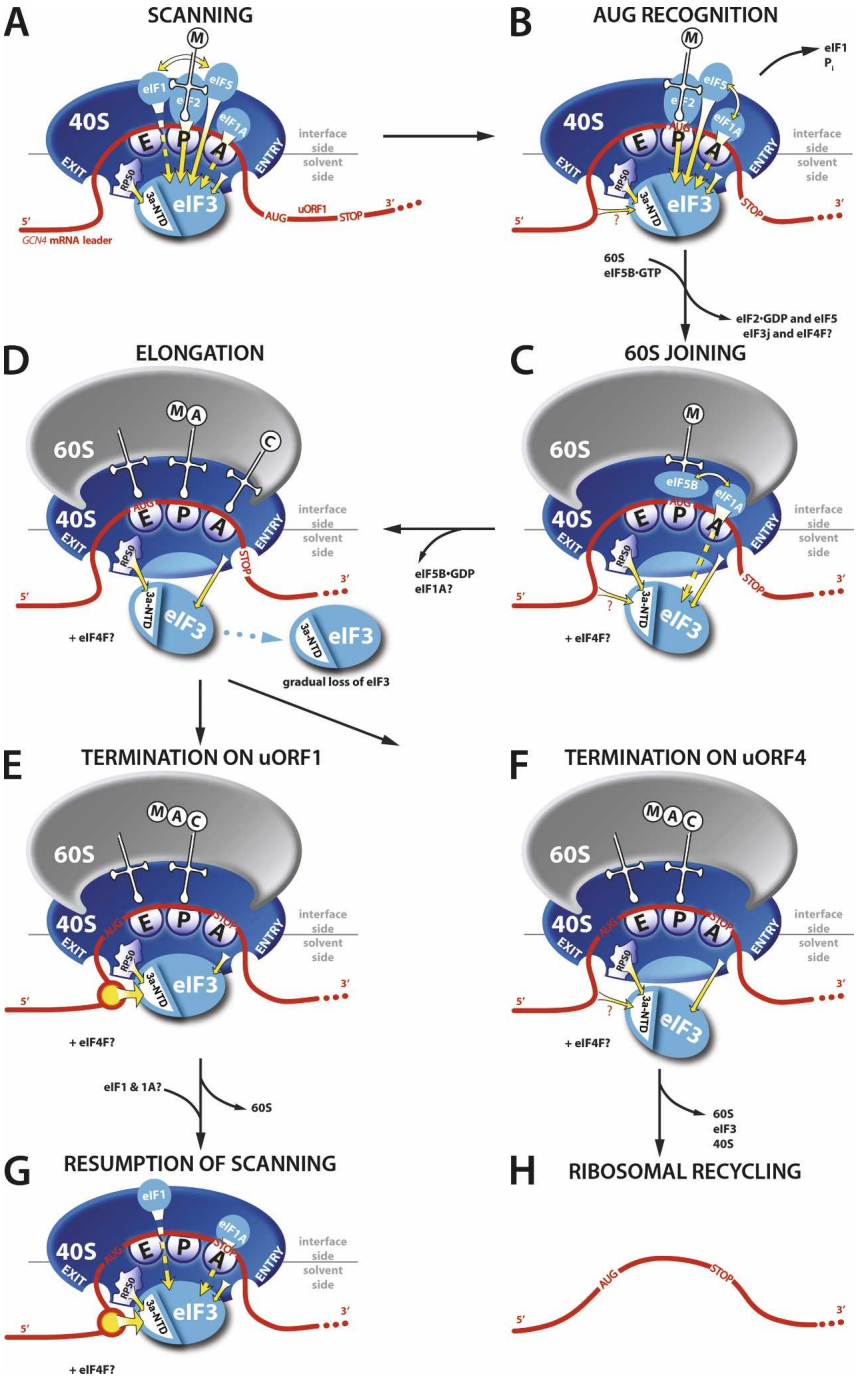

Figure 6. A yeast model for eukaryotic reinitiation following translation of a short uORF. (*A*,*B*) eIF3 association with the scanning 48S PIC is stabilized by supporting contacts with eIF1, eIF1A, eIF5, and the TC. (*C*) Upon subunit joining, eIF3 (and possibly also eIF4F) remains bound to the 80S ribosomes owing to its strategic position on the solvent-exposed side of the 40S ribosome and the contacts that it makes with 40S ribosomal components (e.g., eIF3a-NTD with RPS0A) and presumably also with mRNA. (*D*) During the first few rounds of elongation, weakly associated eIF3 gradually dissociates from the 80S as a function of length and complexity of the translated region. (*E*,*F*) After translation of a short uORF, a certain proportion of 80S ribosomes terminating at its stop codon still contains eIF3, the presence of which is required for resumption of scanning. (*E*,*G*) Binding of the eIF3a-NTD directly to the specific eIF3a-RS 5′ of uORF1 greatly stabilizes association of the post-termination 40S subunit with mRNA following dissociation of the 60S subunit in the first stage of the ribosome recycling reaction and thereby promotes efficient resumption of scanning and REI downstream. (*F*,*H*) Absence of the stimulatory eIF3a-RS, for example at uORF4, results in completion of ribosomal recycling by the majority of terminating 80S ribosomes.

gesting that eIF3 forms an extension of the mRNA-binding channel (Pisarev et al. 2008).

It is noteworthy, however, that *a/tif32-Δ8* does not exacerbate the small reductions in REI produced by lengthening uORF1 by only one or two codons. Likewise, *a/tif32-Δ8* does not diminish the minimal level of REI that wild-type uORF4 (also three codons in length) allows despite lacking stimulatory sequences of uORF1 (Fig. 4G). These results make it unlikely that *a/tif32-Δ8* reduces REI by decreasing eIF3 association with elongating ribosomes during translation of wild-type, three-codon uORF1. Presumably, the effect of *a/tif32-Δ8* in weakening eIF3 binding to the 40S is not great enough to significantly reduce eIF3 occupancy on elongating ribosomes until they have translated more than five codons, as with the elongated versions of uORF1. Hence, we conclude that *a/tif32-Δ8* interferes with a step in REI after termination at the stop codon of wild-type uORF1.

It was shown previously that sequences located upstream of uORF1, and also the last codon and sequences immediately 3′ to the uORF1 stop codon, stimulate REI. The absence of such sequences at uORF4 (Supplemental Fig. 3) contributes to the much lower REI frequency of uORF4 versus uORF1. The fact that *a/tif32-Δ8* has no effect on the low level of REI after uORF4 translation indicates that *a/tif32-Δ8* neutralizes one or more of the features of uORF1 that confer a high REI potential and are absent at uORF4. Importantly, we detected a genetic interaction between *a/tif32-Δ8* and mutations in sequences 5′ of uORF1, wherein the deleterious effect of *a/tif32-Δ8* on REI is blunted or even eliminated by mutations upstream of uORF1 (Fig. 4). These epistatic interactions strongly suggest that the eIF3a-NTD promotes REI by mediating the stimulatory function of the 5′ sequences of uORF1, which we thus refer to as the eIF3a-NTD-responsive site (eIF3a-RS).

We also presented genetic data supporting the idea that the eIF3a-RS of uORF1 must be located at a specific distance upstream of the uORF1 stop codon (Fig. 5). This finding strongly suggests that the efficiency of REI conferred by the eIF3a-RS strictly depends on its proper positioning relative to the 40S mRNA exit channel. Our previous observation that the eIF3a-NTD interacts directly with RPS0A, and the fact that RPS0A occurs near the 40S mRNA exit channel (Spahn et al. 2001), lead us to propose that the eIF3a-NTD binds directly to the stimulatory eIF3a-RS, present at uORF1 but lacking at uORF4, on the solvent side of the 40S when the ribosome is positioned at the uORF1 stop codon (Fig. 6, E vs. F). This interaction would help stabilize association of the 40S subunit with mRNA following dissociation of the 60S subunit in the first stage of the ribosome recycling reaction (Pisarev et al. 2007) and thereby promote efficient resumption of scanning and REI downstream from uORF1 (Fig. 6, G vs. H).

Why is this mechanism so sensitive to the proper placement of the eIF3a-RS? Perhaps the eIF3a-NTD binds to a special mRNA structure whose proper assembly and orientation is critical because the eIF3a-NTD attachment with the 40S is not flexible enough to accommodate even minor alterations. Thus far, we were unable to detect direct binding between purified eIF3a-NTD and the sequences 5′ of uORF1 using conventional UV-cross-linking assays. However, it seems reasonable to suppose that this interaction would be stabilized by simultaneous binding of eIF3 to the back side of the 40S and of mRNA to the mRNA-binding cleft of the 40S (Fig. 6E), making it impossible to detect with eIF3a and mRNA alone. Moreover, the proposed interaction should not be so strong as to impede the rapid resumption of scanning by the post-termination 40S·eIF3 complex.

Alternatively, it is conceivable that eIF3 bound to the post-termination 40S subunit recruits another factor that interacts with the sequences 5′ of uORF1 and possibly even with the eIF3a-NTD itself. Weakening this interaction by *a/tif32-Δ8* that also impairs 40S binding of eIF3 would reduce the recruitment of this hypothetical factor and still diminish the effect on REI of mutating these sequences, as we observed. Interestingly, it was reported that eIF4G/eIF4A must be involved in translating a short uORF to observe efficient REI at a downstream ORF in rabbit reticulocyte lysates (Pöyry et al. 2004). Since eIF3 mediates interaction of eIF4G with the 40S in mammals (Korneeva et al. 2000), eIF3 attachment to the back side of the 40S could allow eIF4G to remain bound temporarily to the ribosome during elongation of a short uORF. As eIF4G has mRNA-binding activity (Lomakin et al. 2000), it could help stabilize the binding of post-termination 40S subunits to the mRNA, as proposed for eIF3; however, eIF4G could also facilitate scanning to the downstream start codon based on its role in ribosomal scanning (Pestova and Kolupaeva 2002). It is true that a direct eIF3–eIF4G interaction has not been observed in yeast; however, this does not exclude a possibility that it occurs only in the ribosomal context, and the hypothetical involvement of eIF4G in translational control of *GCN4* expression has never been systematically investigated.

Our finding that eIF3 is critical for resumption of scanning by post-termination ribosomes and our identification of the eIF3a-RS upstream of the uORF1 stop codon that promotes REI resonate with recent findings on the mechanism of REI after translation of a long ORF. Only recently, Jackson and colleagues (Pöyry et al. 2007) identified eIF3 as a key factor required for REI after translation of a long ORF2 that overlaps the beginning of a downstream ORF3 on polycistronic subgenomic mRNA of feline calicivirus. They found that REI is enhanced by an 87-nt element at the 3′ end of ORF2 that functions at least partly as a binding site for eIF3 (Pöyry et al. 2007). Considering that eIF3 has been implicated in releasing eukaryotic ribosomes from the mRNA after termination of translation at stop codons (Pisarev et al. 2007), it was suggested that the resulting post-termination eIF3/40S complexes at the ORF2 stop codon do not dissociate from the mRNA, but instead get transferred to the 87-nt element by virtue of the eIF3-mRNA contact. This interaction would stabilize mRNA-40S binding and also position the AUG codon of ORF3 in the ribosomal P-site for efficient REI (Pöyry et al. 2007). This mechanism dif-

fers considerably from the canonical REI after a short uORF studied here in that (1) ORF2 is too long to retain eIF3 during translation; (2) eIF3 must be acquired de novo; and (3) there appears to be no scanning after termination of ORF2 before REI at ORF3. Nevertheless, it resembles the model we propose for *GCN4* uORF1 by involving a *cis*-acting enhancer of REI located upstream of the stop codon of the first ORF, which interacts with eIF3 to prevent dissociation of post-termination 40S subunits and stimulate REI.

The fact that translation in general is a rather conserved process in both lower and higher eukaryotes may suggest that our yeast model of REI illustrated in Figure 6 also applies to mammals. However, there are certain aspects by which yeast and mammals differ that ought to be mentioned here: (1) meIF3 contains seven subunits in addition to the yeast six that are conserved (Hinnebusch 2006). Moreover, meIF3a has an extended C terminus compared with its yeast counterpart, though, interestingly, the N termini show the highest degree of similarity. (2) Yeast ribosomes are less sensitive to the start codon context and more sensitive to inhibition by secondary structures (Kozak 2005). (3) REI efficiency in mammalian systems seems to fall off less drastically as the uORF is lengthened in the three to 13 codon range than in yeast (Fig. 5; Kozak 2001). This last fact might indicate that the interaction between eIF3 and the 40S subunit in mammals is stronger and persists longer after initiation at a short uORF, presumably owing to additional contacts that the seven extra mammalian subunits make with the 40S. (4) To our knowledge, there is virtually no information regarding the importance of 5′ and 3′ sequences flanking short uORFs for REI in mammals. Our attempt to compare sequences 5′ of uORF1 of yeast *GCN4* and mammalian *ATF4* and *ATF5* mRNAs, respectively, also did not yield evidence suggesting that the nature of the uORF1-specific post-termination 40S retention on the latter mammalian mRNAs is mechanistically similar to that described for *GCN4*. Thus, whereas it seems fair to propose that at least the basic principles drawn in Figure 6 are shared between the yeast and mammals, the REI mechanism in both systems will likely differ in numerous details.

Our conclusion that eIF3 allows post-termination 40S subunits to remain attached to the mRNA and resume scanning after translation of uORF1 seems at odds with the function of eIF3 in dissociating post-termination ribosomes identified by Pestova and colleagues in a reconstituted system (Pisarev et al. 2007). Moreover, if eIF3 is recruited to all post-termination 80S subunits to participate in ribosome recycling, then why isn't REI efficient after translation of any ORF, regardless of length? Assuming that eIF3 functions in ribosome recycling in vivo, it could be proposed that eIF3 that is acquired de novo from the cytoplasmic pool by post-termination 80S ribosomes at long ORFs differs functionally from eIF3 that is transferred from initiation complexes to elongating ribosomes during translation of a short uORF. In particular, the j-subunit of eIF3 and mRNA are mutually antagonistic for binding to 40S subunits (Unbehaun et al. 2004; Fraser et al. 2007), which might indicate that eIF3j dissociates from eIF3 prior to subunit joining (Fig. 6B). Moreover, eIF3j was shown to promote release of post-termination eIF3·40S complexes from mRNA in the last step of ribosome recycling (Pisarev et al. 2007). Hence, if the eIF3 transferred from the initiation complex to translating ribosomes lacks eIF3j, it would be defective for the last step of ribosome recycling. The persistence of this eIF3j-depleted eIF3 on 80S ribosomes terminating at uORF1 could still promote the eIF3-dependent release of the 60S subunit from the post-termination 80S ribosome (Pisarev et al. 2007), but not dissociation of the 40S from mRNA. Instead, it would stabilize the 40S·mRNA complex (by virtue of eIF3's interaction with eIF3a-RS of uORF1) and promote scanning and reassembly of the 48S PIC for REI downstream.

Materials and methods

Yeast strains and plasmids

Lists of strains and plasmids used in this study and details of their construction can be found in the Supplemental Material.

Biochemical methods

Polysome profile analysis, 1% HCHO-cross-linking, WCE preparation, and fractionation of extracts for analysis of preinitiation complexes were carried out as described by Valášek et al. (2007). β-galactosidase assays were conducted as described previously (Grant and Hinnebusch 1994).

Acknowledgments

We are thankful to Libor Krásný for critical reading of the manuscript, to the members of the Valášek and Krásný laboratories for helpful suggestions, and to Olga Krýdová, Anna Delijannisová, and Ilona Krupičková for technical and administrative assistance. This research was supported for the most part by The Wellcome Trusts Grant 076456/Z/05/Z, and partly also by the Howard Hughes Medical Institute, by NIH Research Grant R01 TW007271 funded by the Fogarty International Center, by the Fellowship of Jan E. Purkyne from the Academy of Sciences of the Czech Republic, by the Institute Research Concept AV0Z50200510, and by the Intramural Research Program of the National Institutes of Health.

References

Algire, M.A., Maag, D., and Lorsch, J.R. 2005. Pi release from eIF2, not GTP hydrolysis, is the step controlled by start-site selection during eukaryotic translation initiation. *Mol. Cell* **20:** 251–262.

Cheung, Y.N., Maag, D., Mitchell, S.F., Fekete, C.A., Algire, M.A., Takacs, J.E., Shirokikh, N., Pestova, T., Lorsch, J.R., and Hinnebusch, A.G. 2007. Dissociation of eIF1 from the 40S ribosomal subunit is a key step in start codon selection in vivo. *Genes & Dev.* **21:** 1217–1230.

ElAntak, L., Tzakos, A.G., Locker, N., and Lukavsky, P.J. 2007. Structure of eIF3b RNA recognition motif and its interaction with eIF3j: Structural insights into the recruitment of eIF3b to the 40 S ribosomal subunit. *J. Biol. Chem.* **282:** 8165–8174.

Fraser, C.S., Berry, K.E., Hershey, J.W., and Doudna, J.A. 2007. 3j is located in the decoding center of the human 40S ribosomal

subunit. *Mol. Cell* **26:** 811–819.
Grant, C.M. and Hinnebusch, A.G. 1994. Effect of sequence context at stop codons on efficiency of reinitiation in *GCN4* translational control. *Mol. Cell. Biol.* **14:** 606–618.
Grant, C.M., Miller, P.F., and Hinnebusch, A.G. 1995. Sequences 5′ of the first upstream open reading frame in *GCN4* mRNA are required for efficient translational reinitiation. *Nucleic Acids Res.* **23:** 3980–3988.
Hinnebusch, A.G. 2005. Translational regulation of GCN4 and the general amino acid control of yeast. *Annu. Rev. Microbiol.* **59:** 407–450.
Hinnebusch, A.G. 2006. eIF3: A versatile scaffold for translation initiation complexes. *Trends Biochem. Sci.* **31:** 553–562.
Jivotovskaya, A., Valášek, L., Hinnebusch, A.G., and Nielsen, K.H. 2006. Eukaryotic translation initiation factor 3 (eIF3) and eIF2 can promote mRNA binding to 40S subunits independently of eIF4G in yeast. *Mol. Cell. Biol.* **26:** 1355–1372.
Kolupaeva, V.G., Unbehaun, A., Lomakin, I.B., Hellen, C.U., and Pestova, T.V. 2005. Binding of eukaryotic initiation factor 3 to ribosomal 40S subunits and its role in ribosomal dissociation and anti-association. *RNA* **11:** 470–486.
Korneeva, N.L., Lamphear, B.J., Hennigan, F.L., and Rhoads, R.E. 2000. Mutually cooperative binding of eukaryotic translation initiation factor (eIF) 3 and eIF4A to human eIF4G-1. *J. Biol. Chem.* **275:** 41369–41376.
Kozak, M. 2001. Constraints on reinitiation of translation in mammals. *Nucleic Acids Res.* **29:** 5226–5232.
Kozak, M. 2005. Regulation of translation via mRNA structure in prokaryotes and eukaryotes. *Gene* **361:** 13–37.
Lomakin, I.B., Hellen, C.U., and Pestova, T.V. 2000. Physical association of eukaryotic initiation factor 4G (eIF4G) with eIF4A strongly enhances binding of eIF4G to the internal ribosomal entry site of encephalomyocarditis virus and is required for internal initiation of translation. *Mol. Cell. Biol.* **20:** 6019–6029.
Marintchev, A. and Wagner, G. 2005. Translation initiation: Structures, mechanisms and evolution. *Q. Rev. Biophys.* **37:** 197–284.
Miller, P.F. and Hinnebusch, A.G. 1989. Sequences that surround the stop codons of upstream open reading frames in *GCN4* mRNA determine their distinct functions in translational control. *Genes & Dev.* **3:** 1217–1225.
Nielsen, K.H., Szamecz, B., Valášek, L.J., Shin, B.S., and Hinnebusch, A.G. 2004. Functions of eIF3 downstream of 48S assembly impact AUG recognition and GCN4 translational control. *EMBO J.* **23:** 1166–1177.
Nielsen, K.H., Valášek, L., Sykes, C., Jivotovskaya, A., and Hinnebusch, A.G. 2006. Interaction of the RNP1 motif in PRT1 with HCR1 promotes 40S binding of eukaryotic initiation factor 3 in yeast. *Mol. Cell. Biol.* **26:** 2984–2998.
Pestova, T.V. and Kolupaeva, V.G. 2002. The roles of individual eukaryotic translation initiation factors in ribosomal scanning and initiation codon selection. *Genes & Dev.* **16:** 2906–2922.
Pestova, T.V., Lomakin, I.B., Lee, J.H., Choi, S.K., Dever, T.E., and Hellen, C.U.T. 2000. The joining of ribosomal subunits in eukaryotes requires eIF5B. *Nature* **403:** 332–335.
Pisarev, A.V., Hellen, C.U.T., and Pestova, T.V. 2007. Recycling of eukaryotic posttermination ribosomal complexes. *Cell* **131:** 286–299.
Pisarev, A.V., Kolupaeva, V.G., Yusupov, M.M., Hellen, C.U.T., and Pestova, T.V. 2008. Ribosomal position and contacts of mRNA in eukaryotic translation initiation complexes. *EMBO J.* **27:** 1609–1621.
Pöyry, T.A., Kaminski, A., and Jackson, R.J. 2004. What determines whether mammalian ribosomes resume scanning after translation of a short upstream open reading frame? *Genes & Dev.* **18:** 62–75.
Pöyry, T.A., Kaminski, A., Connell, E.J., Fraser, C.S., and Jackson, R.J. 2007. The mechanism of an exceptional case of reinitiation after translation of a long ORF reveals why such events do not generally occur in mammalian mRNA translation. *Genes & Dev.* **21:** 3149–3162.
Rajkowitsch, L., Vilela, C., Berthelot, K., Ramirez, C.V., and McCarthy, J.E. 2004. Reinitiation and recycling are distinct processes occurring downstream of translation termination in yeast. *J. Mol. Biol.* **335:** 71–85.
Siridechadilok, B., Fraser, C.S., Hall, R.J., Doudna, J.A., and Nogales, E. 2005. Structural roles for human translation factor eIF3 in initiation of protein synthesis. *Science* **310:** 1513–1515.
Spahn, C.M., Beckmann, R., Eswar, N., Penczek, P.A., Sali, A., Blobel, G., and Frank, J. 2001. Structure of the 80S ribosome from *Saccharomyces cerevisiae*—tRNA–ribosome and subunit–subunit interactions. *Cell* **107:** 373–386.
Srivastava, S., Verschoor, A., and Frank, J. 1992. Eukaryotic initiation factor 3 does not prevent association through physical blockage of the ribosomal subunit–subunit interface. *J. Mol. Biol.* **220:** 301–304.
Unbehaun, A., Borukhov, S.I., Hellen, C.U., and Pestova, T.V. 2004. Release of initiation factors from 48S complexes during ribosomal subunit joining and the link between establishment of codon–anticodon base-pairing and hydrolysis of eIF2-bound GTP. *Genes & Dev.* **18:** 3078–3093.
Valášek, L., Phan, L., Schoenfeld, L.W., Valášková, V., and Hinnebusch, A.G. 2001. Related eIF3 subunits TIF32 and HCR1 interact with an RNA recoginition motif in PRT1 required for eIF3 integrity and ribosome binding. *EMBO J.* **20:** 891–904.
Valášek, L., Nielsen, K.H., and Hinnebusch, A.G. 2002. Direct eIF2–eIF3 contact in the multifactor complex is important for translation initiation in vivo. *EMBO J.* **21:** 5886–5898.
Valášek, L., Mathew, A., Shin, B.S., Nielsen, K.H., Szamecz, B., and Hinnebusch, A.G. 2003. The yeast eIF3 subunits TIF32/a and NIP1/c and eIF5 make critical connections with the 40S ribosome in vivo. *Genes & Dev.* **17:** 786–799.
Valášek, L., Nielsen, K.H., Zhang, F., Fekete, C.A., and Hinnebusch, A.G. 2004. Interactions of eukaryotic translation initiation factor 3 (eIF3) subunit NIP1/c with eIF1 and eIF5 promote preinitiation complex assembly and regulate start codon selection. *Mol. Cell. Biol.* **24:** 9437–9455.
Valášek, L., Szamecz, B., Hinnebusch, A.G., and Nielsen, K.H. 2007. In vivo stabilization of preinitiation complexes by formaldehyde cross-linking. *Methods Enzymol.* **429:** 163–183.
Vattem, K.M. and Wek, R.C. 2004. Reinitiation involving upstream ORFs regulates ATF4 mRNA translation in mammalian cells. *Proc. Natl. Acad. Sci.* **101:** 11269–11274.
Vilela, C., Linz, B., Rodrigues-Pousada, C., and McCarthy, J.E. 1998. The yeast transcription factor genes YAP1 and YAP2 are subject to differential control at the levels of both translation and mRNA stability. *Nucleic Acids Res.* **26:** 1150–1159.
Wang, Z. and Sachs, M. 1997. Ribosome stalling is responsible for arginine-specific translational attenuation in *Neurospora crassa*. *Mol. Cell. Biol.* **17:** 4904–4913.
Yamamoto, Y., Singh, C.R., Marintchev, A., Hall, N.S., Hannig, E.M., Wagner, G., and Asano, K. 2005. The eukaryotic initiation factor (eIF) 5 HEAT domain mediates multifactor assembly and scanning with distinct interfaces to eIF1, eIF2, eIF3, and eIF4G. *Proc. Natl. Acad. Sci.* **102:** 16164–16169.
Zhou, D., Pallam, L.R., Jiang, L., Narasimhan, J., Staschke, K.A., and Wek, R.C. 2008. Phosphorylation of eIF2 directs ATF5 translational control in response to diverse stress conditions. *J. Biol. Chem.* **283:** 7064–7073.

SUPPLEMENTAL MATERIAL

Construction of yeast strains and plasmids

YAH01 was constructed by disrupting the *LEU2* cassette of YLV041 (Valášek 1998) according to the following steps: YLV041, pre-transformed with YCpeIF3a-His-U (Valášek et al. 2003), was introduced with the *leu2::KanMX3* disruption cassette M3926 (Voth et al. 2003) digested with *Bam*HI, and Geneticin G418 resistant colonies were selected on YPD media containing G418. The disruption of the *LEU2* cassette was confirmed by growth on media with and without leucine. Finally, YCpeIF3a-His-U was evicted by growth on 5-FOA media.

To create del'32a9A, H2881-2n (Nielsen et al. 2004) was transformed with the *Eco*RI-*Sac*I 5.6-kb fragment from the *a/tif32*Δ*::hisG-URA3-hisG* pΔeIF3a#4 cassette to delete one chromosomal copy of *a/TIF32*. Uracil auxotrophy was regained by growing the cells on 5-FOA plates. The resulting strain was transformed with YCpeIF3a-His-U carrying wild-type *a/TIF32* and subsequently subjected to tetrad dissection to produce del'32a9A.

To make YBS47, del'32a9A was first transformed with pRSeIF3a-His-L (Valášek et al. 2002) and YCpeIF3a-His-U was evicted by growth on 5-FOA medium. The resulting strain was transformed to Ura^+ with the integrative *GCN2* plasmid pHQ835 (kindly provided by Hongfang Qiu) digested with *Sna*BI. Ura^- segregants were obtained by selecting for growth on medium containing 5-FOA, and the resulting YBS47 was tested for the presence of integrated *GCN2* by testing growth on medium containing 3-aminotriazole (3-AT).

To construct YBS53, YBS47 was transformed with YCpeIF3a-His-U (Valášek et al. 2003) and grown in SD medium supplemented with excess of leucine to enable a spontaneous loss of pRSeIF3a-His-L. The resulting strain, auxotrophic for leucine, was subsequently transformed with pRSeIF3a-Δ8-His-L (Valášek et al. 2002) and YCpeIF3a-His-U was evicted by growth on 5-FOA medium.

pRSeIF3a-Δ7-His was constructed by inserting the *Nde*I-*Sac*I 1.86-kb fragment from YEpeIF3a-His (Valášek et al. 2002) into pRSeIF3a-Δ115-His (Valášek et al. 2002) digested with *Nde*I-*Sac*I.

pRSeIF3a-Δ8-Box6-His-L was made by inserting the 1.08 kb *Nde*I-*Xba*I fragment from pRSeIF3a-Box6-His-L (LB, LV, AGH, unpublished observation) into *Nde*I-*Xba*I digested pRSeIF3a-Δ8-His-L (Valášek et al. 2002) .

To construct pBS62 the following two pairs of primers were used with pM128 (Grant and Hinnebusch 1994) as a template: (i) BS_GCN4_SalI / BS_d40AA_rev and (ii) BS_URF1 / BS_GCN4ORF_rev. The PCR products thus obtained were used in a 1:1 ratio as templates for a third PCR amplification with primers BS_GCN4_SalI and BS_GCN4ORF_rev. The resulting PCR products were digested with *Sal*I and *Bst*EII and ligated with *Sal*I-*Bst*EII cleaved pM128. pBS64 was constructed essentially as described for pBS62 except that the oligonucleotide BS_AAtoCCCCGG_rev was used instead of BS_d40AA_rev. pBS63 was made essentially as described for pBS62 except that the oligonucleotide BS_d160AA_rev was used instead of BS_d140AA_rev .

To create pVM11 the following two pairs of primers were used with pM128 (Grant and Hinnebusch 1994) as a template: BS_GCN4_SalI / VM_61up and VM_15down /

BS_GCN4ORF_rev. The PCR products thus obtained were used in a 1:1 ratio as templates for a third PCR amplification with primers BS_GCN4_SalI and BS_GCN4ORF_rev. The resulting PCR products were digested with *Sal*I and *Bst*EII and ligated with *Sal*I-*Bst*EII cleaved pM128.

pBS71 was constructed in two steps. First, annealed BS_URF1MAAC and BS_URF1MAAC_rev oligonucleotides were ligated into *Hind*III and *Bgl*II digested pM23 (Miller and Hinnebusch 1989). In the second step removing uORF4, the 3.45 kb *Eco*RI fragment was swapped with the *Eco*RI fragment of pM128 (Grant and Hinnebusch 1994) of the same size. pBS72, pBS73, pBS74, pBS75, pBS77 and pBS94, respecitvely, were made essentially as described for pBS71 except that the following pairs of oligonucleotides were used: BS_URF1MAAAC / BS_URF1MAAAC_rev, BS_URF1M6AC / BS_URF1M6AC-rev, BS_URF1M10AC / BS_URF1M10AC-rev, BS_MAAAC_linkerDEL / BS_MAAAC_linkerDEL_rev, BS_MAAAC_linkerEXT / BS_MAAAC_linkerEXT_rev and BS_MAAAAC_linkerDEL9 / BS_MAAAAC_linkerDEL9-rev, respectively.

Northern blot analysis

Northern blot analysis was conducted essentially as described by (Sambrook and Russell 2001) with the following exceptions. Whatman downward capillary transfer procedure was used according to the vendor's instructions and RNA samples for the Northern blotting were separated as in (Masek et al. 2005). A *Bam*HI fragment (~ 3-Kbp) from B180 carrying *GCN4-lacZ* and a 384-bp long PCR product of *ACT1* (exon 2) amplified using genomic DNA isolated from H2880, respectively, were labeled using random hexanucleotides.

References

Abastado, J.P., Miller, P.F., Jackson, B.M., and Hinnebusch, A.G. 1991. Suppression of ribosomal reinitiation at upstream open reading frames in amino acid-starved cells forms the basis for *GCN4* translational control. *Mol Cell Biol* **11**: 486-496.

Grant, C.M. and Hinnebusch, A.G. 1994. Effect of sequence context at stop codons on efficiency of reinitiation in *GCN4* translational control. *Mol Cell Biol* **14**: 606-618.

Grant, C.M., Miller, P.F., and Hinnebusch, A.G. 1994. Requirements for intercistronic distance and level of eIF-2 activity in reinitiation on GCN4 mRNA varies with the downstream cistron. *Mol Cell Biol* **14**: 2616-2628.

Hinnebusch, A.G. 1984. Evidence for translational regulation of the activator of general amino acid control in yeast. *Proc Natl Acad Sci USA* **81**: 6442-6446.

Masek, T., Vopalensky, V., Suchomelova, P., and Pospisek, M. 2005. Denaturing RNA electrophoresis in TAE agarose gels. *Anal Biochem* **336**: 46-50.

Miller, P.F. and Hinnebusch, A.G. 1989. Sequences that surround the stop codons of upstream open reading frames in *GCN4* mRNA determine their distinct functions in translational control. *Genes and Development* **3**: 1217-1225.

Mueller, P.P. and Hinnebusch, A.G. 1986. Multiple upstream AUG codons mediate translational control of *GCN4*. *Cell* **45**: 201-207.

Nielsen, K.H., Szamecz, B., Valasek, L.J., A., Shin, B.S., and Hinnebusch, A.G. 2004. Functions of eIF3 downstream of 48S assembly impact AUG recognition and GCN4 translational control. *EMBO J* **23**: 1166-1177.

Sambrook, J. and Russell, D.W. 2001. *Molecular Cloning, a Laboratory Manual*. Cold Spring Harbor Laboratory, Cold Spring Harbor, NY.

Sikorski, R.S. and Hieter, P. 1989. A system of shuttle vectors and yeast host strains designed for efficient manipulation of DNA in *Saccharomyces cerevisiae*. *Genetics* **122**: 19-27.

Valášek, L. 1998. Characterization of RPG1, the large subunit of the yeast *S. cerevisiae* initiation translation factor 3 (eIF3). *Ph D Thesis*: University of Vienna, Austria.

Valášek, L., Mathew, A., Shin, B.S., Nielsen, K.H., Szamecz, B., and Hinnebusch, A.G. 2003. The Yeast eIF3 Subunits TIF32/a and NIP1/c and eIF5 Make Critical Connections with the 40S Ribosome in vivo. *Genes & Dev* **17**: 786-799.

Valášek, L., Nielsen, K.H., and Hinnebusch, A.G. 2002. Direct eIF2-eIF3 contact in the multifactor complex is important for translation initiation in vivo. *EMBO J* **21**: 5886-5898.

Voth, W.P., Jiang, Y.W., and Stillman, D.J. 2003. New 'marker swap' plasmids for converting selectable markers on budding yeast gene disruptions and plasmids. *Yeast* **20**: 985-993.

Supplemental Table I. Yeast strains used in this study.

Strain	Genotype	Source or reference
YAH01	*MAT*a *ura3::MET3-a/TIF32 ura3 rpg1-del1::leu2::KanMX4 ade2-1 trp1-1 can1-100 leu2-112 his3-11 his3-15*	This study
del'32a9A [a]	*MAT*a *leu2-3, -112 ura3-52 trp1Δ gcn2Δ a/tif32Δ (a/TIF32, URA3)*	This study
YBS47[a]	*MAT*a *leu2-3, -112 ura3-52 trp1Δ gcn2Δ a/tif32Δ URA3::GCN2 ura3* (pRSeIF3a-HIS-L)	This study
YBS53 [a]	*MAT*a *leu2-3, -112 ura3-52 trp1Δ gcn2Δ a/tif32Δ URA3::GCN2 ura3* (pRSeIF3a-Δ8-HIS-L)	This study
H2880[a]	*MAT*a *trp1Δ leu2-3,112 ura3-52*	(Nielsen et al. 2004)
H2881[a]	*MAT*a *trp1Δ leu2-3,112 ura3-52 gcn2::hisG*	(Nielsen et al. 2004)

[a] Isogenic strains.

Supplemental Table II. Plasmids used in this study.

Plasmid	Description	Source of reference
pRS315	Low-copy cloning vector, LEU2	(Sikorski and Hieter 1989)
pRSeIF3a-His-L	Low-copy *a/TIF32-His*, *LEU2* plasmid from pRS315	(Valášek et al. 2002)
pRSeIF3a-Δ8-His-L	Low-copy *a/tif32-Δ8-His* [200-964] , *LEU2* plasmid from pRS315	(Valášek et al. 2002)
pRSeIF3a-Δ7-His-L	Low-copy *a/tif32-Δ7-His* [350-964] , *LEU2* plasmid from pRS315	This study
peIF3a-Δ8-Box6-His-L	Low-copy *a/tif32-Δ8-Box6-His* [200-964] containing 10 Ala substitutions in Box6 [692 – 701] , *LEU2* plasmid from pRS315	This study
p180 (YCp50–GCN4–lacZ)	Low copy *URA3* vector containing wild-type *GCN4* leader	(Mueller and Hinnebusch 1986)
P227	Low copy *URA3* vector containing *GCN4* leader without uORFs.	(Miller and Hinnebusch 1989)
pM226	Derivative of pM199; ORF of uORF1 extends into the *GCN4-lacZ* coding region	(Grant et al. 1994)

pG67	Low copy *URA3* vector containing uORF1 only placed 32 nt from *GCN4-lacZ*	(Grant et al. 1994)
pM199	Low copy *URA3* vector containing uORF1 only at the position of uORF4 (140 nt from *GCN4-lacZ*)	(Grant et al. 1994)
p209	Low copy *URA3* vector containing uORF1 only at its original position (350 nt from *GCN4-lacZ*)	(Grant et al. 1994)
pBS64	Derivative of pM128; Low copy *URA3* vector containing *GCN4* leader with uORF1 at its original position with the CCCCGG substitution of the -21 AAAATT -16 region in its 5' UTR	This study
pBS62	Derivative of pM128; Low copy *URA3* vector containing *GCN4* leader with uORF1 at its original position with 40 nt deletion in its 5' UTR (from -61 to -21)	This study
pVM11	Derivative of pM128; Low copy *URA3* vector containing *GCN4* leader with uORF1 at its original position with 46 deletion in its 5' UTR (from -61 to -15)	This study
pBS63	Derivative of pM128; Low copy *URA3* vector containing *GCN4* leader with uORF1 at its original position with 160 nt deletion in its 5' UTR (from -181 to -21)	This study
pA80z	Low copy *URA3* vector containing *GCN4* leader with solitary uORF4 at the position of uORF1	(Abastado et al. 1991)
pM128	Low copy *URA3* vector containing uORF1 only at its original position (350 nt from *GCN4-lacZ*)	(Grant and Hinnebusch 1994)
pBS71	Derivative of pM23, containing uORF1 only at its original position with a single Ala codon insertion	This study
pBS72	The same as pBS71, except that uORF1 contains 2 Ala codons insertion	This study
pBS73	The same as pBS71, except that uORF1 contains 5 Ala codons insertion	This study
pBS74	The same as pBS71, except that uORF1 contains 10 Ala codons insertion	This study
pBS75	Derivative of pBS72, except that a part of the region designated as linker from nt -9 to -4 is deleted in the 5' UTR of uORF1	This study

pBS77	Derivative of pM23, containing uORF1 only at its original position and a 6 nt insertion between nt -10 and -9 in the 5’ UTR region of uORF1 designated as linker	This study
pBS94	Derivative of pM23, containing uORF1 only at its original position with 3 Ala codons insertion and a part of the region designated as linker from nt -12 to -4 is deleted in the 5’ UTR of uORF1	This study

Supplemental Table III. Oligonucleotides used in this study.

Oligonucleotide	**Sequence (5' to 3')**
BS_GCN4_SalI	TCGGTCGACGGGGAATAAAG
BS_d40AA_rev	CAAGCCATTTTTCAATGATCTTTAATTTTATAAAATATTTTGTTTTGATTGCGAAGTAG
VM_61up	CAAGCCATTTTTCAATGATCTTTATAAAATATTTTGTTTTGATTGCG
VM_15down	AAAGATCATTGAAAAATGGCTTG
BS_d160AA_rev	CAAGCCATTTTTCAATGATCTTTAATTTTTGTTGTGAGTTTTTGTTTTG
BS_URF1	TTAAAGATCATTGAAAAATGGCTTG
BS_GCN4ORF_rev	GGCTGATATTCGGACA
BS_AAtoCCCCGG_rev	AGCAAGCCATTTTTCAATGATCTTTCCGGGGTTAATACGATACTGATAATAACTTAATAAACTG
BS_URF1MAAC	AGCTTAAAGATCATTGAAAAATGGCTGCTTGCTAAACCGATTATATTTTGTTTTTAAAGTA

BS_URF1MAAC_rev	GATCTACTTTAAAAACAAAATATAATCGGTTTAGCAAGCAGCCATTTTTCAATGATCTTTA
BS_URF1MAAAC	AGCTTAAAGATCATTGAAAAATGGCTGCTGCTTGCTAAACCGATTATATTTTGTTTTTAAAGTA
BS_URF1MAAAC_rev	GATCTACTTTAAAAACAAAATATAATCGGTTTAGCAAGCAGCAGCCATTTTTCAATGATCTTTA
BS_URF1M6AC	AGCTTAAAGATCATTGAAAAATGGCTGCTGCTGCTGCTGCTTGCTAAACCGATTATATTTTGTTT TTAAAGTA
BS_URF1M6AC-rev	GATCTACTTTAAAAACAAAATATAATCGGTTTAGCAAGCAGCAGCAGCAGCAGCAGCCATTTTTCAA TGATCTTTA
BS_URF1M10AC	AGCTTAAAGATCATTGAAAAATGGCTGCTGCTGCTGCTGCTGCTGCTGCTGCTTGCTAAACC GATTATATTTTGTTTTTAAAGTA
BS_URF1M10AC-rev	GATCTACTTTAAAAACAAAATATAATCGGTTTAGCAAGCAGCAGCAGCAGCAGCAGCAGCAGC AGCAGCCATTTTTCAATGATCTTTA
BS_MAAAC_linkerDEL	AGCTTAAAGATAAAATGGCTGCTGCTTGCTAAACCGATTATATTTTGTTTTTAAAGTA
BS_MAAAC_linkerDEL_rev	GATCTACTTTAAAAACAAAATATAATCGGTTTAGCAAGCAGCAGCCATTTTATCTTTA
BS_MAAAC_linkerEXT	AGCTTAAAGATCAACAACATTGAAAAATGGCTTGCTAAACCGATTATATTTTGTTTTTAAAGTA
BS_MAAAC_linkerEXT_rev	GATCTACTTTAAAAACAAAATATAATCGGTTTAGCAAGCCATTTTTCAATGTTGTTGATCTTTA
BS MAAAAC linkerDEL9	AGCTTAAAAAAATGGCTGCTGCTGCTTGCTAAACCGATTATATTTTGTTTTTAAAGTA
BS MAAAAC linkerDEL9-rev	GATCTACTTTAAAAACAAAATATAATCGGTTTAGCAAGCAGCAGCAGCCATTTTTTTA

Supplementary Figure 1. Levels of *GCN4-lacZ* mRNAs are similar between WT *a/TIF32* and *a/tif32-Δ8* cells. (A-C) Total RNA was prepared from *a/TIF32* (YBS47; odd lanes) and *a/tif32-Δ8* (YBS53; even lanes) cells expressing WT *GCN4-lacZ* (panel A, first two lanes) or various mutant versions indicated above the Northern blots that were used throughout the study. The same amount of each total RNA was separated by gel electrophoresis, transferred to Nytran SuPerCharge membranes and *GCN4-lacZ* transcripts were visualized by autoradiography using a radiolabeled probe complementary to the *lacZ* reporter gene (upper row). The same membranes were also probed with a radiolabeled actin probe to ensure characterization of similar amounts of RNA (lower row). Relative levels of *GCN4-lacZ* mRNAs in *a/tif32-Δ8* versus *a/TIF32* cells normalized to the *ACT1* signal are shown in the last row of each panel.

Supplementary Figure 2. Proper positioning of the eIF3a-NTD responsive site in the 5' of ORF1 relative to the 40S mRNA exit channel represents a critical requirement for efficient induction of *GCN4* expression by reinitiation. (A-D) Schematics as in Fig. 4A -D. (E-K) Same as in Fig. 3B, except the YBS47 (*a/TIF32*) strain transformed with pM23, pM23-MAAAC, pM23-linkerDEL6-MAAAC, pM23-linkerDEL6, pM23-linkerDEL7, and pM23-linkerDEL9, respectively, was analyzed after 3-AT treatment only.

Supplementary Figure 3. Comparison of sequences surrounding uORF1 and uORF4 of yeast *GCN4*. Numbering is according to (Miller and Hinnebusch 1989). Arrows represent transcription start sites based on (Hinnebusch 1984). uORF1 and uORF4 coding regions are shown in bold with the AUG start and TAA stop codons underlined or in italics, respectively. The last coding triplet of both uORFs, their stop codons and immediately following 6 nucleotides are boxed in grey. Boundaries of all deletions and substitutions in the 5' region of uORF1 tested in Fig. 4 are indicated above the sequences.

A

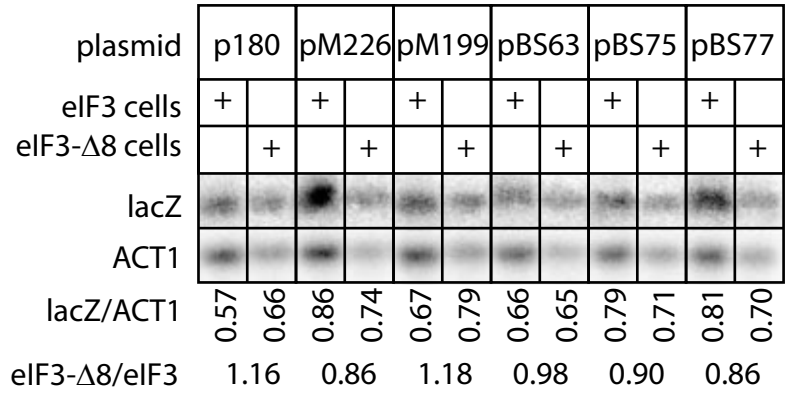
plasmid
p180
pM226
pM199
pBS63
pBS75
pBS77
eIF3 cells
eIF3-Δ8 cells
lacZ
ACT1
lacZ/ACT1
0.57 0.66 0.86 0.74 0.67 0.79 0.66 0.65 0.79 0.71 0.81 0.70
eIF3-Δ8/eIF3
1.16 0.86 1.18 0.98 0.90 0.86

B

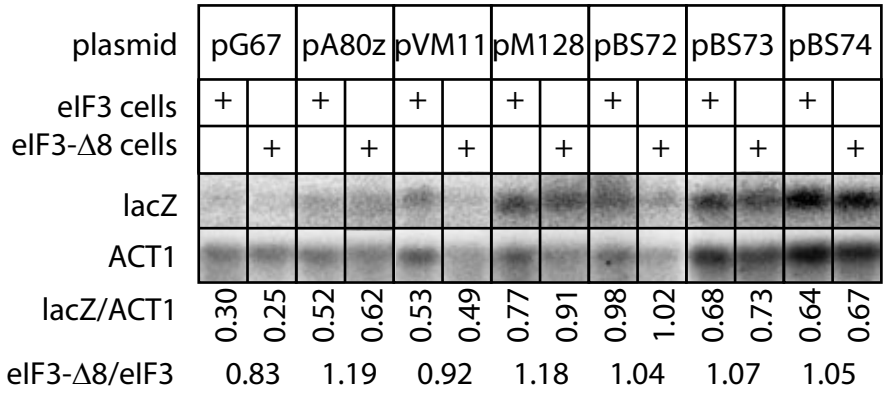
plasmid
pG67
pA80z
pVM11
pM128
pBS72
pBS73
pBS74
eIF3 cells
eIF3-Δ8 cells
lacZ
ACT1
lacZ/ACT1
0.30 0.25 0.52 0.62 0.53 0.49 0.77 0.91 0.98 1.02 0.68 0.73 0.64 0.67
eIF3-Δ8/eIF3
0.83 1.19 0.92 1.18 1.04 1.07 1.05

C

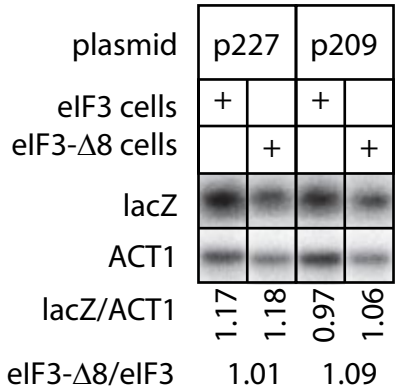
plasmid
p227
p209
eIF3 cells
eIF3-Δ8 cells
lacZ
ACT1
lacZ/ACT1
1.17 1.18 0.97 1.06
eIF3-Δ8/eIF3
1.01 1.09

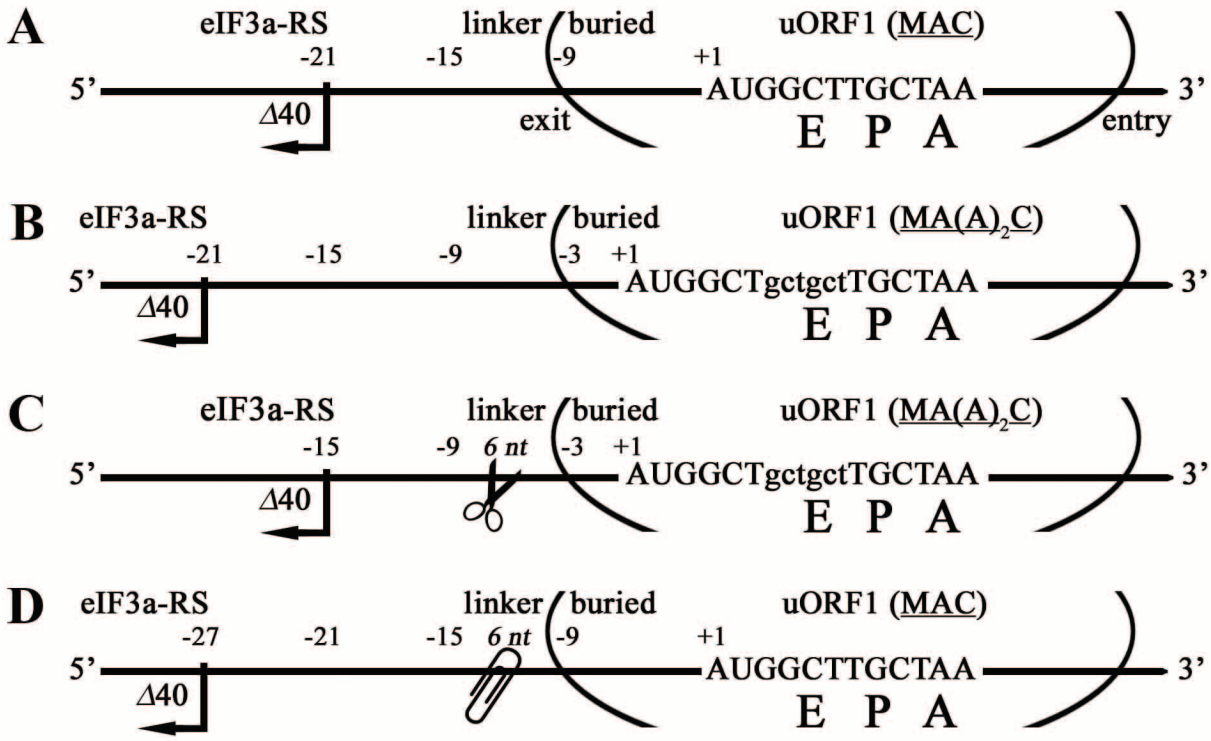

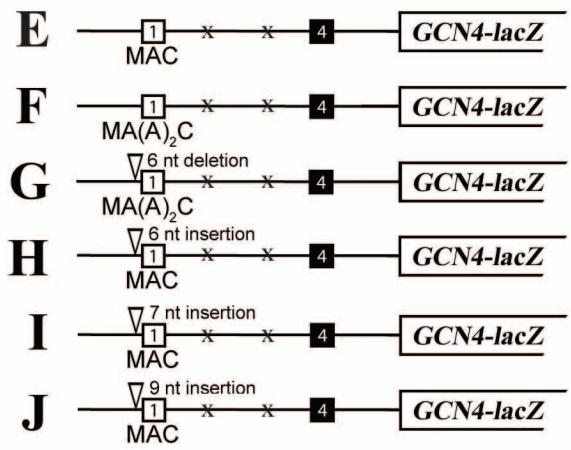

Activity relative to the WT construct	*mut. / WT*
	100±3%
	70±5%
	80±7%
	92±2%
	88±1%
	81±1%

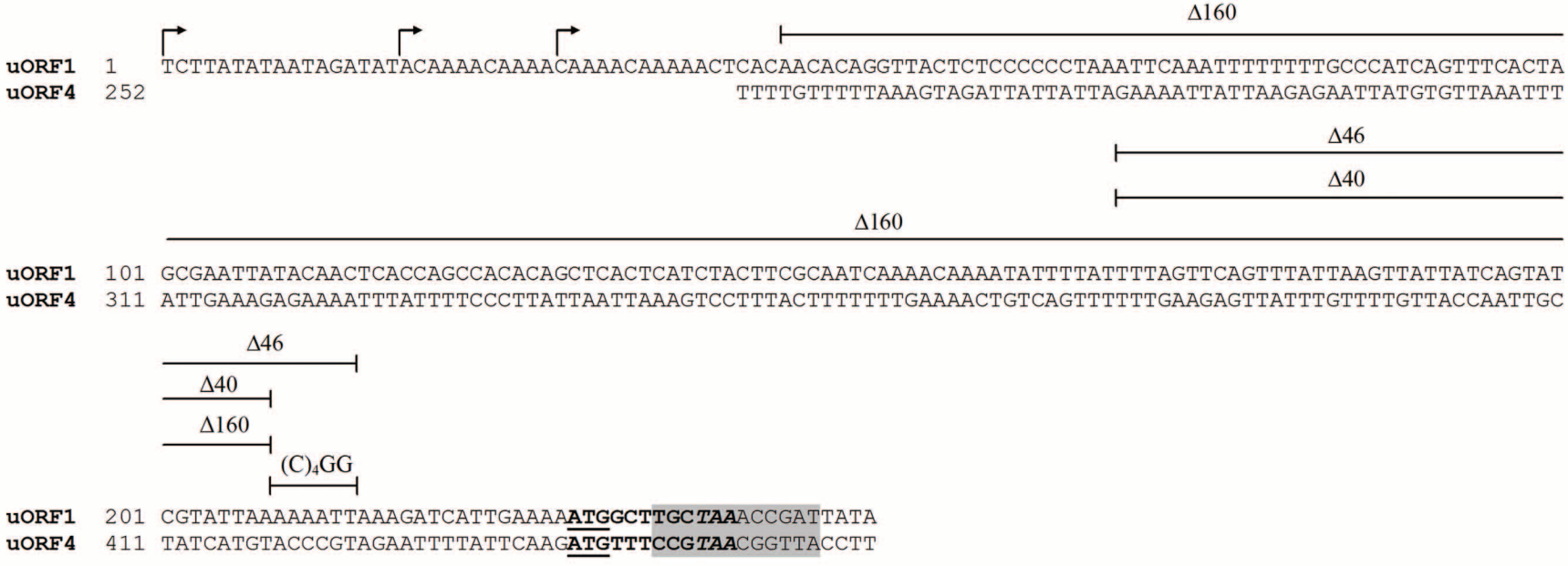
Δ160
uORF1 1 TCTTATATAATAGATATACAAAACAAAACAAAACAAAAACTCACAACACAGGTTACTCTCCCCCCTAAATTCAAATTTTTTTTGCCCATCAGTTTCACTA
uORF4 252 TTTTGTTTTTAAAGTAGATTATTATTAGAAAATTATTAAGAGAATTATGTGTTAAATTT
Δ46
Δ40
Δ160
uORF1 101 GCGAATTATACAACTCACCAGCCACACAGCTCACTCATCTACTTCGCAATCAAAACAAAATATTTTATTTTAGTTCAGTTTATTAAGTTATTATCAGTAT
uORF4 311 ATTGAAAGAGAAAATTTATTTTCCCTTATTAATTAAAGTCCTTTACTTTTTTTGAAAACTGTCAGTTTTTTGAAGAGTTATTTGTTTTGTTACCAATTGC
Δ46
Δ40
Δ160
(C)4GG
uORF1 201 CGTATTAAAAAATTAAAGATCATTGAAAAATGGCTTGCTAAACCGATTATA
uORF4 411 TATCATGTACCCGTAGAATTTTATTCAAGATGTTTCCGTAACGGTTACCTT

The RNA recognition motif of eukaryotic translation initiation factor 3g (eIF3g) is required for resumption of scanning of posttermination ribosomes for reinitiation on GCN4 and together with eIF3i stimulates linear scanning.

Cuchalová L, Kouba T, Herrmannová A, Dányi I, Chiu WL, Valásek L.

Mol Cell Biol. 2010 Oct;30(19):4671-86. doi: 10.1128/MCB.00430-10. Epub 2010 Aug 2.

This work describes functional analysis of two essential eIF3 subunits; i/TIF34 and g/TIF35, whose contributions to general translation initiation have been elusive until now. Here we showed that both subunits stimulate linear scanning and genetically interact with several scanning-promoting initiation factors.

Specific mutants of i/TIF34 and g/TIF35 were found to severely interfere with the translational control mechanism of *GCN4* that relies on reinitiation. Whereas the i/TIF34 mutant blocked upregulation of *GCN4* under starvation conditions owing to its general scanning defect, the g/TIF35 mutant specifically perturbed the reinitiation process by preventing the 40S ribosomes terminating at the first uORF1 to even resume scanning. A similar phenotype was previously associated with partial deletion of the RPS0A-binding site in the a/TIF32-NTD. Detailed genetic analysis revealed, however, that the g/Tif35 RRM and the a/Tif32 NTD ensure efficient resumption of scanning by different mechanisms.

Finally, we found specific interactions between g/TIF35 and ribosomal protein RPS3 and RPS20 suggesting that the g/TIF35–i/TIF34 mini-module of eIF3 occurs somewhere near the mRNA entry channel.

MOLECULAR AND CELLULAR BIOLOGY, Oct. 2010, p. 4671–4686 Vol. 30, No. 19
0270-7306/10/$12.00 doi:10.1128/MCB.00430-10

The RNA Recognition Motif of Eukaryotic Translation Initiation Factor 3g (eIF3g) Is Required for Resumption of Scanning of Posttermination Ribosomes for Reinitiation on *GCN4* and Together with eIF3i Stimulates Linear Scanning▽

Lucie Cuchalová,[1] Tomáš Kouba,[1] Anna Herrmannová,[1] István Dányi,[1] Wen-ling Chiu,[2] and Leoš Valášek[1]*

Laboratory of Regulation of Gene Expression, Institute of Microbiology AVCR, v.v.i., Prague, Czech Republic,[1] and Laboratory of Gene Regulation and Development, Eunice Kennedy Shriver National Institute of Child Health and Human Development, NIH, Bethesda, Maryland 20892[2]

Received 13 April 2010/Returned for modification 25 May 2010/Accepted 26 July 2010

Recent reports have begun unraveling the details of various roles of individual eukaryotic translation initiation factor 3 (eIF3) subunits in translation initiation. Here we describe functional characterization of two essential *Saccharomyces cerevisiae* eIF3 subunits, g/Tif35 and i/Tif34, previously suggested to be dispensable for formation of the 48S preinitiation complexes (PICs) *in vitro*. A triple-Ala substitution of conserved residues in the RRM of g/Tif35 (*g/tif35-KLF*) or a single-point mutation in the WD40 repeat 6 of i/Tif34 (*i/tif34-Q258R*) produces severe growth defects and decreases the rate of translation initiation *in vivo* without affecting the integrity of eIF3 and formation of the 43S PICs *in vivo*. Both mutations also diminish induction of *GCN4* expression, which occurs upon starvation via reinitiation. Whereas *g/tif35-KLF* impedes resumption of scanning for downstream reinitiation by 40S ribosomes terminating at upstream open reading frame 1 (uORF1) in the *GCN4* mRNA leader, *i/tif34-Q258R* prevents full *GCN4* derepression by impairing the rate of scanning of posttermination 40S ribosomes moving downstream from uORF1. In addition, *g/tif35-KLF* reduces processivity of scanning through stable secondary structures, and g/Tif35 specifically interacts with Rps3 and Rps20 located near the ribosomal mRNA entry channel. Together these results implicate g/Tif35 and i/Tif34 in stimulation of linear scanning and, specifically in the case of g/Tif35, also in proper regulation of the *GCN4* reinitiation mechanism.

The initiation phase of protein synthesis is promoted by numerous proteins or protein complexes called eukaryotic initiation factors (eIFs). The multiprotein eIF3 complex, together with eIFs 1, 1A, and 5, promotes recruitment of the Met-tRNA$_i^{Met}$/eIF2/GTP ternary complex (TC) to the small ribosomal subunit (40S), producing the 43S preinitiation complex (PIC). At least in yeast, eIFs 1, 3, and 5 and the TC occur in a preformed unit called the multifactor complex (MFC), which enhances the efficiency of the 43S PIC assembly process (reviewed in reference 20). The eIF4F complex, containing the cap-binding eIF4E and the scaffold protein eIF4G, then mediates recruitment of an mRNA to the 43S PIC with the help of eIF3 and the poly(A)-binding protein. The resulting 48S PIC traverses the 5′ untranslated region (UTR) of mRNA, searching usually for the first AUG codon while unwinding secondary structures in an ATP-dependent reaction stimulated by helicases eIF4A and eIF4B (reviewed in reference 39). This intricate process is called scanning, and its precise molecular mechanism is still poorly understood. It is known that the presence of the TC and eIFs 1, 1A, and 3 in reconstituted mammalian 43S PICs is sufficient for scanning through the unstructured leaders of model mRNAs (38). eIFs 1 and 1A are thought to promote scanning by induction of a conformational change of the 40S head. This change, characterized by opening the latch formed by helices 18 (h18) and 34 (h34) of 18S rRNA and establishing a new interaction between RPS3 and h16, stabilizes the small subunit in an open/scanning-conducive state (36). When the start codon is recognized by the anticodon of Met-tRNA$_i^{Met}$, the concerted action of eIFs 1, 1A, 2, and 5 stimulates a reverse conformational change of the 40S subunit that reforms the h18-h34 latch and arrests scanning (reviewed in reference 27). Upon subunit joining mediated by eIF5B, the 80S couple commences elongation.

Over the last decade, functions of several subunits of the most complex initiation factor, eIF3, and its complete subunit composition have been investigated in yeasts, plants, and mammals (reviewed in reference 17). In *Saccharomyces cerevisiae*, eIF3 comprises five core essential subunits (a/Tif32, b/Prt1, c/Nip1, i/Tif34, and g/Tif35) and one noncore subunit (j/Hcr1). These all have corresponding orthologs in the more complex mammalian eIF3, which contains seven additional nonconserved subunits. Despite recent progress, the true composition of the core of mammalian eIF3 remains somewhat obscure. One study aimed at reconstitution of a human eIF3 *in vitro* suggested that the functional core contains three nonconserved subunits, e, f, and h, in place of eIF3i and -g (25), whereas other work based on tandem mass spectrometry and solution disruption assays identified three stable modules, one of which,

* Corresponding author. Mailing address: Laboratory of Regulation of Gene Expression, Institute of Microbiology AVCR, v.v.i., Videnska 1083, Prague, Czech Republic. Phone: 420 241 062 288. Fax: 420 241 062 665. E-mail: valasekl@biomed.cas.cz.

▽ Published ahead of print on 2 August 2010.

composed of a, b, i, and g subunits, closely resembled the yeast eIF3 core (62).

A systematic effort was devoted to mapping the binding site of eIF3 on the 40S subunit. We found that the extreme N-terminal domain (NTD) of a/Tif32 forms a crucial intermolecular bridge between eIF3 and the 40S subunit (49) and that the RNA recognition motif (RRM) of b/Prt1 and the extreme C-terminal domain (CTD) of c/Nip1 also play direct roles in anchoring eIF3 to the ribosome (9, 33, 51). In addition, we observed that deleting the CTD of a/Tif32 reduced 40S association with the MFC when the connection between eIF3 and eIF5/Tif5 in the MFC was impaired by the *tif5-7A* mutation (51). Importantly, our findings that the a/Tif32 CTD interacts with helices 16 to 18 of 18S rRNA (51) and Rps2 and Rps3 (6), that the a/Tif32 NTD binds to ribosomal proteins Rps0A and Rps10A (51), and that the j/Hcr1 CTD interacts with Rps2 (9) suggested that yeast eIF3 associates with the solvent-exposed side of the 40S subunit, as others have proposed for mammalian eIF3 (45, 48).

Functional studies revealed that j/Hcr1, the only nonessential subunit of yeast eIF3, forms together with the a/Tif32 CTD and the RRM of b/Prt1 an eIF3 subassembly that ensures stringency of the AUG start codon selection by blocking leaky scanning (6, 9, 33). Likewise, the c/Nip1 subunit was implicated in regulation of the AUG decoding mechanism owing to the fact that its NTD associates directly or indirectly with the key actors in this process, such as eIF1, eIF5, and the TC (53). On the other hand, the *prt1-1* point mutation in b/Prt1 and single point substitutions in the conserved KERR motif of a/TIF32-CTD were among other effects suggested to reduce the rate of ribosomal scanning (6, 31). Given the essentiality of all core subunits, a surprising result came from a biochemical study that suggested that the a/Tif32-b/Prt1-c/Nip1 subcomplex lacking g/Tif35 and i/Tif34 subunits is sufficient to stimulate the TC and mRNA recruitment to the 40S subunit and even to promote efficient translation *in vitro* (40). These findings were subsequently supported by pioneering work that used reconstituted mammalian eIF3 and suggested that eIF3i and -g are dispensable for active mammalian eIF3 formation *in vitro* (25).

Besides playing these canonical roles in general translation initiation, eIF3 was also implicated in the gene-specific translational control mechanism termed reinitiation (REI) in yeast, plant, and mammalian cells (35, 42, 49). REI is utilized to up- or downregulate translation of regulatory proteins, such as transcription factors and proto-oncogenes, in response to various environmental stimuli (22). In general, it relies on the ability of the small ribosomal subunit to remain attached to the mRNA following termination of translation on a short upstream ORF (uORF) in order to resume scanning on the same mRNA molecule. The next critical step of REI is *de novo* recruitment of the TC, which is required to recognize the next AUG codon; therefore, REI can be delicately regulated by manipulating the eIF2/GTP levels (8). The uORFs thus possess the exquisite potential to function as context-dependent *cis* regulators of translation.

The best-studied example of the REI mechanism is the translational control of yeast *GCN4*, a transcriptional activator of a large number of biosynthetic genes (reviewed in reference 18). The mRNA leader of *GCN4* contains four short uORFs that differ dramatically in their capacity to promote efficient REI. Whereas uORFs 2 to 4 are very inefficient, uORF1 allows the majority of 40S ribosomes terminating at its stop codon to remain mRNA bound and resume scanning. This ability requires two segments of uORF1: enhancer sequences upstream of its start codon, and the last codon plus ~12 nucleotides (nt) after the stop codon (12, 14). We have recently demonstrated that the 5′ enhancer of uORF1 functionally interacts with the extreme NTD of a/Tif32 at or near the mRNA exit channel of the posttermination 40S subunit. This interaction was proposed to be instrumental in stabilizing the 40S subunit on the mRNA to enable resumption of scanning for efficient REI on a downstream ORF (49). Under nutrient-replete conditions characterized by high levels of the TC, nearly all of the rescanning 40S ribosomes after uORF1 will rebind the TC before reaching uORFs 2 to 4, translate one of these uORFs, and dissociate from the mRNA. Amino acid starvation leads to phosphorylation of eIF2α by the kinase Gcn2, converting eIF2/GDP from a substrate to a competitive inhibitor of its GEF, eIF2B, thus reducing the concentration of TC. Low TC levels derepress *GCN4* translation by allowing ~50% of rescanning 40S ribosomes to rebind TC after bypassing the trap of uORFs 2 to 4 and to reinitiate at *GCN4* instead. Failure to induce expression of *GCN4* in response to a shortage of amino acids in various mutants confers increased sensitivity to inhibitors of amino acid biosynthetic enzymes, and this has been designated the Gcn$^-$ phenotype.

In this report, we performed functional analysis of two small essential eIF3 subunits, g/Tif35 and i/Tif34, whose contributions to general translation initiation were virtually unknown. Site-directed substitutions in the RRM of g/Tif35 in *g/tif35-KLF* produced no impact on its RNA-binding affinity, on the integrity of eIF3 in the MFC, or on formation of the 43S PICs. Nevertheless, the *g/tif35-KLF* mutation markedly reduced rates of translation initiation and decreased the processivity of scanning through a stable secondary structure inserted into the 5′-UTR of uORF-less *GCN4* mRNA. In addition, *g/tif35-KLF* provoked a strong Gcn$^-$ phenotype owing to the inability of posttermination 40S subunits at *GCN4*'s uORF1 to resume scanning for reinitiation downstream; this resembles the previously described phenotype of the *a/tif32-Δ8* mutant (49). Detailed genetic analysis revealed, however, that the g/Tif35 RRM and the a/Tif32 NTD ensure efficient resumption of scanning by different mechanisms. Like *g/tif35-KLF*, the Q258R mutation of the WD40 repeat 6 of i/Tif34 also produced a severe Gcn$^-$ phenotype. However, in contrast to *g/tif35-KLF*, *i/tif34-Q258R* allowed resumption of scanning after uORF1 but significantly reduced the rate of scanning. Consistently, the Gcn$^-$ phenotype of *i/tif34-Q258R* was partially suppressible by cooverexpressing scanning-promoting factors eIF1 and eIF1A. Together these results provide the first insights into the functional contributions of the essential i/Tif34 and g/Tif35 subunits of yeast eIF3 to general translation initiation as well as to translational control of *GCN4* expression.

MATERIALS AND METHODS

Construction of yeast strains and plasmids. To create H464, H421 (Table 1) was first transformed with YEpTIF35-T (Table 2), and YEp-TIF35-U was evicted by growth on 5-fluoroorotic acid (5-FOA) medium. The resulting strain was transformed to Ura$^+$ with the integrative *GCN2* plasmid pHQ835 (kindly provided by Hongfang Qiu) digested with SnaBI. Ura$^-$ segregants were obtained

TABLE 1. Yeast strains used in this study

Strain[a]	Genotype	Source or reference
H464§	*MAT***a** *leu2-3,112 ura3-52*::*GCN2 trp1*Δ *tif35*Δ (YEp-TIF35-U)	This study
H421§	*MAT***a** *leu2-3,112 ura3-52 trp1 gcn2*Δ *tif35*Δ (YEp-TIF35-U)	Klaus H. Nielsen
H111§	*MAT***a** *leu2-3,112 ura3-52*::*GCN2 trp1*Δ *tif35*Δ (YCp22-g/TIF35-screen)	This study
H112§	*MAT***a** *leu2-3,112 ura3-52*::*GCN2 trp1*Δ *tif35*Δ (YCp22-g/tif35-KLF)	This study
YBS47¶	*MAT***a** *leu2-3,112 ura3-52 trp1*Δ *gcn2*Δ *a*/*tif32*Δ *URA3*::*GCN2 ura3* (pRSeIF3a-HIS-L)	49
YBS53¶	*MAT***a** *leu2-3,112 ura3-52 trp1*Δ *gcn2*Δ *a*/*tif32*Δ *URA3*::*GCN2 ura3* (pRSeIF3a-Δ8-HIS-L)	49
H450‖	*MAT***a** *leu2-3,112 ura3-52*::*GCN2 trp1*Δ *tif34*Δ (YEp-TIF34 (*URA3*))	This study
H420‖	*MAT***a** *leu2-3,112 ura3-52 trp1 gcn2*Δ *tif34*Δ (YEp-TIF34 (*URA3*))	Klaus H. Nielsen
H120‖	*MAT***a** *leu2-3,112 ura3-52*::*GCN2 trp1*Δ *tif34*Δ (YCp111-i/TIF34)	This study
H121‖	*MAT***a** *leu2-3,112 ura3-52*::*GCN2 trp1*Δ *tif34*Δ (YCp111-i/tif34-Q258R)	This study

[a] Strains that share a footnote symbol (§, ¶, or ‖) are isogenic strains.

by selecting for growth on medium containing 5-FOA, and the resulting H464 was tested for the presence of integrated *GCN2* by growth on medium containing 3-aminotriazole (3-AT). YEp-TIF35-U was reintroduced into the verified strain, which was then grown on Trp^+ medium to enable spontaneous loss of the *TRP1* covering plasmid, YEpTIF35-T.

To produce H111 and H112, H461 was transformed with YCp22-g/TIF35-screen andYCp22-g/tif35-KLF, respectively, and the resident *g*/*TIF35 URA3* plasmid was evicted on 5-FOA-containing medium.

To create H450, H420 (Table 1) was first transformed with YEpTIF34-T (Table 2), and YEp-TIF34-U was evicted by growth on 5-FOA medium. The resulting strain was transformed to Ura^+ with the integrative *GCN2* plasmid pHQ835 digested with SnaBI. Ura^- segregants were obtained by selecting for growth on medium containing 5-FOA, and the resulting H450 was tested for the presence of integrated *GCN2* by growing on medium containing 3-AT. YEp-TIF34-U was reintroduced into the verified strain, which was then grown on Trp^+ medium to enable spontaneous loss of the *TRP1* covering plasmid, YEpTIF34-T.

To produce H120 and H121, H450 was transformed with YCp111-i/TIF34 and YCp111-i/tif34-Q258R, respectively, and the resident *i*/*TIF34 URA3* plasmid was evicted on medium containing 5-FOA.

YCp22-g/TIF35-screen was generated by fusion PCR. The following pairs of primers were used for separate PCR amplifications using Ycp22-g/TIF35-help (see below) as template: (i) 3gSalIr and 3gHistag and (ii) 3gNdeI and 3gHistagr. The PCR products thus obtained were used in a 1:1 ratio as templates for a third PCR amplification using primers 3gSalIr and 3gNdeI. The resulting PCR product was digested with SalI and NdeI and ligated with SalI-NdeI-cleaved Ycp22-g/TIF35-help (replacing wild-type [WT] *g*/*TIF35* with 8×His-tagged *g*/*TIF35-His*). Ycp22-g/TIF35-help was constructed by inserting the 1,394-bp KpnI-SalI fragment from YEpTIF35-T into YCplac22 digested with KpnI-SalI.

YCp22-g/tif35-KLF was generated by fusion PCR. The following pairs of primers were used for separate PCR amplifications using YCp22-g/tif35-LF (see below) as template: (i) 3gKLF and 3gXhoIr and (ii) 3gNdeI and 3gKLFr. The PCR products thus obtained were used in a 1:1 ratio as templates for a third PCR amplification using primers 3gXhoIr and 3gNdeI. The resulting PCR product was digested with XhoI and NdeI and ligated with XhoI-NdeI-cleaved YCp22-g/tif35-LF (replacing *g*/*tif35-LF* with *g*/*tif35-KLF-His*).

YCp22-g/tif35-LF was also generated by fusion PCR. The following pairs of primers were used for separate PCR amplifications using Ycp22-g/TIF35-screen as template: (i) 3gLF and 3gXhoIr and (ii) 3gNdeI and 3gLFr. The PCR products thus obtained were used in a 1:1 ratio as templates for a third PCR amplification using primers 3gXhoIr and 3gNdeI. The resulting PCR product was digested with XhoI and NdeI and ligated with XhoI-NdeI-cleaved Ycp22-g/TIF35-screen (replacing WT *g*/*TIF35-His* with *g*/*tif35-LF-His*).

pGEX-g/tif35-KLF was made by inserting the XhoI-BamHI-digested PCR product, obtained with primers pGEX35NTD and pGEX35RRMr using the template YCp22-g/tif35-KLF, into XhoI-BamHI-digested pGEX-5X-3.

YEp-SUI1+TIF11was constructed by inserting the 1,134-kb SalI-SacI fragment from pDSO22 into YEpSUI1-U digested with SalI-SacI.

YEpTIF2(4A)-L was constructed by inserting the 2,026-kb SphI-BHI fragment from YEpTIF2(4A)-U into YEplac181 digested with SphI-BHI.

A list of all PCR primers named above can be found in Table 3.

Yeast biochemical methods. Glutathione *S*-transferase (GST) pulldown experiments with GST fusions and *in vitro*-synthesized ^{35}S-labeled polypeptides (see Table 2 for vector descriptions) were conducted as follows. Individual GST-fusion proteins were expressed in *Escherichia coli*, immobilized on glutathione-Sepharose beads, and incubated with 10 μl of ^{35}S-labeled potential binding partners at 4°C for 2 h. The beads were washed three times with 1 ml of phosphate-buffered saline, and bound proteins were separated by SDS-PAGE. Gels were first stained with Gelcode Blue stain reagent (Pierce) and then subjected to autoradiography. Ni^{2+} chelation chromatography of eIF3 complexes containing 8×His-tagged g/Tif35 from yeast whole-cell extracts (WCEs) and Western blot analysis were conducted as described in detail previously (32). In short, WCEs were incubated at 4°C for 2 h with 4 μl of 50% Ni^{2+}-nitrilotriacetic acid–silica resin (Qiagen) suspended in 200 μl of buffer A, followed by washing and elution. β-Galactosidase assays and polysome profile analysis were conducted as described previously (12, 55).

mRNA binding assay. ^{32}P-labeled *Xenopus laevis* β-globin mRNA was prepared *in vitro* using the MAXIscript SP6 transcription kit (Ambion Inc.), [α-^{32}P]UTP (10 mCi/ml), and the pKA18 vector (4) linearized with BamHI, according to the vendor's instructions. The transcript of the first 354 nucleotides of *X. laevis* β-globin mRNA was purified using a size exclusion column (Nuc-Away spin column; Ambion, Inc.).

WT and mutant g/Tif35 proteins fused to the GST moiety and immobilized on glutathione-Sepharose beads were incubated with 100 ng of ^{32}P-labeled *X. laevis* β-globin mRNA in 250 μl of the binding buffer (10 mM HEPES [pH 7.6], 3 mM $MgCl_2$, 40 mM KCl, 5% glycerol, 1 mM dithiothreitol, 1.5% 2-β-mercaptoethanol) for 30 min at 26°C. (To increase specificity of binding, 200 ng of yeast total tRNA [Sigma] was added to each reaction mixture as a competitor RNA.) The beads were then washed three times with 1 ml of binding buffer, and bound β-globin mRNA was separated by electrophoresis on 5.5% denaturing (8 M urea) polyacrylamide gel, followed by autoradiography. For control experiments, the same procedure was carried out using beads containing only the GST moiety or beads preincubated with bacterial extracts derived from plain *E. coli* BL21 cells.

RESULTS

Multiple substitutions of the conserved residues of the RRM of g/Tif35 reduce efficiency of translation initiation. The functionally important yet nonessential C-terminal domain of g/Tif35 is formed by the canonical RRM previously shown to possess nonspecific RNA-binding activity (15). A typical RRM contains two RNP sites in β-sheets 1 and 3, with four highly conserved positions always occupied by a set of either aromatic or basic residues that critically contribute to RNA binding, namely, RNP1 positions 1 (R or K), 3 (F/Y), and 5 (F/Y) and RNP2 position 2 (F/Y) (for a review, see reference 24). An unpublished nuclear magnetic resonance structure of the human heIF3g RRM (K. Tsuda, Y. Muto, M. Inoue, T. Kigawa, T. Terada, M. Shirouzu, and S. Yokoyama, unpublished data) (protein data bank accession code 2CQ0) (Fig. 1A) shows that RNP2 and RNP1 are typically aligned next to each other in a four-stranded anti-parallel β-sheet packed against two perpendicular α-helices. Interestingly, all of the eIF3g RRM homologs differ from the classical RRM at position 2 of RNP2, in

TABLE 2. Plasmids used in this study

Plasmid	Description	Source or reference
p180 (YCp50-*GCN4-lacZ*)	Low-copy-number *URA3* vector containing wild-type *GCN4* leader	29
P227	Low-copy-number *URA3* vector containing *GCN4* leader without uORFs	26
pM226	Derivative of pM199; ORF of uORF1 extends into the *GCN4-lacZ* coding region	13
pA80z	Low-copy-number *URA3* vector containing *GCN4* leader with solitary uORF4 at the position of uORF1	1
pG67	Low-copy-number *URA3* vector containing uORF1 only, placed 32 nt from *GCN4-lacZ*	13
pM199	Low-copy-number *URA3* vector containing uORF1 only, at the position of uORF4 (140 nt from *GCN4-lacZ*)	13
p209	Low-copy-number *URA3* vector containing uORF1 only, at its original position (350 nt from *GCN4-lacZ*)	13
P1014l	Low-copy-number *URA3* vector containing uORF1 only, placed 640 nt from *GCN4-lacZ*	13
pBS64	Derivative of pM128; low-copy-number *URA3* vector containing *GCN4* leader with uORF1 at its original position, with the CCCCGG substitution of the −21 AAAATT −16 region in its 5′-UTR	49
pBS62	Derivative of pM128; low-copy-number *URA3* vector containing *GCN4* leader with uORF1 at its original position with 40-nt deletion in its 5′-UTR (from −61 to −21)	49
pVM11	Derivative of pM128; low-copy-number *URA3* vector containing *GCN4* leader with uORF1 at its original position with 46-nt deletion in its 5′-UTR (from −61 to −15)	49
pBS63	Derivative of pM128; low-copy-number *URA3* vector containing *GCN4* leader with uORF1 at its original position with 160-nt deletion in its 5′-UTR (from −181 to −21)	49
pWCB07	*GCN4-lacZ* lacking all uORFs, with hairpin insertion between nt +481 and +482 in single-copy *URA3* plasmid, from YCp50	This study
pWCB06	*GCN4-lacZ* lacking all uORFs, with hairpin insertion between nt +481 and +482 in single-copy *URA3* plasmid, from YCp50	This study
YCplac22	Single-copy cloning vector, *TRP1*	11
YEp-TIF35	High-copy-number *g/TIF35 URA3* plasmid from YEplac195	3
YEp-TIF34	High-copy-number *i/TIF34 URA3* plasmid from YEplac195	3
YCp22-g/TIF35-screen	Single-copy *g/TIF35-His TRP1* plasmid from YCplac22	This study
YCp22-g/tif35-KLF	Single-copy *g/tif35-KLF-His TRP1* plasmid from YCplac22	This study
pGEX-5X-3	Cloning vector for GST fusions	46
pGEX-g/TIF35	GST-g/Tif35 fusion plasmid from pGEX-5X-3	3
pGEX-g/tif35-KLF	GST-g/tif35-KLF fusion plasmid from pGEX-5X-3	This study
pGBK-T7-RPS3	*RPS3* ORF cloned into pGBKT7, *TRP1* (Clontech)	51
pGBK-T7-RPS20	*RPS20* ORF cloned into pGBKT7, *TRP1* (Clontech)	51
pGBK-T7-RPS2	*RPS2* ORF cloned into pGBKT7, *TRP1* (Clontech)	51
pT7-Δ7-b/PRT1	*b/PRT1*[641–724] ORF cloned under T7 promoter	54
pT7-i/TIF34	*i/TIF34* ORF cloned under T7 promoter	3
YEplac195	High-copy-number cloning vector, *URA3*	11
YEplac181	High-copy-number cloning vector, *LEU2*	11
YEplac112	High-copy-number cloning vector, *TRP1*	11
YEpSUI1-U	High-copy-number *SUI1 URA3* plasmid from YEplac195	53
pDSO22	High-copy-number *TIF11 URA3* plasmid from YEplac195	34
YEp-SUI1+TIF11	High-copy-number *SUI1 TIF11 URA3* plasmid from YEplac195	This study
YEp-SUI1+TIF11-W	High-copy-number *SUI1 TIF11 TRP1* plasmid from YEplac112	10
YEpTIF2(4A)-U	High-copy-number *TIF2 URA3* plasmid from YEplac195	7
YEpTIF2(4A)-L	High-copy-number *TIF2 LEU2* plasmid from YEplac181	This study
YEpTIF4631(4G)-U	High-copy-number *TIF4631 URA3* plasmid from YEplac195	7
pCF82	High-copy-number *SUI1 TRP1* plasmid from YEplac112	10
YCpL-i/TIF34-HA	Single-copy *i/TIF34-HA LEU2* plasmid from YCplac111	3
YCpL-i/tif34-HA-3 (Q258R)	Single-copy *i/tif34-HA-Q258R LEU2* plasmid from YCplac111	3
YEpTIF35-T	High-copy-number *g/TIF35 TRP1* plasmid from YEplac112	54
YEpTIF34-T	High-copy-number *i/TIF34 TRP1* plasmid from YEplac112	54
pKA18	β-Globin under SP6 promoter	4

that eIF3g has a basic as opposed to aromatic residue at that position (Fig. 1B). It is thus conceivable that the stacking interaction that the aromatic residue in position 2 normally establishes with mRNA is replaced by ionic attraction with a phosphate group in the RNA backbone. Surprisingly, the yeast protein also differs in position 3 of RNP1 (L versus F) (Fig. 1B).

In an effort to elucidate the role of g/Tif35 in translation, we first mutated conserved residues in either one or both RNPs (shown schematically in Fig. 1A and B) and tested the resulting mutants for slow growth (Slg^-) and temperature-sensitive (Ts) phenotypes. Whereas neither individual RNP mutant showed any growth defects (data not shown), the combination of both RNP1 and RNP2 mutations in *g/tif35-K194A-L235A-F237A* (henceforth termed *g/tif35-KLF*) resulted in the Ts phenotype without having any effect on the steady-state levels of the g/Tif35 protein in cells (Fig. 1C). The *g/tif35-KLF* mutation was found to provoke substantial (~3-fold) reductions in the polysome:monosome (P/M) ratio at 34°C (Fig. 1D), indicating a marked decrease in the rate of translation initiation *in vivo*.

TABLE 3. Primers used in this study

Primer name	Primer sequence (5′–3′)
3gSalIr	CTGCAGGTCGACCTCTTCACGATCTGCAAAAGTCCCAA
3gNdeI	CGACCATATGACCATGAACTGTCCATT
3gHistagr	AAACAAGTGCAGAGCATATTCTGTGCATCTCGAGCTAATGATGATGATGATGAT GATGATGTTCCTTAACCTTAGGTTTGGACCA
3gHistag	ATGCACAGAATATGCTCTGCACTTGTT
3gLF	CAAAGAAACAGGTAAATCAAGAGGTGCAGCCGCTGTTACCTTTTCGAGCGAAG AAGTTGCCGAACA
3gLFr	TCTTGATTTACCTGTTTCTTTGTTTCT
3gXhoIr	GTGCATCTCGAGCTAATGATGATGATGATG
3gKLFr	AGTACACATATCATCACGTTCTCTAGA
3gKLF	TGATGATATGTGTACTTTGGCAATTATGCAAGTTAATGAAAATGCCGATGAAAA
pGEX35NTD	AATAAGGATCCCCATGAGTGAAGTTGCACCAGAG
pGEX35RRMr	AATAACTCGAGCTATTCCTTAACCTTAGGTTTGGA

g/Tif35 associates with eIF3 via two contacts with subunits i/Tif34 and b/Prt1; it was previously shown that its C-terminal RRM is not required for either of these interactions (3). Indeed, the *g/tif35-KLF* mutation did not affect binding of mutant g/Tif35 (fused to the GST moiety) to radiolabeled i/Tif34 and b/Prt1 in an *in vitro* pulldown experiment (Fig. 2A, second and third panels). It also had no impact on the integrity of the MFC as judged from affinity purification of the WT and mutant 8×His-tagged g/Tif35 proteins by nickel chelation chromatography followed by analysis of the yields of copurifying proteins by Western blot hybridization (Fig. 2B). Finally, no effect on the association of any of the MFC components with the 40S subunits *in vivo* was observed, as expected (data not shown).

To examine whether mutating the RNPs of g/Tif35 affected its RNA-binding affinity, WT and mutant g/Tif35 fused to a GST moiety were incubated with *in vitro*-synthesized ^{32}P-labeled β-globin mRNA, and the amount of bound mRNA species was quantified. As shown in Fig. 2A (fourth panel), the *g/tif35-KLF* mutation had no effect on the affinity of g/Tif35 for β-globin mRNA, indicating that none of the targeted residues critically contributes to g/Tif35's RNA-binding activity. Nevertheless, given the marked impact of the *KLF* mutation on the rate of translation initiation, we decided to explore the nature of its defect further.

The RRM of g/Tif35 is required for full derepression of *GCN4* expression under starvation conditions. According to previous reports, neither yeast nor mammalian eIF3g appears to be required for assembly of the 48S PIC, which includes sequential recruitment of the TC and mRNA to the 40S subunit (25, 40). Hence, we decided to examine whether g/Tif35 might contribute to processes following the assembly of the 48S PIC in living cells, such as scanning and AUG recognition. We tested the *g/tif35-KLF* mutant for specific phenotypes indicating impairment of translational control of *GCN4* expression (18). This mechanism has been extensively used in the past as a valuable genetic tool for dissecting the contributions of individual eIFs to initiation (9, 10, 19, 31, 33, 49, 53, 61). Mutants defective in TC formation and/or its recruitment to the 40S subunit constitutively derepress *GCN4* expression, imparting a so-called Gcd$^-$ phenotype, whereas mutants that fail to derepress *GCN4* under starvation conditions provoke a Gcn$^-$ phenotype, which signals defects in the steps following assembly of 48S PICs such as processivity of scanning, AUG recognition, or subunit joining (9, 16, 23, 31, 53, 60).

In agreement with reports arguing against the involvement of g/Tif35 in stimulation of TC loading onto the 40S subunits, *g/tif35-KLF* did not display the Gcd$^-$ phenotype (data not shown). On the other hand, the *g/tif35-KLF* cells imparted the severe Gcn$^-$ phenotype, as they failed to grow in the presence of 3-AT (an inhibitor of histidine biosynthetic genes) at 34°C (Fig. 3A). The effect of 3-AT can only be overcome by sufficient upregulation of *GCN4* expression, as illustrated by the fact that 30 mM 3-AT completely prevented growth of *g/TIF35*$^+$ *gcn2*Δ cells, in which eIF2α cannot be phosphorylated and thus the TC levels remain high and *GCN4* fully repressed (Fig. 3A). It should be noted that phosphorylation of eIF2α by Gcn2 upon starvation was not affected in *g/tif35-KLF GCN2* cells, ruling out this possible mechanism for the Gcn$^-$ phenotype (data not shown). Using the *GCN4-lacZ* reporter containing all four uORFs, we measured derepression in *g/tif35-KLF* cells in response to 3-AT at 34°C and showed that it was reduced by a factor of ~5 (Fig. 3B, construct i, row 2). The little to no reduction in expression from the uORF-less *GCN4-lacZ* construct clearly suggests that the observed derepression defect is not caused by changes in *GCN4-lacZ* mRNA levels (Fig. 3B, construct ii). (It should be noted that mRNAs produced from all *GCN4-lacZ* constructs used throughout the study are highly stable owing to the fact that they all contain an intact stabilizer element [STE] that prevents the natural *GCN4* mRNA from undergoing nonsense-mediated decay [44, 49].) Together, these results imply that the RRM of g/Tif35 is required for proper upregulation of *GCN4* expression upon starvation and indicate that its function in general translation initiation might be associated with the steps following formation of the 48S PIC.

The RRM of g/Tif35 promotes resumption of scanning of posttermination ribosomes on uORF1 of *GCN4*. To determine what postassembly step(s) might be perturbed by *g/tif35-KLF*, we analyzed a battery of *GCN4-lacZ* reporters that varied in their *GCN4* mRNA leader sequences. Defects in AUG start codon recognition or subunit joining may lead to the Gcn$^-$ phenotype if the 48S PIC scans over the AUG start codon of uORF1 (leaky scanning); this can be monitored with a construct in which uORF1 is elongated and overlaps the beginning of *GCN4*. This elongated version of uORF1 blocks ~99% of all scanning ribosomes from reaching the *GCN4* start site, indicating that only ~1% of ribosomes show leaky scanning of uORF1 in WT cells (13). As shown in Fig. 3B (construct iii), we

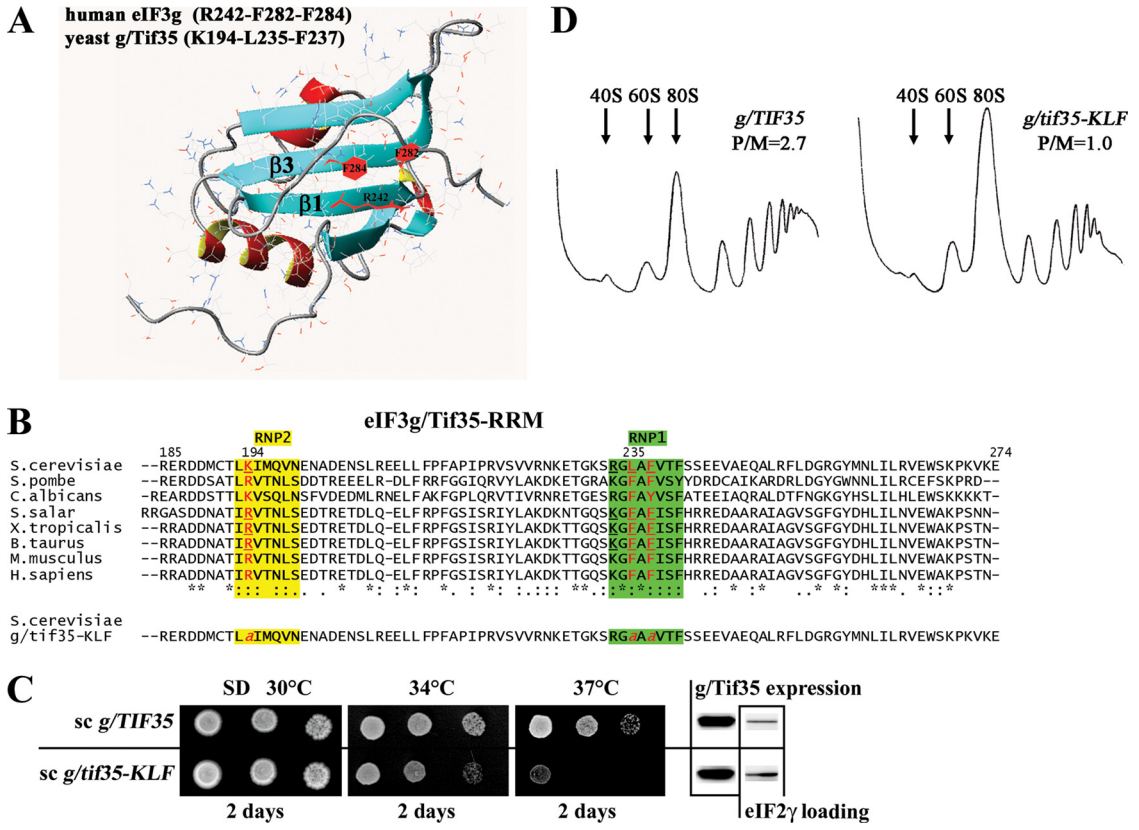

FIG. 1. The triple-Ala substitution of the highly conserved residues in RNPs of the g/Tif35 RRM in *g/tif35-KLF* impairs cell growth and the rate of general translation initiation. (A) The unpublished nuclear magnetic resonance solution structure of the human heIF3g RRM (K. Tsuda et al., unpublished; Protein Data Bank accession code 2CQ0) displays a canonical RRM fold with a four-stranded antiparallel β-sheet packed against two perpendicular α-helices. The highly conserved Arg242 in position 2 of RNP2 in β-sheet 1 and Phe282 and Phe284 in positions 3 and 5 of RNP1 in β-sheet 3 of human eIF3g RRM correspond to Lys194 and to Leu235 and Phe237, respectively, of yeast g/Tif35-RRM and are highlighted in red. (B) Amino acid sequence alignment of g/Tif35-RRM of *Saccharomyces cerevisiae* with that of other species. The amino acid sequence of *S. cerevisiae* g/Tif35 (accession number NP_010717) between residues 185 and 274 (the terminal residue) is aligned with its *Schizosaccharomyces pombe* (accession number CAA18400), *Candida albicans* (accession number Q59ZV5), *Salmo salar* (accession number ACI69727), *Xenopus tropicalis* (accession number Q28CY2), *Bos taurus* (accession number Q3ZC12), *Mus musculus* (accession number Q9Z1D1), and *Homo sapiens* (accession number O75821) homologs. The alignment was conducted with ClustalW (http://www.ch.embnet.org/software/ClustalW.html). Highly conserved sequences of RNP2 and RNP1 are shown in yellow and green, respectively, with the key residues that were subjected to site-directed mutagenesis highlighted in red. The sequence of *g/tif35-KLF* generated in this study is given at the bottom. (C) *g/tif35-KLF* severely impairs cell growth at elevated temperatures. The H464 (*g/tif35*Δ) strain was transformed with YCp22-g/Tif35-screen (top row) and YCp22-g/tif35-KLF (bottom row), and the resident YEp-TIF35-U (*URA3*) plasmid was evicted on medium containing 5-FOA. The resulting strains were then spotted in four serial 10-fold dilutions on SD medium and incubated at 30, 34, and 37°C for 2 days. The far right columns show results of Western analysis of WCEs from the very same strains grown at 34°C, using anti-g/Tif35 (g/Tif35 expression; lane 1) and anti-GCD11 (eIF2γ loading; lane 2) antibodies. (D) The *g/tif35-KLF* mutant reduces rates of translation initiation *in vivo*. Polysome profiles are shown for the strains in panel C cultured in YPD medium at 34°C and treated with cycloheximide just prior to harvesting. WCEs were separated by velocity sedimentation through a 5-to-45% sucrose gradient centrifugation at 39,000 rpm for 2.5 h. The gradients were collected and scanned at 254 nm to visualize the ribosomal species. Positions of 40S, 60S, and 80S species are indicated by arrows, and P/M ratios are given above the profiles.

observed a marginal ~1.5-fold increase in *GCN4-lacZ* expression from this construct in *g/tif35-KLF* cells, which would by no means account for a strong derepression defect (Fig. 3B, construct i). Also, little to no increase in β-galactosidase activity was detected with a construct containing only uORF4 (Fig. 3B, construct iv), which allows a negligible level of REI and thus very effectively blocks translation of downstream ORFs (13). Together these results indicate that the *KLF* mutation does not significantly affect stringency of the start codon selection. It is worth noting that results in Fig. 3B (constructs iii and iv) additionally eliminate the possibility that induction of *GCN4-lacZ* is reduced in *g/tif35-KLF* cells due to a decrease in the reporter mRNA level, as this effect should apply equally to the mutant constructs, yet expression of these constructs was higher than in the WT cells.

The derepression defect in *g/tif35-KLF* cells can be also explained by a reduction in the rate of scanning of ribosomes progressing from uORF1 to uORF4 (i.e., slow scanning) or in their decreased stability on the mRNA during scanning (i.e., abortive scanning). To test this, we analyzed constructs carrying only uORF1 at four different positions relative to *GCN4-lacZ* (Fig. 3B, constructs v to viii). If the 40S subunits were more prone to dissociating from the mRNA during scanning, then a decrease in the *GCN4-lacZ* activity would be expected. This was indeed observed; however, one would also predict that the probability of the 40S falling off would increase with

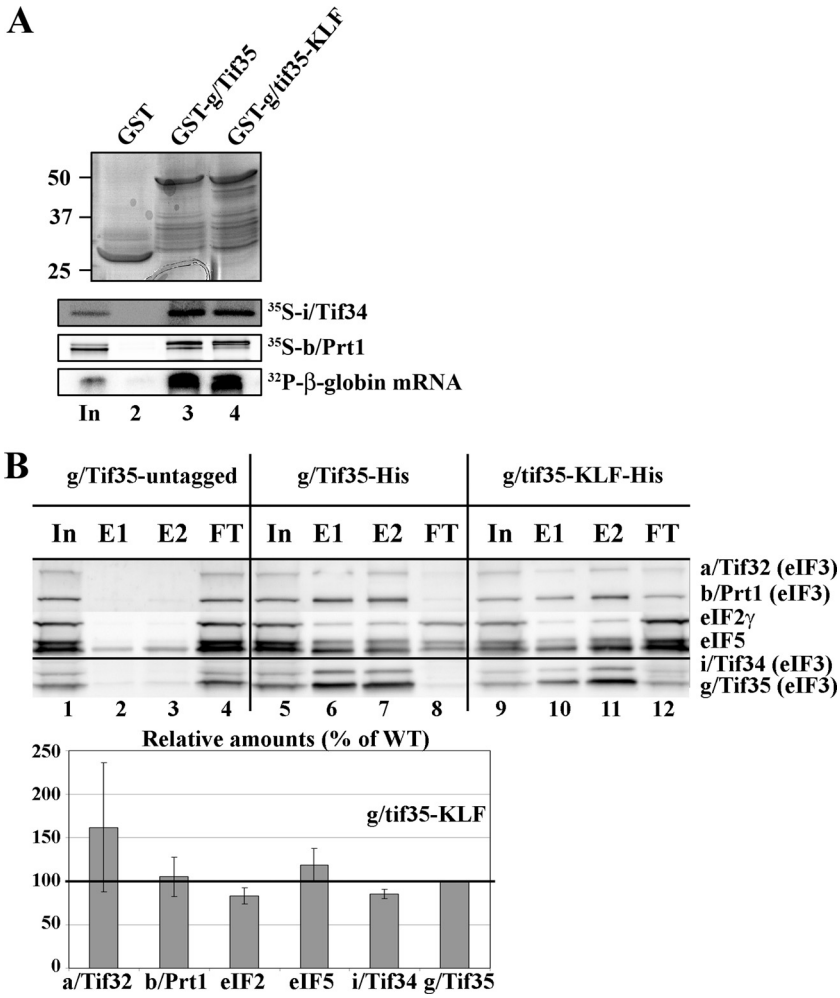

FIG. 2. The *g/tif35-KLF* mutant neither affects the integrity of eIF3 in the MFC nor impairs the RNA-binding activity of g/Tif35. (A) The *g/tif35-KLF* mutation does not reduce binding of g/TIF35 to b/Prt1, i/Tif34, or β-globin mRNA *in vitro*. Full-length WT g/Tif35 (lane 3) and mutant g/tif35-KLF (lane 4) fused to GST, and also GST alone (lane 2), were tested for binding to ^{35}S-labeled b/Prt1 and i/Tif34 and to ^{32}P-labeled β-globin mRNA. Lane 1 (In) contains 10% and 2.5% of input amounts of proteins and RNA, respectively, added to each reaction mixture. (B) The *g/tif35-KLF* mutation does not prevent g/Tif35 from associating with eIF3 in the MFC *in vivo*. WCEs were prepared from H421 (*g/tif35*Δ) bearing untagged g/Tif35 (lanes 1 to 4), H111 expressing 8×His-tagged g/Tif35 (lanes 5 to 8), and H112 expressing 8×His-tagged g/tif35-KLF (lanes 9 to 12). The WCEs were incubated with Ni^{2+}-silica resin, and the bound proteins were eluted and subjected to Western blot analysis. Lanes 1, 5, and 9 contained 5% of the input WCEs (In); lanes 2, 6, and 10 contained 30% fractions eluted from the resin (E1); lanes 3, 7, and 11 contained 60% of the same fractions (E2); lanes 4, 8, and 12 contained 5% of the flowthrough (FT). The Western signals for a/Tif32, b/Prt1, eIF2, eIF5, and i/Tif34 in the E1 and E2 fractions for the WT *g/TIF35* and mutant *g/tif35-KLF* strains were quantified, combined, normalized for the amounts of WT g/Tif35 in these fractions, and these data are plotted in the histogram on the right as percentages of the corresponding values calculated for the WT *g/TIF35*.

the increasing distance to scan through, thus producing a gradual decrease in activity, which is not the case (compare constructs v to viii). Therefore, it is highly unlikely that abortive scanning could explain the Gcn$^-$ phenotype. Slower scanning would, on the other hand, increase *GCN4-lacZ* expression from all four constructs (particularly those with shorter-than-normal spacers between uORF1 and *GCN4-lacZ* [constructs v and vi]) by providing the scanning 40S subunits more time to rebind TC before reaching the next AUG start codon. However, the fact that *g/tif35-KLF* decreased, rather than increased, expression from all four constructs to a similar extent (~57 to 77%) strongly argues against both of these explanations. In fact, the observed phenotype closely resembles that of the *a/tif32-Δ8* mutation only recently shown to interfere with the key first step of REI: resumption of scanning of postterminated ribosomes on the uORF1 stop codon (49).

As shown previously (13), *GCN4-lacZ* expression starts to plateau when the intercistronic distance between uORF1 and *GCN4-lacZ* exceeds the length of the natural 350-nt spacer, indicating saturated TC reacquisition (Fig. 3B, compare constructs viii and vii). The fact that *g/tif35-KLF* plateaus at an equal length but with expression of ~40% of the WT level, as expected, further supports our conclusion that the REI-competent PICs in the mutant cells are reduced to 40% of normal (Fig. 3C). These results hence strongly suggest that besides the NTD of a/Tif32, the RRM of g/Tif35 represents yet another eIF3 domain that is critically required for retention of the postterminated 40S subunits

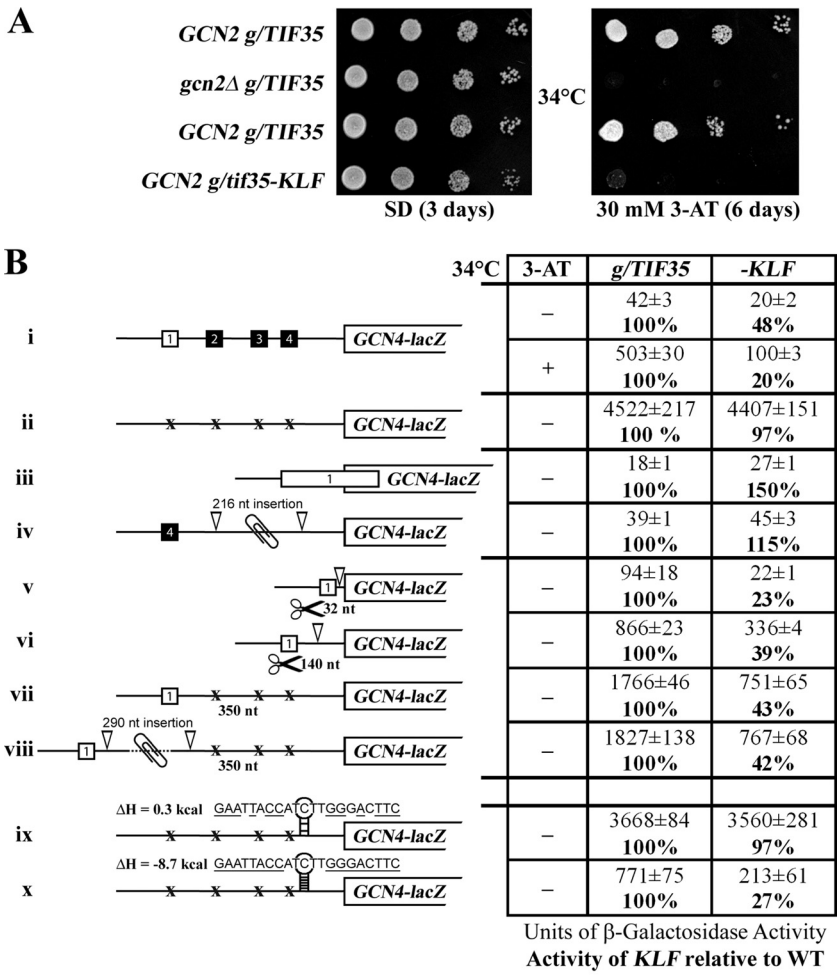

FIG. 3. *g/tif35-KLF* reduces processivity of scanning and interferes with the reinitiation process by preventing posttermination retention of the 40S ribosome on *GCN4* mRNA. (A) *g/tif35-KLF* imparts a strong Gcn$^-$ phenotype, implicating g/Tif35 in regulation of translational control of *GCN4* expression. Isogenic strain H464 (*GCN2 g/TIF35*; row 1) and H421 (*gcn2*Δ *g/TIF35*; row 2) transformed with an empty vector YCplac22 and strain H111 (*GCN2 g/tif35*Δ YCp22-g/TIF35-screen; row 3) and H112 (*GCN2 g/tif35*Δ YCp22-g/tif35-KLF; row 4) were spotted in four serial 10-fold dilutions on SD (left panel) or SD containing 30 mM 3-AT (right panel) and then incubated at 34°C for 3 or 6 days, respectively. (B, construct i) *g/tif35-KLF* reduces basal expression of *GCN4-lacZ* and prevents its full derepression upon starvation. H111 and H112 were transformed with p180 and grown in minimal medium for 6 h, and the β-galactosidase activities were measured in the WCEs and are expressed in units of nmol of *o*-nitrophenyl-β-D-galactopyranoside hydrolyzed per min per mg of protein. To induce *GCN4-lacZ* expression, strains grown in minimal medium for 2 h were treated with 10 mM 3-AT for 6 h. The mean values and standard deviations obtained from at least six independent measurements with three independent transformants, along with the activities the *g/tif35-KLF* mutant strain relative to the corresponding WT, are given in the table. White versus black squares indicate REI-permissive (uORF1) versus REI-nonpermissive (uORFs 2 to 4) uORFs. (Constructs ii to iv) The failure of *g/tif35-KLF* to derepress *GCN4-lacZ* is not caused by leaky scanning. H111 and H112 were transformed with p227 (ii), pM226 (iii), and pA80z (iv) and analyzed as for construct (i), except that they were not treated with 3-AT. Xs point to mutations eliminating the AUG start codons of uORFs 1 to 4. A paperclip symbol indicates an insertion of the nucleotide sequence. (Constructs v to viii) *g/tif35-KLF* blocks induction of *GCN4* expression by reducing the amount of posttermination 40S ribosomes on uORF1, which resume scanning for reinitiation downstream. H111 and H112 were transformed with pG67 (v), pM199 (vi), p209 (vii), or p1014l (viii) and analyzed as described for constructs ii to iv. Scissors indicate deletions of the nucleotide sequence. (Constructs ix and x) *g/tif35-KLF* increases the translation-inhibitory effect of a stable stem-loop structure inserted in the 5′-UTR of uORF-less *GCN4* mRNA. H111 and H112 were transformed with pWCB07 (ix) or pWCB06 (x) and analyzed as described for construct i. Both constructs contain the indicated sequences (with complementary bases underlined) inserted 21 nt 5′ of the *GCN4* AUG codon. (C) β-Galactosidase activities obtained for constructs v to viii in panel B, with WT and *g/tif35-KLF* cells were plotted as a function of the intercistronic distance between uORF1 and the AUG start codon of *GCN4-lacZ*.

on the mRNA, representing a crucial prerequisite for efficient REI.

The g/Tif35 RRM stimulates scanning through structured mRNA leaders. Our finding that the *g/tif35-KLF* mutation impairs resumption of scanning from uORF1 implies that the utility of the *GCN4* translational control as a tool to examine postassembly defects in general translation initiation is in this case limited. In particular, any effect of this mutation on the rate of scanning would be masked by its inability to start scanning downstream of uORF1.

To circumvent this obstacle, we compared WT and mutant *g/tif35-KLF* cells in terms of their abilites to scan through stem-loop structures inserted into the 5′-UTR of a *GCN4-lacZ* fusion lacking all four uORFs (Fig. 3B, constructs ix and x). Whereas a relatively weak stem-loop structure (Δ*H*, 0.3 kcal) reduced the *GCN4-lacZ* expression to the same degree in both WT and *g/tif35-KLF* cells (by ~20%) (Fig. 3B, compare construct ix with ii), a stable stem-loop (Δ*H*, −8.7 kcal) had ~4-fold stronger impact on translation in the mutant versus WT cells, where it diminished *GCN4-lacZ* expression by 85% (Fig. 3B, compare constructs x and ii). These results implicate g/Tif35 in stimulating processivity of scanning on mRNAs with structured 5′-UTRs—the first function in general translation initiation ever attributed to this small essential eIF3 subunit.

The a/Tif32 NTD and g/Tif35 RRM functional domains stimulate resumption of scanning by related but not identical mechanisms. It is believed that linear scanning is promoted by several initiation factors, including eIFs 1, 1A, 4G, 4A, and 4B and a helicase, Ded1, and its yeast homolog Dbp1 (reviewed in reference 39). In addition, eIF4G and eIF4A were shown to be required for resumption of scanning after translation of a short uORF in mammalian cells (43). Thus, we next wished to investigate whether some of these proteins could suppress defects of *g/tif35-KLF* and *a/tif32-Δ8* mutants in processivity of scanning and/or in resumption of scanning that produce the Gcn$^-$ phenotype. Toward this end, we overexpressed the proteins individually or in combinations in our mutant strains while scoring for growth effects on SD and 3-AT plates.

None of the factors suppressed the Gcn$^-$ phenotype of either of the mutants (Fig. 4A and C and data not shown); by contrast, an increased gene dosage of eIF1 (both alone and in combination with high-copy-number [hc] eIF1A) actually exacerbated the Gcn$^-$ phenotype of both of them (Fig. 4A and C, rows 5 and 6 versus 3). This effect of eIF1 was further verified in our reporter assay, which showed that *g/tif35-KLF* introduced with hc eIF1 conferred a severe derepression defect even at 30°C (Fig. 4B). In addition, the Gcn$^-$ phenotype of *a/tif32-Δ8* cells was exacerbated by overexpression of eIF4A or its cooverexpression with eIF4G; however, no such effect was observed in *g/tif35-KLF* cells (Fig. 4A and C). Hence, even though we did not observe any suppression effect and have at present no solid explanation for the exacerbation defects, the latter findings at least indicate that the *g/tif35-KLF* and *a/tif32-Δ8* mutations might differ in their effects on resumption of scanning.

The high propensity of *GCN4*'s uORF1 for REI depends on its short length (three codons) and enhancer sequences both 5′ and 3′ of uORF1 (reviewed in reference 18). The 5′ enhancer promotes retention of posttermination 40S subunits on the *GCN4* mRNA by interacting with the NTD of a/Tif32 (49). To explore whether or not g/Tif35-RRM acts in a similar manner, we transformed the *g/tif35-KLF* strain with *GCN4-lacZ* constructs containing solitary uORF1 with progressive deletions of its 5′ enhancer sequence and examined effects of combining the *KLF* with the 5′ enhancer deletions on REI. Previously, epistatic interactions were observed between the 5′ enhancer deletion mutants and *a/tif32-Δ8* (49). In agreement with this study, replacement of the nt −21-AAAATT-nt 16 stretch with CCCCGG or deletions of 40 (Δ*40*) or 46 (Δ*46*) nt from nt −21 upstream of the 5′ sequences of uORF1 progressively reduced the induction of *GCN4-lacZ* expression in WT cells (Fig. 5B, constructs i to iv). The *g/tif35-KLF* mutation reduced expression of *GCN4-lacZ* in the WT uORF1-only construct by ~50% (Fig. 3B, construct vii, and 5B, construct i), and none of the other deletion constructs further decreased this activity. Essentially the same effect was previously observed in *a/tif32-Δ8* cells. However, in striking contrast to *a/tif32-Δ8*, a complete deletion of the 5′ enhancer in Δ*160*, which diminishes *GCN4-lacZ* induction to ~17% in both WT cells (Fig. 5B, construct v) and *a/tif32-Δ8* cells (49), had a negligible additive effect in *g/tif35-KLF* cells (Fig. 5B, compare the ~45% reduction with construct v versus the ~51% reduction with construct iv). Together these findings further suggest that the g/Tif35 RRM and a/Tif32 NTD make synergistic yet independent contributions to the stabilization of posttermination 40S subunits on the *GCN4* mRNA. The fact that combining the *KLF* and Δ*8* mutations in the *tif35*Δ *tif32*Δ double deletion strain resulted in synthetic lethality corroborates this suggestion (data not shown). More importantly, however, our observations also indicate that even though the *g/tif35-KLF* mutation by itself substantially reduces the resumption-of-scanning capacity of 40S ribosomes after uORF1, it concurrently diminishes the requirement of the uORF1 5′ enhancer sequences for efficient REI (see Discussion).

g/Tif35 interacts with the 40S beak proteins Rps20 and Rps3. To gain more insight into the role of the g/Tif35 RRM in the REI mechanism, we wished to predict the g/Tif35 position on the 40S ribosome. Toward this end we tested GST-g/Tif35 for interactions against all 33 small ribosomal proteins (Rps), which were synthesized and ^{35}S-labeled in rabbit reticulocyte lysates. Among all small ribosomal proteins, only Rps3 and Rps20 strongly interacted with GST-g/Tif35; these interactions were independent of the *KLF* mutation (Fig. 6A and data not shown). (Rps2 is shown for specificity, as it lies near Rps3 and 20 [Fig. 6B].)

Based on homology modeling with *E. coli* ribosomal proteins, both Rps3 and -20 were suggested to form the beak on the solvent-exposed side of the 40S subunit (47) (Fig. 6B). The fact that g/Tif35 specifically interacted only with two Rpss occurring next to each other is significant and suggests that this eIF3 subunit most likely occurs somewhere between the head-lobe and the beak regions (Fig. 6C). Based on these and other interactions identified between the a/Tif32 CTD and Rpss 2 and 3 (6) and between the c/Nip1 and the 40S head proteins (T. Kouba and L. Valášek, unpublished observations), we modified our original model for the position of eIF3 on the 40S subunit (51) as follows. The c/Nip1 CTD and the b/Prt1 CTD interacting with i/Tif34 and g/Tif35 were moved upwards to the head region, with the b/Prt1-CTD/i/Tif34/g/Tif35 module stretching toward the beak in proximity of the mRNA entry

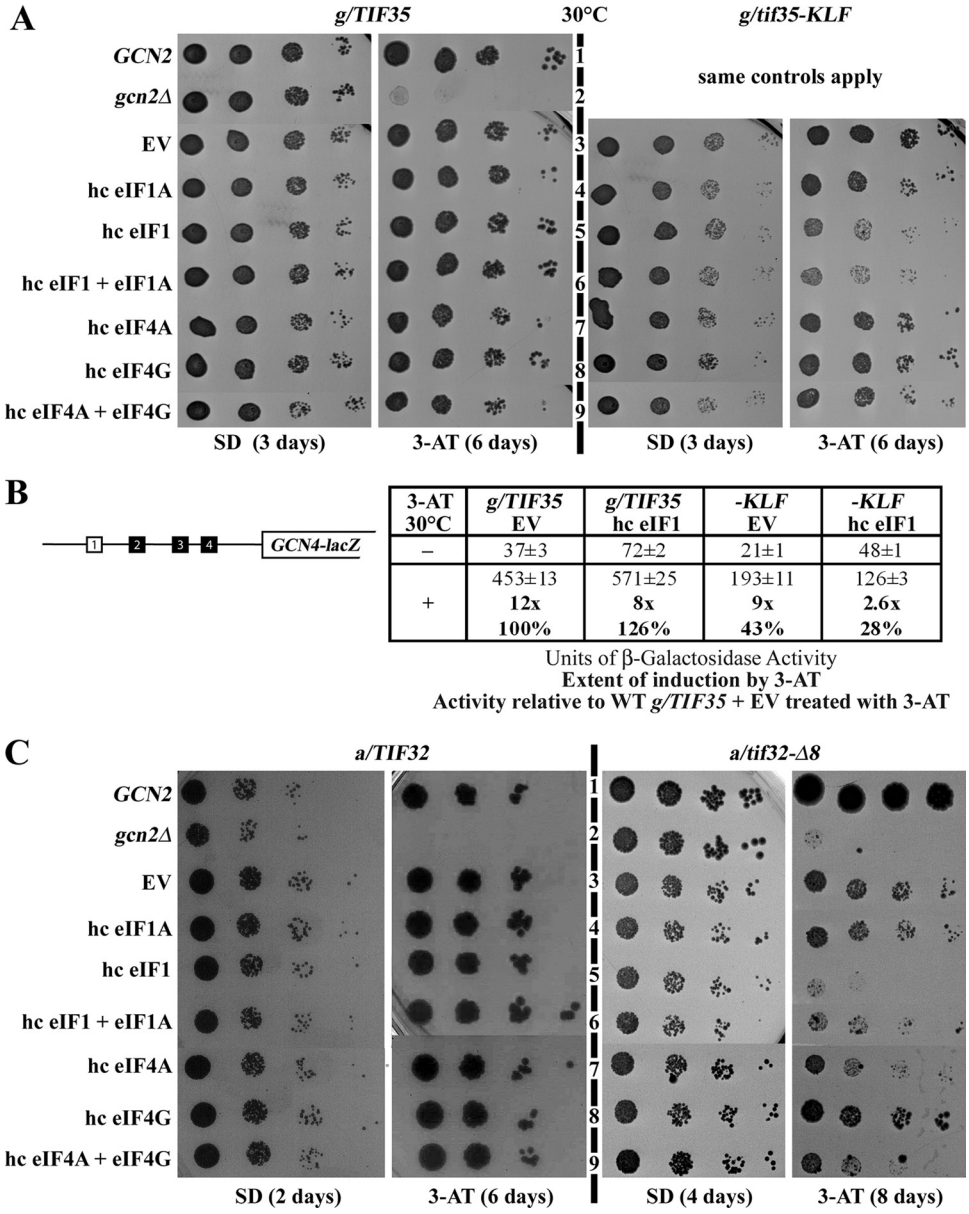

FIG. 4. Overexpression of eIF1 in *g/tif35-KLF* diminishes *GCN4* upregulation upon starvation even at 30°C. (A) Overexpression of eIF1 in *g/tif35-KLF* produces the Gcn$^-$ phenotype at 30°C. Isogenic strains H111(*g/TIF35*) and H112 (*g/tif35-KLF*) were transformed with the following combinations of two vectors: empty vectors YEplac195 and YEplac181 (EV; row 3), pDSO22 and YEplac181 (hc eIF1A; row 4), YEpSUI1-U and YEplac181 (eIF1; row 5), YEp-SUI1 + TIF11 and YEplac181 (eIF1 + eIF1A; row 6), YEpTIF2(4A)-U and YEplac181 (hc eIF4A; row 7), YEpTIF4631(4G)-U and YEplac181 (eIF4G; row 8), YEpTIF2(4A)-L and YEpTIF4631(4G)-U (hc eIF4A + eIF4G; row 9). These strains, together with control strains H464 (*GCN2*; row 1) and H421 (*gcn2*Δ; row 2) transformed with YEplac195 and YEplac181, were spotted in four serial 10-fold dilutions on SD or SD medium containing 30 mM 3-AT and incubated at 30°C for 3 or 6 days, respectively. (B) High-copy-number expression of eIF1 in *g/tif35-KLF* severely blocks induction of *GCN4-lacZ* expression. Isogenic strains H111 (*g/TIF35*) and H112 (*g/tif35-KLF*) transformed either with empty vector YEplac112 (EV) or pCF82 (hc eIF1) were further transformed with p180 and analyzed as described for construct i in Fig. 3B. (C) Overexpression of eIF1 or eIF4A exacerbates the Gcn$^-$ phenotype of *a/tif32-Δ8*. Isogenic strains YBS47 (*a/TIF32*) and YBS53 (*a/tif32-Δ8*) were transformed with the same combinations of two vectors as described for panel A, spotted together with the control strains (as for panel A) in four serial 10-fold dilutions on SD or SD containing 30 mM 3-AT, and incubated at 30°C for 2 to 8 days, as indicated.

channel (Fig. 6C). The a/Tif32 NTD interacts with Rps0 and is thus thought to occur in the vicinity of the mRNA exit channel, where it could interact with the 5′ feature of uORF1 (49). Hence, since both a/Tif32-NTD and g/Tif35-RRM seem to occupy different positions on the back of the 40S, it is indeed conceivable that the nature of their involvement in the initial REI phase is mechanistically different, at least to a certain extent.

i/Tif34 stimulates the rate of scanning. Since eIF3i was, alongside eIF3g, suggested to be dispensable for assembly of the functional 48S PIC in both yeast and mammals (25, 40), we next decided to examine the role of yeast i/Tif34 in scanning

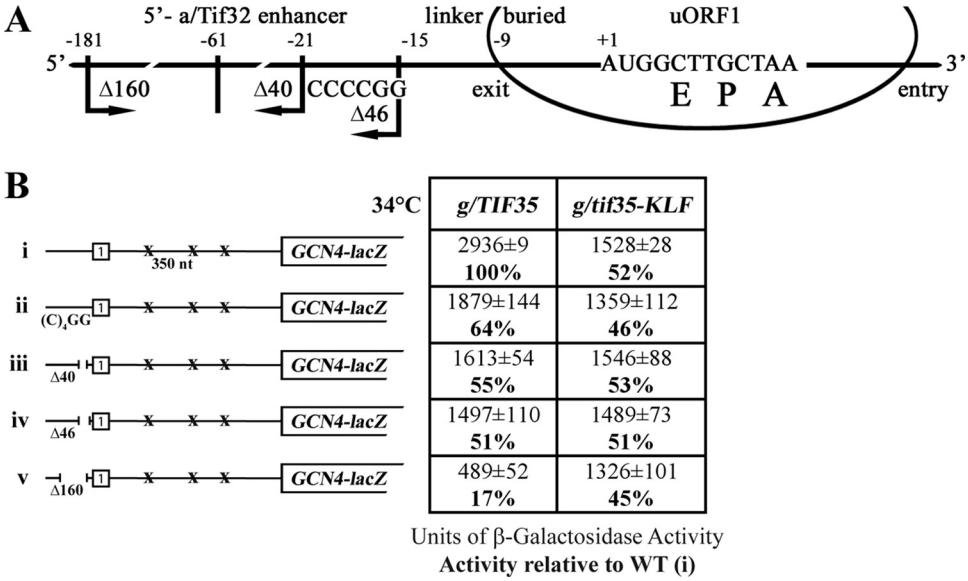

FIG. 5. The *g/tif35-KLF* mutation diminishes the requirement of uORF1 5′ enhancer sequences for efficient REI. (A) Schematic showing the predicted position of the 40S ribosome terminating at the stop codon of uORF1 from the *GCN4* mRNA leader (based on data from reference 49). E, P, and A sites of the 40S ribosomes are aligned with the last two coding triplets and the TAA stop codon. The locations of the 5′ enhancer (labeled 5′-a/Tif32 enhancer to denote the interaction with the NTD of a/Tif32), linker, and buried parts of the sequences upstream of uORF1 are indicated at the top; the 3′ boundaries of the Δ*40* deletion (identical to Δ*160*), Δ*46* deletion, and the $(C)_4GG$ multiple substitution are shown below the line depicting mRNA. (B, constructs i to v) The same experiment as described for construct i in Fig. 3B, except that H111 and H112 were transformed with p209, pBS64, pBS62, pVM11, and pBS63 (constructs i to v, respectively) and analyzed without 3-AT treatment. Activities relative to WT are given as percentages in boldface in the table to the right of the schematics.

and other postassembly processes, in a similar manner as described above for g/Tif35. Yeast i/Tif34 is composed of seven WD40 repeats assembled into a propeller ring and has been shown to interact with the NTD of g/Tif35 and the extreme CTD of b/Prt1 (3, 52). Previously, three growth-defective i/Tif34 mutants were generated and characterized for binding defects (3). Of these, only the *i/tif34-3-HA* (henceforth *i/tif34-Q258R*) mutation, mapping into the WD repeat 6, had no effect on i/Tif34 interactions with g/Tif35 and b/Prt1, yet it showed a >2-fold reduction in the translational rates *in vivo*. These findings indicate that the *Q258R* mutations might have a functional defect rather than a simple assembly problem. Therefore, we selected the *Q258R* mutant for further analysis.

As expected, *i/tif34-Q258R* did not produce the Gcd$^-$ phenotype, which would indicate a defect in TC recruitment *in vivo* (data not shown). However, it did provoke a strong Gcn$^-$ phenotype in the presence of 3-AT (Fig. 7A), resulting from an ~3-fold reduction in the *GCN4* derepression (Fig. 7B, construct i). (This defect was not caused by insufficient phosphorylation of eIF2α [data not shown].) Detailed examination revealed that *i/tif34-Q258R* modestly increases skipping of the AUG start codon of a short uORF preceding the *GCN4-lacZ* gene (by a factor of ~2) (Fig. 7B, constructs iii and iv). More importantly, however, *i/tif34-Q258R* confers strong (~3-fold and ~2.5-fold) increases in expression of the *GCN4-lacZ* constructs containing solitary uORF1 with the 32-nt and 140-nt spacers, respectively (Fig. 7B, constructs v and vi), that are too large to be explained merely by the amount of leaky scanning (compare, for example, construct vi in Fig. 7B, with 1991 − 817, or 1,174 units, with construct iii, with 62 − 28, or 34 units).) Furthermore, increasing the spacing between uORF1 and the *GCN4-lacZ* start site to the natural 350 nt progressively increased *GCN4-lacZ* expression in both strains, as expected; however, the β-galactosidase activity was still ~1.5-fold higher in *i/tif34-Q258R* versus WT cells (Fig. 7B, construct vii). These results are consistent with a defect in the rate of scanning, where the slower-scanning PICs are provided with more time to rebind TC before reaching the next start codon and the closer the solitary uORF1 is to *GCN4-lacZ*, the greater the increase in the frequency of REI. On the other hand, no effect on scanning through stem-loop structures inserted into the uORF-less leader of *GCN4-lacZ* was observed in *i/tif34-Q258R* cells (data not shown), in contrast to *g/tif35-KLF* (Fig. 3B, constructs ix and x). Together, these findings strongly suggest that *i/tif34-Q258R* provokes the Gcn$^-$ phenotype partially by modest leaky scanning over uORF1 but mainly by severe impairment of the rate of scanning between uORF1 and uORF4, which results in an increased number of 40S subunits that rebind TC before reaching inhibitory uORFs 2 to 4. Since *i/tif34-Q258R* has apparently no effect on resumption of scanning, we propose that both observed defects apply equally well to translation of any mRNA in the *Q258R* mutant cells. To our knowledge this is the strongest evidence obtained to date that implicates an eIF3 subunit in stimulating the rate of scanning *in vivo*.

Finally, we examined whether some of the aforementioned scanning-promoting factors could suppress the Gcn$^-$ phenotype of *i/tif34-Q258R*. Strikingly, whereas an increased gene dosage of eIF1 exacerbated the Gcn$^-$ phenotype of the *Q258R* mutant, combined overexpression of eIF1 and eIF1A (i.e., two factors implicated in promotion of scanning [37, 38]) partially suppressed it (Fig. 8A, rows 6 versus 4). This suppression effect

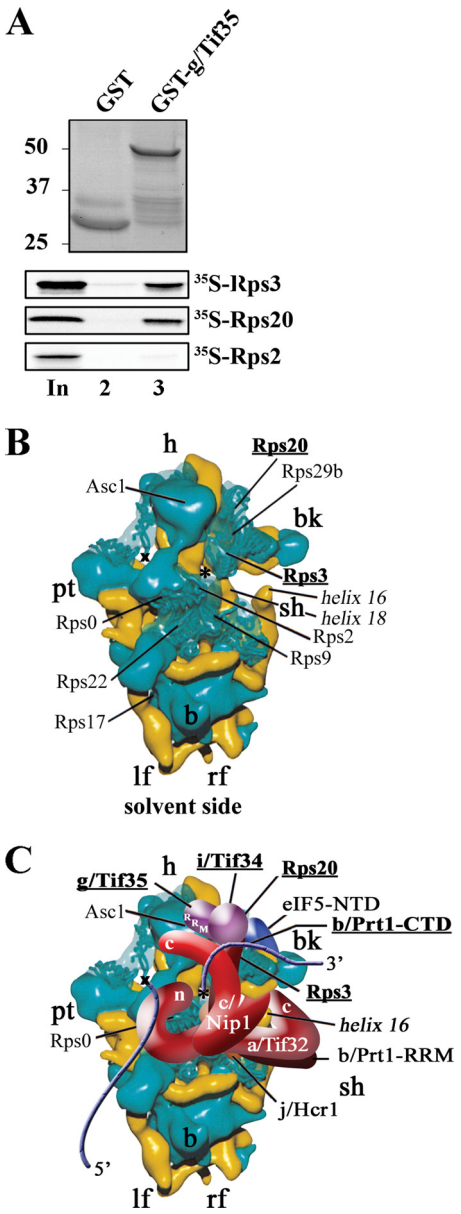

FIG. 6. g/Tif35 specifically interacts with Rps3 and Rps20 situated on the beak of the solvent-exposed side of the 40S subunit. Also shown in a revised model of the hypothetical location of eIF3 on the *S. cerevisiae* small ribosomal subunit. (A) g/Tif35 fused to GST (lane 3) or GST alone (lane 2) was tested for binding to ^{35}S-labeled Rps3, -20, and -2 essentially as described for Fig. 2A. (B and C) Revised hypothetical location of the *S. cerevisiae* eIF3 on the back side of the 40S subunit, based on the data presented in this study and data from reference 51. The cryo-electron microscopy reconstruction of the 40S subunit is shown from the solvent side, with RNA segments in yellow and proteins in green. Positions of Rps3 and Rps20, i/Tif34, the RRM of g/Tif35, and the extreme CTD of b/Prt1 are highlighted in bold. The mRNA entry and exit channels are designated by an asterisk and an X, respectively. The blue lines represent mRNA. Positions of Rps2, -3, and -9 were modified according to findings described in reference 50.

of eIF1 and eIF1A was further verified with the results of our reporter assay, where we showed that simultaneous overexpression of eIF1 and eIF1A increased the *GCN4-lacZ* activity in the *i/tif34-Q258R* cells treated with 3-AT by ~3.5-fold but had no such an effect in the WT cells (Fig. 8B). Finally, we also observed that overexpression of the RNA helicase eIF4A, alone or in combination with eIF4G, greatly exacerbated the Slg$^-$ phenotype of *i/tif34-Q258R*, whereas overexpression of eIF4G alone partially suppressed it (Fig. 8A, rows 7 to 9). Although the molecular basis of these synthetic phenotypes remains to be elucidated, the observed genetic interactions of *i/tif34-Q258R* with the key scanning-promoting factors lend further support to our conclusion that i/Tif34 enhances the rate of the ribosomal scanning.

DISCUSSION

In this paper we have focused on functional characterization of two small subunits of eIF3, g/Tif35 and i/Tif34, the cellular roles of which have remained highly elusive even though these subunits are essential for the viability of yeast cells (15, 21, 30). We found that substitutions of conserved residues of the RRM of g/Tif35 in *g/tif35-KLF* significantly reduced processivity of scanning through a stable stem-loop structure inserted into the uORF-less *GCN4* mRNA leader; this prevented a large proportion of scanning PICs from reaching the coding region (Fig. 3). We also demonstrated that the single point mutation Q258R, mapping to the WD40 repeat 6 of i/Tif34, markedly impairs the rate of scanning of the 40S ribosomes that translate uORF1 and resume scanning downstream (Fig. 7B). The latter severe scanning defect, under starvation conditions with a limited supply of the TC, provides sufficient time for 40S ribosomes en route from uORF1 to *GCN4* to rebind TC before reaching inhibitory uORFs 2 to 4 and thus blocks induction of *GCN4* expression and produces the Gcn$^-$ phenotype (Fig. 7A).

It can be argued that the *GCN4* model system used to explore the scanning properties of posttermination 40S subunits is not suitable for general studies of linear scanning by 48S PICs initiating *de novo* at the mRNA's 5′ end. However, as McCarthy and colleagues elegantly demonstrated, ribosomes scan with the same efficiency after termination on short uORFs as they do when starting from the 5′ cap; therefore, scanning in general is highly processive, with an extremely low off-rate (5). These observations thus validate the employed assay and make our findings applicable to the mechanism of canonical linear scanning. Hence, given that both i/Tif34 and g/Tif35 are dispensable for formation of the 48S PIC at the mRNA's 5′ end in both yeast and mammals (25, 40), and that neither the *i/tif34-Q258R* nor *g/tif35-KLF* mutation affects the integrity of the eIF3 complex (Fig. 2B and reference 3), our results provide the first evidence to date that directly implicates two eIF3 subunits in promoting the rate and processivity of scanning in living cells.

Ostensibly at odds with these conclusions, i/Tif34 and g/Tif35 were found to be dispensable for translation in *in vitro* cell-free systems. Specifically, using the ribosome-binding–toeprinting assay, the mammalian study measured formation of 48S PICs at the AUG codon of β-globin mRNA after a 5-min incubation of all components in a reaction buffer followed by a 10-min incubation with a reverse transcriptase mixture (25). The yeast study monitored the extent of a functional rescue of luciferase mRNA translation in a heat-inactivated *b/prt1-1* extract 70 min after addition of various eIF3 subcomplexes pu-

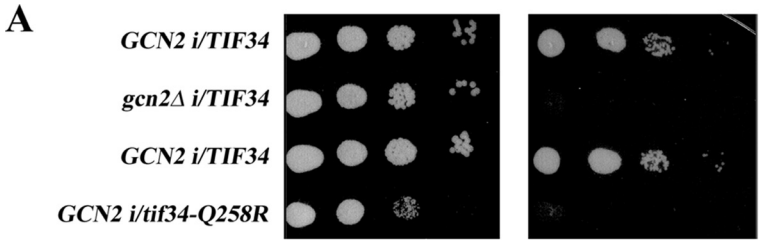

B

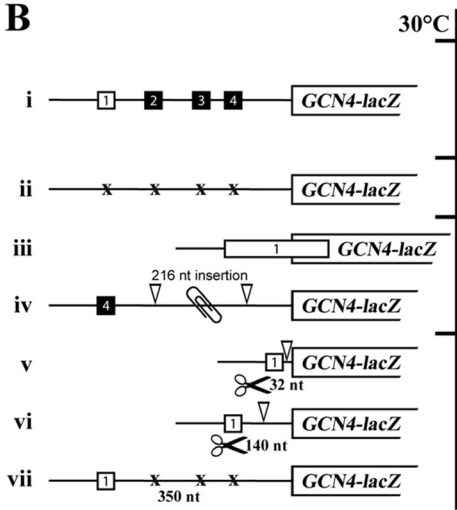

30°C	3-AT	*i/TIF34*	*-Q258R*
i	–	29±2 **100%**	20±4 **69%**
	+	375±22 **100%**	137±7 **37%**
ii	–	6352±534 **100%**	6210±467 **98%**
iii	–	28±1 **100%**	62±3 **221%**
iv	–	33±1 **100%**	56±3 **170%**
v	–	111±13 **100%**	321±18 **289%**
vi	–	817±10 **100%**	1991±53 **244%**
vii	–	2108±101 **100%**	3035±87 **144%**

Units of β-Galactosidase Activity
Activity of i/tif34-*Q258R* relative to WT

FIG. 7. Genetic evidence that *i/tif34-Q258R* prevents induction of *GCN4* expression by a combination of modestly increased leaky scanning of uORF1 and a severe reduction in the rate of scanning from uORF1. (A) *i/tif34-Q258R* imparts a strong Gcn$^-$ phenotype, implicating i/Tif34 in regulation of translational control of *GCN4*. Isogenic strains H450 (*GCN2 i/TIF34*; row 1) and H420 (*gcn2*Δ *i/TIF34*; row 2) transformed with empty vector YCplac111 and strains H120 (*GCN2 i/tif34*Δ YCp111-i/TIF34; row 3) and H121 (*GCN2 i/tif34*Δ YCp111-i/tif34-Q258R; row 4) were spotted in four serial 10-fold dilutions on SD (left panel) or SD containing 30 mM 3-AT (right panel) and then incubated at 30°C for 6 or 8 days, respectively. (B, construct i) *i/tif34-Q258R* prevents full derepression of *GCN4-lacZ* expression upon starvation. Isogenic strains H120 (*i/TIF34*) and H121 (*i/tif34-Q258R*) were transformed with p180 and analyzed as described for construct i in Fig. 3B. (Constructs ii to iv) The *i/tif34-Q258R* mutation increases leaky scanning over the AUG start codon. H120 and H121 were transformed with p227 (ii), pM226 (iii), and pA80z (iv) and analyzed as described for constructs ii to iv in Fig. 3B. (Constructs v to vii) The *i/tif34-Q258R* mutation reduces the rate of scanning of posttermination 40S ribosomes from uORF1. H120 and H121 were transformed with pG67 (v), pM199 (vi), or p209 (vii) and analyzed as described for constructs ii to iv in Fig. 3B.

rified by Ni chelation chromatography (40). In this way the a/Tif32-b/Prt1-c/Nip1 subcomplex was found to be nearly as active as the five-subunit complex, whereas the b/Prt1-i/Tif34-g/Tif35 subcomplex was practically inactive. It must be noted, however, that both approaches focused on the end points of the reactions that were monitored and did not follow the kinetics. As such, neither of them would likely be sensitive enough to detect qualitative defects in the rate and processivity of scanning.

At the same time, it is fair to note that the simple assumption that i/Tif34 and g/Tif35 are merely required to augment activities of other eIFs in scanning would not explain their essentiality for cellular viability in yeasts. To account for this fact, we propose the following. It has been established by numerous labs that the "strength" of a particular mRNA is determined by the presence of stable secondary structures in its 5′-UTR; in general, the closer these structures are to the 5′ cap, the more inhibitory they become (reviewed in reference 22). It is conceivable that a suboptimal rate of scanning might have dramatically diverse effects on translatability of mRNAs differing in both the length and the complexity of their 5′-UTRs. The essential character of both small eIF3 subunits might explained by suggesting that the loss of their stimulatory effects on scanning predominantly compromises translation of a subset of critical mRNAs encoding tightly regulated genes, such as those involved in cell cycle regulation, signal transduction, etc.—mRNAs which often have long 5′-UTRs rich in secondary structures (22, 56). This proposal is consistent with earlier observations showing that (i) specific mutations in i/Tif34 or overexpression of its fission yeast homolog Sum1 deregulates progression through the cell cycle and affects mating and the osmotic stress response (21, 57) and (ii) overexpression of human eIF3i, often observed in carcinomas, resulted in cell size increase, proliferation enhancement, cell cycle progression, and anchorage-independent growth (2). Indeed, we cannot rule out that there might be other essential functions for these two proteins in translation or even func-

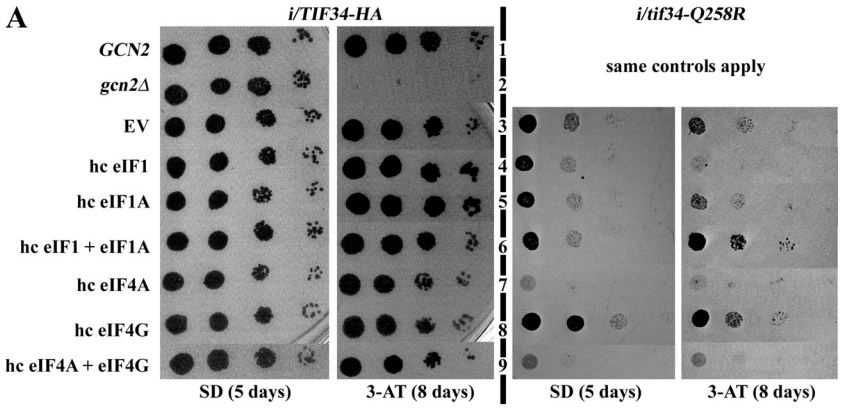

B

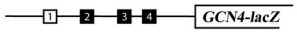

3-AT 34°C	*i/TIF34* EV	*i/TIF34* hc eIFs 1+1A	*-Q258R* EV	*-Q258R* hc eIFs 1+1A
-	23±1	26±1	31±1	40±1
+	379±2 **16x** **100%**	255±4 **10x** **67%**	47±2 **1.5x** **12%**	172±20 **4.3x** **45%**

Units of β-Galactosidase Activity
Extent of induction by 3-AT
Activity relative to WT *i/TIF34* + EV treated with 3-AT

FIG. 8. Simultaneous overexpression of eIFs 1 and 1A partially suppresses the Gcn⁻ phenotype of *i/tif34-Q258R*. (A) Isogenic strains H120 (*i/TIF34*) and H121 (*i/tif34-Q258R*) were transformed with the same combinations of two vectors as for Fig. 4A, spotted together with H450 (*GCN2*; row 1) and H420 (*gcn2*Δ; row 2) transformed with YEplac195 and YEplac181 in four serial 10-fold dilutions on SD or SD containing 10 mM 3-AT, and incubated at 30°C for 5 or 8 days. (B) High-copy-number expression of eIFs 1 and 1A increases the *GCN4-lacZ* activity in the *i/tif34-Q258R* cells treated with 3-AT. Isogenic strains H120 (*i/TIF34*) and H121 (*i/tif34-Q258R*) transformed either with empty vector YEplac112 (EV) or YEp-SUI1+TIF11-W (hc eIF1 + eIF1A) were further transformed with p180 and analyzed as described for construct i in Fig. 3B.

tions that are independent of eIF3. It will be important to subject those regions of both subunits that were not studied here to systematic mutagenesis and investigate their potential roles in translation and beyond.

In support of the *i/TIF34* role in scanning, the Gcn⁻ phenotype of its Q258R mutant was partially suppressed by simultaneous overexpression of eIFs 1 and 1A (Fig. 8), i.e., the two master regulators of scanning (38). Interestingly, overexpression of only eIF1 conversely worsened the effect of *i/tif34-Q258R* on derepression of *GCN4*, as did overexpression of eIF1 alone or in combination with eIF1A in *g/tif35-KLF* cells (Fig. 4). In addition, sole overexpression of the eIF4A helicase exacerbated the Slg⁻ phenotype of *i/tif34-Q258R* but not that of *g/tif35-KLF* cells (Fig. 4 and 8). In both mutants, no effects were associated with other helicases implicated in translation initiation, such as Ded1, Dbp1, and eIF4B. Scanning consists of two linked processes: unwinding of secondary structures in the 5′-UTR and ribosomal movement along it. The 43S PICs can scan unstructured 5′-UTRs without factors associated with RNA unwinding and are thus intrinsically capable of movement along mRNA (38). Omission of eIF1A substantially reduces this ability and lack of eIF1 almost abrogates it, indicating that movement of the 43S complexes requires the open/scanning-conducive conformation induced by the synergistic actions of eIF1 and eIF1A (36). Furthermore, scanning along 5′-UTRs containing even weak secondary structures requires ATP and eIF4A, eIF4G, and eIF4B (38). However, the mechanism by which these factors assist scanning remains unknown. That said, our suppression and synthetic exacerbation genetic data might indicate that *i/tif34-Q258R* impedes full opening of the mRNA entry channel (i.e., the adoption of the scanning-conducive conformation), perhaps in a manner that could be corrected by the mass action of eIF1 and eIF1A. Alternatively, or in addition, both the *Q258R* and *KLF* mutations could predominantly interfere with the action of at least one of the initiation-specific helicases. Given the fact that g/Tif35 specifically interacts with Rps20 and mainly with Rps3 (Fig. 6), which is directly involved in transition between the closed/scanning-incompetent and open/scanning-conducive conformations of the 40S ribosome (36), it could be further proposed that this g/Tif35-Rps3 contact places i/Tif34 in a favorable position to influence the latter conformational transitions. (It should be noted that we did not detect any specific interactions between i/Tif34 and any of the 33 ribosomal proteins.) At the same time, the predicted position of g/Tif35 above the mRNA entry channel may enable its RRM to stimulate scanning by presenting mRNAs to the decoding center and/or by promoting the action of helicases. These options resonate with recent findings suggesting that mammalian eIF3 forms an extension of the mRNA-binding channel that might contribute to scanning (41). g/Tif35 could, for example, act in cooperation with eIF4B, a cofactor for the RNA helicase activity of eIF4F, since yeast g/Tif35 and eIF4B were found to interact (58). At odds with this scenario, however, we did not observe any binding between these two proteins in our GST pulldown assays (data not shown).

It is intriguing that the *g/tif35-KLF* mutation dramatically reduced induction of *GCN4* expression under amino acid starvation by impairing resumption of scanning of posttermination ribosomes from uORF1. The strongest evidence supporting

the nature of this defect was provided by demonstrating that irrespective of the intercistronic distance between uORF1 and the start codon of *GCN4-lacZ*, the efficiency of REI on *GCN4* in the *g/tif35-KLF* cells remained at ~30 to 40% of the WT (Fig. 3). These and other results thus implicate the RRM of g/Tif35, along with the a/Tif32 NTD, in stabilizing uORF1 posttermination 40S ribosomes on *GCN4* mRNA and/or in promoting resumption of scanning for REI downstream. Intriguingly, eIF3g has also been shown to play a critical role in the REI mechanism in plants, where it interacted with the cauliflower mosaic virus transactivator, TAV, and promoted translation reinitiation of viral polycistronic mRNAs (35).

The key feature of *GCN4*'s uORF1 is its ability to allow a high frequency of resumption of scanning after its translation; this ability depends on its short length (three codons) and its 5′ and 3′ enhancer sequences (18). Importantly, we have recently demonstrated that the postinitiation retention of eIF3 on 80S ribosomes translating uORF1 is likewise critical for uORF1's full REI capacity, owing to the fact that the 5′ enhancer sequences interact with the NTD of a/Tif32 and thus stabilize the posttermination 40S subunit on *GCN4* mRNA (49).

Several lines of evidence suggest that even though both the a/Tif32 NTD and the g/Tif35 RRM are critical for this initial REI phase, their individual roles differ. First, combining *g/tif35-KLF* with the N-terminal deletion of a/Tif32 in *a/tif32-Δ8* resulted in a synthetic lethal phenotype. Also, our suppression/exacerbation analysis with scanning-promoting eIFs at high copy numbers revealed different effects on the Gcn$^-$ phenotypes of *g/tif35-KLF* versus *a/tif32-Δ8* mutants (Fig. 4). Third, the a/Tif32 NTD and the g/Tif35 RRM domains seem to occur on opposing pores of the mRNA-binding channel. Furthermore, our detailed genetic analysis strongly suggests that the g/Tif35 RRM does not promote resumption of scanning in cooperation with the 5′ enhancer of uORF1 (Fig. 5). Finally, the indisputable functional importance of uORF1's 5′ enhancer is practically eliminated in the background of the *KLF* mutation (Fig. 5B, construct v). Interestingly, somewhat similar results were observed when the *GCN4* leader lacking the 5′ enhancer sequences of uORF1 was placed in front of the recombinant *GAL1-lacZ* gene (28). The resulting construct was unexpectedly fully capable of conferring the *GCN4*-like mode of translational control upon the *GAL1-lacZ* transcript. Besides the coding sequence, the only other region in which the *GCN4-lacZ* and *GAL1-lacZ* constructs differed were their 3′-UTRs, which corresponded to the genuine chromosomal sequence of each gene. These findings might imply that the *GCN4* 3′-UTR plays an inhibitory role in the *GCN4* translational control mechanism, perhaps as a part of the 5′-cap/eIF4E/eIF4G/PAB1/3′-UTR closed-loop structure (59). It will be intriguing to examine how exactly the g/Tif35 RRM and the *GCN4* 3′-UTR contribute to reinitiation and whether there is any functional connection between them.

ACKNOWLEDGMENTS

We are thankful to the members of the Valášek and Krásný laboratories for helpful comments and to Olga Krydová for technical and administrative assistance. We are also indebted to Monica Liu for critical reading of the manuscript and Olga Janoušková and Edit Rutkai for their help with site-directed mutagenesis of the g/Tif35-RRM and GST pulldown experiments with the small ribosomal proteins, respectively.

This research was supported by the Howard Hughes Medical Institute, The Wellcome Trust grant 076456/Z/05/Z, a Fellowship of Jan E. Purkyne from the Academy of Sciences of the Czech Republic, and Institutional Research Concept AV0Z50200510.

REFERENCES

1. **Abastado, J. P., P. F. Miller, B. M. Jackson, and A. G. Hinnebusch.** 1991. Suppression of ribosomal reinitiation at upstream open reading frames in amino acid-starved cells forms the basis for *GCN4* translational control. Mol. Cell. Biol. **11:**486–496.
2. **Ahlemann, M., R. Zeidler, S. Lang, B. Mack, M. Münz, and O. Gires.** 2006. Carcinoma-associated eIF3i overexpression facilitates mTOR-dependent growth transformation. Mol. Carcinog. **45:**957–967.
3. **Asano, K., L. Phan, J. Anderson, and A. G. Hinnebusch.** 1998. Complex formation by all five homologues of mammalian translation initiation factor 3 subunits from yeast *Saccharomyces cerevisiae*. J. Biol. Chem. **273:**18573–18585.
4. **Asano, K., H.-P. Vornlocher, N. J. Richter-Cook, W. C. Merrick, A. G. Hinnebusch, and J. W. B. Hershey.** 1997. Structure of cDNAs encoding human eukaryotic initiation factor 3 subunits: possible roles in RNA binding and macromolecular assembly. J. Biol. Chem. **272:**27042–27052.
5. **Berthelot, K., M. Muldoon, L. Rajkowitsch, J. Hughes, and J. E. G. McCarthy.** 2004. Dynamics and processivity of 40S ribosome scanning on mRNA in yeast. Mol. Microbiol. **51:**987–1001.
6. **Chiu, W. L., S. Wagner, A. Herrmannova, L. Burela, F. Zhang, A. K. Saini, L. Valasek, and A. G. Hinnebusch.** 28 June 2010. The C-terminal region of eIF3a promotes mRNA recruitment, scanning and, together with eIF3j and the eIF3b RRM, selection of AUG start codons. Mol. Cell Biol. doi:10.1128/MCB.00280-10.
7. **de la Cruz, J., I. Iost, D. Kressler, and P. Linder.** 1997. The p20 and Ded1 proteins have antagonistic roles in eIF4E-dependent translation in Saccharomyces cerevisiae. Proc. Natl. Acad. Sci. U. S. A. **94:**5201–5206.
8. **Dever, T. E., L. Feng, R. C. Wek, A. M. Cigan, T. D. Donahue, and A. G. Hinnebusch.** 1992. Phosphorylation of initiation factor 2α by protein kinase GCN2 mediates gene-specific translational control of *GCN4* in yeast. Cell **68:**585–596.
9. **ElAntak, L., S. Wagner, A. Herrmannova, M. Karáskova, E. Rutkai, P. J. Lukavsky, and L. Valášek.** 2010. The indispensable N-terminal half of eIF3j co-operates with its structurally conserved binding partner eIF3b-RRM and eIF1A in stringent AUG selection. J. Mol. Biol. **396:**1097–1116.
10. **Fekete, C. A., S. F. Mitchell, V. A. Cherkasova, D. Applefield, M. A. Algire, D. Maag, A. K. Saini, J. R. Lorsch, and A. G. Hinnebusch.** 2007. N- and C-terminal residues of eIF1A have opposing effects on the fidelity of start codon selection. EMBO J. **26:**1602–1614.
11. **Gietz, R. D., and A. Sugino.** 1988. New yeast-Escherichia coli shuttle vectors constructed with in vitro mutagenized yeast genes lacking six-base pair restriction sites. Gene **74:**527–534.
12. **Grant, C. M., and A. G. Hinnebusch.** 1994. Effect of sequence context at stop codons on efficiency of reinitiation in *GCN4* translational control. Mol. Cell. Biol. **14:**606–618.
13. **Grant, C. M., P. F. Miller, and A. G. Hinnebusch.** 1994. Requirements for intercistronic distance and level of eIF-2 activity in reinitiation on GCN4 mRNA varies with the downstream cistron. Mol. Cell. Biol. **14:**2616–2628.
14. **Grant, C. M., P. F. Miller, and A. G. Hinnebusch.** 1995. Sequences 5′ of the first upstream open reading frame in *GCN4* mRNA are required for efficient translational reinitiation. Nucleic Acids Res. **23:**3980–3988.
15. **Hanachi, P., J. W. B. Hershey, and H. P. Vornlocher.** 1999. Characterization of the p33 subunit of eukaryotic translation initiation factor-3 from *Saccharomyces cerevisiae*. J. Biol. Chem. **274:**8546–8553.
16. **Hannig, E. M., A. M. Cigan, B. A. Freeman, and T. G. Kinzy.** 1992. *GCD11*, a negative regulator of *GCN4* expression, encodes the γ subunit of eIF-2 in *Saccharomyces cerevisiae*. Mol. Cell. Biol. **13:**506–520.
17. **Hinnebusch, A. G.** 2006. eIF3: a versatile scaffold for translation initiation complexes. Trends Biochem. Sci. **31:**553–562.
18. **Hinnebusch, A. G.** 2005. Translational regulation of GCN4 and the general amino acid control of yeast. Annu. Rev. Microbiol. **59:**407–450.
19. **Hinnebusch, A. G., K. Asano, D. S. Olsen, L. O. N. Phan, K. H. Nielsen, and L. Valasek.** 2004. Study of translational control of eukaryotic gene expression using yeast. Ann. N. Y. Acad. Sci. **1038:**60–74.
20. **Hinnebusch, A. G., T. E. Dever, and K. A. Asano.** 2007. Mechanism of translation initiation in the yeast Saccharomyces cerevisiae, p. 225–268. *In* N. Sonenberg, M. Mathews, and J. W. B. Hershey (ed.), Translational control in biology and medicine. Cold Spring Harbor Laboratory Press, Cold Spring Harbor, NY.
21. **Humphrey, T., and T. Enoch.** 1998. Sum1, a highly conserved WD-repeat protein, suppresses S-M checkpoint mutants and inhibits the osmotic stress cell cycle response in fission yeast. Genetics **148:**1731–1742.
22. **Kozak, M.** 2005. Regulation of translation via mRNA structure in prokaryotes and eukaryotes. Gene **361:**13–37.
23. **Lee, J. H., T. V. Pestova, B. S. Shin, C. Cao, S. K. Choi, and T. E. Dever.** 2002. Initiation factor eIF5B catalyzes second GTP-dependent step in eu-

karyotic translation initiation. Proc. Natl. Acad. Sci. U. S. A. **99:**16689–16694.
24. **Maris, C., C. Dominguez, and F. H.-T. Allain.** 2005. The RNA recognition motif, a plastic RNA-binding platform to regulate post-transcriptional gene expression. FEBS J. **272:**2118–2131.
25. **Masutani, M., N. Sonenberg, S. Yokoyama, and I. H.** 2007. Reconstitution reveals the functional core of mammalian eIF3. EMBO J. **26:**3373–3383.
26. **Miller, P. F., and A. G. Hinnebusch.** 1989. Sequences that surround the stop codons of upstream open reading frames in *GCN4* mRNA determine their distinct functions in translational control. Genes Dev. **3:**1217–1225.
27. **Mitchell, S. F., and J. R. Lorsch.** 2008. Should I stay or should I go? Eukaryotic translation initiation factors 1 and 1a control start codon recognition. J. Biol. Chem. **283:**27345–27349.
28. **Mueller, P. P., S. Harashima, and A. G. Hinnebusch.** 1987. A segment of *GCN4* mRNA containing the upstream AUG codons confers translational control upon a heterologous yeast transcript. Proc. Natl. Acad. Sci. U. S. A. **84:**2863–2867.
29. **Mueller, P. P., and A. G. Hinnebusch.** 1986. Multiple upstream AUG codons mediate translational control of *GCN4*. Cell **45:**201–207.
30. **Naranda, T., M. Kainuma, S. E. McMillan, and J. W. B. Hershey.** 1997. The 39-kilodalton subunit of eukaryotic translation initiation factor 3 is essential for the complex's integrity and for cell viability in *Saccharomyces cerevisiae*. Mol. Cell. Biol. **17:**145–153.
31. **Nielsen, K. H., B. Szamecz, L. J. Valasek, A., B. S. Shin, and A. G. Hinnebusch.** 2004. Functions of eIF3 downstream of 48S assembly impact AUG recognition and GCN4 translational control. EMBO J. **23:**1166–1177.
32. **Nielsen, K. H., and L. Valášek.** 2007. In vivo deletion analysis of the architecture of a multi-protein complex of translation initiation factors. Methods Enzymol. **431:**15–32.
33. **Nielsen, K. H., L. Valášek, C. Sykes, A. Jivotovskaya, and A. G. Hinnebusch.** 2006. Interaction of the RNP1 motif in PRT1 with HCR1 promotes 40S binding of eukaryotic initiation factor 3 in yeast. Mol. Cell. Biol. **26:**2984–2998.
34. **Olsen, D. S., E. M. Savner, A. Mathew, F. Zhang, T. Krishnamoorthy, L. Phan, and A. G. Hinnebusch.** 2003. Domains of eIF1A that mediate binding to eIF2, eIF3 and eIF5B and promote ternary complex recruitment *in vivo*. EMBO J. **22:**193–204.
35. **Park, H. S., A. Himmelbach, K. S. Browning, T. Hohn, and L. A. Ryabova.** 2001. A plant viral "reinitiation" factor interacts with the host translational machinery. Cell **106:**723–733.
36. **Passmore, L. A., T. M. Schmeing, D. Maag, D. J. Applefield, M. G. Acker, M. A. Algire, J. R. Lorsch, and V. Ramakrishnan.** 2007. The eukaryotic translation initiation factors eIF1 and eIF1A induce an open conformation of the 40S ribosome. Mol. Cell **26:**41–50.
37. **Pestova, T. V., S. I. Borukhov, and C. U. T. Hellen.** 1998. Eukaryotic ribosomes require initiation factors 1 and 1A to locate initiation codons. Nature **394:**854–859.
38. **Pestova, T. V., and V. G. Kolupaeva.** 2002. The roles of individual eukaryotic translation initiation factors in ribosomal scanning and initiation codon selection. Genes Dev. **16:**2906–2922.
39. **Pestova, T. V., J. R. Lorsch, and C. U. T. Hellen.** 2007. The mechanism of translation initiation in eukaryotes, p. 87–128. *In* N. Sonenberg, M. Mathews, and J. W. B. Hershey (ed.), Translational control in biology and medicine. Cold Spring Harbor Laboratory Press, Cold Spring Harbor, NY.
40. **Phan, L., L. W. Schoenfeld, L. Valášek, K. H. Nielsen, and A. G. Hinnebusch.** 2001. A subcomplex of three eIF3 subunits binds eIF1 and eIF5 and stimulates ribosome binding of mRNA and $tRNA_i^{Met}$. EMBO J. **20:**2954–2965.
41. **Pisarev, A. V., C. U. T. Hellen, and T. V. Pestova.** 2007. Recycling of eukaryotic posttermination ribosomal complexes. Cell **131:**286–299.
42. **Pöyry, T. A., A. Kaminski, E. J. Connell, C. S. Fraser, and R. J. Jackson.** 2007. The mechanism of an exceptional case of reinitiation after translation of a long ORF reveals why such events do not generally occur in mammalian mRNA translation. Genes Dev. **21:**3149–3162.
43. **Pöyry, T. A., A. Kaminski, and R. J. Jackson.** 2004. What determines whether mammalian ribosomes resume scanning after translation of a short upstream open reading frame? Genes Dev. **18:**62–75.
44. **Ruiz-Echevarria, M. J., and S. W. Peltz.** 2000. The RNA binding protein Pub1 modulates the stability of transcripts containing upstream open reading frames. Cell **101:**741–751.
45. **Siridechadilok, B., C. S. Fraser, R. J. Hall, J. A. Doudna, and E. Nogales.** 2005. Structural roles for human translation factor eIF3 in initiation of protein synthesis. Science **310:**1513–1515.
46. **Smith, D. B., and K. S. Johnson.** 1988. Single-step purification of polypeptides expressed in Escherichia coli as fusions with glutathione S-transferase. Gene **67:**31–40.
47. **Spahn, C. M., R. Beckmann, N. Eswar, P. A. Penczek, A. Sali, G. Blobel, and J. Frank.** 2001. Structure of the 80S ribosome from Saccharomyces cerevisiae-tRNA ribosome and subunit-subunit interactions. Cell **107:**373–386.
48. **Srivastava, S., A. Verschoor, and J. Frank.** 1992. Eukaryotic initiation factor 3 does not prevent association through physical blockage of the ribosomal subunit-subunit interface. J. Mol. Biol. **220:**301–304.
49. **Szamecz, B., E. Rutkai, L. Cuchalova, V. Munzarova, A. Herrmannova, K. H. Nielsen, L. Burela, A. G. Hinnebusch, and L. Valášek.** 2008. eIF3a cooperates with sequences 5′ of uORF1 to promote resumption of scanning by post-termination ribosomes for reinitiation on GCN4 mRNA. Genes Dev. **22:**2414–2425.
50. **Taylor, D. J., B. Devkota, A. D. Huang, M. Topf, E. Narayanan, A. Sali, S. C. Harvey, and J. Frank.** 2009. Comprehensive molecular structure of the eukaryotic ribosome. Structure **17:**1591–1604.
51. **Valášek, L., A. Mathew, B. S. Shin, K. H. Nielsen, B. Szamecz, and A. G. Hinnebusch.** 2003. The yeast eIF3 subunits TIF32/a and NIP1/c and eIF5 make critical connections with the 40S ribosome in vivo. Genes Dev. **17:**786–799.
52. **Valášek, L., K. H. Nielsen, and A. G. Hinnebusch.** 2002. Direct eIF2-eIF3 contact in the multifactor complex is important for translation initiation in vivo. EMBO J. **21:**5886–5898.
53. **Valášek, L., K. H. Nielsen, F. Zhang, C. A. Fekete, and A. G. Hinnebusch.** 2004. Interactions of eukaryotic translation initiation factor 3 (eIF3) subunit NIP1/c with eIF1 and eIF5 promote preinitiation complex assembly and regulate start codon selection. Mol. Cell. Biol. **24:**9437–9455.
54. **Valášek, L., L. Phan, L. W. Schoenfeld, V. Valášková, and A. G. Hinnebusch.** 2001. Related eIF3 subunits TIF32 and HCR1 interact with an RNA recoginition motif in PRT1 required for eIF3 integrity and ribosome binding. EMBO J. **20:**891–904.
55. **Valášek, L., B. Szamecz, A. G. Hinnebusch, and K. H. Nielsen.** 2007. In vivo stabilization of preinitiation complexes by formaldehyde cross-linking. Methods Enzymol. **429:**163–183.
56. **van der Velden, A. W., and A. A. M. Thomas.** 1999. The role of the 5′ untranslated region of an mRNA in translation regulation during development. Int. J. Biochem. Cell Biol. **31:**87–106.
57. **Verlhac, M.-H., R.-H. Chen, P. Hanachi, J. W. B. Hershey, and R. Derynck.** 1997. Identification of partners of TIF34, a component of the yeast eIF3 complex, required for cell proliferation and translation initiation. EMBO J. **16:**6812–6822.
58. **Vornlocher, H. P., P. Hanachi, S. Ribeiro, and J. W. B. Hershey.** 1999. A 110-kilodalton subunit of translation initiation factor eIF3 and an associated 135-kilodalton protein are encoded by the *Saccharomyces cerevisiae TIF32* and *TIF31* genes. J. Biol. Chem. **274:**16802–16812.
59. **Wells, S. E., P. E. Hillner, R. D. Vale, and A. B. Sachs.** 1998. Circularization of mRNA by eukaryotic translation initiation factors. Mol. Cell **2:**135–140.
60. **Williams, N. P., A. G. Hinnebusch, and T. F. Donahue.** 1989. Mutations in the structural genes for eukaryotic initiation factors 2α and 2β of *Saccharomyces cerevisiae* disrupt translational control of *GCN4* mRNA. Proc. Natl. Acad. Sci. U. S. A. **86:**7515–7519.
61. **Yamamoto, Y., C. R. Singh, A. Marintchev, N. S. Hall, E. M. Hannig, G. Wagner, and K. Asano.** 2005. The eukaryotic initiation factor (eIF) 5 HEAT domain mediates multifactor assembly and scanning with distinct interfaces to eIF1, eIF2, eIF3, and eIF4G. Proc. Natl. Acad. Sci. U. S. A. **102:**16164–16169.
62. **Zhou, M., A. M. Sandercock, C. S. Fraser, G. Ridlova, E. Stephens, M. R. Schenauer, T. Yokoi-Fong, D. Barsky, J. A. Leary, J. W. Hershey, J. A. Doudna, and C. V. Robinson.** 2008. Mass spectrometry reveals modularity and a complete subunit interaction map of the eukaryotic translation factor eIF3. Proc. Natl. Acad. Sci. U. S. A. **105:**18139–18144.

Structural analysis of an eIF3 subcomplex reveals conserved interactions required for a stable and proper translation pre-initiation complex assembly.

Herrmannová A, Daujotyte D, Yang JC, Cuchalová L, Gorrec F, Wagner S, Dányi I, Lukavsky PJ, Valásek LS.

Nucleic Acids Res. 2012 Mar;40(5):2294-311. doi: 10.1093/nar/gkr765. Epub 2011 Nov 15.

This study describes the first structural information (a crystal structure at 2 2.2 Å) on a yeast core eIF3 subunit, i/TIF34, bound to the C-terminus of the eIF3 scaffold protein b/PRT1. Mutating the conserved residues mediating the b/PRT1—i/TIF34 contact results in lethality or severe growth phenotypes owing to the loss of the i/TIF34-g/TIF35 mini-module from the rest of eIF3 and from pre-initiation complexes (PICs). Since binding of the remaining a/TIF32-b/PRT1-c/NIP1 subcomplex and eIF5 is also unexpectedly destabilized, aberrant PICs containing eIFs 2 and 1 accumulate and dramatically increase leaky scanning over the AUG start codon in the manner suppressible by overexpression of g/TIF35 and eIF1. Hence, we propose that stable association of the i/TIF34–g/TIF35 mini-module with the rest of eIF3 via b/PRT1 significantly stabilizes binding of eIF3 and eIF5 to the nascent pre-initiation complexes in vivo. This way these critical interactions serve to prevent accumulation of mis-assembled PICs on mRNAs and thus ensure stringent selection of the AUG start codon.

2294–2311 *Nucleic Acids Research, 2012, Vol. 40, No. 5* *Published online 15 November 2011*
doi:10.1093/nar/gkr765

Structural analysis of an eIF3 subcomplex reveals conserved interactions required for a stable and proper translation pre-initiation complex assembly

Anna Herrmannová[1], Dalia Daujotytė[2], Ji-Chun Yang[2], Lucie Cuchalová[1], Fabrice Gorrec[2], Susan Wagner[1], István Dányi[1], Peter J. Lukavsky[2,*] and Leoš Shivaya Valášek[1,*]

[1]Laboratory of Regulation of Gene Expression, Institute of Microbiology ASCR, v.v.i., Videnska 1083, Prague, 142 20, the Czech Republic and [2]MRC-Laboratory of Molecular Biology, Structural Studies Division, Hills Road, Cambridge, CB2 0QH, UK

Received May 24, 2011; Revised August 31, 2011; Accepted September 1, 2011

ABSTRACT

Translation initiation factor eIF3 acts as the key orchestrator of the canonical initiation pathway in eukaryotes, yet its structure is greatly unexplored. We report the 2.2 Å resolution crystal structure of the complex between the yeast seven-bladed β-propeller eIF3i/TIF34 and a C-terminal α-helix of eIF3b/PRT1, which reveals universally conserved interactions. Mutating these interactions displays severe growth defects and eliminates association of eIF3i/TIF34 and strikingly also eIF3g/TIF35 with eIF3 and 40S subunits *in vivo*. Unexpectedly, 40S-association of the remaining eIF3 subcomplex and eIF5 is likewise destabilized resulting in formation of aberrant pre-initiation complexes (PICs) containing eIF2 and eIF1, which critically compromises scanning arrest on mRNA at its AUG start codon suggesting that the contacts between mRNA and ribosomal decoding site are impaired. Remarkably, overexpression of eIF3g/TIF35 suppresses the leaky scanning and growth defects most probably by preventing these aberrant PICs to form. Leaky scanning is also partially suppressed by eIF1, one of the key regulators of AUG recognition, and its mutant *sui1*^{G107R} but the mechanism differs. We conclude that the C-terminus of eIF3b/PRT1 orchestrates co-operative recruitment of eIF3i/TIF34 and eIF3g/TIF35 to the 40S subunit for a stable and proper assembly of 48S pre-initiation complexes necessary for stringent AUG recognition on mRNAs.

INTRODUCTION

Canonical translation initiation ensures timely and spatially coordinated formation of the trimeric complex between the 40S small ribosomal subunit (40S subunit), initiator Met-tRNA$_i^{Met}$ and an mRNA at its extreme 5′ end, and concludes with the assembly of an elongation-competent 80S ribosome at the authentic AUG start codon. The entire process is orchestrated by numerous eukaryotic initiation factors (eIFs) with eIF3 representing the most intricate factor (1). The multiple essential roles of eIF3 during initiation include stabilization of eIF2/GTP/Met-tRNA$_i^{Met}$ ternary complex (TC) binding to 40S subunits, recruitment of 5′-^{7m}G capped mRNAs to 40S subunits, assistance in scanning of the 5′ untranslated region (5′ UTR) of the mRNA, and finally in aiding AUG initiation codon recognition (2).

This crucial involvement of eIF3 in nearly every step of translation initiation is also reflected in its structural complexity. Mammalian eIF3 consists of at least 13 subunits (eIF3a-m) assembled into a 750 kDa particle. In budding yeast, eIF3 comprises five essential core subunits (a/TIF32, b/PRT1, c/NIP1, i/TIF34, g/TIF35) and one loosely associated, non-essential subunit j/HCR1, all of which have corresponding orthologs in mammals (1).

*To whom correspondence should be addressed. Tel: +42 (0) 241 062 288; Fax: +42 (0) 241 062 665; Email: valasekl@biomed.cas.cz
Correspondence may also be addressed to Peter J. Lukavsky. Tel: +41 (0)44 633 39 40; Fax: +41 (0)44 633 12 94; Email: lpeter@mol.biol.ethz.ch
Present addresses:
Peter J. Lukavsky, Institute of Molecular Biology and Biophysics, ETH Hönggerberg, Schafmattstrasse 20, Zürich, Switzerland.
Dalia Daujotyte, Lexogen GmbH, Campus Vienna Biocenter 5, 1030 Vienna, Austria.

The authors wish it to be known that, in their opinion, the first two authors should be regarded as joint First Authors.

At least in yeast, this core eIF3 complex associates with eIFs 1, 5 and the TC *in vivo* to form the so-called multifactor complex (MFC). Surprisingly, detailed biochemical analysis carried out with purified eIF3 subcomplexes identified that the trimeric complex of a/TIF32, b/PRT1 and c/NIP1 promoted TC and mRNA recruitment to the 40S subunit and even stimulated translation *in vitro* on a model mRNA as efficiently as the wild-type (wt) five subunit complex (3). Hence given the fact that i/TIF34 and g/TIF35 subunits are otherwise essential for cell proliferation and their individual depletions result in a typical polysome run-off (4), these results perhaps indicate that their contributions to general translation initiation have a more stimulatory character. Indeed, we have recently shown that both small eIF3 subunits augment various aspects of linear scanning and, as such, may have differential effects on efficiency of translation of coding mRNAs containing short, less structured versus long, highly structured 5′ UTRs (5). Interestingly, *in vitro* reconstitution of human eIF3 also supported the dispensability of highly conserved eIF3g and eIF3i in stimulation of canonical eIF3 functions. Instead, non-conserved eIF3e, eIF3f and eIF3h in complex with eIF3a, eIF3b, and eIF3c were proposed to be the functionally indispensable subunits of mammalian eIF3 (6). In contrast, however, two other groups reported purification of a human eIF3 subcomplex closely resembling the yeast core eIF3 complex (7,8). Hence more experiments are required to clarify these discrepancies.

The structural complexity of eIF3 is well illustrated by its elaborate subunit–subunit interaction web, which has been mapped in great detail for yeast eIF3 and its associated eIFs (9). The b/PRT1 subunit serves as the major scaffolding subunit of eIF3 and associates with the other core subunits in both yeast and mammals (7–10). The b/PRT1 N-terminal domain (NTD) contains a conserved RNA recognition motif (RRM) (11,12), which provides an interaction surface for the C-terminal half of a/TIF32 and the NTD of j/HCR1 (12,13), followed by a middle domain predicted to fold into two β-propeller structures (14), the second of which contains a binding site for c/NIP1. Finally, the extreme C-terminal domain (CTD) of the b/PRT1 scaffold is required for association of i/TIF34 and g/TIF35 subunits (10). Whereas i/TIF34 is predicted to adopt a seven-bladed β-propeller structure made up of seven WD-40 repeats with unknown binding sites for b/PRT1 and g/TIF35, the latter subunit interacts with i/TIF34 and b/PRT1 through its NTD containing a predicted Zn-finger domain (10). The g/TIF35-CTD then adopts an RRM fold that is not involved in any subunit–subunit interactions (9,10). Better understanding of all functions of individual interactions among eIF3 subunits clearly requires more detailed information at the molecular level; however, no atomic structures of any yeast eIF3 subunits have been determined to date.

Here we report the 2.2 Å resolution crystal structure of the i/TIF34 subunit in complex with the minimal CTD of b/PRT1 (654–700), the boundaries of which we defined by solution NMR spectroscopy. Mutating the conserved residues mediating the b/PRT1—i/TIF34 contact results in lethality or severe growth phenotypes owing to the loss of the i/TIF34-g/TIF35 mini-module from the rest of eIF3 and from pre-initiation complexes (PICs). Since binding of the remaining a/TIF32-b/PRT1-c/NIP1 subcomplex and eIF5 is also unexpectedly destabilized, aberrant PICs containing eIFs 2 and 1 accumulate and dramatically increase leaky scanning over the AUG start codon in the manner suppressible by overexpression of g/TIF35 and eIF1. Hence we propose that stable association of the i/TIF34–g/TIF35 mini-module with the rest of eIF3 *via* b/PRT1 significantly stabilizes binding of eIF3 and eIF5 to the nascent pre-initiation complexes *in vivo*. This way these critical interactions serve to prevent accumulation of mis-assembled PICs on mRNAs and thus ensure stringent selection of the AUG start codon.

MATERIALS AND METHODS

Protein expression and purification

DNA fragments encoding yeast i/TIF34 and b/PRT1(630–724) were prepared by PCR from pGEX–TIF34 or pGEX–PRT1, respectively (10), using appropriate primers and subcloned into pET28a vector (Novagen) with a Tobacco Etch Virus (TEV) protease cleavage site instead of the original thrombin cleavage site. A DNA fragment encoding b/PRT1(654–700) was prepared by PCR from b/PRT1(630–724) plasmid DNA and subcloned into a modified pET28a vector (Novagen, containing an N-terminal His_6-tag fused to a lipoyl domain (12,15) followed by a TEV cleavage site and the standard pET28a multiple cloning site). Point mutations in b/PRT1(630–724) were introduced following the QuickChange protocol (Stratagene). Proteins were expressed in *Escherichia coli* Rosetta(DE3) cells (Novagen) in LB rich or M9 minimal media supplemented with $^{15}NH_4Cl$ or $^{15}NH_4Cl$ and ^{13}C-glucose. Protein expression was induced by addition of 1 mM IPTG at OD_{600} of ~0.8 and further incubation for 14 h at 16° C. All proteins were purified using two 5 mL HiTrap chelating columns (HiTrap, GE Healthcare) in series and charged with nickel sulfate under standard conditions (lysis and loading buffer A: 20 mM HEPES pH 7.5, 500 mM NaCl, 30 mM imidazole, 10% glycerol (w/v), 5 mM 2-mercaptoethanol; elution buffer B: same as buffer A with 300 mM imidazole). For b/PRT1 peptides this was followed by TEV protease cleavage for His_6-tag or His_6-tag lipoyl fusion removal (dialysis buffer for TEV cleavage at room temperature: 20 mM HEPES pH 7.5, 150 mM NaCl, 10% glycerol, 5 mM 2-mercaptoethanol), while i/TIF34 was left uncleaved. TEV cleavage reaction mixtures were then reloaded onto HiTrap chelating columns to remove the His_6-TEV protease, the His_6-tag or His_6-tag lipoyl fusion as well as minor contaminating proteins using buffers A and B (see above). After purification, the proteins were dialyzed 3 times against 2 L storage/NMR buffer (50 mM sodium phosphate buffer pH 7.5, 150 mM NaCl, 5 mM 2-mercaptoethanol).

Purified His_6–i/TIF34 and b/PRT1 proteins were assembled into complexes at a 1:1.2 molar ratio, concentrated using Vivaspin 20 mL centrifugal devices

with 10 000 MWCO (Sartorius) and passed over a Sephacryl S-200 gel filtration column (GE Healthcare) using storage/NMR buffer as running buffer. Fractions corresponding to the 1:1 complex were pooled, concentrated to 7–10 mg/ml and either used directly for NMR experiments or dialyzed against 2 times 2 L crystallization buffer (20 mM HEPES pH 7.5, 150 mM NaCl, 5 mM 2-mercaptoethanol) using Slide-A-Lyzer 0.5 mL dialysis cassettes with 10 000 MWCO (Thermo Scientific).

NMR spectroscopy

NMR experiments were performed on Bruker DMX600 or AVANCE800 spectrometers equipped with cryoprobes. Partial protein backbone assignments of $^{13}C/^{15}N$-labeled b/PRT1(630–724) in complex with unlabeled His_6–i/TIF34 were achieved by means of through-bond heteronuclear scalar correlations with standard pulse sequences from the Bruker pulse sequence library. Chemical shift patterns upon binding of ^{15}N-labeled b/PRT1(630–724) or b/PRT1(654–700) to His_6–i/TIF34 were compared using standard ^{15}N-HSQC and ^{15}N-TROSY pulse sequences. All NMR samples were prepared in NMR buffer (see above) with addition of 10% D_2O (v/v) at protein concentrations of 100–200 μM. All spectra were recorded at 20° C.

Defining the minimal i/TIF34-binding domain of b/PRT1 by NMR spectroscopy

Residues 641–724 of b/PRT1 were previously shown to be required for i/TIF34-binding *in vitro* (9,10). Crystallization of proteins and their complexes is often hindered by flexible, unstructured tails and this prompted us to further define the precise boundaries of the interaction site by NMR spectroscopy (16,17). To achieve this, we expressed unlabeled i/TIF34 and a $^{13}C,^{15}N$-labeled C-terminal fragment of b/PRT1 spanning residues 630–724 and recorded ^{15}N-HSQC spectra of the peptide both in the free and i/TIF34-bound form. The spectrum of the free 10 kDa peptide displays severe resonance overlap in the amide region and mainly random coil chemical shifts indicative of no intrinsic secondary structure as also confirmed by CD spectroscopy (data not shown and Supplementary Figure S1A). Upon binding of i/TIF34 to the b/PRT1 peptide, a 50 kDa complex is formed with much slower tumbling times of the bound peptide in solution resulting in shorter transverse relaxation times and concomitant broadening of amide signals from b/PRT1 residues participating in the interaction with i/TIF34. On the other hand, a significant portion of the sharper random coil crosspeaks of b/PRT1 remains unchanged indicating that they are not part of the i/TIF34 binding interface. For several of these random coil resonances much longer transverse relaxation times allowed us to obtain backbone assignments using standard triple resonance experiments. We unambiguously assigned a four amino acid stretch spanning residues Q651-M654 from the N-terminus as well as the entire extreme C-terminus starting at residue A701 of b/PRT1, while the middle segment spanning residues 655–700 could not be assigned due to short transverse relaxation times from an interaction with i/TIF34. We therefore designed and expressed a ^{15}N-labeled peptide comprising residues 654–700 of the C-terminus of b/PRT1. This shorter peptide displays the same broad, shifted resonances when bound to i/TIF34 as the longer ^{15}N-labeled peptide comprising residues 630–724, including a downfield shifted Trp-NεH crosspeak of W674, but lacks the sharp random coil Trp-NεH crosspeak (W644) from the N-terminal half of the longer peptide (Supplementary Figure S1B). This unambiguously defines that the minimum i/TIF34 binding site of b/PRT1 comprises residues 654–700. This conclusion is also confirmed by isothermal titration calorimetry (ITC), which displays very similar affinities for the long b/PRT1(630–724) and the minimal C-terminal peptide of b/PRT1(654–700) with K_D-values of 81 nM and 160 nM, respectively (Supplementary Figure S1C). Thus optimized complex of yeast full-length i/TIF34 and the 654–700 fragment of b/PRT1, lacking b/PRT1 random coil segments, was subjected to crystallization and after optimization yielded well diffracting crystals suitable for structure determination of the complex.

Crystallization

Crystallization screening by sitting drop vapor diffusion was performed with 200 nl drops (1:1 ratio of protein solution to mother liquor) against 1600 commercial conditions at room temperature. Crystals were obtained in 0.1 M Tris–HCl pH 8.8, 0.1 M Li_2SO_4, 28% PEG 4000, 2–8% 1,5-diAminoPentane dihydrochloride. Heavy atom derivatives were obtained by soaking crystals in saturated solutions of K_2PtCl_4 (potassium tetrachloroplatinate (II) and $C_2H_5HgSC_6H_4CO_2Na$ (sodium ethyl-mercurithiosalicylate, thiomersal) for 2–5 min.

Diffraction data collection and structure determination

Native diffraction dataset was collected from a single crystal at 100K at the Diamond synchrotron facility (UK) on beamline I03. Data of heavy atom derivatives were collected using a MAR-DTB image-plate detector and rotating anode X-ray generator. The data were indexed with MOSFLM (18) and further processed using SCALA (19) and TRUNCATE (20) from CCP4 package (21). Experimental phases were obtained by MIR, combining Pt and Hg derivatives, scaling them to the native dataset and further processing with SHARP (22). Although the phase information from the Pt derivative was weak beyond (and at) 3.8 Å resolution, adding it significantly improved the experimental map. PHYRE server (23) homology modeling solution of i/TIF34 was used as a search model in Phaser (24) to find second molecule in the asymmetric unit. Map was improved with solvent flattening in Parrot (25). Major part of the model was built with Buccaneer (26), with remaining parts hand-built using Coot (27). Iterative rounds of model building in Coot, refinement with Refmac (28) and validation using MolProbity server (29) were ultimately performed without non-crystallographic symmetry (NCS). Initially, NCS was applied during the first rounds of

refinement but no significant improvement was observed. Therefore we decided not to use NCS in the refinement, especially since one part of the protein (the flexible loop) was different between the two molecules. The final structure consists of four protein chains: B and D—i/TIF34, E and F—b/PRT1(654–700). Chains B and D have TEV protease cleavage site, and therefore start at the residue Glu-9 leaving methionine as the first amino acid. Chain B contains residues −9 to 259 and 273 to 342, chain D −9 to 342, chains E and F 661 to 699. Data collection and refinement statistics are summarized in Supplementary Table S1.

Yeast strains, plasmids, and biochemical methods

Lists of strains and plasmids used in this study (Supplementary Tables S3–S5), details of their construction, as well as description of all well-established biochemical assays used throughout the study can be found in the Supplementary Data.

RESULTS

The overall crystal structure of i/TIF34–b/PRT1(654–700) complex

Using solution NMR spectroscopy, we defined the minimal C-terminal i/TIF34-binding site of b/PRT1(654–700) lacking any b/PRT1 random coil segments, which could hinder crystallization (16,17) (Figure 1A, Supplementary Figures S1 and S2A, 'Material and Methods' section). The crystallographic structure of thus optimized yeast i/TIF34–b/PRT1(654–700) complex was determined at 2.2 Å resolution by MIR heavy atom phasing (data statistics in Supplementary Table S1). Two complexes were found in the asymmetric unit and both of them displayed excellent electron density (Supplementary Figures S3 and S4) except for a few terminal residues of both the b/PRT1 and i/TIF34 molecules and a specific loop region spanning well-conserved residues 260–272 in one of the two i/TIF34 molecules (discussed in more detail later).

The i/TIF34 subunit adopts a seven-bladed β-propeller fold with a short, bent α-helix at the C-terminus (Figure 1B). As commonly seen in β-propeller structures (30), one β-sheet of the last blade 7 is formed by N-terminal residues 1–7, while the subsequent amino acid residues consecutively form blades 1–7 (Figure 1C). Phylogenetic analysis shows that the most conserved residues comprise blades 1, 2, 6 and 7 (Figure 1D and Supplementary Figure S2A) and that several loops between the blades also include highly conserved residues. The β-propeller structure usually serves as a platform for protein–protein interactions (31). Interacting protein partners often bind to the top or bottom of the β-propeller structure, but binding along the groove between blades has also been observed (32–34). The b/PRT1(654–700) fragment binds to the bottom side of the β-propeller along the loops of blades 5 and 6 of i/TIF34 (Figure 1B). The b/PRT1 residues 663 to 689 form a long α-helix while the extended C-terminus (residues 690–699) advances towards the central cavity of the i/TIF34 β-propeller and is held mostly by contacts *via* main chain atoms (Figure 1B). These interactions are independent of the contacts between the two complexes within the asymmetric unit (Supplementary Figures S3 and S4).

The b/PRT1-binding interface of i/TIF34 comprises residues from β-sheets and loops in blades 5 and 6 (Figure 1B). The total buried surface area of the b/PRT1–i/TIF34 interface is 1028.7 $Å^2$ and 1054.6 $Å^2$ (complex I and complex II, respectively, in Supplementary Figure S4) as calculated using PISA (35). The b/PRT1-interacting surface of i/TIF34 bears a few important charged regions (Figure 2A; left). The remaining surface of this side of the β-propeller shows dominantly negative charge, while patches of positive charge dominate around the central cavity on the top side of the β-propeller (formed by blades 2–5, Figure 2A; right). This charge distribution is conserved suggesting distinct interfaces for the interactions with other components of the translational machinery (Figures 1D, 2A and Supplementary Figure S2A).

Seven residues of the b/PRT1(654–700) fragment are in close proximity (<3.5 Å apart) for direct contact with eight residues of i/TIF34. In both proteins, the interacting residues involve highly conserved amino acids (Figure 1D and Supplementary Figure S2A; and also listed in Supplementary Table S2). At the b/PRT1–i/TIF34 interface hydrogen bonds are formed between the most conserved residues Y677-D224 and R678-D207/T209 (Figure 2B and Supplementary Figure S2B), implying that these residues are crucial for b/PRT1–i/TIF34 complex formation. The second important feature of the complex interface is the insertion of the aromatic ring of b/PRT1 W674 into a pocket of i/TIF34 formed by hydrophobic amino acids (L231 and I281 as well as the conserved L222) and the side chains of polar amino acids (Y210 and K280 as well as the conserved K232 and E250) (Figure 2C, D and Supplementary Figure S2B). The nearest i/TIF34 residues are within 3.8–4.8 Å of W674. W674 probably makes a π–cation interaction with K280 (36) and additional hydrophobic interactions with the other 'pocket' residues (Figure 2D). Phylogenetic investigation shows that in other organisms including human, frog and *Drosophila*, Phe or Tyr is found instead of Trp and K280 replaced by either Leu or Val, implying conservation of the hydrophobic nature of this interaction (Supplementary Figure S2A). In addition to the specific side chain contacts along the α-helix of b/PRT1, there is a series of interactions between main chain atoms of the extended C-terminal part of b/PRT1 starting with N690 and i/TIF34 residues in blades 5 and 6 (Supplementary Table S2). Interestingly, none of the i/TIF34 residues directly interacting with b/PRT1 appeared in previous mutational studies by Asano and co-workers (10). For direct comparison see Supplementary Figure S5 and the corresponding text.

The major difference between the two i/TIF34–b/PRT1(654–700) complexes in the asymmetric unit lies within the loop made of residues 260–272 in blade 6 of i/TIF34 on the opposite side of the b/PRT1 binding interface. One of the complexes has well-defined electron

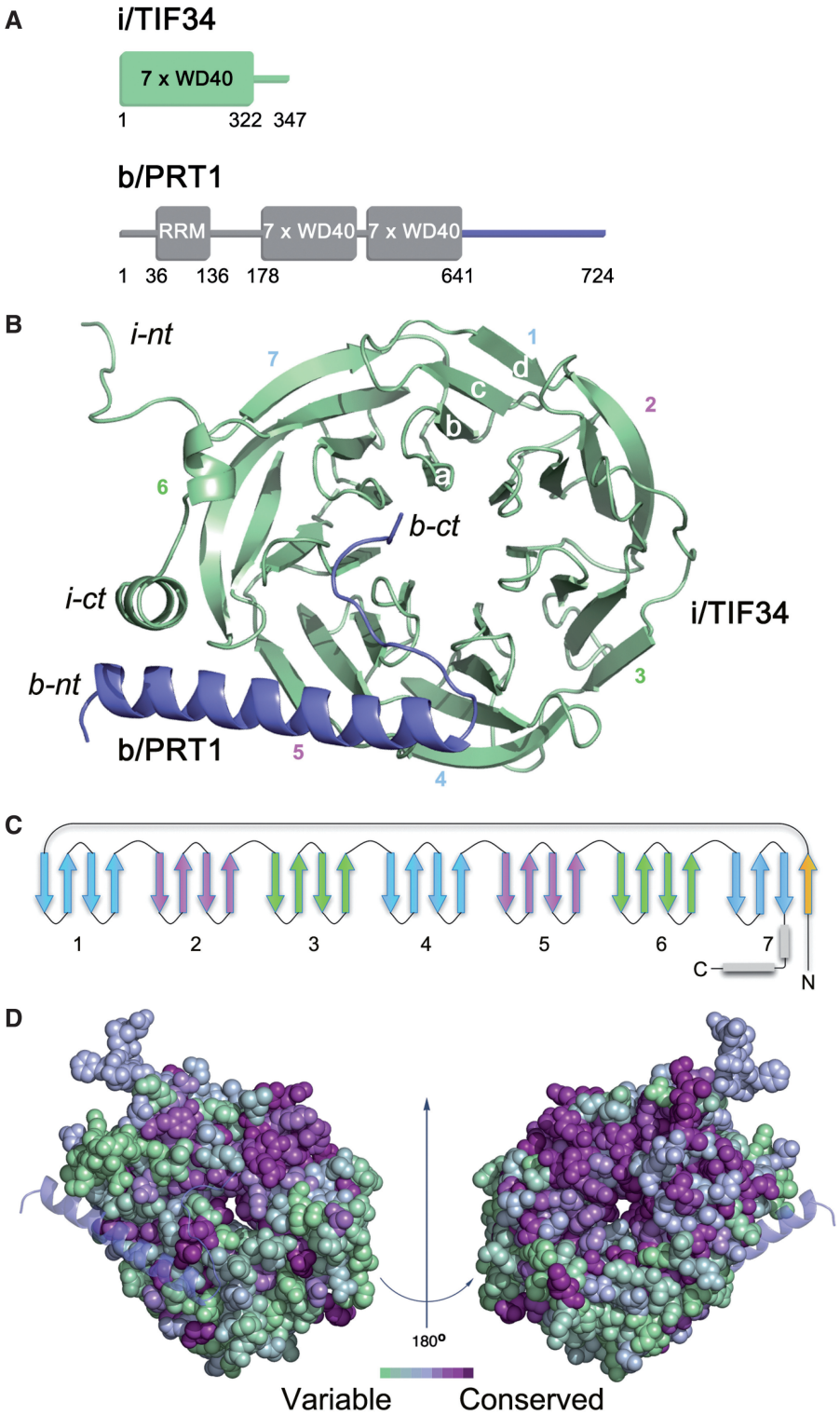

Figure 1. Structure of i/TIF34–b/PRT1 complex. (**A**) Schematic drawing of the predicted protein domains of yeast i/TIF34 (top) and b/PRT1 subunits of eIF3 (bottom). The folded domains and their boundaries are indicated. Predicted unstructured regions are shown as lines. (**B**) Overview of the structure: cartoon representation of i/TIF34 (green) and b/PRT1(654–700) (blue). WD-40 blades 1–7, β-strands a–d of blade 1 and N-terminus (nt) and C-terminus (ct) are labeled. The complex is shown from the bottom side of the β-propeller, where loops occur between strands a–b and c–d. (**C**) Topology diagram of the i/TIF34 fold. (**D**) Space-filling view of the i/TIF34 in complex with b/PRT1 (bottom view, left and top view, right), colored according to sequence conservation. A gradient of green to purple indicates the degree of phylogenetic conservation, with variable shown as green and most conserved as dark purple. The conservation heat plot of the i/TIF34 surface was generated by ConSurf using multiple alignment of Human, *Drosophila*, *Arabidopsis* and *Saccharomyces cerevisiae* i/TIF34 protein homologues. All structural figures were generated using PyMOL (http://www.pymol.org).

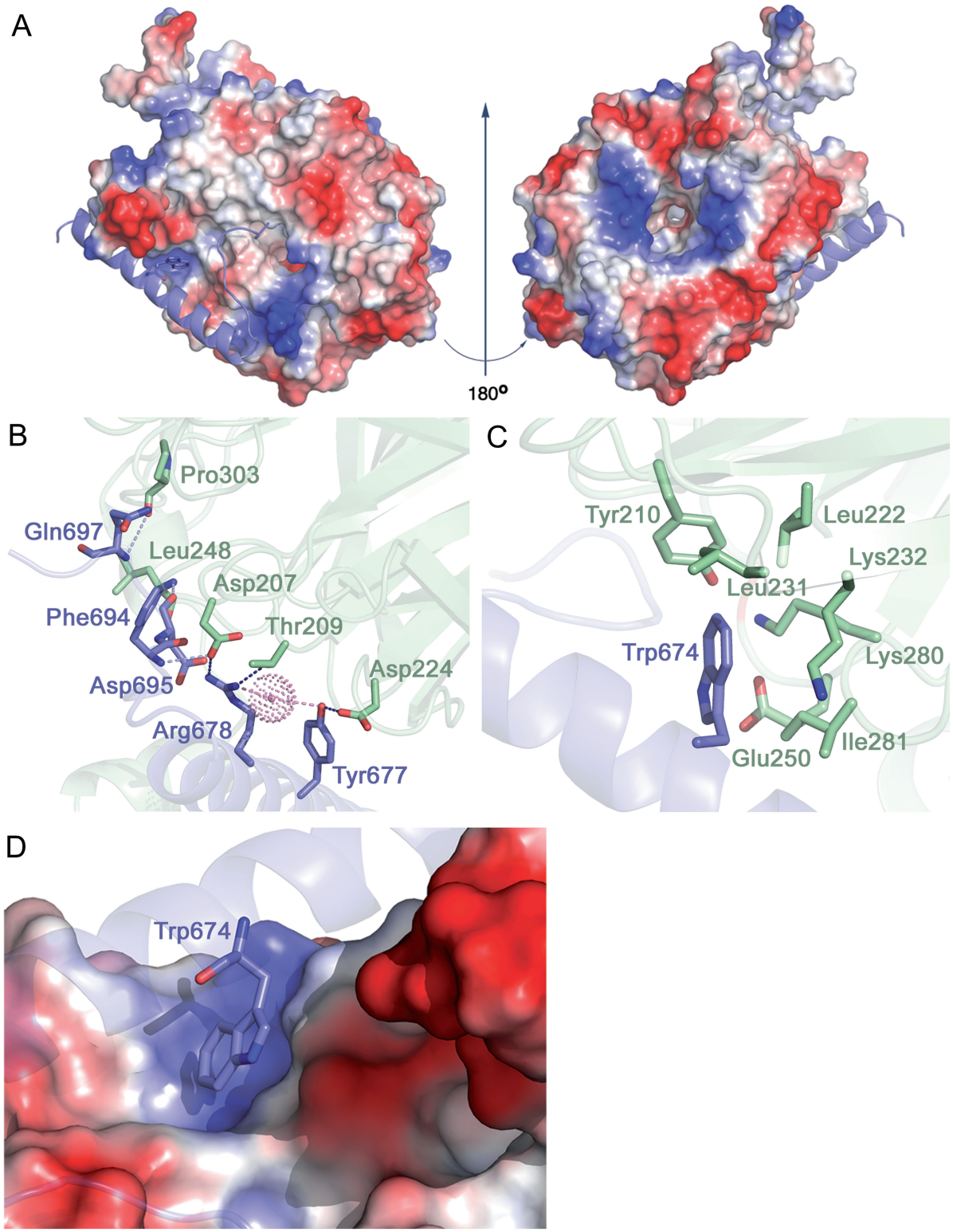

Figure 2. Molecular details of i/TIF34 and b/PRT1 interactions. (**A**) Electrostatic potential (±5kT/e) of the solvent-accessible surface of i/TIF34 in complex with b/PRT1(654–700) rendered on the molecular surface of the complex. A gradient of blue to red shows positive to negative charge, respectively, as calculated using PyMOL built-in APBS tools (55). PQR file for analysis of Poisson–Boltzmann electrostatics calculations was generated using PDB2PQR tool (56) and further used for APBS. b/PRT1(654–700) is shown as a cartoon in blue. View from the b/PRT1 binding site is shown on the left; the 'reverse' side of i/TIF34 shown on the right has negative charge clustering at the highly conserved blade 1 (upper part), blades 4 and 5 (the bottom part) and positive charge around the central cavity. (**B–C**) The i/TIF34-b/PRT1 binding interface involves highly conserved amino acids from both proteins. i/TIF34 is shown in green, b/PRT1 in blue. (**B**) Y677 and R678 from b/PRT1 form H-bonds (blue) with D207, T209 and D224 from i/TIF34 (only interacting side chains are shown). Other residues making contacts (light blue) via main chain atoms are also shown in sticks. One water molecule (shown in dots) is in close proximity (light pink) to R678 NH1 (2.6 Å) and Y677 OH (3.3 Å). (**C**) b/PRT1 W674 is surrounded by hydrophobic and charged amino acids (only side chains are shown), which form a shallow pocket. (**D**) Surface representation of the i/TIF34 hydrophobic pocket, which accommodates b/PRT1 W674. This interaction serves as a 'lock' for the i/TIF34 and b/PRT1 interaction interface.

density surrounding these residues (complex II in Supplementary Figure S6A), whereas the other molecule lacks defined electron density around this area (position of the residues omitted from the PDB file are indicated by the red arrow in Supplementary Figure S6A). The well-defined loop in complex II contacts another symmetry-related i/TIF34 molecule (residues 80–87 and 130–139; not shown) and forms a salt bridge between E270 and K91 in the same chain of the symmetry-related complex fixing the loop in a detectable state. The flexible loop residues are predominantly negatively charged (Supplementary Figure S6B) and residues 260–279 display high sequence conservation from yeast to human (Supplementary Figure S2A) suggesting an important interaction module with either the 40S subunits or other partners within the eIF3 complex.

Disrupting the conserved b/PRT1–i/TIF34 interaction results in lethality or severe growth phenotypes

To confirm the critical aspects of the b/PRT1–i/TIF34 contacts revealed by the structure analysis and to investigate the functional consequences of their loss in living cells, we first substituted Y677 and R678 (alone or in combination), or W674 of b/PRT1 with Ala, Asp or Phe residues, respectively, and tested them for growth phenotypes. The corresponding mutations were generated in a plasmid copy of *PRT1-His*, encoding His_8-tagged b/PRT1, and introduced into a *prt1Δ* strain harboring wt *PRT1* on a *URA3* plasmid, which was subsequently evicted by counter-selection on medium containing 5-fluoroorotic acid (5-FOA). Whereas the double *Y677A R678D* mutation is lethal and the *Y677A R678A* (dubbed *YR/AA* herein) double mutant imparts a very severe slow growth (Slg–) phenotype, individual *Y677A* and *R678A* substitutions show little to no effect on growth rates (Figure 3A). Severe Slg^- and temperature sensitive (Ts^-) phenotypes are also found associated with the *W674A* mutation. Strikingly, the 'phylogenetic correction' substitution in *W674F* (see above) displays wt-like behavior under all tested conditions (Figure 3A; summarized in 3C). Importantly, *in vitro* electrophoretic mobility shift assays performed with recombinant purified i/TIF34 and b/PRT1-CTD(630–724) variants confirm these *in vivo* results: b/prt1-W674F mutant protein competes well with wt b/PRT1-CTD for i/TIF34 binding, whereas b/prt1-W674A and the YR/AA double mutant are not able to compete for i/TIF34 binding at all (Supplementary Figure S7). These results confirm that an aromatic side chain (Phe or Trp) is required to fill the hydrophobic pocket on i/TIF34 and indicate that the contacts of Y677 and R678 with D207 and D224, respectively, are redundant (see more biochemical evidence further below).

In a similar fashion, specific substitutions of D207 and D224 (alone or in combination), or L222 of i/TIF34, generated in a plasmid copy of *TIF34-HA* encoding HA-tagged i/TIF34, were tested for growth defects in a *tif34Δ* strain. In agreement with the aforementioned results, individual *D207K* and *D224K* substitutions produce no effects; however, the combined *D207K D224K* (dubbed *DD/KK* herein) mutant displays a severe Ts^- phenotype (Figure 3B). Finally, both charge substitutions of L222 in *L222D* or *L222K*, which probably drastically disturb the L222-containing hydrophobic pocket or perhaps even the entire local structure around blades 5 and 6 (Figure 2C and D), also impart severe Ts^- and Slg^- phenotypes (Figure 3B; summarized in 3C).

Impairment of the contact between b/PRT1 and i/TIF34 eliminates association of i/TIF34 and g/TIF35 from the rest of eIF3 *in vivo*

To further test whether the mutations under study impair a direct contact between b/PRT1 and i/TIF34 proteins we introduced three single-Ala-substitution mutations into full length b/PRT1, synthesized and radiolabeled the resulting mutant proteins *in vitro* and tested their binding affinities towards i/TIF34 and g/TIF35 fused with the GST moiety. As shown in Figure 4A, all three completely eliminate binding of b/PRT1 specifically to i/TIF34 but not to g/TIF35. Similarly, both single D/K substitutions and the *DD/KK* double mutation of i/TIF34, the latter of which was chosen for further analysis, abolished binding of [^{35}S]-labeled i/TIF34 to GST-b/PRT1 but not to GST-g/TIF35 (Figure 4B and data not shown).

Next we wished to demonstrate the effect of our mutations on the association of i/TIF34 with the rest of eIF3 *in vivo*. Towards this end we analyzed formation of the entire eIF3-containing MFC (see our model in Figure 4C) in yeast cells by Ni^{2+}-chelation chromatography using His_8-tagged *PRT1* as bait. As reported previously (13), a fraction of a/TIF32, j/HCR1, eIF2, eIF5 and eIF1 co-purified specifically with wt b/PRT1-His but not with its untagged version (Figure 5A, lanes 4–6 versus 1–3). The *prt1-W674A* mutation of one of the two contacts between i/TIF34 and b/PRT1 severely diminishes (by >90%) association of i/TIF34, and in contrast to the above *in vitro* experiments, also that of g/TIF35 with the MFC, whereas *prt1-W674F* shows no effects (Figures 5A and B, lanes 7–9 versus 10–12). This concurs well with our genetic data (Figure 3A). In addition, the overall integrity of the MFC also seems to be modestly affected. Similarly, the *tif34-DD/KK* mutation of the other contact also severely reduces binding of i/TIF34 and g/TIF35 to the purified b/PRT1-His complex (Figures 5C and D, lanes 9–12 versus 5–8). Importantly, overexpressing His_8-tagged *TIF35* as bait in the background of *tif34-DD/KK* further supported these novel observations as g/TIF35-His practically failed to pull down any of the MFC components with the exception of i/TIF34 (Supplementary Figure S8A). The fact that the *DD/KK* mutation does not affect the mutual interaction between i/TIF34 and g/TIF35 *in vivo* is in perfect agreement with our *in vitro* binding data (Figure 4B). Together these results strongly suggest that binding of i/TIF34 with b/PRT1, in addition to the direct g/TIF35–b/PRT1 interaction, is a necessary prerequisite for stable eIF3-association of g/TIF35 *in vivo* indicating that the observed growth phenotypes are a direct consequence of the loss of the essential i/TIF34–g/TIF35 mini-module from the rest of eIF3. Hence the fact that the individual

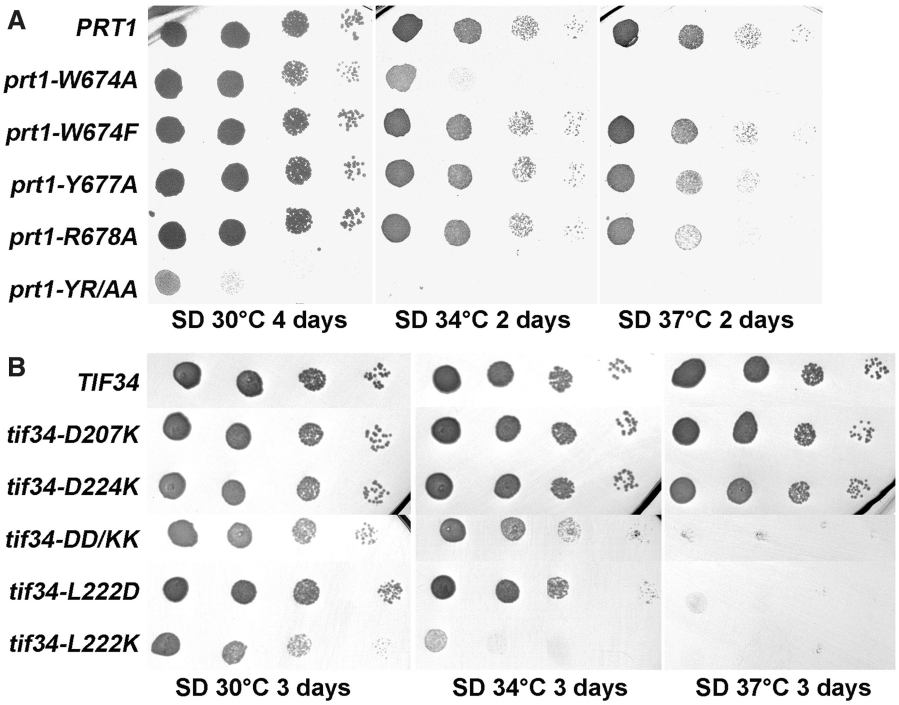

C

PRT1 mutations	30°C	34°C	37°C
W674A	WT	Slg$^-$	severe Ts$^-$
W674F	WT	WT	WT
Y677A	WT	WT	WT
R678A	WT	WT	mild Slg$^-$
Y677A R678A	severe Slg$^-$	severe Ts$^-$	severe Ts$^-$
Y677A R678D		lethal	
***TIF34* mutations**			
D207K	WT	WT	mild Slg$^-$
D224K	WT	WT	WT
D207K D224K	WT	Slg$^-$	severe Ts$^-$
L222D	WT	Slg$^-$	severe Ts$^-$
L222K	Slg$^-$	severe Slg$^-$	severe Ts$^-$

Figure 3. Phenotypic and biochemical analysis of i/TIF34 and b/PRT1 mutations that disrupt subunit interactions. (**A**) The *prt1-W674A* and *-YR/AA* but not *-W674F* mutations produce severe slow growth and temperature sensitive phenotypes. The YAH06 (*prt1Δ*) strain was transformed with the corresponding plasmids carrying individual mutant alleles and the resident pCR52 (*PRT1,URA3*) covering plasmid was evicted on 5-FOA. The resulting strains were then spotted in four serial 10-fold dilutions on SD medium and incubated at 30, 34 and 37°C. (**B**) The *tif34-DD/KK, -L222D* and *L222K* mutations produce severe slow growth and temperature sensitive phenotypes. The H450 (*tif34Δ*) strain was transformed with the corresponding plasmids carrying individual mutant alleles and the resident YEp-i/TIF34-U (*TIF34, URA3*) covering plasmid was evicted on 5-FOA. The resulting strains were then spotted in four serial 10-fold dilutions on SD medium and incubated at 30, 34 and 37°C. (**C**) Summary of phenotypes of mutations analyzed in this study.

prt1-Y677A, *prt1-R678A*, *tif34-D207K* and *tif34-D224K* mutations diminish the b/PRT1–i/TIF34 interaction *in vitro* (Figure 4) yet produce no significant growth phenotypes (Figure 3) can be explained by proposing that their impact *in vivo* is largely overcome by a stabilization effect of simultaneous binding of g/TIF35 to i/TIF34 and b/PRT1 in the context of the entire eIF3 complex, as was observed (Supplementary Figure S8B and C). In other words, their aforementioned redundancy is dependent on the presence of g/TIF35 *in vivo*. Indeed, this effect is not powerful enough in the case of more deleterious double mutations. Since we had confirmation that genetic and molecular defects of both *prt1-W674A* and *tif34-DD/KK* mutations have the same nature, we decided to focus our further analysis on the latter.

Disruption of the b/PRT1–i/TIF34 interaction prevents 40S-binding of the i/TIF34–g/TIF35 mini-module and selectively affects stability of pre-initiation complexes *in vivo*

We showed previously that a partial eIF3 subcomplex containing a/TIF32 and c/NIP1, and eIF5, but lacking

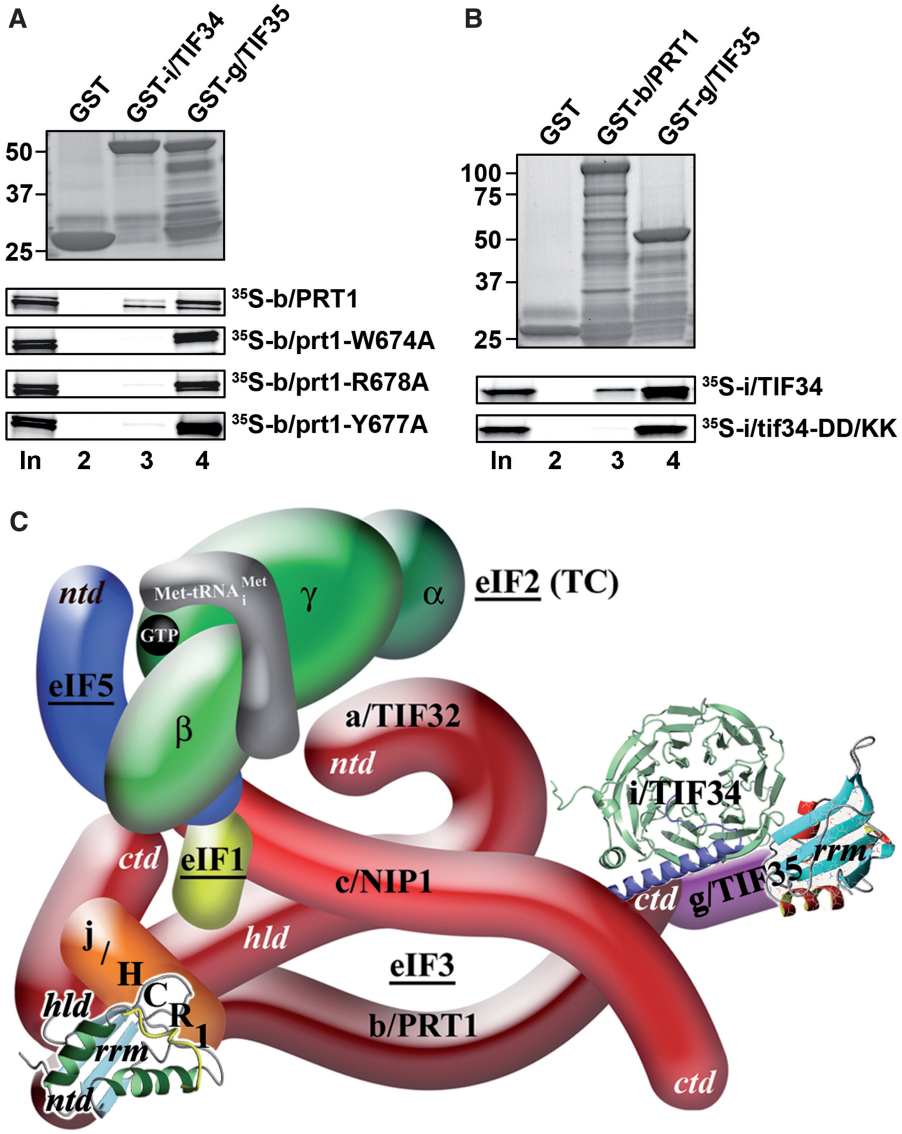

Figure 4. The *tif34-DD/KK* mutation impairs the direct interaction between i/TIF34 and b/PRT1 *in vitro* and the revised 3D model of eIF3 in the MFC. (**A**) The *prt1-W674A*, *-Y677A*, and *-R678A* mutations impair the direct interaction between b/PRT1 and i/TIF34 *in vitro*. Full-length i/TIF34 (lane 3) and g/TIF35 (lane 4) fused to GST, and GST alone (lane 2), were tested for binding to ^{35}S-labeled wt b/PRT1 and its mutant derivatives; 10% of input amounts added to each reaction is shown in lane 1 (In). (**B**) Full-length b/PRT1 (lane 3) and g/TIF35 (lane 4) fused to GST, and GST alone (lane 2), were tested for binding to ^{35}S-labeled wt i/TIF34 and the *DD/KK* mutant derivative. (**C**) A revised 3D model of eIF3 and its associated eIFs in the MFC (based on the data from (9); *ntd*, N-terminal domain; *ctd*, C-terminal domain; *hld*, HCR1-like domain; *rrm*, RNA recognition motif; TC, ternary complex). The NMR structure of the interaction between the RRM of human eIF3b (green and light blue) and the N-terminal peptide of human eIF3j (yellow) (12), the NMR structure of the C-terminal RRM of human eIF3g (red and sky-blue) (5), and the X-ray structure of the yeast i/TIF34–b/PRT1 complex (this study), were used to replace the original schematic representations of the corresponding molecules.

the b/PRT1, i/TIF34 and g/TIF35 subunits, still interacted with the 40S ribosomes *in vivo* (albeit with ~2-fold reduced affinity compared to wt 5-subunit eIF3), whereas the b/PRT1–i/TIF34–g/TIF35 subcomplex lacking the N-terminal RRM of b/PRT1 did not (13,37). Hence given that mutating the contact residues between b/PRT1 and i/TIF34 strongly impairs association of i/TIF34 and g/TIF35 with eIF3 in the MFC (Figure 5), it could be consequently expected that the ribosome occupancy of only i/TIF34 and g/TIF35 gets impaired. To examine this, we measured binding of selected eIF3 subunits and other MFC components to 40S subunits by formaldehyde cross-linking followed by high velocity sedimentation in sucrose gradients, as this method provides the best available approximation of the native composition of 43S/48S pre-initiation complexes *in vivo* (38). In accord with our prediction, we observed a relative ~90% decrease in the amounts of i/TIF34 and g/TIF35 associated with 40S subunits in whole-cell extracts (WCEs) obtained from the *tif34-DD/KK* cells grown at the semipermissive temperature (Figure 6A, '43–48S' lanes). Surprisingly, rather significant reductions in

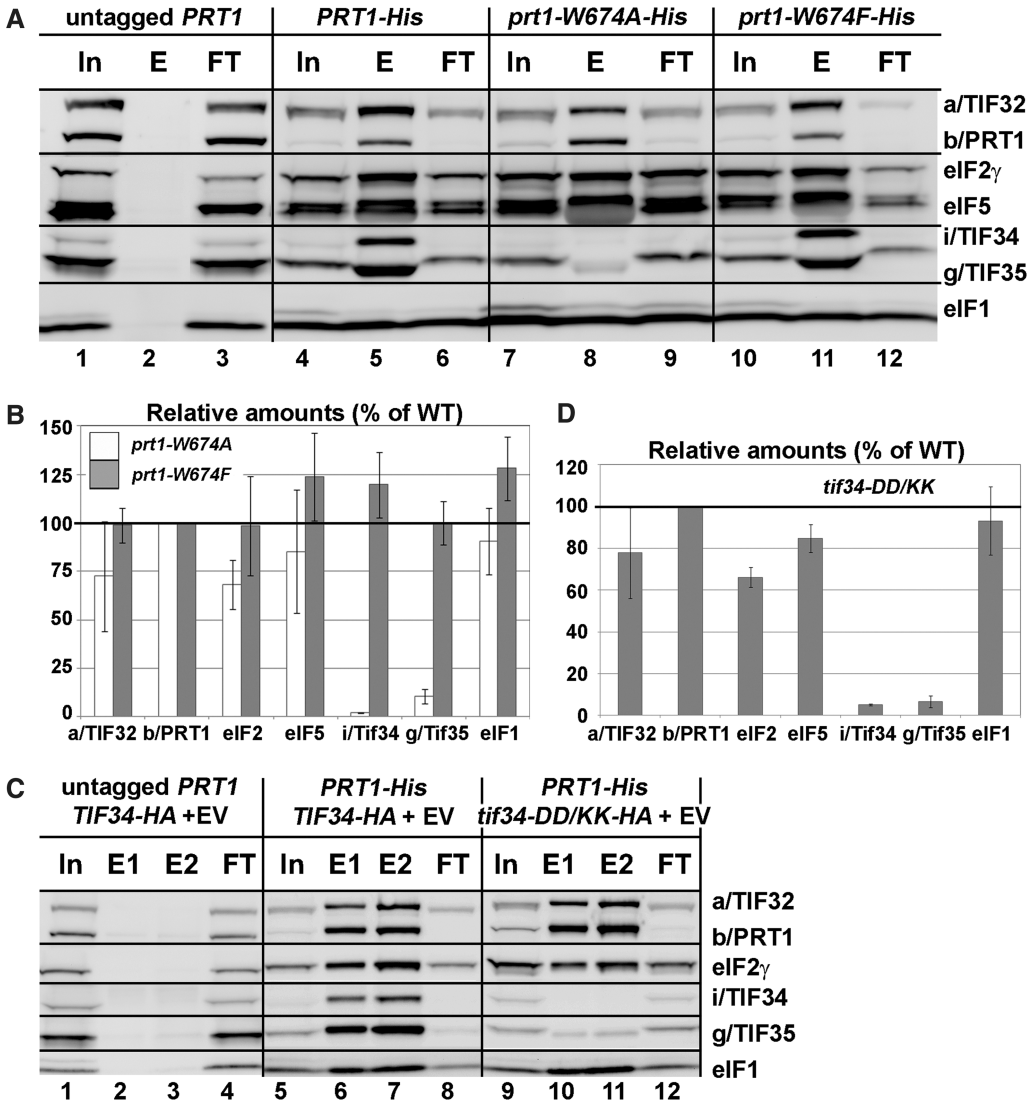

Figure 5. Disrupting the b/PRT1–i/TIF34 interaction eliminates association of the i/TIF34-g/TIF35 mini-module from the MFC *in vivo*. (**A** and **B**) WCEs prepared from YAH06 (*prt1Δ*) bearing untagged b/PRT1 (lanes 1–3), 8xHis-tagged b/PRT1 (lanes 4–6), and two of its mutant derivatives (lanes 7–9 and 10–12) were incubated with Ni^{2+} agarose and the bound proteins were eluted and subjected to western blot analysis with the antibodies indicated in each row. (In) lanes contained 5% of the input WCEs; (E) lanes contained 100% of eluate from the resin; (FT) lanes contained 5% of the flow through. (**B**) The Western signals for indicated proteins in the E fractions of the wt *PRT1-His* and its mutants were quantified, normalized for the amounts of the wt b/PRT1 in these fractions and plotted in the histogram as percentages of the corresponding values calculated for the wt b/PRT1. (**C** and **D**) WCEs were prepared from YAH12 (*prt1Δ tif34Δ*) bearing untagged *PRT1* and wt *TIF34* (lanes 1–4) and from YAH11 (*prt1Δ tif34Δ*) bearing 8xHis-tagged *PRT1* and either wt *TIF34* plus empty vector (lanes 5–8) or mutant *tif34-DD/KK* plus empty vector (lanes 9–12) and analyzed analogously to (A and B).

40S-binding (~40%) were also observed for other eIF3 subunits and eIF5, whereas binding of eIF2 (TC) and eIF1 was reduced only marginally (~20%). The lack of an increase in abundance of unbound eIF3 and eIF5 factors in the *tif34-DD/KK* gradients, which might have been expected given the pronounced loss of these proteins from the PICs, is attributed to an increased instability of eIFs defective to properly bind to 40S relative to those tightly bound in PICs during sedimentation. This phenomenon was also observed by us and others in the past (39–41). Quantification of input lanes ruled out a possibility of an increased proteolysis of eIF3 and eIF5 in the living cells as well as in the WCEs even after prolonged incubation on ice (Figure 6A). We conclude that the physical detachment of i/TIF34 and g/TIF35 from the rest of eIF3 not only prevents their binding to the 40S ribosome but also significantly weakens 40S-association of the remaining a/TIF32-b/PRT1-c/NIP1 subcomplex and eIF5. Remarkably, these findings thus may suggest that the mutant cells contain a subpopulation of PICs containing only eIF1 and the TC (see further below).

Detachment of the i/TIF34–g/TIF35 mini-module from eIF3 dramatically increases leaky scanning over the AUG start site producing a severe Gcn$^-$ phenotype

To elucidate the functional consequences of this PIC-assembly defect, we employed the translational

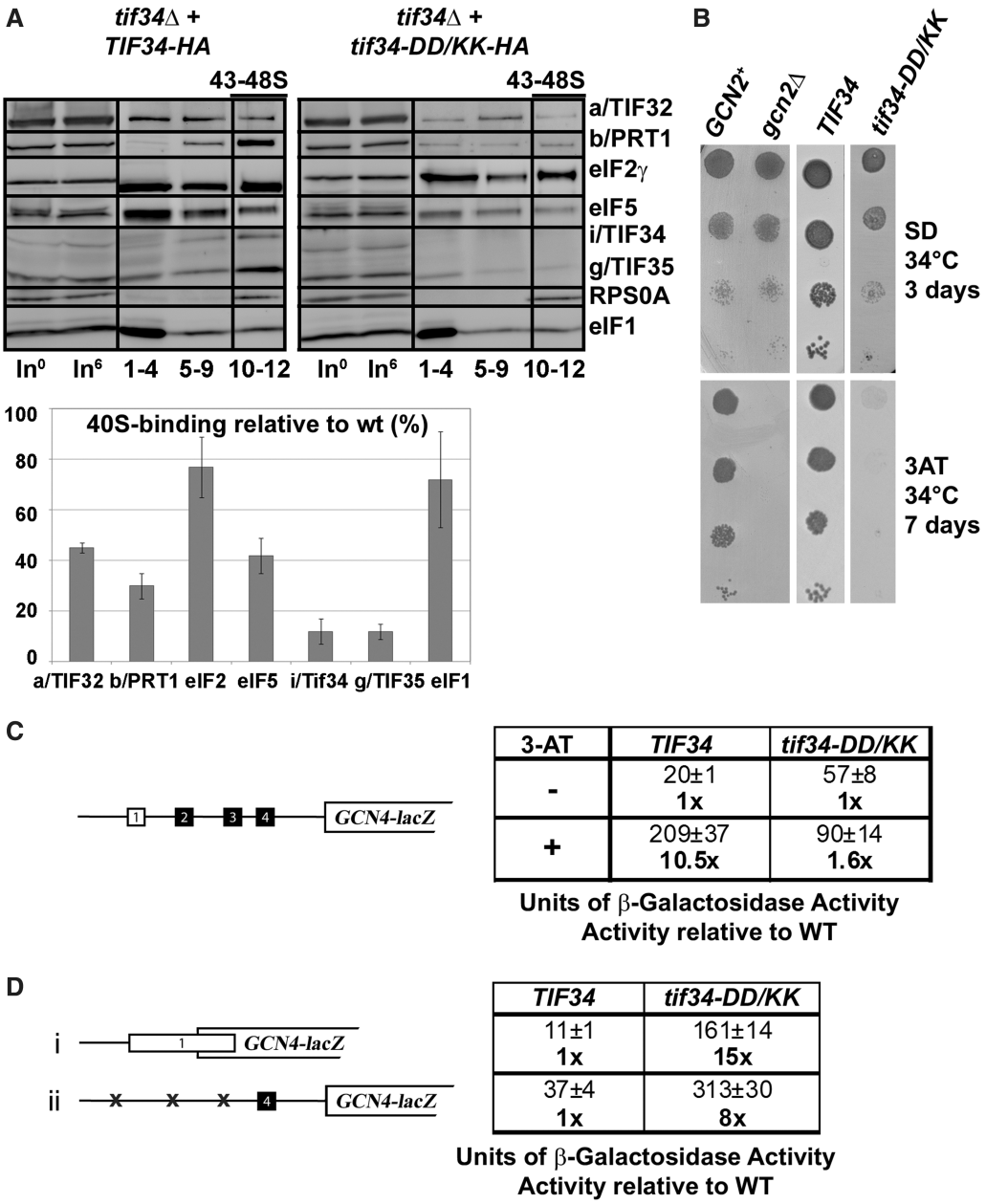

Figure 6. Disruption of the b/PRT1–i/TIF34 interaction prevents 40S-binding of the i/TIF34–g/TIF35 mini-module and dramatically increases leaky scanning over the AUG start site producing a severe Gcn$^-$ phenotype. (**A**) Physical detachment of i/TIF34 and g/TIF35 from the rest of eIF3 selectively affects stability of pre-initiation complexes *in vivo*. Transformants of H450 (*tif34Δ*) bearing wt or mutant *i/TIF34-HA* were grown in SD medium at 34 C to an OD_{600} of approximately 1.5 and cross-linked with 2% HCHO prior to harvesting. WCEs were prepared, separated on a 7.5–30% sucrose gradient by centrifugation at 41 000 rpm for 5 h and subjected to western blot analysis (note that the anti-RPS0A antibodies were generated in this study; see Supplementary Data). Fractions 1–4, 5–9, and 10–12 (43–48S) were pooled; lanes 'In^0' and 'In^6' show samples of the input WCEs (5%) that were processed immediately before (h0) or after (h6) incubation for 6 h on ice, mimicking the duration of the HCHO fractionation experiment to document the stability of the factors of interest in WCEs. Proportions of the 40S-bound proteins relative to the amount of 40S subunits were calculated using NIH ImageJ from three independent experiments. The resulting values obtained with the wt strain were set to 100% and those obtained with mutant strains were expressed as percentages of the wt (SDs are given). This experiment was repeated seven times with similar results. (**B**) *tif34-DD/KK* imparts the Gcn$^-$ phenotype. H417 (*GCN2*), H418 (*gcn2Δ*) and H450 (*tif34Δ*) bearing wt or mutant *i/TIF34-HA* were spotted in four serial 10-fold dilutions on SD (upper panel) or SD containing 30 mM 3-AT (lower panel) and then incubated at 34°C for 3 and 7 days, respectively. (**C**) *tif34-DD/KK* severely prevents derepression of *GCN4-lacZ* upon starvation. The H450 strains as in panel A were transformed with the *GCN4-lacZ* reporter p180 and grown in SD medium at 34°C to an OD_{600} of approximately 1. The β-galactosidase activities were measured in the WCEs and expressed in units of nmol of *O*-nitrophenyl-β-D-galactopyranoside hydrolyzed per minute per mg of protein. To induce *GCN4-lacZ* expression, strains were grown in minimal medium to an OD_{600} approximately 0.5 and then treated with 10 mM 3-AT for 6 h. The table gives mean values and standard deviations obtained from at least six independent measurements with three independent transformants, and activities with 3-AT-induction relative to those without induction. (**D**) Detachment of the i/TIF34–g/TIF35 mini-module from eIF3 provokes unusually severe leaky scanning defect. The H450 strains as in (A) were transformed with the *GCN4-lacZ* reporter plasmids pM226 (i) and plig102-3 (ii) and analyzed as in (C). The table gives activities in mutant relative to wt cells.

control mechanism of *GCN4*, which depends on four short upstream open reading frames (uORFs) found in its mRNA leader and has been adapted to serve as an experimental tool for monitoring various translational steps [reviewed in (42)]. The expression of *GCN4*, a transcriptional activator of many biosynthetic genes, is delicately regulated in a nutrient-dependent manner by the GCN2 kinase. Under nutrient-replete conditions the kinase is inactive and the *GCN4* expression is repressed. Upon amino-acid starvation, GCN2 becomes activated and derepresses *GCN4* synthesis by reducing the steady state levels of the TC. Mutants defective in the TC formation and/or its recruitment to the 40S subunit mimic starvation conditions and constitutively derepress *GCN4* even under nutrient-replete conditions, producing the Gcd$^-$ phenotype. Conversely, mutants that fail to derepress *GCN4* under starvation conditions provoke the Gcn$^-$ phenotype, which signals defects in the steps following assembly of 48S PICs, such as processivity of scanning, AUG recognition or subunit joining (42).

In accord with the nearly wt levels of 40S-bound TC (Figure 6A), *tif34-DD/KK* did not display the Gcd$^-$ phenotype; however, it did impart the severe Gcn$^-$ phenotype characterized by a failure to grow in the presence of 3-aminotriazole (3-AT) at 34°C (Figure 6B, column 4; 3-AT is an inhibitor of histidine biosynthetic genes.) Using the wt *GCN4-lacZ* reporter plasmid we indeed confirmed almost an absolute failure to derepress *GCN4* in response to 3-AT in the *DD/KK* cells (Figure 6C). The fact that the *tif34-DD/KK* cells sport the Gcn$^-$ phenotype as severe as the deletion of *GCN2* by itself (Figure 6B, column 2) suggests that the *DD/KK* mutation deregulates *GCN4* translational control by a dramatic impairment of one or more initiation steps following the TC recruitment.

To investigate this, we decided to employ the *GCN4-lacZ* reporter constructs with specific modifications in the *GCN4* mRNA leader, which have been successfully used in the past to reveal malfunctioning in scanning processivity, scanning rates, stringency of AUG selection or in subunit joining (12,39,40,43). Defects in recognition of the AUG start codon resulting in so-called leaky scanning can be identified with two *GCN4-lacZ* constructs: one where the first uORF (uORF1) is elongated and overlaps the beginning of *GCN4* (Figure 6D, constructs i); the other where only the last uORF (uORF4), non-permissive for reinitiation (44,45), is preserved in the mRNA leader of *GCN4-lacZ* (Figure 6D, construct ii). Only those ribosomes that skip (leaky scan) AUGs of the corresponding uORFs in both constructs may initiate on *GCN4-lacZ*, thereby producing an increase in β-galactosidase activity. Accordingly, both *tif34-DD/KK* and *prt1-W674A* show an unusually robust increase (up to 15-fold) of expression from both of these constructs (Figure 6D and Supplementary Figure S8D). Surprisingly, further analysis of other potential defects described above did not reveal any clearly distinguishable defects (see 'Discussion' section). Taken together these results strongly suggest that stable association of the i/TIF34–g/TIF35 mini-module with the rest of eIF3 stabilizes binding of eIF3 and eIF5 to the PICs to ensure their proper assembly required for stringent AUG recognition.

Increased gene dosage of *TIF35* suppresses growth and leaky scanning defects of the *i/tif34-DD/KK* mutant by preventing formation of aberrant PICs

Given the close interdependence of both small eIF3 subunits in terms of their stability and incorporation into the eIF3 complex it may be possible to suppress some of the observed phenotypes of *tif34-DD/KK* by increasing the gene dosage of *TIF35*. Accordingly, overexpressing *TIF35* significantly suppressed its growth deficiency (Figure 7A), unexpectedly, however, it did not strengthen association of i/TIF34 and g/TIF35 with b/PRT1-His in the MFC (Figure 7B, lanes 5–8 versus 1–4 and versus Figure 5C, lanes 9–12; these experiments were carried out at the same time and are summarized in the quantification plot of Figure 7B). Instead, it repeatedly decreased the amounts of eIF5, and mainly of eIF2 and eIF1 co-purifying with the rest of eIF3 suggesting that the increased dosage of g/TIF35 destabilized formation of the MFC *in vivo*. Sequestration of eIF2 and eIF1 in a separate complex by excess of g/TIF35 in cells could explain this unexpected phenomenon; however, was not observed (Supplementary Figure S8A). Hence, the molecular details of this mechanism are at present unknown to us. Most importantly, whereas it had no impact on the amounts of the 40S-bound eIF3 subunits and eIF5 when compared to wt and *i/tif34-DD/KK* cells bearing an empty vector, high dosage of g/TIF35 significantly decreased the amounts of eIF2 (~2-fold) and evened the eIF1 amounts to wt levels (Figure 7C, compare 43–48S fractions and the quantification plot summarizing results from Figures 6A and 7C). (Increased amounts of g/TIF35 in the ribosomal fractions are caused by trailing of the large excess of this protein through sucrose gradients and thus are not significant.) Importantly, the fact that the eIF2 levels actually matched those of eIF3 and eIF5 suggests that destabilization of the MFC in turn prevents formation of the aberrant TC-containing PICs. We therefore propose that the presence of aberrant PICs in the cell interferes with the canonical initiation process and significantly contributes to the observed growth defects associated with the loss of the i/TIF34–g/TIF35 mini-module from the rest of eIF3.

Hence it is likely that the robustly increased tendency to leaky scan initiating AUGs in *tif34-DD/KK* (Figure 6D) comes from malfunctioning of these erroneous PICs during the AUG recognition process. In strong support of this assumption, high dosage g/TIF35 fully suppressed the severe leaky scanning defect of the *DD/KK* mutant as well as its Gcn$^-$ phenotype (Figure 8A and B). These findings also argue that this unusually severe leaky scanning defect is actually the primary cause of the Gcn$^-$ phenotype in the mutant cells. To our knowledge, this type of a direct causal dependence has not been observed before.

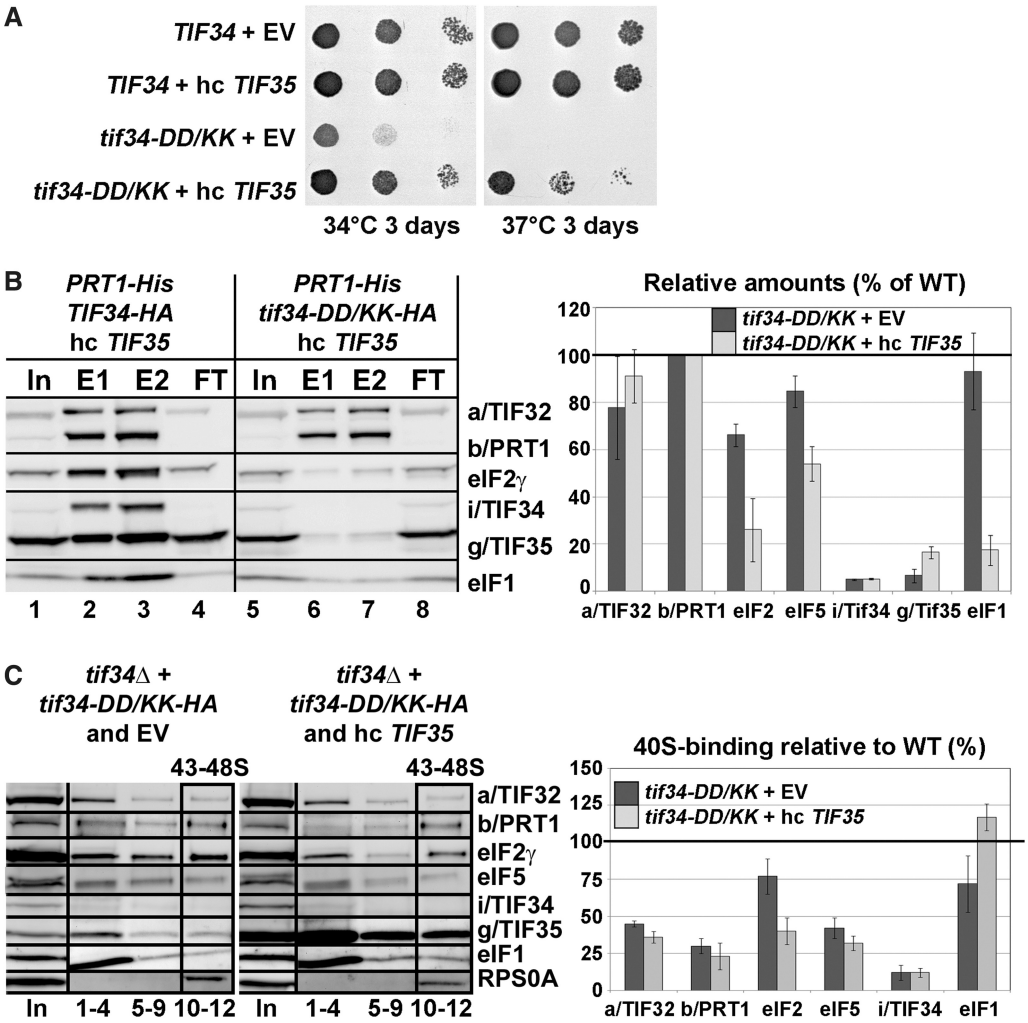

Figure 7. Increased gene dosage of *TIF35* partially suppresses growth defects of *tif34-DD/KK* mutant by preventing formation of the aberrant PICs. (**A**) High copy expression of *TIF35* partially suppresses growth phenotypes of *DD/KK*. The H450 strains as in Figure 6A were transformed with empty vector or hc *TIF35* and spotted in three serial 10-fold dilutions on SD medium and incubated at 34°C and 37°C for 3 days. (**B**) High dosage of g/TIF35 destabilizes formation of the MFC *in vivo*. The YAH12 (*prt1Δ tif34Δ*) strains as in Figure 5C were transformed with hc *TIF35* and subjected to Ni^{2+}-chelation chromatography as described in Figure 5A. The histogram shown on the right combines data from Figure 5C and D and this panel; the data were obtained in parallel experiments carried out at the same time. (**C**) High dosage of g/TIF35 prevents formation of aberrant TC-containing PICs *in vivo*. The H450 transformants as in (A) were subjected to formaldehyde cross-linking as described in Figure 6A. Proportions of the 40S-bound proteins relative to the amount of 40S subunits are shown in the histogram on the right. The resulting values obtained with the wt strain were set to 100% and those obtained with the *DD/KK* strain transformed with empty vector or high copy *TIF35* were expressed as percentages of the former (SDs are given).

Increased gene dosage of *SUI1* (eIF1) selectively suppresses the Gcn$^-$ and leaky scanning phenotypes of the *tif34-DD/KK* mutant

Initiation factors eIF1, eIF1A and eIF5 are considered to be the key controllers of the start selection process in eukaryotes (46). To examine their effect in the background of our leaky scanning *DD/KK* mutant, we overexpressed them individually in the *DD/KK* mutant strain while scoring for suppression of its Gcn$^-$ phenotype on 3-AT plates. Interestingly, overexpressing eIF1 but not eIF1A and eIF5 markedly suppressed the Gcn$^-$ but not the Slg$^-$ phenotype of *DD/KK* (Figures 8A and data not shown). To test whether this pronounced effect requires stable PIC association of eIF1, we examined eIF1 mutants with either severely weakened (*sui1*^{Q84P}, *sui1*^{D83G}, *sui1*$^{93\text{-}97}$) or wt (*sui1*^{G107R}) PIC affinity (41,47) for their ability to suppress the Gcn$^-$ phenotype. Out of these mutants, only high copy (hc) *sui1*^{G107R} with wt PIC affinity was capable of nearly wt Gcn$^-$ phenotype suppression (Figure 8A, right-hand panel). Hence, in order to suppress the *DD/KK* mutant, eIF1 must be capable of stable 40S-binding. Accordingly, high dosage of wt eIF1 as well as sui1^{G107R} also considerably suppressed the leaky scanning defect (Figure 8B). As expected, overexpressing eIF1A and eIF5 had no effect (data not shown). These experiments thus further support the idea that the leaky scanning defect is the main contributor to the failure of mutant cells to induce *GCN4* expression under starvation conditions.

In contrast to increased dosage of g/TIF35, which destabilized formation of the MFC *in vivo* (Figure 7B),

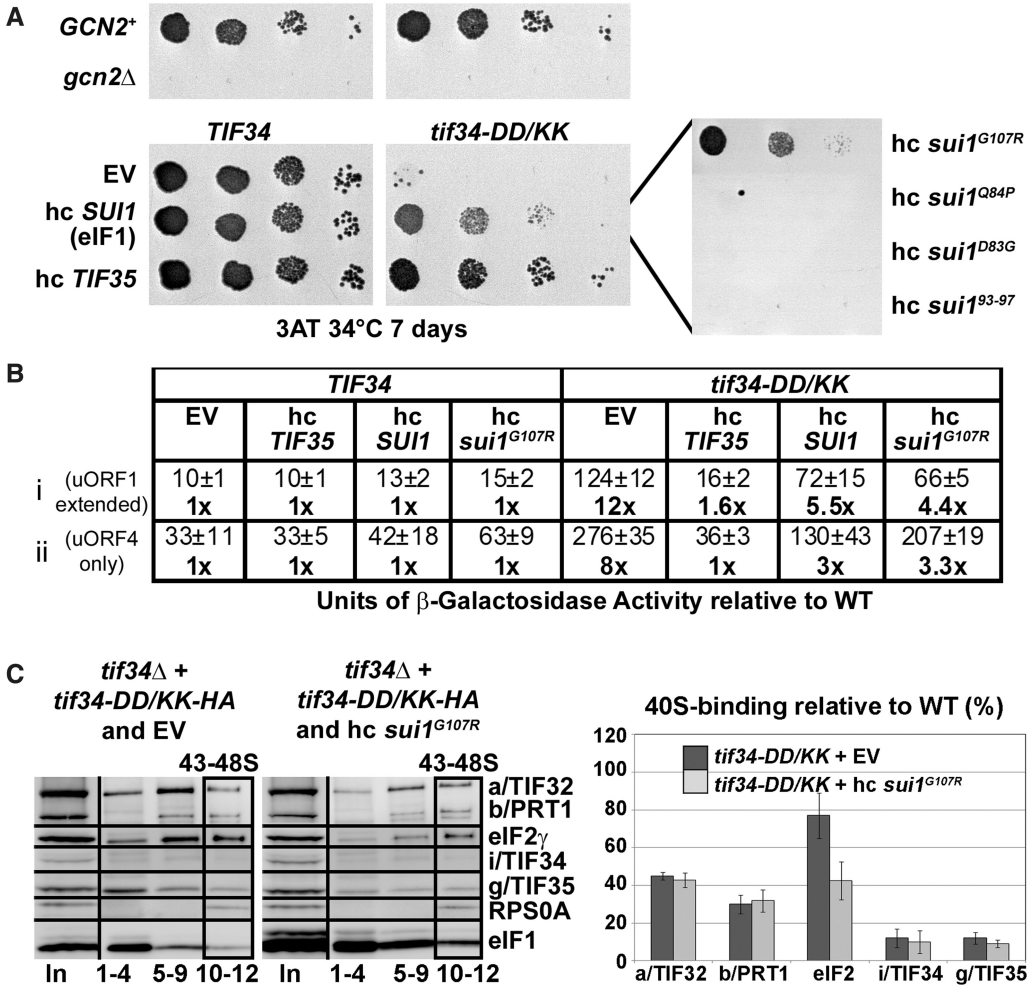

Figure 8. Increased gene dosage of *TIF35*, *SUI1* (eIF1), and its mutant allele $sui1^{G107R}$ suppresses the Gcn$^-$ phenotype of *tif34-DD/KK* as well as its severe leaky scanning defect; and high copy $sui1^{G107R}$ disrupts aberrant PICs *in vivo*. (**A**) The H450 strains as in Figure 6A were transformed with empty vector, hc *SUI1* (eIF1) or its mutant alleles, and with hc *TIF35*, respectively, spotted in four serial 10-fold dilutions on 3-AT containing SD media and tested for growth at 34°C for 7 days. (**B**) The strains as in (A) were further transformed with constructs shown in Figure 6D and analyzed as described in there. (**C**) High dosage of $sui1^{G107R}$ disrupts the aberrant TC-containing PICs *in vivo*. The H450 transformants as in panel A were subjected to formaldehyde cross-linking as described in Figure 6A. Proportions of the 40S-bound proteins relative to the amount of 40S subunits are shown in the histogram on the right. The resulting values obtained with the wt strain were set to 100% and those obtained with the *DD/KK* strain transformed with empty vector or hc $sui1^{G107R}$ were expressed as percentages of the former (SDs are given).

Ni^{2+}-chelation experiments from WCE of the *tif34-DD/KK* cells overexpressing either wt eIF1 or $sui1^{G107R}$ repeatedly showed no further destabilization of the MFC integrity in the mutant cells (data not shown). However, we did observe a clear negative effect of overexpressing $sui1^{G107R}$ on the amount of TC associated with 40S subunits in the *DD/KK* mutant *in vivo* reminiscent of that displayed by hc *TIF35* (Figure 8C compare with Figure 7C). Interestingly, no similar TC reduction was detected in cells overexpressing wt eIF1 (data not shown).

DISCUSSION

In this study we show that residues 654–700 of b/PRT1 are sufficient for i/TIF34 binding and present, to our knowledge, the first atomic-resolution structure of the interaction between two essential core eIF3 subunits. Our structure reveals that the two major contacts between i/TIF34 and b/PRT1(654–700) occur on the bottom side of the i/TIF34 β-propeller through conserved residues in blades 5 and 6. Disrupting the first contact between D207 and D224 of i/TIF34 and the corresponding Y677 and R678 of b/PRT1 produces lethal or Ts$^-$ phenotypes and severely diminishes MFC- and 40S-association of i/TIF34, and also that of g/TIF35, *in vivo* (Figures 3–6). Importantly, it also destabilizes binding of the rest of eIF3 and eIF5 to the 40S subunit (Figure 6). Likewise, disrupting the second contact between W674 of b/PRT1 and the hydrophobic pocket of i/TIF34 confers essentially the same phenotypes (Figures 3–5, Supplementary Figure S8D, and data not shown). Together these results clearly indicate that both contacts between b/PRT1 and i/TIF34 critically stabilize association of the i/TIF34–g/TIF35 mini-module with the rest of eIF3, in close co-operation with those contacts that g/TIF35 makes with both subunits. This in turn ensures efficient loading of these

two small eIF3 subunits onto the 40S where they are subsequently required for proper assembly of the 48S PICs.

Several important intermolecular bridges between yeast eIF3 and the solvent-exposed side of the 40S ribosome were previously identified, including those between the NTD of a/TIF32 and the small ribosomal protein RPS0A, the a/TIF32-CTD and helices 16–18 of 18S rRNA and RPS2 and RPS3, and the CTD of j/HCR1 and RPS2 (12,37,44,48). Note that both RPS2 and 3 are situated near the mRNA entry pore (Figure 9, upper panel). Besides them, the CTD of c/NIP1 and the b/PRT1-RRM were also shown to critically contribute to the eIF3 affinity for the 40S subunit; however, their binding partners remain to be identified (12,37). Whether or not the remaining eIF3 subunits in i/TIF34 and g/TIF35 likewise participate in this functionally crucial eIF3-ribosome binding activity remained unclear until now. On the one hand a partial subcomplex composed of i/TIF34, g/TIF35 and b/PRT1 lacking its N-terminal RRM showed zero 40S-binding affinity *in vivo* (9). On the other hand, another subcomplex comprising c/NIP1, the critical N-terminal half of a/TIF32, and eIF5 showed a substantial affinity for the 40S subunits *in vivo*, though not as strong as that of the wt 6-subunit eIF3 (37). Based on these findings and the data presented here, we propose that whereas the major and essential driving force of the 40S-binding affinity of yeast eIF3 lies in the three largest subunits, as proposed earlier (37), i/TIF34 and g/TIF35 provide complementary 40S-binding activity that is required for stabilization of the entire 48S PICs. It is therefore conceivable that the proper establishment of all intermolecular bridges between eIF3 and the 40S ribosome is needed to ensure precise positioning of eIF3 on the small subunit and thereby flawless functioning of eIF3 not only in formation of 43S and 48S PICs, but also in the subsequent initiation steps.

This last notion resonates with our findings that the *DD/KK* mutation produces severe Gcn$^-$ phenotype owing to the robustly increased skipping of the AUG start codon (Figure 6). It is assumed that this so-called leaky scanning phenotype results from an inability of the 48S PIC to switch from the open/scanning-conducive conformation of the 40S head region to the closed/scanning-arrested one that occurs upon AUG recognition and is strictly regulated by eIFs 1 and 1A (reviewed in (46)). The conformational change upon scanning arrest is characterized by dissolution of the contact between RPS3 and helix 16 of 18S rRNA and reformation of the helix18–helix34-RPS3 connection designated as the latch on the mRNA entry channel (49). Interestingly, the leaky scanning phenotype was also observed with mutations disrupting the web of interactions among the a/TIF32-CTD, the b/PRT1-RRM and j/HCR1 located most likely below the mRNA entry channel (12,48) (Figure 9, lower panel). Likewise, g/TIF35 was recently found to interact with RPS3 and RPS20, two subunits located above the mRNA entry channel (5) (Figure 9). This advocates that both termini of b/PRT1 and their associated eIF3 subunits can influence the precision and/or timing of this critical conformational transition upon AUG start codon

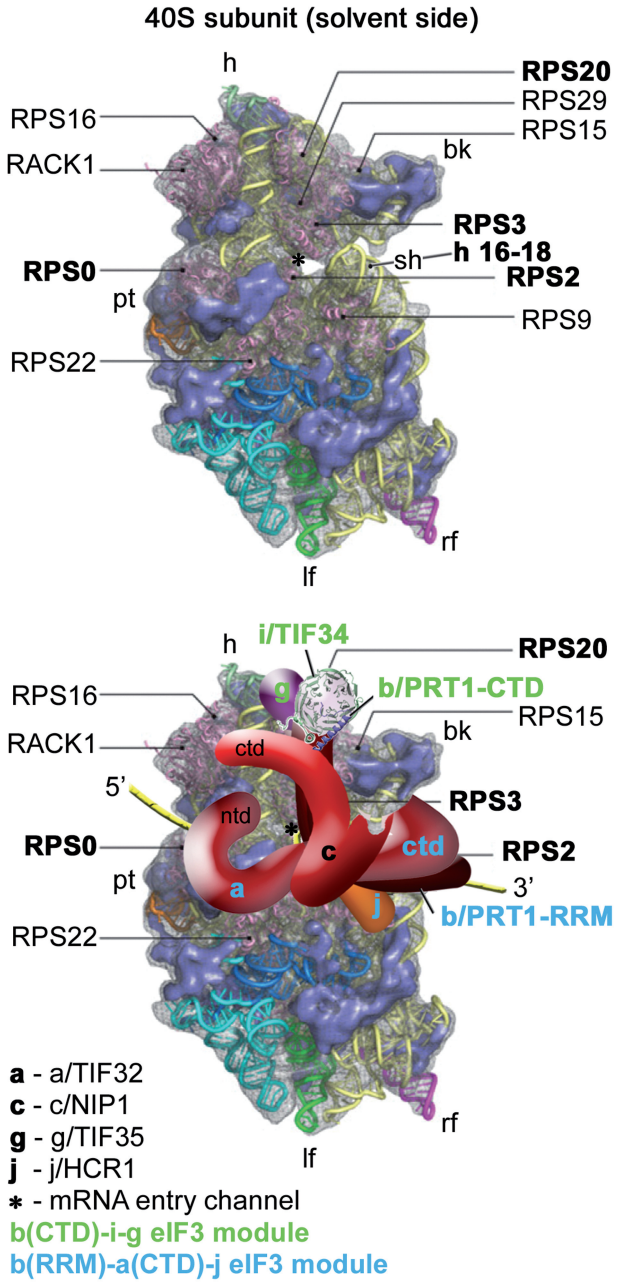

Figure 9. A model of two eIF3 modules bound to the opposite termini of the scaffold b/PRT1 subunit situated near the mRNA entry channel of the 40S subunit. (Upper panel) The Cryo-EM reconstruction of the 40S subunit is shown from the solvent side with ribosomal RNA represented as tubes. Ribosomal proteins, with known bacterial homologs and placement, are shown as pink cartoons and labeled (adapted from (57)). Positions of RPS0, 2, 3 and 20 and 18S rRNA helices 16–18 are highlighted in bold. The mRNA entry channel is designated by an asterisk. (Lower panel) Hypothetical location of *S. cerevisiae* eIF3 on the back side of the 40S subunit based on the data presented in this study and elsewhere, including the interactions between RPS0 and a/TIF32-NTD; RPS2 and j/HCR1; RPS2 and 3 and a/TIF32-CTD; helices 16-18 of 18S rRNA and a/TIF32-CTD; and RPS3 and 20 and g/TIF35 (see text for details). The schematic representations of b/PRT1-CTD and i/TIF34 were replaced with the X-ray structure as in Figure 4C. Two eIF3 modules represented by the b/PRT1-CTD–i/TIF34–g/TIF35 and the b/PRT1-RRM–a/TIF32-CTD–j/HCR1 are color-coded in green and blue, respectively. The yellow lines represent mRNA.

recognition (see our model in Figure 9, lower panel). We envisage three functional consequences of our mutants that could explain the leaky scanning as well as growth defects.

First, the lack of i/TIF34 and g/TIF35 may change the overall conformation and/or orientation of the rest eIF3 on the ribosome in a way that interferes with dynamics of the latch closing upon start codon recognition, allowing the 40S ribosome to skip the authentic AUG codon and continue scanning downstream. The aforementioned fact that g/TIF35 interacts with RPS20 and mainly with RPS3, which is one of the main components of the 'latch mechanism' (5), is consistent with this hypothesis. If true, the scaffold b/PRT1 subunit would serve to connect two eIF3 modules at each of its termini as indicated in Figure 9 (a/TIF32-CTD–j/HCR1 at the N-terminal RRM, and i/TIF34–g/TIF35 at the C-terminal α-helix) that would work together and with c/NIP1 (39) and other eIFs (46) to fine-tune the AUG selection process.

The second contributor to the leaky scanning phenotype might originate from defects in the interaction of the PICs with mRNA in the background of the disrupted interactions between eIFs. It is evident now that eIF3 is crucial for productive mRNA recruitment (50,51) and there is also evidence that eIF3 directly interacts with mRNA (5,44,52). This might suggest that changes in how eIF3 interacts with the PICs could negatively affect the way the mRNA interacts with the mRNA binding channel having an ultimate impact on fidelity of start codon recognition.

The third contribution could arise from our finding that breaking the contact between b/PRT1 and i/TIF34 subunits leads to accumulation of erroneous PICs containing the TC and eIF1 (Figure 6A), the amounts of which can be reduced by overexpressing *TIF35* (Figure 7C) or *sui1*^{G107R} (Figure 8C). The fact that high dosage of g/TIF35 suppresses the Gcn$^-$ and partially also the Slg$^-$ phenotypes of *tif34-DD/KK* but paradoxically does not better the assembly of the MFC and 48S PICs indicates that the presence of these aberrant complexes has a dominant negative effect on the initiation process reducing the overall fitness of mutant cells. Given the lack of any precedent for these repeatedly observable effects, we can only hypothesize that such forms of aberrant PICs would originate from simultaneous binding of all eIFs associated around eIF3 in the MFC to the ribosome followed by rapid dissociation of the unstably bound eIF3 (since lacking the i/TIF34–g/TIF35 mini-module) and eIF5 (eIF5 is known to bind to eIF3 very tightly (3)). It is assumed that the MFC has to undergo a relatively extensive rearrangement when it associates with the 40S subunit (37), as eIFs 1, 2, and most probably also 5 occur on the 40S interface side, whereas eIF3 binds to the solvent-exposed side [reviewed in (2)]. Hence we can stipulate that eIF3 and eIF5 preferentially fall off during this rearrangement period. We further stipulate that the resulting TC-eIF1-rich PICs would have the TC locked in a conformation conducive to scanning but incompatible with initiation (the so-called the P^{out} conformation of the TC), as recently described for some eIF1A mutants (53), and as such they would be skipping the AUG start codons with dramatically increased frequency, as observed with our mutants. How to explain the paradox mentioned above? We propose that the increased dosage of g/TIF35 completely eliminates the MFC-driven PIC assembly pathway that is considered to be the most efficient way of the PIC formation (1). As a consequence, PICs in the mutant cells overexpressing *g/TIF35* must form solely by a less efficient yet still fully functional stochastic association of individual eIFs with the 40S ribosome, reminiscent of the bacterial initiation reaction, with no need for ribosomal rearrangement.

The fact that high dosage of sui1^{G107R} also reduced amounts of TC-containing PICs in *tif34-DD/KK* (Figure 8C) but, in contrast to high copy *TIF35*, did not further destabilize the MFC in the mutant cells suggests a different molecular mechanism of suppression. In the light of earlier observations with reconstituted translational systems showing that mammalian eIF1 disrupts aberrantly formed PICs *in vitro* (54), we could speculate that an increased dosage of eIF1 disrupts the aberrant PICs directly also *in vivo*. In support, we found that the *sui1*^{G107R} mutant, which in contrast to other *sui1* mutants decreases the fidelity of start codon recognition without increasing the rate of eIF1 release from the PICs, suppressed the Gcn$^-$ and leaky scanning phenotypes of the *DD/KK* mutant like wt eIF1 (Figure 8A and B). These results imply that the eIF1 effect in *DD/KK* cells requires its stable physical presence on the 40S ribosome, where it could directly manipulate the aberrant PICs. However, at odds with this scenario, overexpression of wt eIF1 had no impact on the amounts of the 40S-bound TC in *tif34-DD/KK*. Hence at present we cannot offer any satisfactory explanation for this rather intriguing observation.

The aforementioned paradox that overexpressing *TIF35* significantly suppresses the growth defect of the *tif34-DD/KK* mutant without rescuing the 40S association of eIF3 and eIF5 may also evoke a notion that the yeast cells can grow at wt rates with only a relatively small fraction (~40%) of the normal amounts of eIF3, eIF2 and eIF5 bound to 40S PICs. While we indeed cannot rule out this possibility, we think that in reality the 40S-binding of all factors in the living cells is most likely not as dramatically affected as we see in our cross-linking experiments, where the effect of a weaker 40S-association might get magnified by a mechanical breakage of cells and all other *in vitro* manipulations.

Finally, it should also be noted that we recently generated and analyzed two specific mutations in i/TIF34 and g/TIF35, neither of which had any effects on eIF3 and PIC assembly, that produced a severe slow scanning defect and significantly reduced processivity of scanning through stable secondary structures (5). Neither of these scanning phenotypes was, however, found associated with the *W674A* and *DD/KK* mutations analyzed here. This is not surprising, since the latter mutations affect translation by destabilizing the MFC and PIC formation, while the former mutations, which have no assembly defects, primarily disrupt eIF3 functions downstream of the 48S PIC assembly. This is consistent with the dual role of eIF3 as a central hub required for

mRNA binding to the 43S PIC (48,50,51) as well as a crucial player in scanning and AUG recognition (5,12,39). It will now be intriguing to investigate the binding determinants of g/TIF35 in a partial subcomplex with i/TIF34 and b/PRT1-CTD and their interactions with the 40S subunit using the powerful combination of structural, genetic and biochemical approaches in order to continue replacing the *hic sunt leones* on our illustrative model of eIF3 with real structures as presented in Figure 4C.

ACCESSION CODES

Structure factors and coordinates for the i/TIF34-b/PRT1(654-700) complex have been deposited in the Protein Data Bank under accession code 3zwl.

SUPPLEMENTARY DATA

Supplementary Data are available at NAR Online: Supplementary Tables 1–5, Supplementary Figures 1–9, Supplementary Methods, Supplementary References [58–64].

ACKNOWLEDGEMENTS

We are thankful to Jon Lorsch, Monica Liu and Phil Evans for critical reading of the manuscript and to an unknown reviewer for his insightful comments. We are indebted to Phil Evans and Gerhard Reitmayr for help with diffraction data analysis and Python scripting. We also gratefully acknowledge members of Lukavsky, Valášek, Neuhaus, Nagai and Krásný laboratories for numerous discussions.

FUNDING

The Wellcome Trust grant (090812/B/09/Z); Howard Hughes Medical Institute, and Inst. Research Concept (AV0Z50200510 to L.S.V.); the Medical Research Council and HFSP (RGP0024/2008 to P.J.L.); EMBO Long-term fellowship (to D.D.). Funding for open access charge: The Wellcome Trust grant (090812/B/09/Z).

Conflict of interest statement. None declared.

REFERENCES

1. Hinnebusch,A.G. (2006) eIF3: a versatile scaffold for translation initiation complexes. *Trends Biochem Sci.*, **31**, 553–562.
2. Jackson,R.J., Hellen,C.U.T. and Pestova,T.V. (2010) The mechanism of eukaryotic translation initiation and principles of its regulation. *Nat. Rev. Mol. Cell Biol.*, **11**, 113–127.
3. Phan,L., Schoenfeld,L.W., Valášek,L., Nielsen,K.H. and Hinnebusch,A.G. (2001) A subcomplex of three eIF3 subunits binds eIF1 and eIF5 and stimulates ribosome binding of mRNA and $tRNA_i^{Met}$. *EMBO J.*, **20**, 2954–2965.
4. Naranda,T., Kainuma,M., McMillan,S.E. and Hershey,J.W.B. (1997) The 39-kilodalton subunit of eukaryotic translation initiation factor 3 is essential for the complex's integrity and for cell viability in *Saccharomyces cerevisiae*. *Mol. Cell. Biol.*, **17**, 145–153.
5. Cuchalová,L., Kouba,T., Herrmannová,A., Danyi,I., Chiu,W.-l. and Valášek,L. (2010) The RNA recognition motif of eukaryotic translation initiation factor 3g (eIF3g) is required for resumption of scanning of posttermination ribosomes for reinitiation on GCN4 and together with eIF3i stimulates linear scanning. *Mol. Cell. Biol.*, **30**, 4671–4686.
6. Masutani,M., Sonenberg,N., Yokoyama,S. and Imataka,H. (2007) Reconstitution reveals the functional core of mammalian eIF3. *EMBO J.*, **26**, 3373–3383.
7. Fraser,C.S., Lee,J.Y., Mayeur,G.L., Bushell,M., Doudna,J.A. and Hershey,J.W. (2004) The j-subunit of human translation initiation factor eIF3 is required for the stable binding of eIF3 and its subcomplexes to 40S ribosomal subunits in vitro. *J. Biol. Chem.*, **279**, 8946–8956.
8. Zhou,M., Sandercock,A.M., Fraser,C.S., Ridlova,G., Stephens,E., Schenauer,M.R., Yokoi-Fong,T., Barsky,D., Leary,J.A., Hershey,J.W. *et al.* (2008) Mass spectrometry reveals modularity and a complete subunit interaction map of the eukaryotic translation factor eIF3. *Proc. Natl Acad. Sci. USA*, **105**, 18139–18144.
9. Valášek,L., Nielsen,K.H. and Hinnebusch,A.G. (2002) Direct eIF2-eIF3 contact in the multifactor complex is important for translation initiation in vivo. *EMBO J.*, **21**, 5886–5898.
10. Asano,K., Phan,L., Anderson,J. and Hinnebusch,A.G. (1998) Complex formation by all five homologues of mammalian translation initiation factor 3 subunits from yeast *Saccharomyces cerevisiae*. *J. Biol. Chem.*, **273**, 18573–18585.
11. ElAntak,L., Tzakos,A.G., Locker,N. and Lukavsky,P.J. (2007) Structure of eIF3b RNA recognition motif and its interaction with eIF3j: structural insights into the recruitment of eIF3b to the 40 S ribosomal subunit. *J. Biol. Chem.*, **282**, 8165–8174.
12. ElAntak,L., Wagner,S., Herrmannová,A., Karásková,M., Rutkai,E., Lukavsky,P.J. and Valášek,L. (2010) The indispensable N-terminal half of eIF3j co-operates with its structurally conserved binding partner eIF3b-RRM and eIF1A in stringent AUG selection. *J. Mol. Biol.*, **396**, 1097–1116.
13. Valášek,L., Phan,L., Schoenfeld,L.W., Valášková,V. and Hinnebusch,A.G. (2001) Related eIF3 subunits TIF32 and HCR1 interact with an RNA recognition motif in PRT1 required for eIF3 integrity and ribosome binding. *EMBO J.*, **20**, 891–904.
14. Marintchev,A. and Wagner,G. (2005) Translation initiation: structures, mechanisms and evolution. *Q. Rev. Biophys.*, **37**, 197–284.
15. Dodd,R.B., Allen,M.D., Brown,S.E., Sanderson,C.M., Duncan,L.M., Lehner,P.J., Bycroft,M. and Read,R.J. (2004) Solution structure of the Kaposi's sarcoma-associated Herpesvirus K3 N-terminal domain reveals a novel E2-binding C4HC3-type RING domain. *J. Biol. Chem.*, **279**, 53840–53847.
16. Muchmore,S.W., Sattler,M., Liang,H., Meadows,R.P., Harlan,J.E., Yoon,H.S., Nettesheim,D., Chang,B.S., Thompson,C.B., Wong,S.-L. *et al.* (1996) X-ray and NMR structure of human Bcl-xL, an inhibitor of programmed cell death. *Nature*, **381**, 335–341.
17. Szymczyna,B.R., Taurog,R.E., Young,M.J., Snyder,J.C., Johnson,J.E. and Williamson,J.R. (2009) Synergy of NMR, computation, and X-ray crystallography for structural biology. *Structure*, **17**, 499–507.
18. Leslie,A. (2006) The integration of macromolecular diffraction data. *Acta Cryst.Section D*, **62**, 48–57.
19. Evans,P. (2006) Scaling and assessment of data quality. *Acta Cryst. Section D*, **62**, 72–82.
20. French,S. and Wilson,K. (1978) On the treatment of negative intensity observations. *Acta Cryst Section A*, **34**, 517–525.
21. Collaborative Computational Project,N. (1994) The CCP4 suite: programs for protein crystallography. *Acta Crystallogr. D Biol Crystallogr.*, **50**, 760–763.
22. de La Fortelle,E. and Bricogne,G. (1997) Maximum-likelihood heavy-atom parameter refinement for multiple isomorphous replacement and multiwavelength anomalous diffraction methods. *Methods Enzymol.*, **276**, 472–494.
23. Kelley,L.A. and Sternberg,M.J.E. (2009) Protein structure prediction on the Web: a case study using the Phyre server. *Nat. Protocols*, **4**, 363–371.
24. McCoy,A.J., Grosse-Kunstleve,R.W., Storoni,L.C. and Read,R.J. (2005) Likelihood-enhanced fast translation functions. *Acta Cryst. Section D*, **61**, 458–464.

25. Zhang,K.Y., Cowtan,K. and Main,P. (1997) Combining constraints for electron-density modification. *Methods Enzymol.*, **277**, 53–64.
26. Cowtan,K. (2006) The Buccaneer software for automated model building. 1. Tracing protein chains. *Acta Cryst. Section D*, **62**, 1002–1011.
27. Emsley,P. and Cowtan,K. (2004) Coot: model-building tools for molecular graphics. *Acta Cryst. Section D*, **60**, 2126–2132.
28. Murshudov,G.N., Vagin,A.A. and Dodson,E.J. (1997) Refinement of macromolecular structures by the maximum-likelihood method. *Acta Cryst. Section D*, **53**, 240–255.
29. Davis,I.W., Leaver-Fay,A., Chen,V.B., Block,J.N., Kapral,G.J., Wang,X., Murray,L.W., Arendall,W.B. III, Snoeyink,J., Richardson,J.S. *et al.* (2007) MolProbity: all-atom contacts and structure validation for proteins and nucleic acids. *Nucleic Acids Res.*, **35**, W375–383.
30. Coyle,S.M., Gilbert,W.V. and Doudna,J.A. (2009) Direct Link between RACK1 function and localization at the ribosome in vivo. *Mol. Cell. Biol.*, **29**, 1626–1634.
31. Li,D. and Roberts,R. (2001) Human genome and diseases: WD-repeat proteins: structure characteristics, biological function, and their involvement in human diseases. *Cell. Mol. Life Sci.*, **58**, 2085–2097.
32. Jennings,B.H., Pickles,L.M., Wainwright,S.M., Roe,S.M., Pearl,L.H. and Ish-Horowicz,D. (2006) Molecular recognition of transcriptional repressor motifs by the WD domain of the groucho/TLE corepressor. *Mol. Cell*, **22**, 645–655.
33. Oliver,A.W., Swift,S., Lord,C.J., Ashworth,A. and Pearl,L.H. (2009) Structural basis for recruitment of BRCA2 by PALB2. *EMBO Rep.*, **10**, 990–996.
34. ter Haar,E., Harrison,S.C. and Kirchhausen,T. (2000) Peptide-in-groove interactions link target proteins to the Î²-propeller of clathrin. *Proc. Natl Acad. Sci. USA*, **97**, 1096–1100.
35. Krissinel,E. and Henrick,K. (2007) Inference of macromolecular assemblies from crystalline state. *J. Mol. Biol.*, **372**, 774–797.
36. Gallivan,J.P. and Dougherty,D.A. (1999) Cation-pi interactions in structural biology. *Proc. Natl Acad. Sci. USA*, **96**, 9459–9464.
37. Valášek,L., Mathew,A., Shin,B.S., Nielsen,K.H., Szamecz,B. and Hinnebusch,A.G. (2003) The yeast eIF3 subunits TIF32/a and NIP1/c and eIF5 make critical connections with the 40S ribosome in vivo. *Genes Dev.*, **17**, 786–799.
38. Valášek,L., Szamecz,B., Hinnebusch,A.G. and Nielsen,K.H. (2007) In vivo stabilization of preinitiation complexes by formaldehyde cross-linking. *Methods Enzymol.*, **429**, 163–183.
39. Valášek,L., Nielsen,K.H., Zhang,F., Fekete,C.A. and Hinnebusch,A.G. (2004) Interactions of eukaryotic translation initiation factor 3 (eIF3) subunit NIP1/c with eIF1 and eIF5 promote preinitiation complex assembly and regulate start codon selection. *Mol. Cell. Biol.*, **24**, 9437–9455.
40. Fekete,C.A., Mitchell,S.F., Cherkasova,V.A., Applefield,D., Algire,M.A., Maag,D., Saini,A.K., Lorsch,J.R. and Hinnebusch,A.G. (2007) N- and C-terminal residues of eIF1A have opposing effects on the fidelity of start codon selection. *EMBO J.*, **26**, 1602–1614.
41. Nanda,J.S., Cheung,Y.-N., Takacs,J.E., Martin-Marcos,P., Saini,A.K., Hinnebusch,A.G. and Lorsch,J.R. (2009) eIF1 controls multiple steps in start codon recognition during eukaryotic translation initiation. *J. Mol. Biol.*, **394**, 268–285.
42. Hinnebusch,A.G. (2005) Translational regulation of GCN4 and the general amino acid control of yeast. *Annu. Rev. Microbiol.*, **59**, 407–450.
43. Nielsen,K.H., Szamecz,B., Valasek,L., Jivotoskaya,A., Shin,B.S. and Hinnebusch,A.G. (2004) Functions of eIF3 downstream of 48S assembly impact AUG recognition and GCN4 translational control. *EMBO J.*, **23**, 1166–1177.
44. Szamecz,B., Rutkai,E., Cuchalova,L., Munzarova,V., Herrmannova,A., Nielsen,K.H., Burela,L., Hinnebusch,A.G. and Valášek,L. (2008) eIF3a cooperates with sequences 5′ of uORF1 to promote resumption of scanning by post-termination ribosomes for reinitiation on GCN4 mRNA. *Genes Dev.*, **22**, 2414–2425.
45. Munzarová,V., Pánek,J., Gunišová,S., Dányi,I., Szamecz,B. and Valášek,L.S. (2011) Translation reinitiation relies on the interaction between eIF3a/TIF32 and progressively folded cis-acting mRNA elements preceding short uORFs. *PLoS Genet.*, **7**, e1002137.
46. Mitchell,S.F. and Lorsch,J.R. (2008) Should I stay or should i go? Eukaryotic translation initiation factors 1 and 1a control start codon recognition. *J. Biol. Chem.*, **283**, 27345–27349.
47. Cheung,Y.N., Maag,D., Mitchell,S.F., Fekete,C.A., Algire,M.A., Takacs,J.E., Shirokikh,N., Pestova,T., Lorsch,J.R. and Hinnebusch,A.G. (2007) Dissociation of eIF1 from the 40S ribosomal subunit is a key step in start codon selection in vivo. *Genes Dev.*, **21**, 1217–1230.
48. Chiu,W.-L., Wagner,S., Herrmannova,A., Burela,L., Zhang,F., Saini,A.K., Valasek,L. and Hinnebusch,A.G. (2010) The C-terminal region of eukaryotic translation initiation factor 3a (eIF3a) promotes mRNA recruitment, scanning, and, together with eIF3j and the eIF3b RNA recognition motif, selection of AUG start codons. *Mol. Cell. Biol.*, **30**, 4415–4434.
49. Passmore,L.A., Schmeing,T.M., Maag,D., Applefield,D.J., Acker,M.G., Algire,M.A., Lorsch,J.R. and Ramakrishnan,V. (2007) The eukaryotic translation initiation factors eIF1 and eIF1A induce an open conformation of the 40S ribosome. *Mol. Cell*, **26**, 41–50.
50. Mitchell,S.F., Walker,S.E., Algire,M.A., Park,E.-H., Hinnebusch,A.G. and Lorsch,J.R. (2010) The 5′-7-Methylguanosine Cap on eukaryotic mRNAs serves both to stimulate canonical translation initiation and to block an alternative pathway. *Mol. Cell*, **39**, 950–962.
51. Jivotovskaya,A., Valášek,L., Hinnebusch,A.G. and Nielsen,K.H. (2006) Eukaryotic translation initiation factor 3 (eIF3) and eIF2 can promote mRNA binding to 40S subunits independently of eIF4G in yeast. *Mol. Cell. Biol.*, **26**, 1355–1372.
52. Pisarev,A.V., Kolupaeva,V.G., Yusupov,M.M., Hellen,C.U.T. and Pestova,T.V. (2008) Ribosomal position and contacts of mRNA in eukaryotic translation initiation complexes. *EMBO J.*, **27**, 1609–1621.
53. Saini,A.K., Nanda,J.S., Lorsch,J.R. and Hinnebusch,A.G. (2010) Regulatory elements in eIF1A control the fidelity of start codon selection by modulating tRNAiMet binding to the ribosome. *Genes Dev.*, **24**, 97–110.
54. Pestova,T.V., Borukhov,S.I. and Hellen,C.U.T. (1998) Eukaryotic ribosomes require initiation factors 1 and 1A to locate initiation codons. *Nature*, **394**, 854–859.
55. Baker,N.A., Sept,D., Joseph,S., Holst,M.J. and McCammon,J.A. (2001) Electrostatics of nanosystems: Application to microtubules and the ribosome. *Proc. Natl Acad. Sci. USA*, **98**, 10037–10041.
56. Dolinsky,T.J., Czodrowski,P., Li,H., Nielsen,J.E., Jensen,J.H., Klebe,G. and Baker,N.A. (2007) PDB2PQR: expanding and upgrading automated preparation of biomolecular structures for molecular simulations. *Nucleic Acids Res.*, **35**, W522–W525.
57. Taylor,D.J., Devkota,B., Huang,A.D., Topf,M., Narayanan,E., Sali,A., Harvey,S.C. and Frank,J. (2009) Comprehensive molecular structure of the eukaryotic ribosome. *Structure*, **17**, 1591–1604.
58. Kuzmic,P. (2009) DynaFit–a software package for enzymology. *Methods in Enzymology*, **467**, 247–280.
59. Kuzmic,P. (1996) Program DYNAFIT for the analysis of enzyme kinetic data: Application to HIV proteinase. *Analyt. Biochem.*, **237**, 260–273.
60. Nielsen,K.H. and Valášek,L. (2007) In vivo deletion analysis of the architecture of a multi-protein complex of translation initiation factors. *Methods Enzymol.*, **431**, 15–32.
61. Grant,C.M., Miller,P.F. and Hinnebusch,A.G. (1994) Requirements for intercistronic distance and level of eIF-2 activity in reinitiation on GCN4 mRNA varies with the downstream cistron. *Mol. Cell. Biol.*, **14**, 2616–2628.
62. Cigan,A.M., Foiani,M., Hannig,E.M. and Hinnebusch,A.G. (1991) Complex formation by positive and negative translational regulators of *GCN4*. *Mol. Cell. Biol.*, **11**, 3217–3228.
63. Smith,D.B. and Johnson,K.S. (1988) Single-step purification of polypeptides expressed in *Escherichia coli* as fusions with glutathione S-transferase. *Gene*, **67**, 31–40.
64. Gietz,R.D. and Sugino,A. (1988) New yeast-*Escherichia coli* shuttle vectors constructed with in vitro mutagenized yeast genes lacking six-base pair restriction sites. *Gene*, **74**, 527–534.

SUPPLEMENTARY INFORMATION

MATERIALS AND METHODS

i/TIF34-b/PRT1 Affinity Analysis Using Gel Mobility Shift Assays.
The [^{35}S]-labeled C-terminal b/PRT1 peptides were prepared using the TnT coupled rabbit reticulocyte *in vitro* translation and transcription system (Promega). Proteins were synthesized by incubating 1 μg of plasmid in 40 μl of TnT Quick Master mixture with 2 μl of L-[^{35}S] methionine (Amersham Biosciences) for 2 hours at 25°C. The *in vitro* translated products were then purified using HIS-Select™ spin columns (Sigma) according to the manufacturer's instructions. Unlabeled C-terminal b/PRT1 peptides and i/TIF34 were expressed in *E. coli* and purified as above. Dissociation constant of b/PRT1(630-724) was determined by titrating purified [^{35}S]-b/PRT1 (0.1 μM final concentration) with increasing amount of purified i/ TIF34 (0, 0.1, 0.25, 0.5, 1.0, 5.0, 10, 25.0 μM final concentration) in a final volume of 20 μl reaction mix containing 20 mM Hepes pH 7.5, 50 mM NaCl and 5% glycerol. For competition assay, 0.2 μM#[^{35}S]-b/PRT1 (630-724) was first mixed with 1 μM i/TIF34, then unlabeled b/PRT1 peptides were added to increasing concentrations at the following ratios of unlabelled to labelled protein: 0.1, 0.5, 1, 10, 25, 50, 100 for b(630-724); 1, 2, 10, 25, 50, 100 for W674F; 1, 10, 25, 50, 100, 200 for W674A; 1, 10, 25, 50, 200 for Y677A/R68A; and 1, 5, 50, 100, 200 for b(654-700). Complexes were formed at 30°C and analyzed on 4-16% native polyacrylamide BisTris gels (Invitrogen). Gel electrophoresis was performed for 2 h at 100 V at 4 °C using NativePAGE running buffer (Invitrogen). Gels were then dried on Whatman paper and exposed overnight on a PhosphorImager screen. Bound and free radioactive b/PRT1 bands were quantified using ImageQuantTL image analysis tool. Data analysis was performed using DynaFit software (58,59). Direct and competition titration data were fit using equilibrium binding or displacement models for single site binding.

Calorimetry (ITC) Analysis of i/TIF34-b/PRT1 Interactions.
All calorimetric titrations were performed on a VP-ITC microcalorimeter (Microcal). Protein samples were dialyzed against the same storage/NMR buffer (see Materials and Methods in the main text). The sample cell was filled with 200 μl of 26 μM solution of i/TIF34 and the injection syringe with 288 μM or 200 μM of b/PRT1(654-700) or b/PRT1(630-724), respectively. Each titration typically consisted of a preliminary 0.5 μl injection followed by 20 subsequent 2-μl injections every 120 seconds. All of the experiments were performed at 25 °C. Data for the preliminary injection, which are affected by diffusion of the solution from and into the injection syringe during the initial equilibration period, were discarded. Binding isotherms were generated by plotting heats of reaction normalized by the moles of injectant versus the ratio of total injectant to total protein per injection. The data were fitted to single site binding model using Origin 7.0 (Microcal).

Yeast Genetic and Biochemical Methods.

GST pull-down assays with GST fusions and *in vitro*-synthesized [^{35}S]-labeled polypeptides were conducted as follows. Individual GST-fusion proteins were expressed in *E. coli*, immobilized on glutathione-Sepharose beads and incubated with 10 μl of [^{35}S]-labeled potential binding partners at 4°C for 2 h. The beads were washed 3 times with 1 ml of phosphate-buffered saline and bound proteins separated by SDS-PAGE. Gels were first stained with Gelcode Blue Stain Reagent (Pierce) and then subjected to autoradiography. Ni^{2+}-chelation chromatography of eIF3 complexes containing His_8-tagged b/PRT1 or g/TIF35 from yeast whole-cell extracts (WCEs) and Western blot analysis were conducted as described in detail previously (60). In short, WCEs were incubated with 15 μL of 50% Ni^{2+}-NTA-silica resin (GE Healthcare) suspended in 200 μL of buffer A for 2 h at 4°C, followed by washing and elution. 2% HCHO cross-linking followed by WCE preparation and fractionation of extracts for analysis of pre-initiation complexes were carried out as described previously (38). β-galactosidase assays were conducted as described previously (61).

Preparation of Antibodies Against RPS0A.

The GST-RPS0A fusion protein encoded by pGEX-RPS0A was expressed in *E. coli* and purified from the WCE by incubation with Glutathione-Sepharose 4B beads (Pharmacia). The isolated protein was resolved by SDS-PAGE (4-20% gels), excised from the gel, and washed with 1x PBS. Rabbits were injected with the purified protein and serum containing polyclonal antibodies against RPS0A was obtained commercially by Apronex (Prague, the Czech Republic).

Construction of Yeast Strains and Plasmids.

List of all strains named below can be found in Tables S3.

To create AY134 strain, YAH06 was transformed with pRS-b/PRT1-HisXS and the original covering plasmid carrying *PRT1 URA3* was evicted on 5-FOA.

YAH11 was generated by a genetic cross of H420 and AY134 as a haploid ascospore resistant to 3-AT, unable to grow on 5-FOA, unable to evict a resident *LEU2* covering plasmid, and autotrophic for tryptophan.

To create YAH12 strain, YAH11 was transformed with pCR52-1 (62) and grown on SD media containing Leucine to get rid of the original pRS-b/PRT1-HisXS plasmid.

List of all plasmids and PCR primers named below can be found in Tables S4 and S5, respectively.

pRS-b/PRT1-W674A-His was generated by fusion PCR. The following pairs of primers were used for separate PCR amplifications using pRS-b/PRT1-His as template: (1) AH-PRT1-BamHI and AH-PRT1-W674A-R, respectively, (2) AH-PRT1-W674A and AH-PRT1-NotI-R, respectively. The PCR products thus obtained were used in a 1:1 ratio as templates for a third PCR amplification using primers AH-PRT1-BamHI and AH-PRT1-NotI-R. The resulting PCR product was digested with BamHI and NotI and ligated with BamHI-NotI-cleaved pRS-b/PRT1-His.

pRS-b/PRT1-W674F-His – was generated by fusion PCR. The following pairs of primers were used for separate PCR amplifications using pRS-b/PRT1-His as template: (1) AH-PRT1-BamHI and AH-PRT1-W674F-R, respectively, (2) AH-PRT1-W674F and AH-PRT1-NotI-R, respectively. The PCR products thus obtained were used in a 1:1 ratio as templates for a third PCR amplification using primers AH-PRT1-BamHI and AH-PRT1-NotI-R. The resulting PCR product was digested with BamHI and NotI and ligated with BamHI-NotI-cleaved pRS-b/PRT1-His.

pRS-b/PRT1-Y677A-His was made by inserting the BamHI-MscI digested PCR product obtained with primers AH-PRT1-BamHI and AH-PRT1-Y677A-R using pRS-b/PRT1-HisXS as a template into BamHI-MscI digested pRS-b/PRT1-HisXS.

pRS-b/PRT1-R678A-His was made by inserting the BamHI-MscI digested PCR product obtained with primers AH-PRT1-BamHI and AH-PRT1-R678A-R using pRS-b/PRT1-HisXS as a template into BamHI-MscI digested pRS-b/PRT1-HisXS.

pRS-b/PRT1-Y677A-R678A-His was made by inserting the BamHI-MscI digested PCR product obtained with primers AH-PRT1-BamHI and AH-PRT1-YR-AA-R using pRS-b/PRT1-HisXS as a template into BamHI-MscI digested pRS-b/PRT1-HisXS.

pRS-b/PRT1-Y677A-R678D-His was made by inserting the BamHI-MscI digested PCR product obtained with primers AH-PRT1-BamHI and AH-PRT1-YR-AD-R using pRS-b/PRT1-HisXS as a template into BamHI-MscI digested pRS-b/PRT1-HisXS.

YCp-i/TIF34-D207K-HA was generated by fusion PCR. The following pairs of primers were used for separate PCR amplifications using YCp-i/TIF34-HA as template: (1) y3iKpnI and D207Kr, respectively, (2) D207K and BmgBIr, respectively. The PCR products thus obtained were used in a 1:1 ratio as templates for a third PCR amplification using primers y3iKpnI and BmgBIr. The resulting PCR product was digested with KpnI and BmgBI and ligated with KpnI-BmgBI-cleaved YCp-i/TIF34-HA.

YCp-i/TIF34-D224K-HA was generated by fusion PCR. The following pairs of primers were used for separate PCR amplifications using YCp-i/TIF34-HA as template: (1) y3iKpnI and D224Kr, respectively, (2) D224K and BmgBIr, respectively. The PCR products thus obtained were used in a 1:1 ratio as templates for a third PCR amplification using primers y3iKpnI and BmgBIr. The resulting PCR product was digested with KpnI and BmgBI and ligated with KpnI-BmgBI-cleaved YCp-i/TIF34-HA.

YCp-i/TIF34-D207K-D224K-HA was generated by fusion PCR. The following pairs of primers were used for separate PCR amplifications using YCp-i/TIF34-D207K-HA as template: (1) y3iKpnI and D224Kr, respectively, (2) D224K and BmgBIr, respectively. The PCR products thus obtained were used in a 1:1 ratio as templates for a third PCR amplification using primers y3iKpnI and BmgBIr. The resulting PCR product was digested with KpnI and BmgBI and ligated with KpnI-BmgBI-cleaved YCp-i/TIF34-D207K-HA.

YCp-i/TIF34-L222D-HA was generated by fusion PCR. The following pairs of primers were used for separate PCR amplifications using YCp-i/TIF34-HA as template: (1) y3iKpnI and LC3iLr, respectively, (2) LC3iL222D and BmgBIr, respectively. The PCR products thus obtained were used in a 1:1 ratio as templates for a third PCR amplification using primers y3iKpnI and BmgBIr. The resulting PCR product was digested with KpnI and BmgBI and ligated with KpnI-BmgBI-cleaved YCp-i/TIF34-HA.

YCp-i/TIF34-L222K-HA was generated by fusion PCR. The following pairs of primers were used for separate PCR amplifications using YCp-i/TIF34-HA as template: (1) y3iKpnI and LC3iLr, respectively, (2) LC3iL222K and BmgBIr, respectively. The PCR products thus obtained were used in a 1:1 ratio as templates for a third PCR amplification using primers y3iKpnI and BmgBIr. The resulting PCR product was digested with KpnI and BmgBI and ligated with KpnI-BmgBI-cleaved YCp-i/TIF34-HA.

YCp-i/TIF34-HA-W was constructed by inserting the 2223bp SacI-DrdI fragment from YCp-i/TIF34-HA into YCplac22 digested with SacI-DrdI.

YCp-i/TIF34-D207K-D224K-HA-W was constructed by inserting the 2223bp SacI-DrdI fragment from YCp-i/TIF34-D207K-D224K-HA into YCplac22 digested with SacI-DrdI.

YCp-i/TIF34-D207K-HA-W was constructed by inserting the 2223bp SacI-DrdI fragment from YCp-i/TIF34-D207K-HA into YCplac22 digested with SacI-DrdI.

YCp-i/TIF34-D224K-HA-W was constructed by inserting the 2223bp SacI-DrdI fragment from YCp-i/TIF34-D224K-HA into YCplac22 digested with SacI-DrdI.

YEp-g/TIF35-His was constructed by inserting the 2112bp EcoRI-PstI fragment from YCp-g/TIF35-His-screen into YEplac195 digested with EcoRI-PstI.

YEp-SUI1-G107R was constructed by inserting the 287bp BamHI-SacII fragment from pCFB134 into YEp-SUI1 digested with BamHI-SacII.

pT7-b/PRT1-W674A was constructed by inserting the 1222bp NsiI-MscI fragment from pRS-b/PRT1-W674A-His into pT7-b/PRT1 digested with NsiI-MscI.

pT7-b/PRT1-Y677A was constructed by inserting the 1222bp NsiI-MscI fragment from pRS-b/PRT1-Y677A-His into pT7-b/PRT1 digested with NsiI-MscI.

pT7-b/PRT1-R678A was constructed by inserting the 1222bp NsiI-MscI fragment from pRS-b/PRT1-R678A-His into pT7-b/PRT1 digested with NsiI-MscI.

pT7-i/TIF34-D207K-D224K was constructed by inserting the 587bp KpnI-EcoRI fragment from YCp-i/TIF34-D207K-D224K-HA into pT7-i/TIF34 digested with KpnI-EcoRI.

pGEX-RPS0A was constructed in two steps. First, the intron was removed by a fusion PCR using pGBK-RPS0A (37) as a template and the following pair of primers for two separate PCR reactions producing exon 1 (O1-BamHI x BSRPS0Aexon1-r) and exon2 (BSRPS0Aexon2 x O2-KpnI-XhoI-r), respectively. Both PCR products thus obtained were used in a 1:1 ratio as templates for a third PCR amplification using primers O1-BamHI and O2-KpnI-XhoI-r. The resulting PCR

product was digested with BamHI and XhoI and ligated with BamHI-XhoI-cleaved pGEX-4T-1 (63).

REFERENCES

58. Kuzmic, P., Michael, L.J. and Ludwig, B. (2009), *Methods in Enzymology*. Academic Press, Vol. Volume 467, pp. 247-280.
59. Kuzmic, P. (1996) Program DYNAFIT for the Analysis of Enzyme Kinetic Data: Application to HIV Proteinase. *Analytical Biochemistry*, **237**, 260-273.
60. Nielsen, K.H. and Valášek, L. (2007) In vivo deletion analysis of the architecture of a multi-protein complex of translation initiation factors. *Methods Enzymol.*, **431**, 15-32.
38. Valášek, L., Szamecz, B., Hinnebusch, A.G. and Nielsen, K.H. (2007) In Vivo Stabilization of Preinitiation Complexes by Formaldehyde Cross-Linking. *Methods Enzymol.*, **429**, 163-183.
61. Grant, C.M., Miller, P.F. and Hinnebusch, A.G. (1994) Requirements for intercistronic distance and level of eIF-2 activity in reinitiation on GCN4 mRNA varies with the downstream cistron. *Mol Cell Biol*, **14**, 2616-2628.
62. Cigan, A.M., Foiani, M., Hannig, E.M. and Hinnebusch, A.G. (1991) Complex formation by positive and negative translational regulators of *GCN4*. *Mol Cell Biol*, **11**, 3217-3228.
37. Valášek, L., Mathew, A., Shin, B.S., Nielsen, K.H., Szamecz, B. and Hinnebusch, A.G. (2003) The Yeast eIF3 Subunits TIF32/a and NIP1/c and eIF5 Make Critical Connections with the 40S Ribosome in vivo. *Genes Dev*, **17**, 786-799.
63. Smith, D.B. and Johnson, K.S. (1988) Single-step purification of polypeptides expressed in Escherichia coli as fusions with glutathione S-transferase. *Gene*, **67**, 31-40.
10. Asano, K., Phan, L., Anderson, J. and Hinnebusch, A.G. (1998) Complex formation by all five homologues of mammalian translation initiation factor 3 subunits from yeast *Saccharomyces cerevisiae*. *J Biol Chem*, **273**, 18573-18585.
29. Davis, I.W., Leaver-Fay, A., Chen, V.B., Block, J.N., Kapral, G.J., Wang, X., Murray, L.W., Arendall, W.B., III, Snoeyink, J., Richardson, J.S. *et al.* (2007) MolProbity: all-atom contacts and structure validation for proteins and nucleic acids. *Nucleic Acids Research*, **35**, W375-383.
35. Krissinel, E. and Henrick, K. (2007) Inference of Macromolecular Assemblies from Crystalline State. *J Mol Biol.*, **372**, 774-797.
12. ElAntak, L., Wagner, S., Herrmannová, A., Karásková, M., Rutkai, E., Lukavsky, P.J. and Valášek, L. (2010) The indispensable N-terminal half of eIF3j co-operates with its structurally conserved binding partner eIF3b-RRM and eIF1A in stringent AUG selection. *J Mol Biol.*, **396**, 1097-1116.
64. Gietz, R.D. and Sugino, A. (1988) New yeast-Escherichia coli shuttle vectors constructed with in vitro mutagenized yeast genes lacking six-base pair restriction sites. *Gene*, **74**, 527-534.
5. Cuchalová, L., Kouba, T., Herrmannová, A., Danyi, I., Chiu, W.-l. and Valášek, L. (2010) The RNA Recognition Motif of Eukaryotic Translation Initiation Factor 3g (eIF3g) Is Required for Resumption of Scanning of Posttermination Ribosomes for Reinitiation on GCN4 and Together with eIF3i Stimulates Linear Scanning. *Mol Cell Biol*, **30**, 4671-4686.

39. Valášek, L., Nielsen, K.H., Zhang, F., Fekete, C.A. and Hinnebusch, A.G. (2004) Interactions of Eukaryotic Translation Initiation Factor 3 (eIF3) Subunit NIP1/c with eIF1 and eIF5 Promote Preinitiation Complex Assembly and Regulate Start Codon Selection. *Mol. Cell. Biol.*, **24**, 9437-9455.
47. Cheung, Y.N., Maag, D., Mitchell, S.F., Fekete, C.A., Algire, M.A., Takacs, J.E., Shirokikh, N., Pestova, T., Lorsch, J.R. and Hinnebusch, A.G. (2007) Dissociation of eIF1 from the 40S ribosomal subunit is a key step in start codon selection in vivo. *Genes Dev*, **21**, 1217-1230.
13. Valášek, L., Phan, L., Schoenfeld, L.W., Valášková, V. and Hinnebusch, A.G. (2001) Related eIF3 subunits TIF32 and HCR1 interact with an RNA recoginition motif in PRT1 required for eIF3 integrity and ribosome binding. *EMBO J*, **20**, 891-904.

FIGURE LEGENDS

Figure S1. Identification of the minimal i/TIF34-binding site of b/PRT1. (**A**) Overlay of $^{1}H,^{15}N$-TROSY (transverse relaxation optimized spectroscopy) spectra of ^{13}C, ^{15}N-labelled b/PRT1(630-724) in the free form (purple) or bound to unlabelled i/TIF34 (pink). Assigned amide crosspeaks from bound b/PRT1(630-724) which display sharp resonance lines and random coil chemical shifts are labeled. The NεH side chain crosspeaks of W644 and W674, which resonate downfield of the backbone amide NH crosspeaks are shown in an inset. Only the W674-NεH resonances display large chemical changes upon i/TIF34 binding, while W644-NεH remains unchanged suggesting that the middle part if b/PRT1(630-724) comprises the i/TIF34 binding site. (**B**) Overlay of $^{1}H,^{15}N$-TROSY spectra of ^{15}N-labelled b/PRT1(630-724; purple) or ^{15}N-labelled b/PRT1(654-700; pink) both bound to unlabelled i/TIF34. The shorter b/PRT1 peptide lacks most of the sharp, random coil amide NH resonances from the longer b/PRT1 peptide, while very similar, broad amide NH resonances close to the noise level arising from i/TIF34-interacting parts of b/PRT1 are observed in both peptides. The Trp-NεH side chain crosspeaks are shown in an inset. The shorter b/PRT1 peptide (pink) lacks the sharp, random coil W644-NεH resonances of the longer peptide (purple), but displays the same broad, downfield-shifted crosspeak for W674-NεH as found for the longer peptide suggesting a very similar binding mode of both peptides. (**C**) Isothermal calorimetric titration of i/TIF34 with b/PRT1(630-724) and b/PRT1(654-700) reveal comparable binding affinities. The panels show experimental data and the fitted binding isotherms. The data was analyzed using Origin 7.0 (MicroCal) software. Data points were obtained by integration of heat signals plotted against the molar ratio of i/TIF34 to b/PRT1 variants in the reaction cell. The solid line represents a calculated curve using the best-fit parameters obtained by a nonlinear least squares fit. The b/PRT1 construct used for each experiment is indicated in the panel.

Figure S2. Sequence alignment of i/TIF34 and b/PRT1 from different species and stereo view of the i/TIF34 - b/PRT1 binding interface. (**A**) Sequence alignment of eIF3i/TIF34 and eIF3b/PRT1 from *S. cerevisiae*, human, *Drosophila*, frog, *Neurospora*, Mouse and *Arabidopsis*. Phylogenetic analysis reveals a high level of

eIF3i/TIF34 and eIF3b/PRT1 conservation between species. In eIF3b/PRT1, only the C-terminus is shown; blue triangles indicate boundaries of our eIF3b/PRT1 construct, residues important for the interaction and discussed in the text are numbered according to *S. cerevisiae*. Secondary structure elements are shown above the aligned sequences. (**B**) Interface of i/TIF34 and b/PRT1(654-700) interactions. i/TIF34 is in green, b/PRT1(654-700) in blue. Cross-eye stereo image was generated using PyMOL (http://www.pymol.org).

Figure S3. Structure of the i/TIF34-b/PRT1(654-700) complex. (**A**) Left, experimentally phased, solvent-flattened electron density map with the refined model superimposed. Right, part of the experimental electron density map in the region of b/PRT1(654-700). Protein backbones are shown as ribbons. (**B**) Overall view of the i/TIF34-b/PRT1(654-700) complex (two complexes in asymmetric unit) with the corresponding 2mFo-DFc electron density map shown contoured at 1 sigma. i/TIF34 is in green, b/PRT1(654-700) in blue. Ray-traced images were generated using PyMOL (http://www.pymol.org).

Figure S4. Two i/TIF34-b/PRT1 complexes are present in the asymmetric unit. i/TIF34 chains are shown in green, b/PRT1 in blue. Blades in the β-propeller structure of i/TIF34 are numbered from 1 to 7 (N to C-terminus). The two complexes in the asymmetric unit interact through the surface-exposed loop (residues 112-121 in blade 4) of one i/TIF34 molecule with β-sheet in blade 1 and loop in blade 2 of another i/TIF34 molecule, as depicted by the red arrow. Complex I denotes chains E and B, as named in the pdb file, and complex II – chains F and D.

Figure S5. Positional comparison of the i/TIF34 residues directly interacting with b/PRT1 with those identified in previous mutational studies by Asano and co-workers (10), which cluster on opposite sides of beta-propeller. Positions of eight lethal mutations are shown as red dots. The residues include Y18, C28, H51, D61, G257 (to D or S), G294 and D314. Ts^- changes at positions G311 and P247 are shown as blue dots. In the latter work, amino acids conferring Ts^- or Slg^- mutations were identified in blades 6 (*P247L* and *Q258R*) and 7 (*G311S*). Direct comparison shown here clearly reveals that none of these residues form contacts to b/PRT1(654-700). Mutations *P247L* and *G311S* were proposed to affect mainly binding of g/TIF35, since overexpression of g/TIF35 could fully suppress the observed phenotypes (10). Notably, P247 is in close proximity to the extended C-terminal part of b/PRT1 (starting with residue 689) suggesting that both b/PRT1 and g/TIF35 might share the same binding surface on i/TIF34. In agreement with this proposal, the Ts^- mutation *Q258R*, which was only weakly suppressed by the high copy *TIF35* plasmid and conferred no defects in binding to b/PRT1 or g/TIF35 (10), resides at the base of the flexible loop (residues 260-272) on the opposite site of the b/PRT1 binding site.

Figure S6. i/TIF34 residues 260-272 fold into a flexible loop. (**A**) The flexible loop within blade 6 (residues 260-272) displays well-defined electron density only in one

molecule of the asymmetric unit (complex II, chain D in the pdb file - shown with the corresponding 2mFo-DFc electron density map contoured at 1.0 sigma). The loop in another molecule (complex I, chain B) is not visible and therefore the residues have been omitted from the pdb file. The red arrow indicates the site of the lacking flexible loop in the complex I. (**B**) Side view showing the flexible loop (indicated by black bracket), which bears neutral-to-negative charge.

Figure S7. Gel shift analysis of i/TIF34 binding to b/PRT1 mutants. (**A**) b/PRT1(630-739) binds i/TIF34 with a K_D of 0.26 μM±0.15, as determined by directly titrating 0.1 μM [^{35}S]-b/PRT1 with increasing amounts of i/TIF34 (0.1-25 μM) and calculated using DynaFit software (58,59). (**B**) Competition assays were used to test binding of b/PRT1 mutants. 0.2 μM [^{35}S]-b/PRT1(630-724) was mixed with 1 μM i/TIF34, and increasing amounts of unlabeled b/PRT1 peptides were added to the reaction mixture (see Supplementary Materials and Methods). Complexes were incubated at 30°C temperature in a final volume of 20 μl reaction mix containing 20 mM Hepes pH 7.5, 50 mM NaCl and 5% glycerol for 20 min and analyzed on 4-16% native polyacrylamide BisTris gels (Invitrogen). The b/PRT1(654-700) peptide and W674F mutant bind i/TIF34 with similar affinity as the b/PRT1(630-724). The increments of increase (the ratio of concentrations of unlabeled to labeled proteins) were as follows: panel b(630-724): 0.1, 0.5, 1, 10, 25, 50, 100; panel W674F: 1, 2, 10, 25, 50, 100; panel W674A: 1, 10, 25, 50, 100, 200; panel Y677A/R678A: 1, 10, 25, 50, 200; panel b(654-700): 1, 5, 50, 100, 200.

Figure S8. (**A**) The *tif34-DD/KK* mutation disrupts i/TIF34 binding to b/PRT1 while preserving its contact with g/TIF35 *in vivo*. WCEs were prepared from H450 (*tif34Δ*) bearing wt *TIF34-HA* and empty vector (lanes 1 – 4), wt *TIF34-HA* and 8x His-tagged hc *TIF35* (lanes 5 – 8) and mutant *tif34-DD/KK-HA* and 8x His-tagged hc *TIF35* (lanes 9 – 12) and analyzed as in Figure 5A - B. (In) lanes contained 5% of the input WCEs; (E1) lanes contained 10% of eluate from the resin; (E2) lanes contained 20% of eluate from the resin; and (FT) lanes contained 5% of the flow through. (**B**) The *tif34-D207K* and *tif34-D224K* mutations are redundant and have only mild effect on the MFC composition *in vivo*. WCEs were prepared from YAH12 (*prt1Δ tif34Δ*) bearing untagged *PRT1* and wt *TIF34* on sc plasmids (lanes 1-3), or from YAH11 (*prt1Δ tif34Δ*) bearing 8x His-tagged *PRT1* and either wt *TIF34* (lanes 4-6), mutant *tif34-D207K* (lanes 7-9) or mutant *tif34-D224K* (lanes 10-12), and analyzed as in Figure 5A - B. (In) lanes contained 5% of the input WCEs; (E) lanes contained 100% of eluate from the resin; and (FT) lanes contained 5% of the flow through. (**C**) The *prt1-R678A* and *prt1-Y677A* mutations are redundant and have only mild effect on the MFC composition *in vivo*. WCEs were prepared from YAH06 (*prt1Δ*) bearing untagged *PRT1* (lanes 1 – 3), 8x His-tagged *PRT1* (lanes 4 – 6) and two of its mutant derivatives (lanes 7 – 9 and 10 - 12) and analyzed as in Figure 5A - B. (In) lanes contained 5% of the input WCEs; (E) lanes contained 100% of eluate from the resin; and (FT) lanes contained 5% of the flow through. (**D**) The *prt1-W674A* mutation provokes severe leaky scanning defect. The YAH06 (*prt1Δ*) strains bearing either wt

PRT1 or mutant *prt1-W674A* were transformed with the *GCN4-lacZ* reporter plasmids pM226 (i) and plig102-3 (ii), grown in SD medium at 34°C and analyzed as in Figure 6D.

Supplementary Table S1. Data collection and refinement statistics (MIR)

	D61 (native)	HgThioMer	Pt
Data collection[a]			
Space group	$P3_1$ 2 1	$P3_1$ 2 1	$P3_1$ 2 1
Cell dimensions			
a, *b*, *c* (Å)	126.28 126.28 105.64	125.9 125.9 105.45	125.9 125.9 107.58
α, β, γ (°)	90 90 120	90 90 120	90 90 120
Resolution (Å)	54.7-2.2 (2.32-2.2)[b]	75.8-2.99 (3.15-2.99)	54.5-3.8 (4-3.8)
R_{merge} (%)[c]	13.5	22.0	31.8
$\langle\langle I\rangle/\sigma(\langle I\rangle)\rangle$	10.2 (2.2)	9.3 (2.1)	2.9 (1.1)
Completeness (%)	99.9 (100)	97.5 (83.1)	99.9 (100)
Multiplicity	7.4 (7.6)	7.6 (7.3)	3.8 (3.7)
Wavelength (Å)	1.0000	1.5418	1.5418
Phasing			
Phasing power, acentric (Isomorphous/Anomalous)		0.98/0.21	0.25/0.05
Mean Figure of merit, acentric (inner resolution bin)	0.16 (0.81)		
<FoM> after solvent flattening (53%)	0.69		
Refinement			
No. reflections	47261		
R_{work} / R_{free} (%)	19/24		
No. atoms			
Protein	6145		
Water	237		
<B> factors (Å^2)			
Protein	37.6		
Water	38.9		
R.m.s. deviations			
Bond lengths (Å)	0.022		
Bond angles (°)	1.867		
Ramachandran plot (%)[d]			
Favoured	96.31		
Allowed	3.43		
Outliers	0.26		

[a] Data were collected on a single crystal, and in the refinement, 5% of unique reflections were removed as a test set for R_{free} calculation.

[b] Values in parentheses are for highest-resolution shell.

[c] $R_{merge} = \Sigma_{hl} | I_{hl} - \langle I_h \rangle | / \Sigma_{hl} \langle I_h \rangle$ where I_{hl} is the l^{th} measurement of reflection h.

[d] From MolProbity (29)

Supplementary Table S2. The i/TIF34-b/PRT1 interaction interface#

b/PRT1	Distance, Å	i/TIF34
Contacts involving side chains		
F:Tyr677 (OH)[a]	2.70	D:Asp224 (OD1)[a]
F:Arg678 (NH1)	3.49	D:Thr209 (OG1)
Main-chain contacts		
F:Phe694 (N)	3.35	D:Asp207 (OD2)
F:Met689 (O)	2.96	D:Lys164 (NZ)
Salt bridges		
F:Arg678 (NH1)	2.99	D:Asp207 (OD2)
F:Arg678 (NH2)	2.75	D:Asp207 (OD2)

[a] F, D is the chain id. Contacts in another complex from the ASU, between chains E and B are the same with minor distance deviations. The interaction parameters were calculated using PISA tool (35).

Table S3. Yeast strains used in this study

Strain	Genotype	Source or reference
YAH06	*MATa leu2-3,112 ura3-52 trp1Δ prt1::hisG GCN2* (hc *PRT1 URA3*)	(12)
AY134	*MATa leu2-3,112 ura3-52 trp1Δ prt1::hisG GCN2* (lc *PRT1 LEU2*)	This study
YAH11	*MATa leu2-3,112 ura3-52 trp1Δ prt1::hisG tif34Δ GCN2* (lc *PRT1-His LEU2* and hc *TIF34 URA3*)	This study
YAH12	*MATa leu2-3,112 ura3-52 trp1Δ prt1::hisG tif34Δ GCN2* (hc *PRT1,URA3* and sc *TIF34-HA TRP1*)	This study
H450	*MATa leu2-3,-112 ura3-52::GCN2 trp1Δ tif34Δ* (hc *TIF34 URA3*)	L. Cuchalová
H420	*MATa leu2-3, -112 ura3-52 trp1 gcn2Δ tif34Δ* (hc *TIF34 URA3*)	Klaus H. Nielsen
H417	*MATa leu2-3, -112 ura3-52 trp1*	Klaus H. Nielsen
H418	*MATa leu2-3, -112 ura3-52 trp1 gcn2Δ*	Klaus H. Nielsen

Table S4. Plasmids used in this study

Plasmid	Description	Source of reference
pRS-b/PRT1-HisXS	low copy wt *PRT1* in *LEU2* plasmid from pRS315	(12)
pRS-b/PRT1-W674A-His	low copy *PRT1* containing the *W674A* mutation in *LEU2* plasmid from pRS315	This study
pRS-b/PRT1-W674F-His	low copy *PRT1* containing the *W674F* mutation in *LEU2* plasmid from pRS315	This study
pRS-b/PRT1-Y677A-His	low copy *PRT1* containing the *Y677A* mutation in *LEU2* plasmid from pRS315	This study
pRS-b/PRT1-R678A-His	low copy *PRT1* containing the *R678A* mutation in *LEU2* plasmid from pRS315	This study
pRS-b/PRT1-Y677A-R678A-His	low copy *PRT1* containing *Y677A* and *R678A* mutations in *LEU2* plasmid from pRS315	This study
pRS-b/PRT1-Y677A-R678D-His	low copy *PRT1* containing *Y677A* and *R678D* mutations in *LEU2* plasmid from pRS315	This study
YEp-TIF34-U	high copy *TIF34 URA3* plasmid from YEplac195	(10)
YCp-i/TIF34-HA	single copy wt *TIF34-HA* in *LEU2* plasmid from YCplac111	(10)
YCp-i/TIF34-D207K-HA	single copy wt *TIF34-HA* containing the *D207K* mutation in *LEU2* plasmid from YCplac111	This study
YCp-i/TIF34-D224K-HA	single copy wt *TIF34-HA* containing the *D224K* mutation in *LEU2* plasmid from YCplac111	This study
YCp-i/TIF34-D207K-D224K-HA	single copy wt *TIF34-HA* containing *D207K* and *D224K* mutations in *LEU2* plasmid from YCplac111	This study
YCp-i/TIF34-L222D-HA	single copy wt *TIF34-HA* containing the *L222D* mutation in *LEU2* plasmid from YCplac111	This study
YCp-i/TIF34-L222K-HA	single copy wt *TIF34-HA* containing the *L222K* mutation in *LEU2* plasmid from YCplac111	This study
YCp-i/TIF34-HA-W	single copy wt *TIF34-HA* in *TRP1* plasmid from YCplac22	This study
YCp-i/TIF34-D207K-D224K-HA-W	single copy wt *TIF34-HA* containing *D207K* and *D224K* mutations in *TRP1* plasmid from YCplac22	This study
YCp-i/TIF34-D207K-HA-W	single copy wt *TIF34-HA* containing *D207K* mutation in *TRP1* plasmid from YCplac22	This study
YCp-i/TIF34-D224K-HA-W	single copy wt *TIF34-HA* containing *D224K* mutation in *TRP1* plasmid from YCplac22	This study
YEplac195	high copy *URA3* plasmid	(64)
YEp-g/TIF35	high copy wt *TIF35* in *URA3* plasmid from YEp352	(10)
YCp-g/TIF35-His-screen	single copy wt *TIF35-His* in *TRP1* plasmid from YCplac22	(5)
YEp-g/TIF35-His	high copy wt *TIF35-His* in *URA3* plasmid from YEplac195	This study
YEp-SUI1	high copy *SUI1* (eIF1) in *URA3* plasmid from YEplac195	(39)
pCFB130	high copy *sui1-His* containing the 93-97 mutation in *LEU2* plasmid form YEplac181	(47)
pJCB02	high copy *sui1-His* containing the D83G mutation in *LEU2* plasmid form YEplac181	(47)
pJCB04	high copy *sui1-His* containing the Q84P mutation in *LEU2* plasmid form YEplac181	(47)
pCFB134	high copy *sui1-His* containing the G107R mutation in *LEU2* plasmid form YEplac181	(47)
YEp-SUI1-G107R	high copy *sui1* containing the G107R mutation in *URA3* plasmid from YEplac195	This study
pGEX-5X-3	cloning vector for GST fusions	(63)

pGEX-i/TIF34	GST-i/TIF34 fusion plasmid from pGEX-5X-3	(10)
pGEX-g/TIF35	GST-g/TIF35 fusion plasmid from pGEX-5X-3	(10)
pGEX-b/PRT1	GST-b/PRT1 fusion plasmid from pGEX-5X-3	(13)
pGEX-RPS0A	GST-RPS0A fusion plasmid from pGEX-4T-1	This study
pT7-b/PRT1	*PRT1* ORF cloned under T7 promoter into pT7-7	(10)
pT7-b/PRT1-W674A	*PRT1* ORF containing the *W674A* mutation cloned under T7 promoter into pT7-7	This study
pT7-b/PRT1-Y677A	*PRT1* ORF containing the *Y677A* mutation cloned under T7 promoter into pT7-7	This study
pT7-b/PRT1-R678A	*PRT1* ORF containing the *R678A* mutation cloned under T7 promoter into pT7-7	This study
pT7-i/TIF34	*TIF34* ORF cloned under T7 promoter into pT7-7	(10)
pT7-i/TIF34-D207K-D224K	*TIF34* ORF containing *D207K* and *D224K* mutations cloned under T7 promoter into pT7-7	This study
pM226	Derivative of pM199; ORF of uORF1 extends into the *GCN4-lacZ* coding region	(61)
plig102-3	Low copy *URA3* vector with *GCN4* leader point mutations containing uORF4 only at its original position in front of the *GCN4-lacZ* coding region	(61)

Table S5. Primers used in this study

Primer name	Primer sequence (5´to 3´)
AH-PRT1-BamHI	TCACTTGGGATCCATCTGGTA
AH-PRT1-NotI-R	CGCGGTGGCGGCCGCGGATCT
AH-PRT1-W674A-R	TGCTTGCTTCAATAATTCACGTTG
AH-PRT1-W674A	CAACGTGAATTATTGAAGCAAGCAACCGAATATAGAGAAAAAATT
AH-PRT1-W674F-R	GAATTGCTTCAATAATTCACGTTG
AH-PRT1-W674F	CAACGTGAATTATTGAAGCAATTCACCGAATATAGAGAAAAAATT
AH-PRT1-YR-AA-R	TTTTTCCATTTCTTGGCCAATTTTTTCTGCTGCTTCGGTCCATTGCTTCAATAA
AH-PRT1-YR-AD-R	TTTTTCCATTTCTTGGCCAATTTTTTCATCTGCTTCGGTCCATTGCTTCAATAA
AH-PRT1-Y677A-R	TTCCATTTCTTGGCCAATTTTTTCTCTTGCTTCGGTCCATTGCTTCAA
AH-PRT1-R678A-R	TTCCATTTCTTGGCCAATTTTTTCTGCATATTCGGTCCATTGCTTCAA
y3iKpnI	TACTTTGGATGGTCACACCGGTACCAT
BmgBIr	CGGCCTTCTCCACGTCGTATTTGAAAT
D207K	GTGACATGCAATTTTCTCCTAAGTTAACATACTTTATTACATCATCCAGAGATA
D207Kr	AGGAGAAAATTGCATGTCACTGATGGA
D224K	ATACTAACTCGTTCTTGGTCAAGGTATCGACTCTACAAGTTCTTAAGAAATACG
D224Kr	GACCAAGAACGAGTTAGTATCTCTGGA
LC3iL222D	ACATCATCCAGAGATACTAACTCGTTCGACGTCGATGTATCGACTCTACAAGTTCTT
LC3iLr	GAACGAGTTAGTATCTCTGGATGATGT
LC3iL222K	ACATCATCCAGAGATACTAACTCGTTCAAGGTCGATGTATCGACTCTACAAGTTCTT
O1-BamHI	AATAGGATCCCATATGTCCTTACCAGCTACTTTTGAC
BSRPS0Aexon1-r	TGAAAACATACGGTTCTTGGTGAACTTGAACGTTTCTAGCAC
BSRPS0Aexon2	CAAGAACCGTATGTTTTCAACGCAAGACC
O2-KpnI-XhoI-r	TTCTCGAGATGGTACCACTTACCACTCGACGTTGTCAGCATTTTC

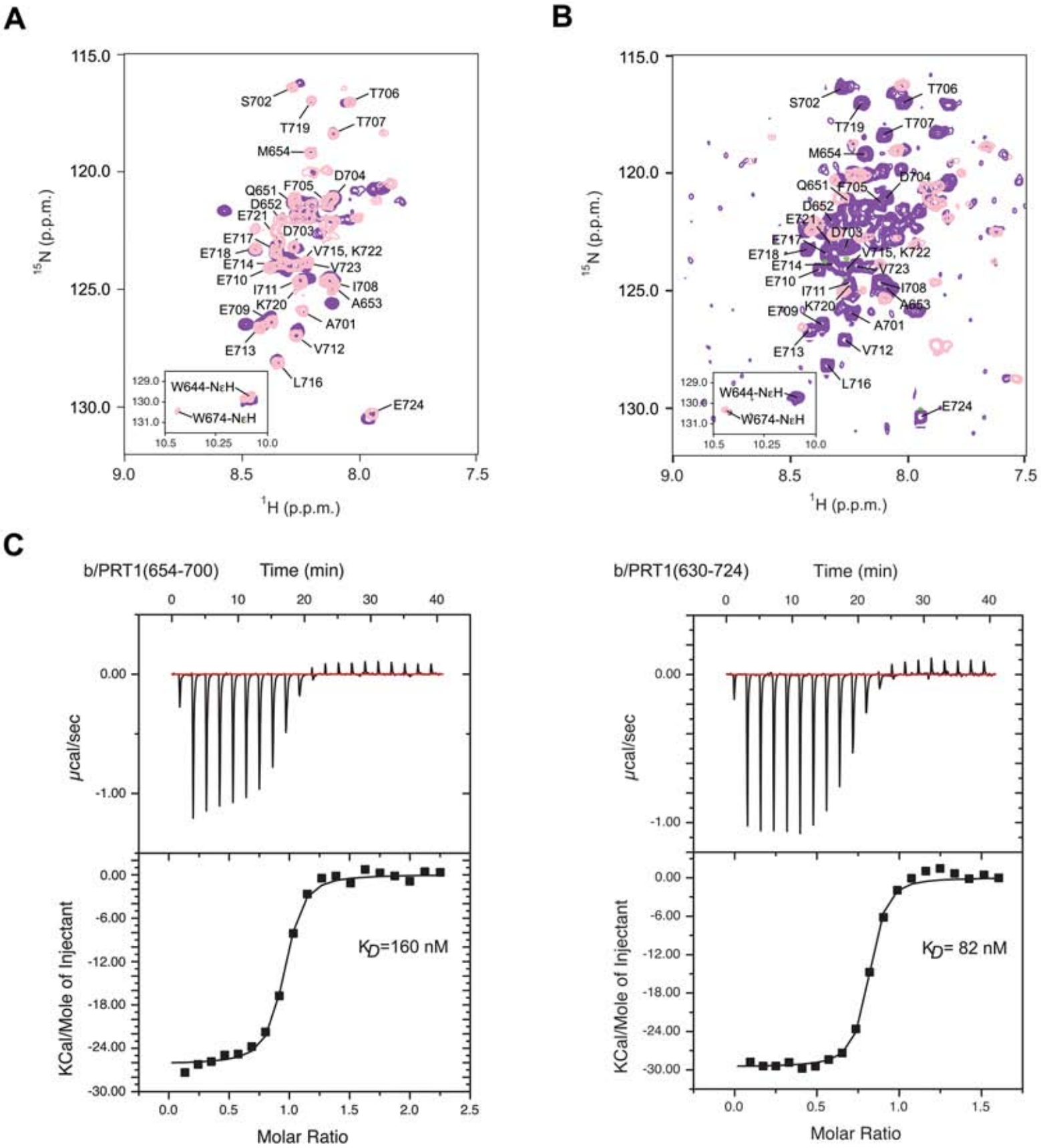
A
B
C
^{15}N (p.p.m.)
^{1}H (p.p.m.)
S702
T706
T719
T707
M654
D704
Q651
F705
D652
E721
D703
E717
E718
V715, K722
E714
V723
E710
I711
I708
A653
E709
K720
A701
E713
V712
L716
E724
W644-NεH
W674-NεH
b/PRT1(654-700)
Time (min)
μcal/sec
KCal/Mole of Injectant
Molar Ratio
K_D=160 nM
b/PRT1(630-724)
K_D= 82 nM

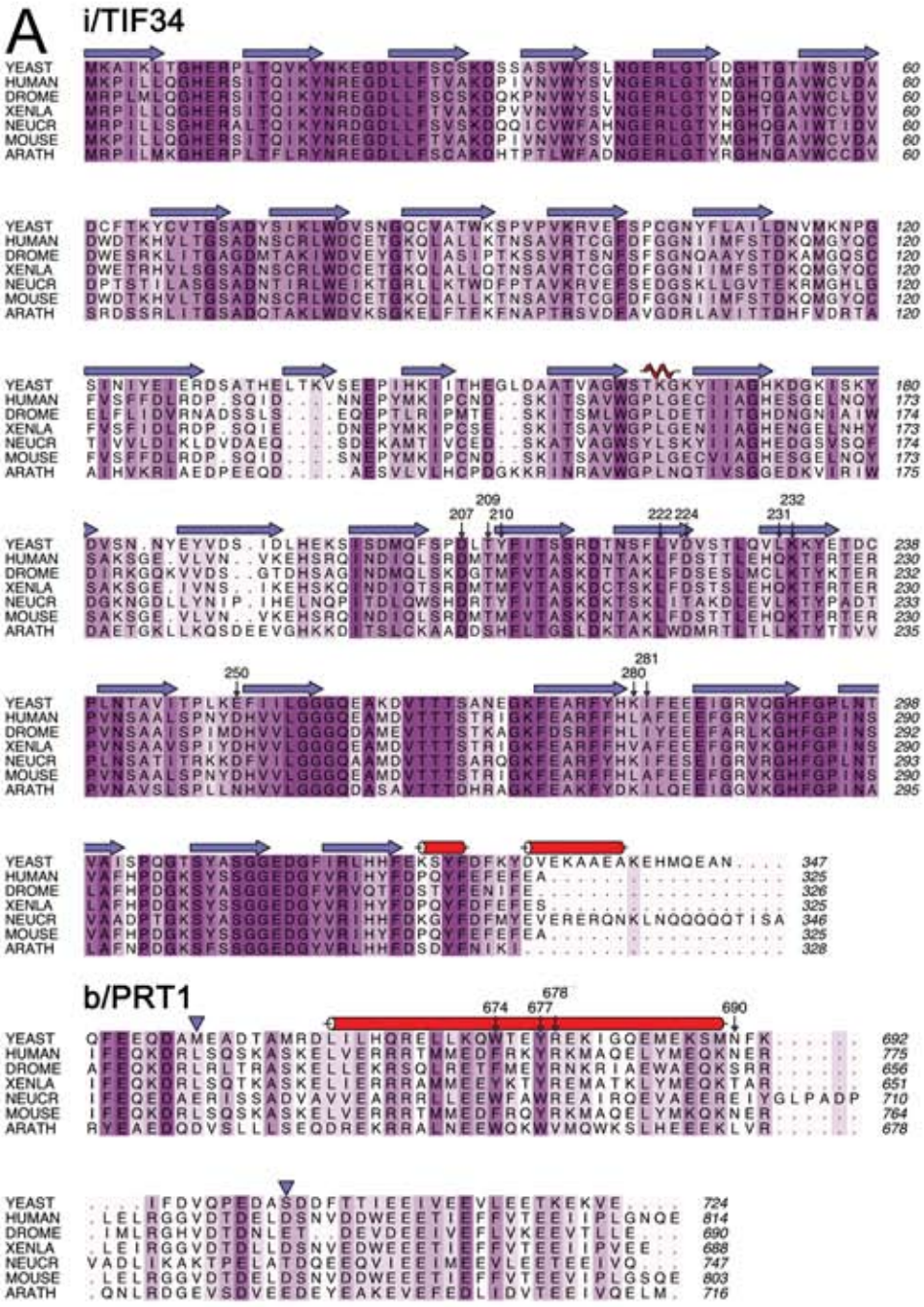
A
i/TIF34
YEAST
HUMAN
DROME
XENLA
NEUCR
MOUSE
ARATH
b/PRT1
YEAST
HUMAN
DROME
XENLA
NEUCR
MOUSE
ARATH

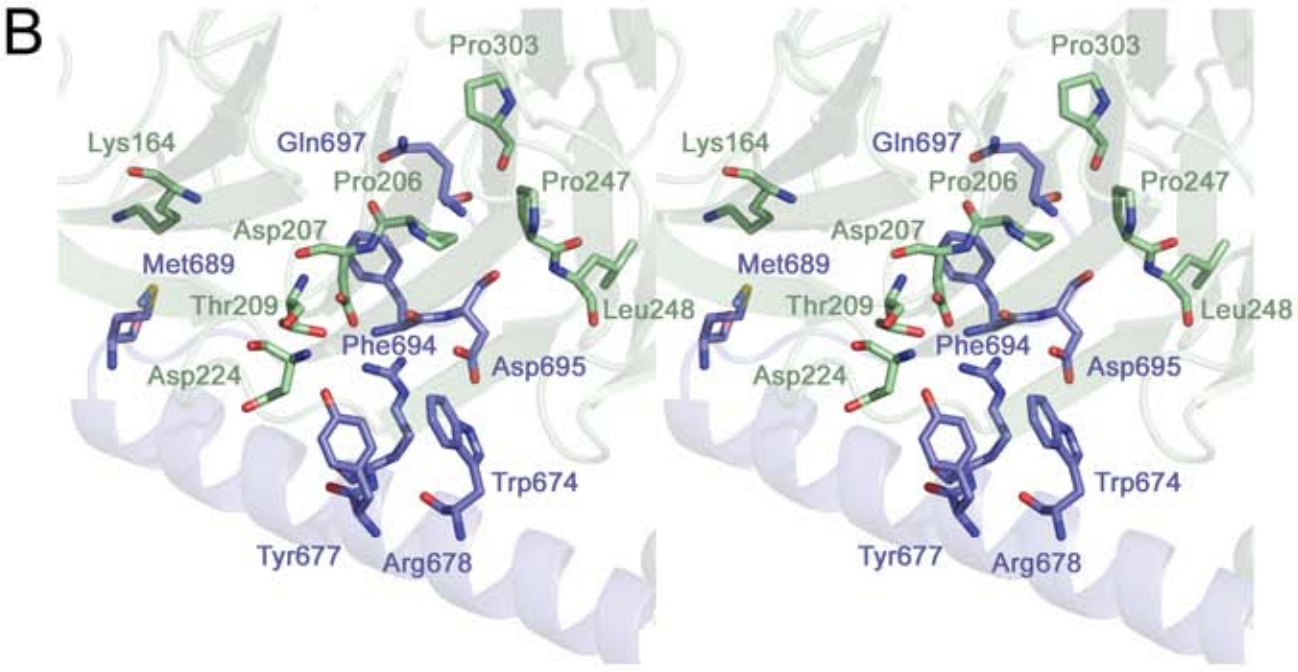
B
Pro303
Lys164
Gln697
Pro206
Pro247
Asp207
Met689
Thr209
Leu248
Phe694
Asp695
Asp224
Trp674
Tyr677
Arg678

A

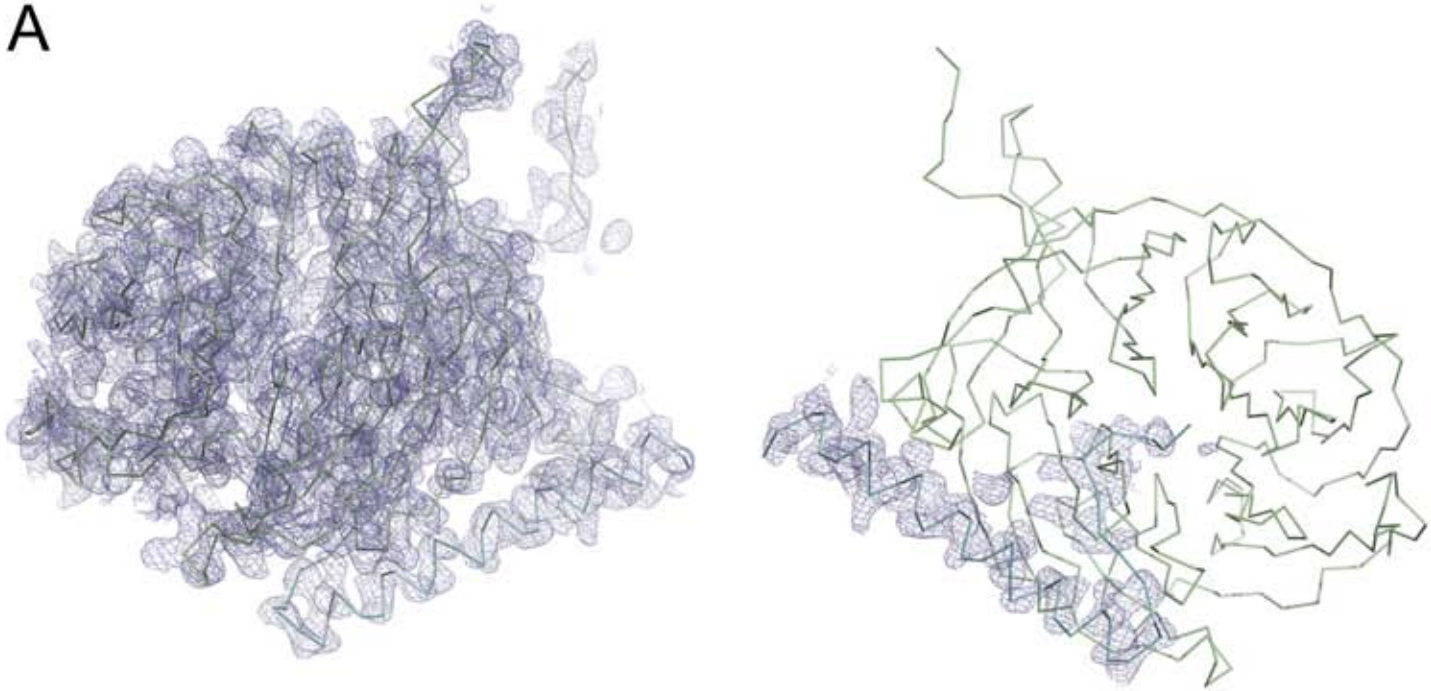

B

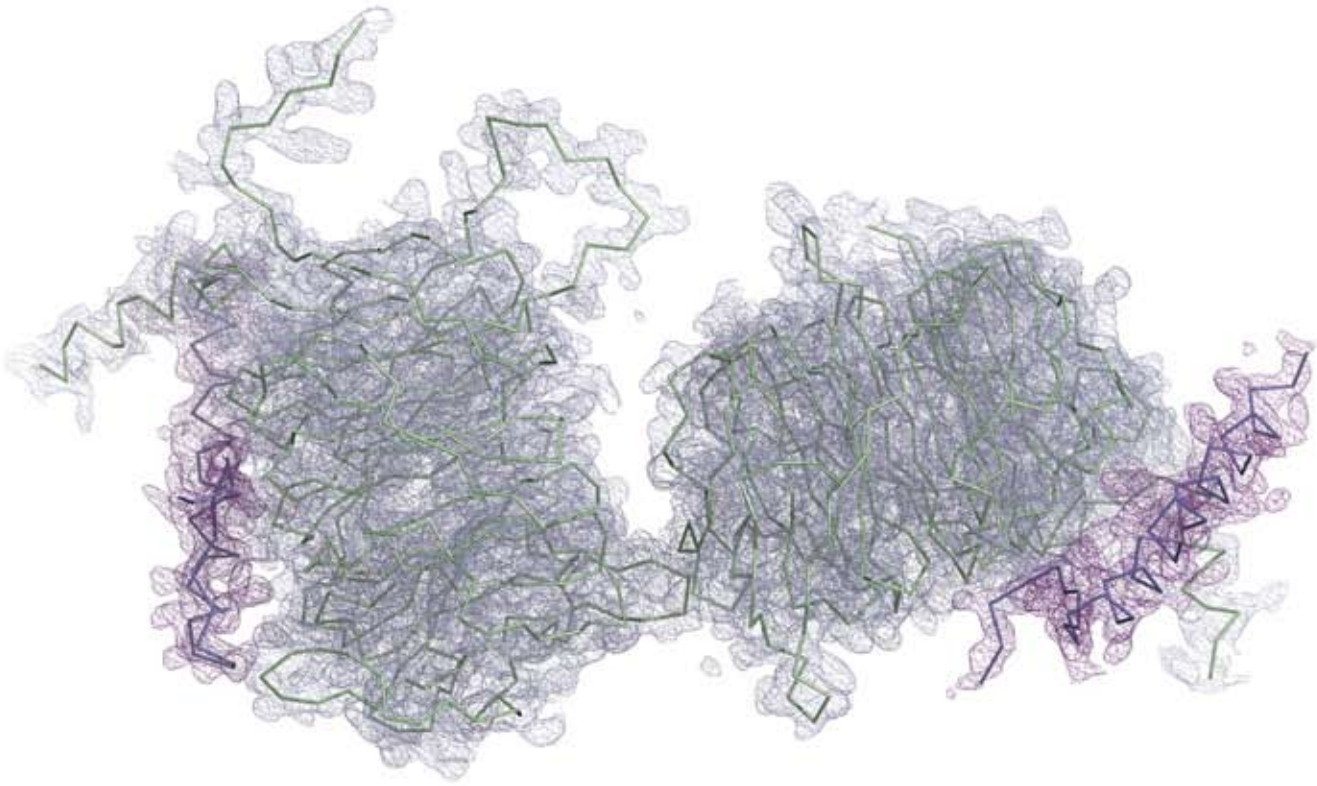

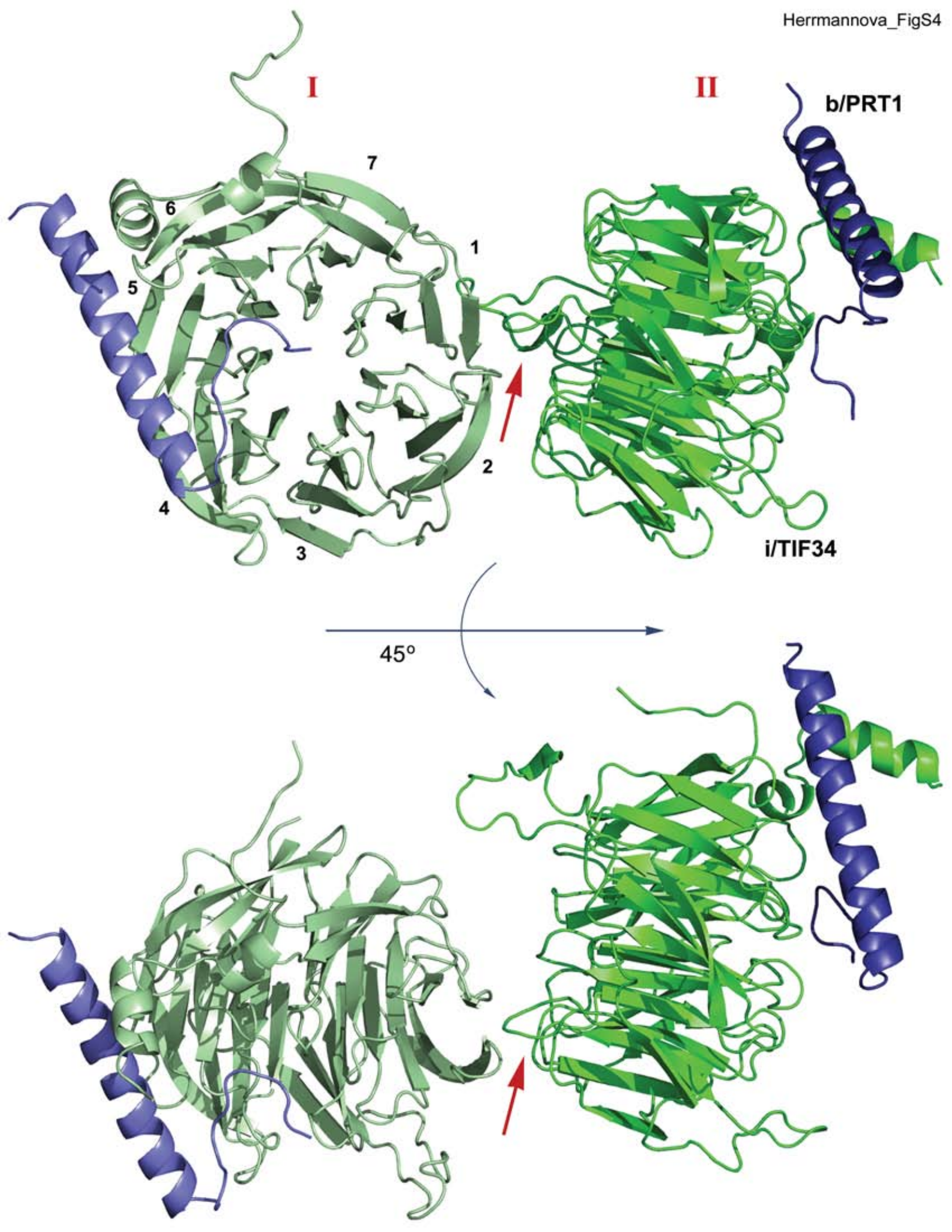
I
II
b/PRT1
7
6
1
5
2
4
3
i/TIF34
45°

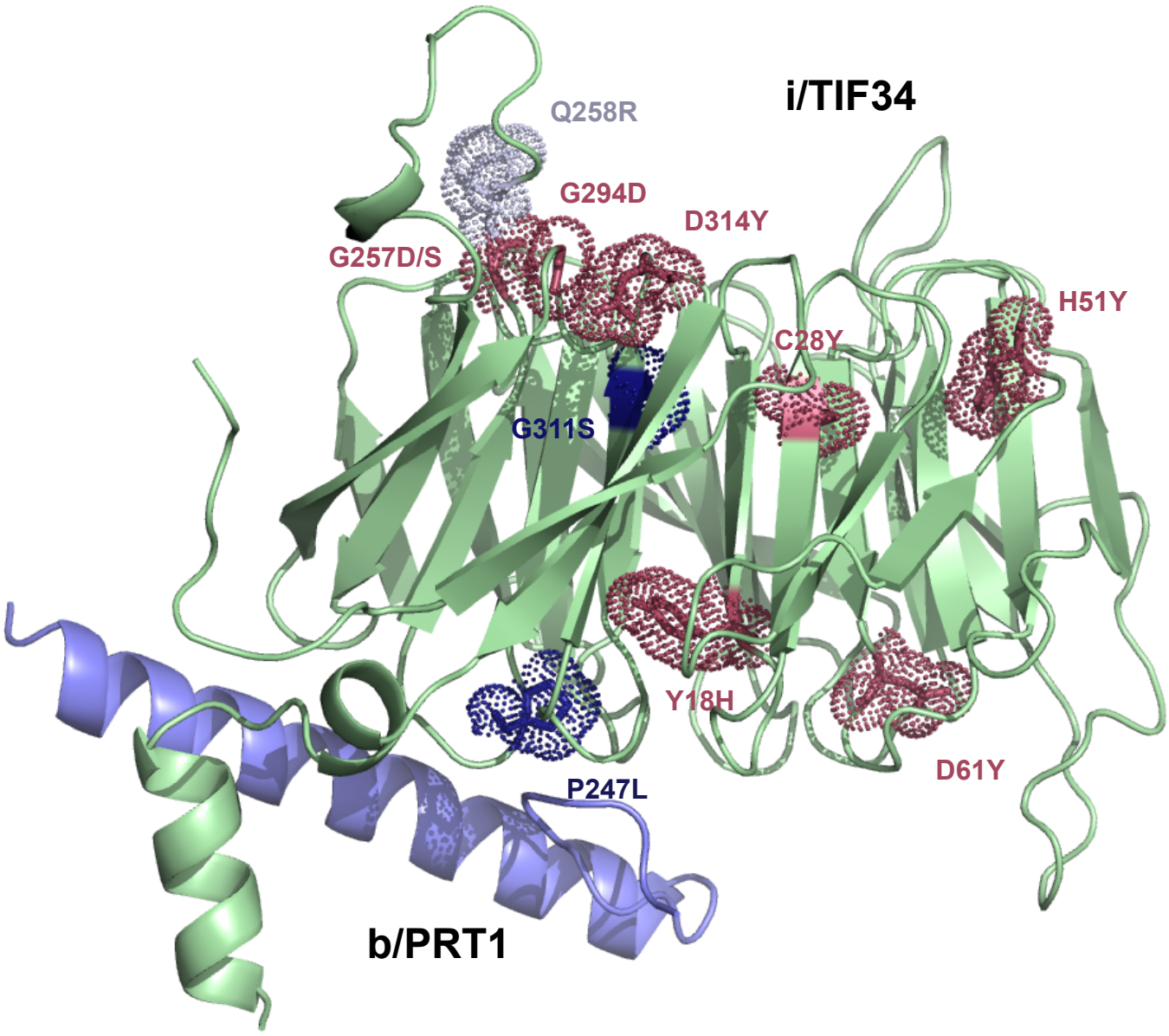
i/TIF34
Q258R
G294D
D314Y
G257D/S
H51Y
C28Y
G311S
Y18H
D61Y
P247L
b/PRT1

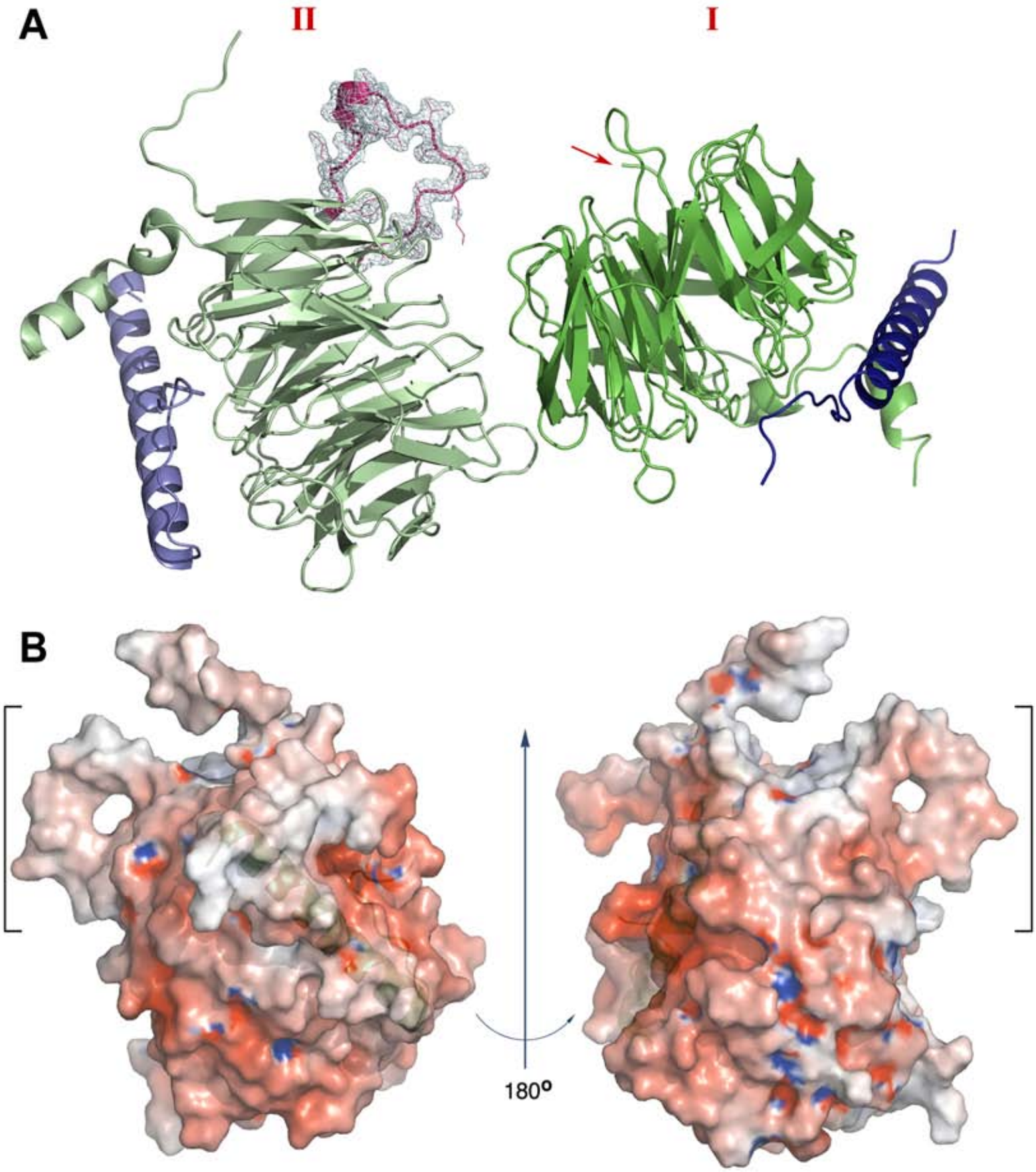
A
II
I
B
180°

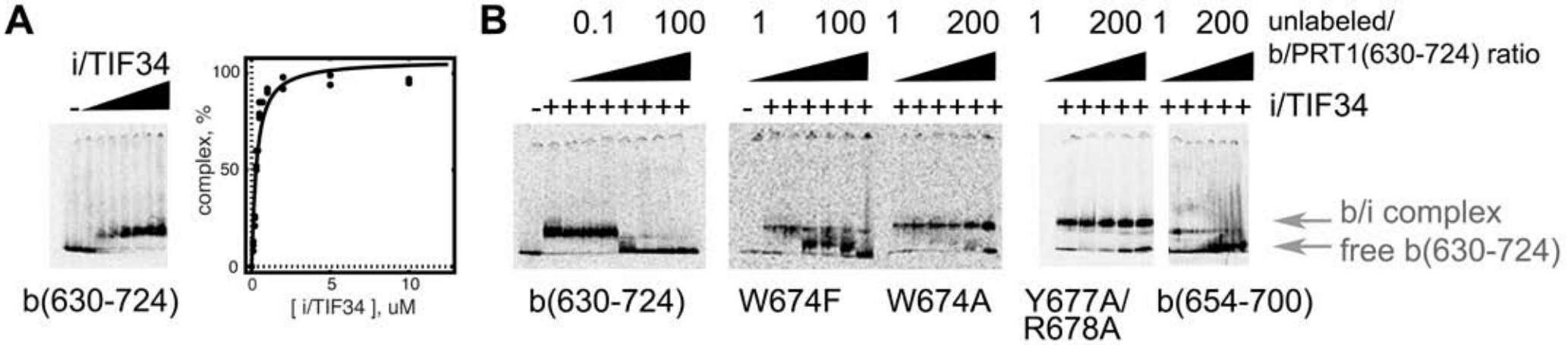
A
i/TIF34
-
b(630-724)
complex, %
100
50
0
0
5
10
[i/TIF34], uM
B
0.1
100
1
100
1
200
1
200
1
200
unlabeled/
b/PRT1(630-724) ratio
-++++++++
- ++++++
++++++
+++++
+++++
i/TIF34
b/i complex
free b(630-724)
b(630-724)
W674F
W674A
Y677A/
R678A
b(654-700)

A

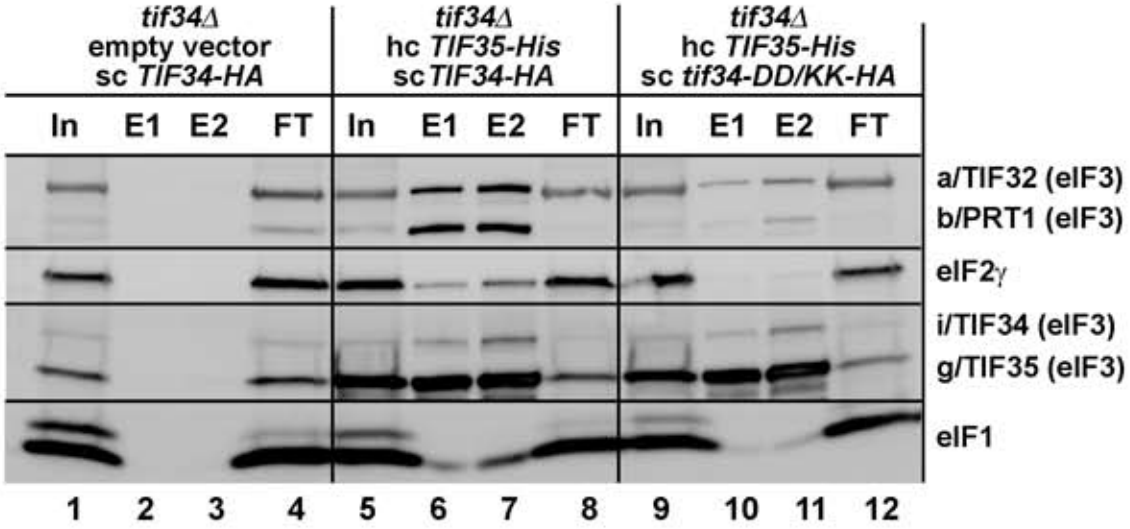

B

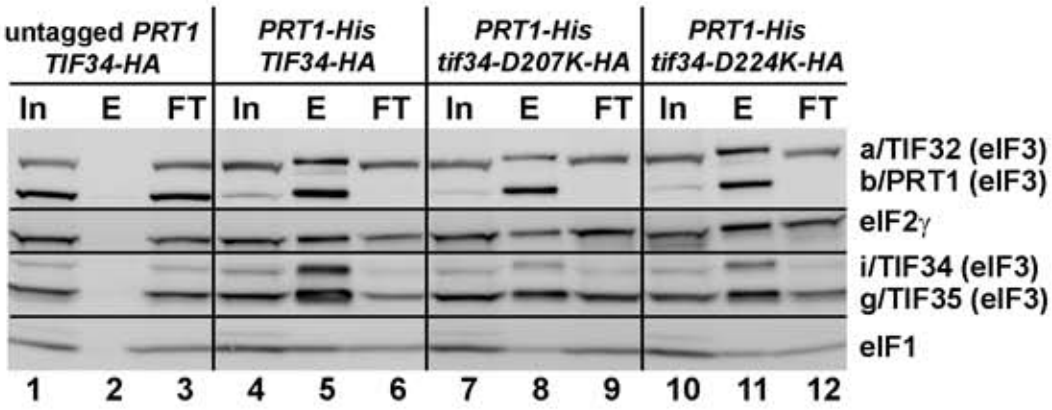

C

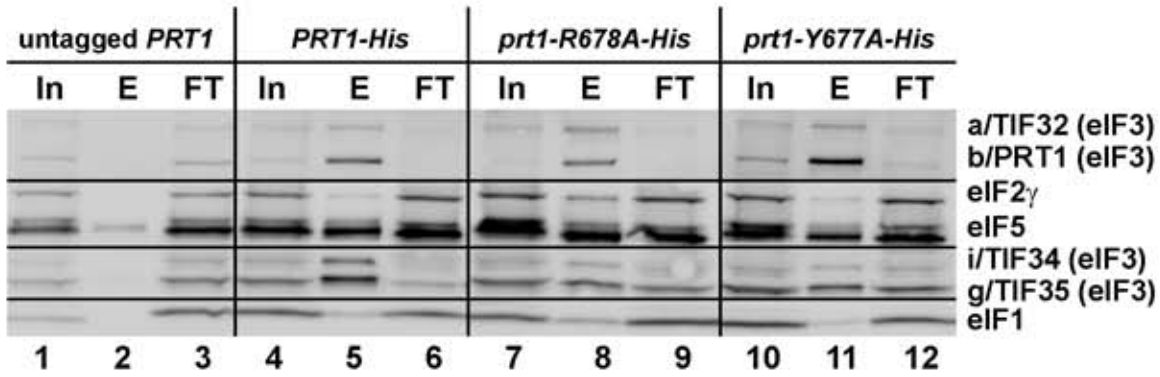

D

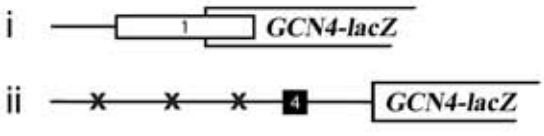

PRT1	*prt1-W674A*
10±1 **1x**	139±6 **13.9x**
42±3 **1x**	278±17 **6.6x**

Units of β-Galactosidase Activity
Activity relative to WT

Small ribosomal protein RPS0 stimulates translation initiation by mediating 40S-binding of eIF3 via its direct contact with the eIF3a/TIF32 subunit.

Kouba T, Dányi I, Gunišová S, Munzarová V, Vlčková V, Cuchalová L, Neueder A, Milkereit P, Valášek LS.

PLoS One. 2012;7(7):e40464. doi: 10.1371/journal.pone.0040464. Epub 2012 Jul 5.

Here we completed the analysis for the a/TIF32-NTD–RPS0A interaction by analyzing the RPS0A contribution to the stable 40S-binding of eIF3. RPS0A is a non-essential protein situated near the mRNA exit channel on the solvent side of the 40S subunit, functionally contributing to its cytoplasmic maturation characterized by a final processing of the 20S rRNA precursor to 18S rRNA (the so called cleavage D). In the recently solved crystal structure of 80S ribosome the last 45 C-terminal residues of RPS0 (C-terminal tail - CTT) are missing suggesting that they are flexible, exposed to the solvent, where they could interact with some ribosome-binding factors. By generating a conditional depletion mutant of RPS0A we demonstrated that its depletion impairs recruitment and/or stable association of eIF3 and other MFC components with 40S subunits resulting in a significant decrease in the translation initiation rates. Importantly, a viable truncation of the RPS0A-CTT, shown to contribute to the RPS0A affinity towards a/TIF32-NTD in vitro, produces similar although less pronounced effects. In support, the FLAG-tagged ΔCTT mutant also loses to wt RPS0A in an *in vivo* competition assay for eIFs recruitment. Hence we conclude that the N-terminal residues 200 through 400 a/TIF32 establish an important intermolecular bridge between eIF3 and the small ribosomal subunit via the flexible CTT of RPS0A.

OPEN ACCESS Freely available online

PLoS one

Small Ribosomal Protein RPS0 Stimulates Translation Initiation by Mediating 40S-Binding of eIF3 *via* Its Direct Contact with the eIF3a/TIF32 Subunit

Tomáš Kouba[1☯], István Dányi[1☯], Stanislava Gunišová[1], Vanda Munzarová[1], Vladislava Vlčková[1], Lucie Cuchalová[1], Andreas Neueder[2], Philipp Milkereit[2], Leoš Shivaya Valášek[1]*

1 Laboratory of Regulation of Gene Expression, Institute of Microbiology ASCR, v.v.i., Prague, The Czech Republic, **2** Institut für Biochemie, Genetik und Mikrobiologie, University of Regensburg, Regensburg, Germany

Abstract

The ribosome translates information encoded by mRNAs into proteins in all living cells. In eukaryotes, its small subunit together with a number of eukaryotic initiation factors (eIFs) is responsible for locating the mRNA's translational start to properly decode the genetic message that it carries. This multistep process requires timely and spatially coordinated placement of eIFs on the ribosomal surface. In our long-standing pursuit to map the 40S-binding site of one of the functionally most complex eIFs, yeast multisubunit eIF3, we identified several interactions that placed its major body to the head, beak and shoulder regions of the solvent-exposed side of the 40S subunit. Among them is the interaction between the N-terminal domain (NTD) of the a/TIF32 subunit of eIF3 and the small ribosomal protein RPS0A, residing near the mRNA exit channel. Previously, we demonstrated that the N-terminal truncation of 200 residues in *tif32-Δ8* significantly reduced association of eIF3 and other eIFs with 40S ribosomes *in vivo* and severely impaired translation reinitiation that eIF3 ensures. Here we show that not the first but the next 200 residues of a/TIF32 specifically interact with RPS0A via its extreme C-terminal tail (CTT). Detailed analysis of the RPS0A conditional depletion mutant revealed a marked drop in the polysome to monosome ratio suggesting that the initiation rates of cells grown under non-permissive conditions were significantly impaired. Indeed, amounts of eIF3 and other eIFs associated with 40S subunits in the pre-initiation complexes in the RPS0A-depleted cells were found reduced; consistently, to the similar extent as in the *tif32-Δ8* cells. Similar but less pronounced effects were also observed with the viable CTT-less mutant of RPS0A. Together we conclude that the interaction between the flexible RPS0A-CTT and the residues 200–400 of the a/TIF32-NTD significantly stimulates attachment of eIF3 and its associated eIFs to small ribosomal subunits in vivo.

Citation: Kouba T, Dányi I, Gunišová S, Munzarová V, Vlčková V, et al. (2012) Small Ribosomal Protein RPS0 Stimulates Translation Initiation by Mediating 40S-Binding of eIF3 *via* Its Direct Contact with the eIF3a/TIF32 Subunit. PLoS ONE 7(7): e40464. doi:10.1371/journal.pone.0040464

Editor: Mick F. Tuite, University of Kent, United Kingdom

Received February 8, 2012; **Accepted** June 7, 2012; **Published** July 5, 2012

Funding: This research was supported by The Wellcome Trusts Grants 076456/Z/05/Z and 090812/Z/09/Z, and the Czech Science Foundation P305-11-0172 (http://www.wellcome.ac.uk/). The funders had no role in study design, data collection and analysis, decision to publish, or preparation of the manuscript.

Competing Interests: The authors have declared that no competing interests exist.

* E-mail: valasekl@biomed.cas.cz

☯ These authors contributed equally to this work.

Introduction

Initiation of protein synthesis is one of the key points in regulation of gene expression in eukaryotes, playing a role in processes from neuronal function to development. It requires the coordinated action of large cellular ribonucleoprotein assemblies called ribosomes, initiation Met-tRNA$_i^{Met}$, mRNA, and at least 12 eukaryotic initiation factors (eIFs). Among them, the multiprotein eIF3 complex deserves a special attention owing to a broad range of functions that it is believed to promote (reviewed in [1]). eIF3, together with eIFs 1, 1A and 5 promotes recruitment of the Met-tRNA$_i^{Met}$·eIF2·GTP ternary complex (TC) to the small 40S ribosomal subunit (40S) to assemble the 43S pre-initiation complex (PIC) [1]. Furthermore, it significantly stimulates mRNA recruitment to the 43S PICs in co-operation with the poly(A)-binding protein and eIF4F complex, containing the mRNA cap-binding factor eIF4E [2–5]. At least in yeast, eIF3 was also implicated in promoting the scanning of the mRNA's 5′ untranslated region (UTR) for the nearest AUG start codon to be recognized by the anti-codon of Met-tRNA$_i^{Met}$ [6,7]. Finally, recent reports ascribe eIF3 a coordinating role also in the intricate AUG recognition process by itself [8–12].

Flawless execution of all these functions depends on proper and stable association of eIF3 with the small ribosomal subunit mediated by number of interactions between its subunits and the ribosomal components. Given the fact that eIF3 associates together with eIF1, TC, and eIF5 in the Multifactor Complex (MFC) [13–15], which enhances the efficiency of the PIC assembly process [4,7–9,16,17], it is conceivable that timely and spatially coordinated attachment of eIF3 to the 40S subunit also significantly influences binding of the other MFC components. Among the points of contacts between eIF3 and 40S subunit that have been mapped so far are those between (i) the C-terminal domain (CTD) of a/TIF32 and helices 16–18 of 18S rRNA [18] and small ribosomal proteins RPS2 and RPS3 [11], all of which constitute the mRNA entry channel [19]; (ii) the CTD of j/HCR1

and RPS2 and RPS23 [10]; (iii) the g/TIF35 subunit of eIF3 and the 40S beak proteins RPS3 and RPS20 [6]; (iv) the C-terminal PCI domain of c/NIP1 and RACK1/ASC1/RPS33 and probably also 18S rRNA segments of the solvent-exposed head region [20]; and (v) the N-terminal domain (NTD) of a/TIF32 and RPS0A [18,21]. Based on these findings we have proposed that eIF3 is attached to the rear, solvent-exposed side of the small ribosomal subunit in the area of the head, beak, and shoulder regions (Figure 1) [6,20]. However, with the exception of the c/NIP1–ASC1 contact, and partly also that between the a/TIF32-NTD and RPS0A, the true physiological importance of most of these interactions remains to be corroborated by *in vivo* approaches.

Here we completed this type of analysis for the a/TIF32-NTD–RPS0A interaction by analyzing the RPS0A contribution to the stable 40S-binding of eIF3. RPS0A is a non-essential protein situated near the mRNA exit channel on the solvent side of the 40S subunit [22], functionally contributing to its cytoplasmic maturation characterized by a final processing of the 20S rRNA precursor to 18S rRNA (the so called cleavage D) [23]. Yeast genome also contains the RPS0B gene whose protein product is about 95% identical to RPS0A. Deletion of both genes is lethal and one can substitute for the other in a higher copy number [24]. In the recently solved crystal structure of 80S ribosome the last 45 C-terminal residues of RPS0 (residues 208–252) are missing [25] suggesting that they are flexible, exposed to the solvent, where they could interact with some ribosome-binding factors. Interestingly, the sequence of the missing C-terminal tail (CTT) is the only region in RPS0 which slightly differs between the A and B isoforms in *S. cerevisiae*. By generating a conditional depletion mutant of RPS0A we demonstrate that its depletion impairs recruitment and/or stable association of eIF3 and other MFC components with 40S subunits resulting in a significant decrease in the translation initiation rates. Importantly, a viable truncation of the RPS0A-CTT, shown to contribute to the RPS0A affinity towards a/TIF32-NTD *in vitro*, produces similar although less pronounced effects. In support, the FLAG-tagged ΔCTT mutant also loses to wt RPS0A in an *in vivo* competition assay for eIFs recruitment. Hence we conclude that the N-terminal residues 200 through 400 a/TIF32 establish an important intermolecular bridge between eIF3 and the small ribosomal subunit via the flexible CTT of RPS0A.

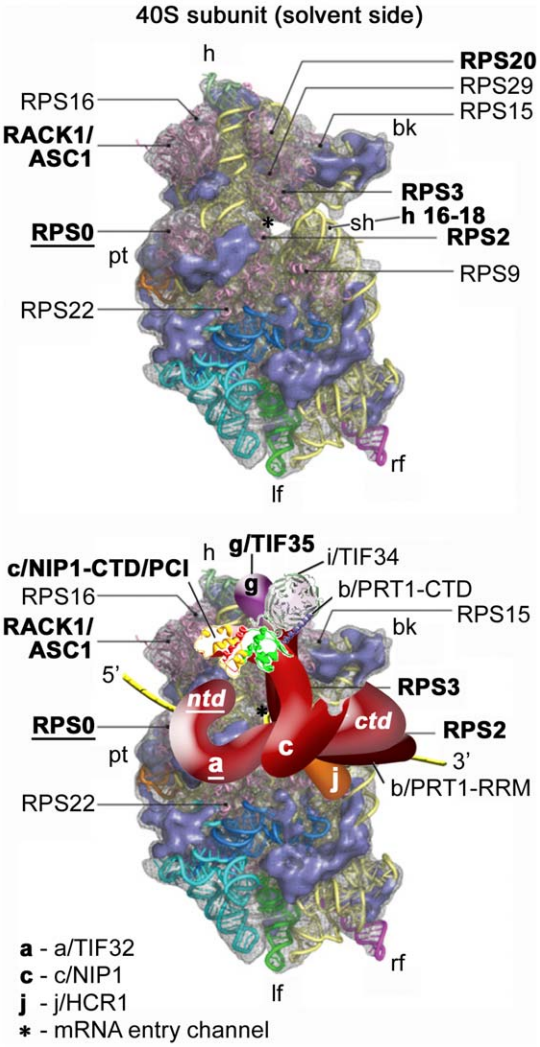

Figure 1. Model of the hypothetical location of eIF3 on the *S. cerevisiae* small ribosomal subunit. (Upper panel) The Cryo-EM reconstruction of the 40S subunit is shown from the solvent side with ribosomal RNA represented as tubes. Ribosomal proteins, with known homologs and placement, are shown as pink cartoons and labeled (adapted from [40]). The positions of helices 16–18 of 18S rRNA, and ribosomal proteins RACK1/ASC1, RPS2, 3, and 20 are highlighted in bold. The position of RPS0, the subject of this study, is highlighted in bold and underlined. The mRNA entry channel is designated by an asterisk. (Lower panel) Hypothetical location of *S. cerevisiae* eIF3 on the back side of the 40S subunit based on the data presented in this study and elsewhere, including the interactions between RPS0 and the NTD of a/TIF32 (in bold and underlined); the c/NIP1-CTD and RACK1/ASC1; RPS2 and j/HCR1; helices 16–18 of 18S rRNA and RPS2 and 3 with the a/TIF32-CTD; and RPS3 and 20 and g/TIF35 (all in bold). The 3D structural model of the c/NIP1-CTD/PCI domain [20] and the X-ray structure of the yeast i/TIF34 – b/PRT1-CTD complex [12] were used to replace the original schematic representations of the same molecules. The yellow lines represent mRNA.
doi:10.1371/journal.pone.0040464.g001

Results

Small ribosomal protein RPS0A interacts with the region spanning amino acid residues 200 and 400 of eIF3a/TIF32 *via* its extreme C-terminus

We previously demonstrated that the C-terminal 117 amino acid residues of RPS0A (at positions 135–252) were sufficient for wild type (wt) *in vitro* interaction with the N-terminal half (residues 1–490) of the a/TIF32 subunit of yeast eIF3 [18]. Our yeast two hybrid analysis then suggested that merely the N-terminal 396 residues of a/TIF32 suffice for strong binding to full length RPS0A. Finally, since the deletion of the extreme N-terminal 200 residues of a/TIF32 in the mutant, but still viable *tif32-Δ8* allele markedly reduced 40S-binding affinity of eIF3 *in vivo* [21], we assumed that the RPS0A binding site resides most likely in the first 200 residues of a/TIF32. To test this assumption experimentally, we fused full length RPS0A with the GST moiety and examined the resulting recombinant protein for binding to three N-terminal segments of a/TIF32 synthesized and radiolabeled in rabbit reticulocyte lysates. In accord with our two hybrid data, the longest segment (NTD [1–400]) shows specific binding to GST-RPS0A (Figure 2A, lane 3, second panel). At odds with our prediction, however, removal of the extreme 200 residues (NTD-Δ8 [201–400]) did not abolish but perhaps even improved the quality of this interaction (third panel). This suggests that not the N-terminal stretch of 200 residues but the immediately following one is sufficient for wt binding. Indeed, expression of the 1–200 segment (NTD-N200) completely disrupted binding. Together these data clearly argue that the a/TIF32 residues 201 through

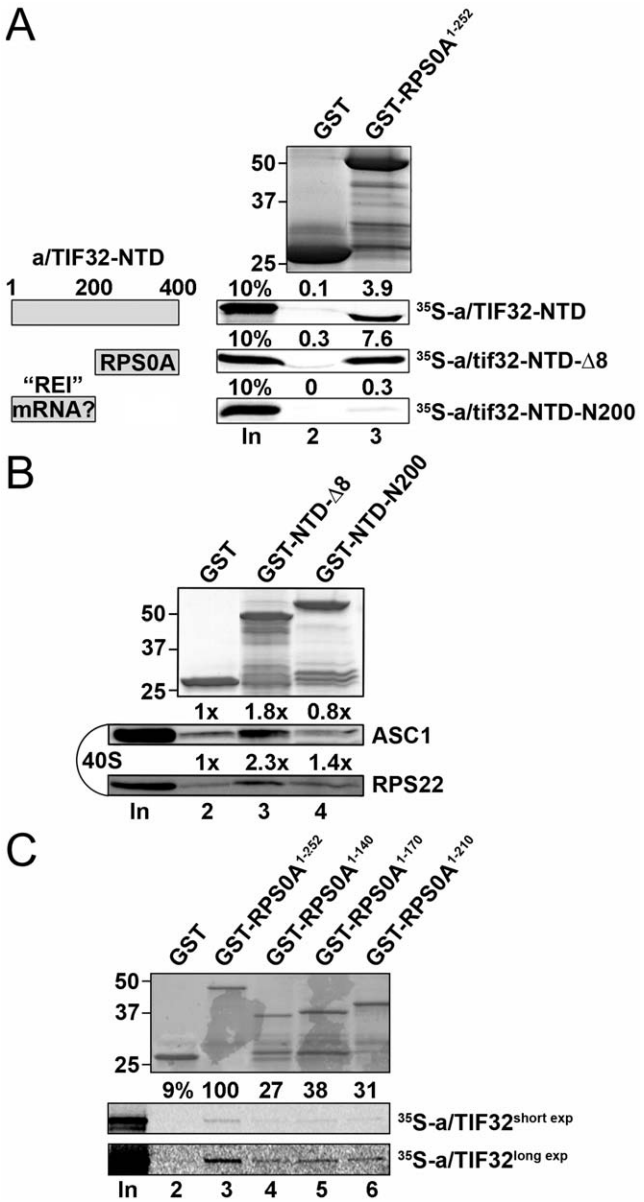

Figure 2. Small ribosomal protein RPS0A interacts with the region spanning amino acid residues 200 and 400 of eIF3a/TIF32 *via* its extreme C-terminal tail *in vitro*. (A) Full-length RPS0A fused to GST (lane 3) and GST alone (lane 2) were tested for binding to ^{35}S-labeled wt a/TIF32-NTD [amino acid residues 1–400] and its N- and C-terminal halves; 10% of input amounts added to each reaction is shown in lane 1 (In). The schematic to the right illustrates two discernible regions of the a/TIF32-NTD, one of which promotes reinitiation after translation of short uORFs by contacting specific mRNA regions preceding these uORFs [21,32], and the other interacts with RPS0A. (B) GST fusions of two consecutive segments of the a/TIF32-NTD in NTD-Δ8 [residues 200–400] and NTD-N2–200 [201–400] in lanes 3 and 4, respectively, or GST alone (lane 2) were tested for binding to the purified wt 40S ribosomal subunits. Lane 1 (In) contains 2.5% of input amounts of 40S subunits added to each reaction mixture. Binding to 40S ribosomes was detected by Western blotting with antibodies against ASC1 and RPS22. (C) Full-length RPS0A (lane 3) and its C-terminal truncations (lanes 4–6) fused to GST, and GST alone (lane 2), were tested for binding to ^{35}S-labeled wt a/TIF32; 10% of input amounts added to each reaction is shown in lane 1 (In); short and long exposures are displayed as indicated.
doi:10.1371/journal.pone.0040464.g002

400 are not only sufficient but also necessary for a/TIF32 binding to RPS0A.

To further support this conclusion by demonstrating that the latter a/TIF32 residues contact RPS0A also in the context of the entire ribosome, we decided to examine *in vitro* binding of both halves of the a/TIF32-NTD directly to the purified 40S subunits. To do that, we performed GST pull down assays with the NTD-Δ8 and NTD-N200 fragments fused to GST moiety and the 40S ribosomal subunits isolated from the wt H503 strain. Even though this type of an in vitro assay is not very efficient [20], we repeatedly detected a weak but specific interaction between the minimal RPS0A-binding domain in GST-NTD-Δ8 and purified 40S subunits (Figure 2B, lane 3). In contrast, the extreme N-terminal segment in GST-NTD-N200 showed only background binding comparable to the GST alone control sample (Figure 2B, lanes 4 and 2).

Having shown earlier that the C-terminal 117 residues of RPS0A are sufficient for a/TIF32 binding [18], as noted above, we also wished to examine what part of the RPS0A-CTT is necessary for this contact. Towards this end we generated three C-terminal RPS0A truncations fused to GST and examined their binding affinities towards a/TIF32 *in vitro*. As shown in Figure 2C (lanes 4–6), even the shortest truncation (by 42 residues, lane 6) markedly reduced binding and no further decrease was observed with more progressive truncations. (Note that compared to Figure 2A, we had to use ~20-fold smaller amounts of GST fusion proteins to reach the ratio at which the decrease in binding was observable; more quantitative measurements will be required in the future to address the effect of individual truncations more specifically.) Nevertheless, it is worth noting that almost exactly this minimal part of RPS0A (precisely the last 45 residues) was found missing in the recently solved crystal structure of the 80S ribosome [25], indicating that it is free to interact with ribosome-accessory factors. Taking together, we propose that the extreme, solvent-exposed RPS0A-CTT is necessary for binding to a/TIF32; at the same time, however, it is not fully sufficient as more N-terminal part of RPS0A is needed for full affinity interaction.

Rapid depletion of RPS0A significantly decreases translation initiation rates

As mentioned above, we previously proposed that the RPS0A–a/TIF32 interaction represents an important intermolecular bridge between eIF3 and the small ribosomal subunit [21]. However, the true importance of RPS0A in this bridging interaction has never been directly examined. The yeast genome also contains a *RPS0A* paralogue in *RPS0B* and these two genes can substitute for each other in their essential roles when overexpressed [24]. Hence to address the role of RPS0A in mediating the binding of eIF3 to the 40S, we constructed an *rps0AΔ rps0BΔ* double deletion strain harboring the *RPS0A* allele on a high copy vector under control of the *MET3* promoter. Expression from this promoter can be turned off by supplementing the medium with methionine and we reasoned that a rapid turnover of RPS0A in the cells will allow us to determine the consequences of its depletion on eIF3/MFC association with the 40S ribosome *in vivo*. As expected, addition of methionine to the media promptly ceased the cell growth (Figure 3A). Importantly, this growth defect was fully complemented by co-overexpression of the wt allele under its endogenous promoter from a separate plasmid (Figure S1). To estimate the depletion rates of the RPS0A protein, we grew the *rps0AΔ rps0BΔ* cells in the absence of methionine to an O.D.$_{600}$~0.3, transferred one half of the culture to the media containing methionine, incubated the cells for up to 12 hrs and monitored the RPS0A decrement by Western blotting.

As can be seen in Figure 3B, majority of RPS0A was efficiently eliminated after 6–8 hours in the Met^+ media; however, trace amounts similar to those observed after 8 hr were still detectable even after 10 or 12 hours in non-permissive conditions (lanes 3 and 4, and data not shown). Based on these observations we decided to use the 8-hour interval of depletion as the gold standard for our further analysis. It is worth noting that under these conditions, the growth defect was still reversible on shifting the mutant back to permissive conditions (data not shown).

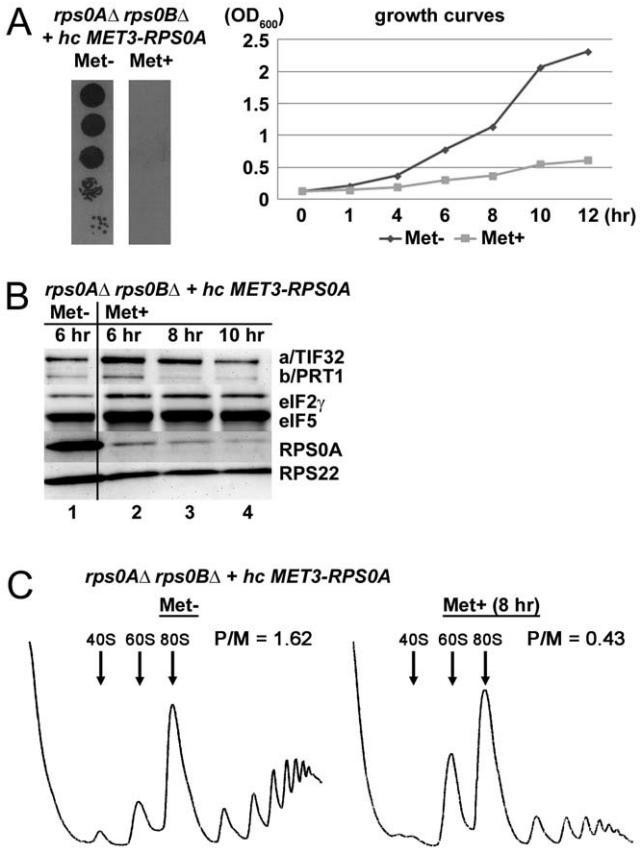

Figure 3. Conditional depletion of RPS0A significantly decreases translation initiation rates. (A) The RPS0A-depletion ceases the growth of mutant cells in non-permissive conditions. Strain YID16 (*rps0aΔ rps0bΔ* YEpMET-RPS0A-U) bearing the *RPPS0A* WT allele under control of *MET3* promoter was spotted in five serial 10-fold dilutions on SD medium +/− methionine and incubated at 30°C for 2.5 days. Growth curves of the same cells grown in liquid SC media lacking methionine at 30°C to an optical density (OD_{600}) of 0.15, split into two halves, and further cultivated under the permissive (Met−) and non-permissive (Met+; with 20 mM methionine) conditions for the indicated time intervals at which OD_{600} readings were taken. (B) Rapid depletion of the RPS0A protein in the non-permissive media. The YID16 cells were grown in liquid SC media lacking methionine at 30°C to OD_{600} of 0.3, split into two halves, grown without (lane 1) or with (lanes 2–4) methionine for the indicated time intervals, and WCEs were prepared and subjected to Western analysis using antibodies against the indicated proteins. (C) Rapid depletion of RPS0A dramatically reduces the polysome content. The YID16 cells were cultured under the same conditions as in panel B (the 8 hr interval was chosen for Met^+ culture) and treated with cycloheximide (5 mg/100 ml) for 5 min prior to harvesting. WCE were prepared and subsequently separated on a 5%–45% sucrose gradient by centrifugation at 39,000 rpm for 2.5 h. The gradients were collected and scanned at 254 nm to visualize the ribosomal species. Positions of 40S, 60S and 80S species are indicated by arrows and polysome to monosome (P/M) ratios are given above the profiles.

doi:10.1371/journal.pone.0040464.g003

Having established the depletion conditions, we first analyzed the effect of RPS0A-depletion on the polysome content in *rps0AΔ rps0BΔ* cells cultivated for 8 hrs in the presence of methionine. To compare the amount of translating ribosomes under permissive versus non-permissive conditions, both Met^- and Met^+ cultures were treated with cycloheximide for 5 minutes prior to their harvest to lock the polyribosomes on mRNAs. This so called polysome profile analysis is the most common and established way of monitoring the translational status of cells grown under various conditions [26]. A decrease in the initiation rate results in the typical polysome run-off with a concomitant increase in the amount of free 80S ribosomes, seen as a large monosomal peak in a polysome profile. Indeed, a substantial polysomal run-off reflected in the 3.8-fold reduction in the polysome/monosome (P/M) ratio was found to accompany a loss of RPS0A (Fig. 3C) implicating RPS0A in ensuring optimal initiation rates in wt cells. Even though we cannot completely rule out that some secondary effects arising after 8 hours of depletion could contribute to the observed phenotype, we think that a clear time correlation of the RPS0A-depletion with growth cessation and polysome run-off entitles us to propose that the impact of the RPS0A loss from the cells on translational rates is immediate and hence direct (see also discussion). As expected, we also observed reduced levels of the 40S subunits and, as a consequence, an accumulation of free 60S subunits owing to a defect in 40S biogenesis that occurs in RPS0A or RPS0B mutants [23].

RPS0A mediates association of eIF3 and its associated eIFs with the 40S ribosomal subunit partly also *via* its C-terminal tail

To answer the key question of this study, we grew the cells as described above and at the point of harvest, we subjected them to 1 hour treatment with 2% formaldehyde. The advantage of the formaldehyde treatment is that it cross-links eIFs to 40S ribosomes, minimizing dissociation of PICs during sedimentation and thus provides the best available approximation of the native 43S/48S PICs composition *in vivo* [26]. Whole cell extracts (WCEs) derived from thus pre-treated cells were then resolved by velocity sedimentation through 7–30% sucrose gradients, fractioned, and the resulting samples were analyzed for the distribution of selected eIFs and ribosomal proteins across the individual fractions by Western blotting. As shown in Fig. 4, no RPS0A signal was detected in the 40S-containing fractions 10 to 12 derived from the Met^+ cells that were pooled together. Also note that overexpression of RPS0A under wt Met^- conditions produces more protein than it can be incorporated into a natural pool of 40S subunits (Fig. 4, lanes Met^-, 1–5 and 6–9). Despite an apparent instability of the small ribosomal species (Fig. 4, lanes Met^+, 1–5 and 6–7), a sizeable fraction of the 40S subunits (~45% of those found in the Met^- cells as calculated from the RPS22 signal using NIH Image J) sedimented in fractions 10–12 indicating that the RPS0A-depleted cells still contain sufficient supply of relatively intact and presumably still active 40S species. (It should be noted that even the immature small ribosomal subunits (deficient in the cleavage D) can interact with eIF3 and other eIFs and fully engage in translation initiation [27]). Importantly, we observed a clear shift in the overall distribution of the amounts of selected eIF3 subunits, and to a similar but perhaps a little less pronounced extent also that of eIF5 and the TC (represented by its eIF2γ subunit), from the 40S-containing fractions 10–12 to the pooled upper fractions 1–5 and 6–9 in the Met^+ versus Met^- cells. With respect to these distribution changes, approximately 4-fold reduction in the

amounts of the latter 40S-associated eIFs was detected in fractions 10–12, dropping down from ~20–45% in Met− to ~5–10% in Met^+ cells. These values nicely correlate with those obtained with the *a/tif32-Δ8* mutant cells lacking the NTD of a/TIF32 [21]. Hence, we conclude that depletion of RPS0A significantly affects 40S-binding of the MFC-associated eIFs, providing a direct evidence for the role of RPS0A in anchoring eIF3 to the solvent side of the small ribosomal subunit.

Next we wished to demonstrate that the extreme CTT of RPS0A, making a direct contact with the a/TIF32-NTD (Figure 2C), significantly contributes to this role of RPS0A in translation initiation using the *in vivo* formaldehyde cross-linking approach. To do that, we introduced the FLAG-tagged truncation of RPS0A (residues 1–197) – removing all of its flexible C-terminal 45 residues – on high copy plasmid into the YID16 *rps0aΔ rps0bΔ* double deletion strain and analyzed the phenotype of the resulting mutant in comparison with the YID16 strain overexpressing wt RPS0A-FLAG. Importantly, affinity purification of FLAG-tagged full length RPS0A or of this C-terminal truncated form from the corresponding WCEs followed by Northern blotting indicated that both variants were efficiently assembled into 40S subunits and its precursors, and that deletion of the CTT of RPS0A does not lead to major pre-rRNA processing defects ([28] and data not shown). Hence any potential defects associated with this mutant should be directly attributable to the impairment of the RPS0A role in translation only. Growth analysis revealed mild growth phenotype at 37°C (compare doubling times (dt) in Figure 5A) suggesting that

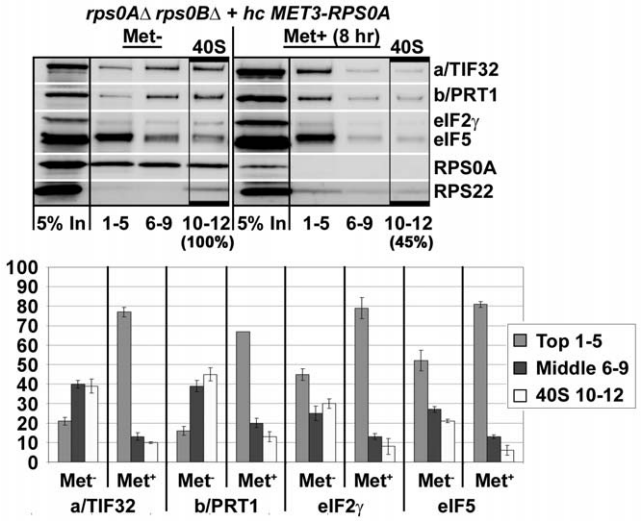

Figure 4. RPS0A mediates *in vivo* association of eIF3 and its associated eIFs with the 40S ribosomal subunit. The same as in Figure 3C, except that the cells were treated with 2% formaldehyde instead of cycloheximide and WCEs were separated on a 7.5%–30% sucrose gradient by centrifugation at 41,000 rpm for 5 h. Proteins from the collected fractions were subjected to Western analysis using antibodies against the proteins listed on the right-hand side of the blots. An aliquot of each WCE was analyzed in parallel (In, input); fractions 1–5, 6–9, and 10–12 were combined. Rectangles indicate fractions where the 43S and 48S pre-initiation complexes sediment (40S); percentages indicate the relative amount of the 40S species in the cells grown under non-permissive versus permissive conditions. Amounts of the each individual factor in the pooled fractions from three independent experiments were quantified by fluorescence imaging, combined and the percentage representation of the signal corresponding to the Top (1–5), Middle (6–9) or 40S (10–12) fractions was calculated and plotted.
doi:10.1371/journal.pone.0040464.g004

the extreme RPS0A-CTT does contribute to the efficiency of the cell proliferation rates. Gradient analysis of the PIC composition then showed modest but reproducible redistribution of eIF3, eIF2 and eIF5 from the 40S-containing fractions into the lighter fractions (Figure 5A). Importantly, the levels of small ribosomal subunits remained unchanged, as expected (compare ASC1 and RPS0A signals in fractions 10–12). The difference in the eIFs amounts in the 40S fractions between the wt and mutant forms of FLAG-tagged RPS0A was between 10–15%. In contrast, the distribution of eIF1A, which is not a part of the MFC, did not change at all. The smaller effect observed in comparison with the depletion of the entire protein is in agreement with i) the fact that besides the CTT, the a/TIF32-NTD contacts also more N-terminal part of RPS0A (Figure 2A); and ii) the modest growth defect associated with the loss of the CTT (Figure 5A). Also note that the wt RPS0A-FLAG but not the CTT-less RPS0A-FLAG protein appears free in the upper fractions suggesting that the wt protein expressed from a high copy plasmid occurs in molar excess over small subunits, as could be expected, and as a result not all RPS0A molecules that are synthesized get incorporated into 40S ribosomes. The fact that no free form of the CTT-less RPS0A-FLAG was observed in the top fractions could be explained by a modestly decreased (by ~15%) stability of the mutant protein (Figure 5A – left panel) that had, however, no effect on the overall amounts of the 40S subunits, as mentioned above.

Further supporting evidence for the role of the RPS0A-CTT in anchoring eIF3 to the 40S ribosome comes from our last experiment, where we expressed either the FLAG-tagged full length RPS0A or its C-terminally truncated form in otherwise wt cells and affinity purified specifically those ribosomal subunits, which contained either of the FLAG-tagged proteins using anti-FLAG matrix. As shown in Figure 5B, the amounts of 40S-associated eIF3 and eIF2 and eIF5 were reduced by ~50 and 70%, respectively, when comparing the IP sample containing mutant rps0A-ΔCTT-FLAG versus wt RPS0A-FLAG ribosomes (lanes 2 vs. 4). (Since the rps0A-ΔCTT-FLAG protein runs at the same size as heavy chains of anti-FLAG antibodies (data not shown), obtained results were normalized to the amount of recovered 40S subunits with help of ASC1 instead; comparable expression levels of both FLAG-tagged proteins are shown in Figure 5C.) Together these results demonstrate that 40S ribosomes containing mutant rps0A-ΔCTT-FLAG compete less efficiently with native ribosomes for binding to eIFs than those containing wt RPS0A-FLAG.

Discussion

Over the last decade we and others have mapped several binding domains within the eIF3 subunits and its associated eIFs that promote stable association of these eIFs with the 40S ribosome [6,9–12,18,20,21,29,30]. In many of these cases specific binding partners in ribosomal components were also identified with help of yeast two-hybrid and *in vitro* binding assays; however, a solid *in vivo* evidence underpinning physiological importance of these interactions, especially with respect to ribosomal components, has been largely missing. In fact, the only exception is the recently reported bridging interaction between the PCI domain of the c/NIP1 subunit of eIF3 and the small ribosomal protein RACK1/ASC1, and probably also 18S rRNA segments of the head region [20]. Besides that, N-terminal deletion of RPS5 was previously also shown to affect 40S-binding of eIF3 [31], however, since it is not known whether and how RPS5 contacts eIF3, the molecular nature of this effect is unknown. Here we investigated physiological consequences of disrupting yet another important

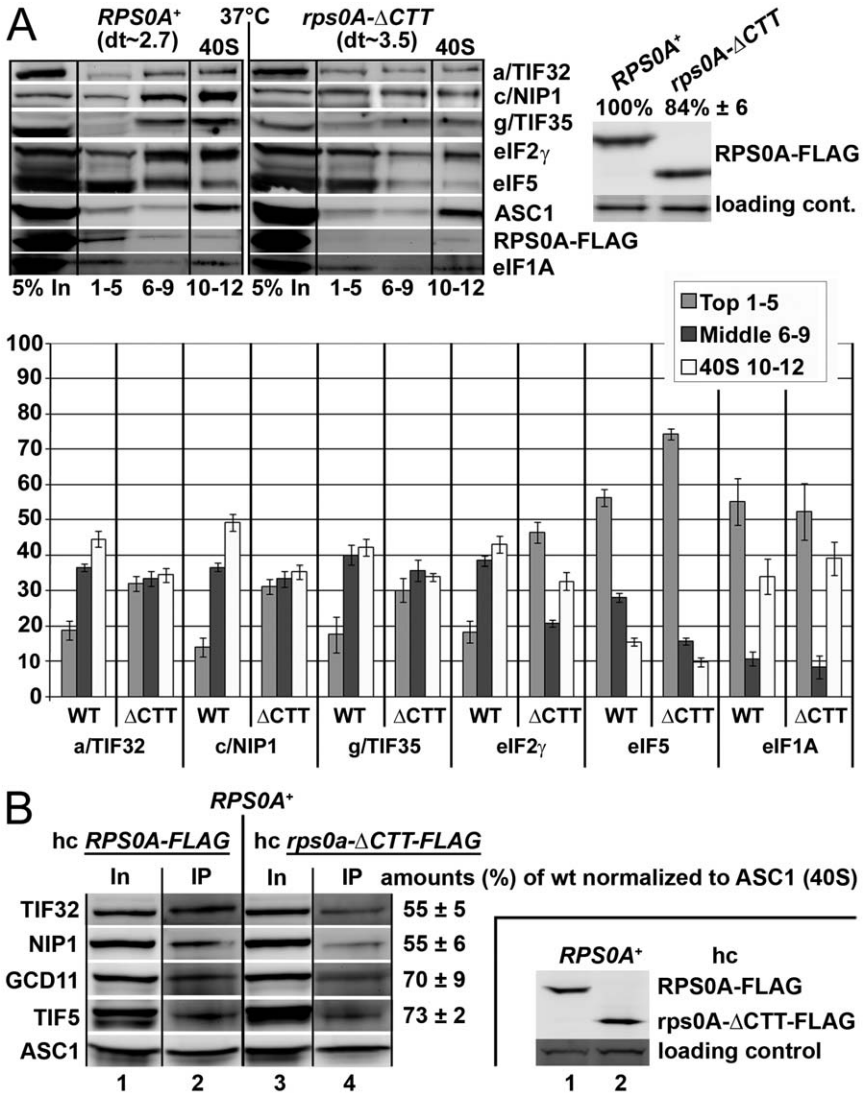

Figure 5. The CTT of RPS0A, making a direct contact with the a/TIF32-NTD, contributes to the RPS0A role in anchoring eIF3 to the small ribosomal subunit. (A) The same as in Figure 4, except that the YID16 cells transformed with a high copy plasmid bearing either wt *RPS0A-FLAG* (in TK156) or *rps0A-ΔCTT-FLAG* (in TK157) alleles under control of the *RPS28* promoter, as the only source of the RPS0A protein product, were grown at 37°C and subsequently subjected to the 2% formaldehyde cross-linking procedure; dt indicates doubling times measured at 37°C. (Expression levels of both FLAG-tagged RPS0A protein variants in TK156 and 157 strains are shown in the right-handed panel). (B) Small ribosomal subunits containing C-terminally truncated RPS0A do not compete well for eIFs recruitment with native ribosomes. A FLAG-tag affinity purification of 40S ribosomes and its associated eIFs from WCEs prepared from the H2880 wt strain overexpressing either wt or C-terminally truncated RPS0A-FLAG followed by Western blotting. (Expression levels of both FLAG-tagged proteins in high copy number in H2880 are shown in the right-handed panel).
doi:10.1371/journal.pone.0040464.g005

40S – eIF3 bridging interaction between RPS0A and a/TIF32 [18,21] by mutating the RPS0A part of the contact.

Our *in vitro* binding analysis (Figure 2A and C) suggest that the major molecular determinants of this interaction occur in the N-terminal segment of a/TIF32 encompassing the residues 201 through 400 and in the extreme CTT of RPS0A, which is supposed to be free, sticking form the 40S body out into the space [19,25]. In support, the latter a/TIF32 segment fused to GST but not the preceding one between residues 1 and 200 interacted with the isolated 40S species *in vitro* (Figure 2B). These results seem at odds with our previous finding that the deletion of the first 200 residues in *tif32-Δ8* markedly reduced 40S-binding of eIF3 *in vivo* [21], naturally indicating that the RPS0A binding site resides in this very first 200-residue segment. To reconcile these observations we propose that the entire NTD of a/TIF32 adopts a specific fold that presents the RPS0A-binding site situated between residues 201 through 400 for proper and stable interaction with RPS0A near the mRNA exit pore. Deletion of the first 200 amino acid residues disrupts this fold in such a way that the RPS0A-binding site is, in the context of the entire pre-initiation complex, no longer suitably positioned for a stable binding to RPS0A. It is worth noting that whereas the residues 201 through 400 interact with RPS0A, the extreme N-terminal 200 residues are crucial for efficient reinitiation after translation of short uORFs in yeast by contacting specific mRNA features that precede them (Figure 2A) [21,32].

An important milestone of our task to implicate RPS0A in promoting assembly of PICs was to demonstrate that mutating *RPS0A* will bear direct consequences in efficiency of translation initiation; i.e. will reduce initiation rates (the P/M ratio) as was

observed with our RPS0A-conditional depletion strain (Figure 3). Indeed, it can be argued that depletion of a ribosomal protein, which is an integral part of the export machinery for 20S rRNA-containing pre-40S ribosomes [33], will affect the polysome to monosome ratio primarily by decreasing the levels of mature 40S subunits. However, there are examples of mutant strains (carrying mutations in either 18S rRNA or small ribosomal proteins) with a pronounced defect in 40S biosynthesis showing that a shortage of mature 40S subunits as the primary defect actually leads to a clear decrease not only in the amounts of free 40S subunits and polysomes, but also in the amounts of 80S couples [33,34]. As a result, these strains display a relatively mild effect on the P/M ratio than could have been expected. This contrasts with our rps0A-depletion data showing significant (~3.8-fold) reduction in the P/M ratio. Even though it is very likely that a part of this effect can be attributed to a misbalanced ribosome biogenesis, we propose that the main source of the polysome run-off in the rps0A-depletion strain is the inability of the mutant 40S subunits to function properly in translation initiation. An important supporting evidence for this proposal was obtained in our cross-linking experiments, where we showed that the rps0A-depletion impaired association of eIF3, eIF5 and the TC with 40S subunits to a similar extent (~35%) as observed before with *tif32-Δ8* lacking the a/TIF32-NTD (Figure 4). Further support comes from the analysis of the viable C-terminally truncated *RPS0A-FLAG* allele that, despite having no major defect in ribosome biogenesis (data not shown), also reduced 40S-binding of eIF3 and eIF5 *in vivo*, though to a smaller degree (Figure 5A). Consistently, ribosomes containing rps0A-ΔCTT-FLAG could not compete well with native ribosomes for recruitment of eIFs in otherwise wt cells when compared to the wt "RPS0A-FLAG" ribosomes (Figure 5B). Hence, besides the aforementioned interaction of the c/NIP1-PCI with RACK1/ASC1 and 18S rRNA [20], this work concludes characterization of another important intermolecular bridge spanning between the RPS0A-CTT and the a/TIF32-NTD that anchors the MFC to the small ribosomal subunit in a co-operative manner with another, yet to be identified 40S-eIF3 contacts.

Materials and Methods

Yeast strains and plasmids

Strain YID16 (*leu2-3,-112 ura3-52 trp1 rps0a::kanMX3::TRP1 rps0b::kanMX* [YEpMET-RPS0A-U]) was constructed in the following steps. (i) To delete a chromosomal copy of *RPS0A*, two primers, RPS0A-A 5′ AATTAACTTCGTAGGCTGGAACAG 3′ and RPS0A-D 5′ CCAGTTTTGTTCATGGATAAGAGGT 3′, were used to PCR amplify a DNA fragment containing the *rps0A*::*kanMX* allele from strain BY4844 obtained from Research Genetics. The purified DNA fragment was used to transform strain H2880 (*MATa leu2-3,-112 ura3-52 trp1*) [7] to G418 resistance. The deletion of *RPS0A* was verified by PCR. The resulting strain YID08 (*leu2-3,-112 ura3-52 trp1 rps0a::kanMX3*) was transformed with the *kanMX::TRP1* cassette (a *Not*I fragment of M4757 [35]) to tryptophan prototrophy and regained sensitivity to G418, producing yID14 (*leu2-3,-112 ura3-52 trp1 rps0a::kanMX3::TRP1*). (iii) Subsequently, YID14 was introduced with YEpMET-RPS0A-U and a chromosomal copy of *RPS0B* was deleted by transforming the resulting strain by a *rps0b::KanMX4* cassette obtained from BY4741 (Research Genetics) back to G418 resistance using primers BSRPS0A 5′ CATGCATTCATGACAATTTTACCTA 3′ and BSRPS0D 5′ CTAGCATTGAAAACGTATGGTTCTT 3′. Thus generated YID16 was verified by Western analysis using antibodies against RPS0A (see below).

To create TK156 and TK157, YID16 was first transformed with YCpMETRPS0A-W and the Uracil auxotrophy was regained by growing the cells on SD plates containing 5-fluoro-orotic acid. The resulting strain was subsequently transformed with YEp-pRPS28B-FLAG-RPS0A and YEp-pRPS28B-FLAG-RPS0A-ΔCTT *LEU2*-based plasmids, respectively, and the tryptophan auxotrophy was regained by growing the cells in liquid media containing tryptophan; cells that lost YCp-METRPS0A-W were selected based on a growth test on SD plates lacking or supplemented with tryptophan. Thus generated TK156 and TK157 strains were verified by Western blotting analysis using anti-FLAG M2 antibody (Sigma).

H503 (*MAT*a *leu2-3 112 his4-539 trp1 ura3-52 cup1::LEU2/PGK1pG/MFA2pG*) was used for purification of the 40S ribosomal species.

Construction of YEpMET-RPS0A-U was done in the following three steps. (i) A 1222-bp *Bam*HI-*Sal*I fragment from pGBKRPS0A [18] was inserted between *Bam*HI-*Sal*I multicloning sites of YCplac22MET-W (a kind gift of Kim Nasmyth). (ii) Thus created YCpMETRPS0A-W was cut with *Xba*I-*Sph*I and the resulting 1553-bp fragment was inserted between *Xba*I-*Sph*I sites of YEplac112 [36] producing YEpMET-RPS0A-W. (iii) Subsequently, a 2025-bp *Sac*I-*Sph*I fragment from YEpMET-RPS0A-W was inserted between *Sac*I-*Sph*I sites of YEplac195 [36] producing YEpMET-RPS0A-W.

pGEX-RPS0A was constructed in two steps. First, the intron was removed by a fusion PCR using pGBK-RPS0A [18] as a template and the following pair of primers for two separate PCR reactions producing exon 1 (O1-BamHI 5′ AATAGGATCCCATATGTCCTTACCAGCTACTTTTGAC 3′ and BSRPS0exon1-r 5′ TGAAAACATACGGTTCTTGGTGAACTTGAACGTTTCTAGCAC 3′) and exon2 (BSRPS0exon2 5′ CAAGAACCGTATGTTTTCAACGCAAGACC 3′ and O2-KpnI-XhoI-r 5′ TTCTCGAGATGGTACCACTTACCACTCGACGTTGTCAGCATTTTC 3′), respectively. Both PCR products thus obtained were used in a 1:1 ratio as templates for third PCR amplification using primers O1-BamHI and O2-KpnI-XhoI-r. The resulting PCR product was digested with *Bam*HI and *Xho*I and ligated with *Bam*HI-*Xho*I-cleaved pGEX-4T-1 [37].

pGEX-RPS0A$^{1–140}$, pGEX-RPS0A$^{1–170}$ and pGEX-RPS0A$^{1–210}$ were made by inserting the corresponding *Bam*HI-*Sph*I digested PCR products obtained with primers O1-BamHI and IDRPS0A-1–140-r (5′ ATAGCATGCTTAGTTAACGTAAGAAGCTTCCT 3′) or IDRPS0A-1–170-r (5′ ATAGCATGCATTAAATGGAGTGCTTACCTCTGT 3′) or IDRPS0A-1–210-r (5′ ATATGCATGCATTAAACTTCTTCAGGGTCTCTGT 3′), respectively, using pGEX-RPS0A as a template into *Bam*HI-*Sph*I digested pGEX-RPS0A.

Construction of pT7-TIF32 and pGAD-a/TIF32-NTD was described in [30,32], respectively. Plasmids pGAD-a/TIF32-NTD-Δ8 and pGAD-a/TIF32-NTD-N200 were generated by inserting the *Nde*I-*Xho*I-digested fragments obtained by PCR using YCp-a/TIF32-His-screen as a template and the following pairs of primers: SGTIF32d8NDEIF 5′ CATCAAGCATATGAGATTAGCTGAAATG 3′ and SGTIF32NTDXHOIR 5′ CCCCCTCGAGTTAATCAAAGTTAACTTCAATG 3′; and SGTIF32NDEIF 5′ GAAGGATCCATATGGCCCCCCCAC 3′ and SGTIF32NTD200XHOIR 5′ CCCCCTCGAGTTACTTGAATTCGTTTTTACGC 3′, respectively, into *Nde*I-*Xho*I-cut pGADT7 (Clontech).

To construct pGEX-a/TIF32-NTD, pGEX-a/TIF32-NTD-Δ8 and pGEX-a/TIF32-NTD-N200, the corresponding a/TIF32-NTD segments were PCR out using the following three sets of primers (VVTIF32NTDXMAIF_5′ CACCCGGGGCATGGC-

CCCCCCAC 3′ and SGTIF32NTDXHOIR_5′ CCCCCTCGAGTTAATCAAAGTTAACTTCAATG 3′; VVTIF32NTDXMAIF_5′ CACCCGGGGCATGGCCCCCCCAC 3′ and SGTIF32NTDXHOIR_5′ CCCCCTCGAGTTAATCAAAGTTAACTTCAATG 3′; and VVTIF32d8XMAIF_5′ CACCCGGGGCATGAGATTAGCTGAAATGT 3′ and SGTIF32NTDXHOIR_5′ CCCCCTCGAGTTAATCAAAGTTAACTTCAATG 3′) and pT7-a/TIF32-NTD, pT7-a/TIF32-NTD-Δ8 and pT7-a/TIF32-NTD-N200 vectors, respectively, as templates (the reverse primers introduced the *Xma*I restriction site at the 3′ end of all three PCR products). Thus obtained PCR products were cut with *Xho*I and *Xma*I and ligated with *Xho*I-*Xma*I-cleaved pGEX-5X-3 [37].

YEp-pRPS28B-FLAG-RPS0A (request number K421, [28]) is based on vector YEplac195 [36] into which a PCR amplicon, which was produced using oligos O581_5′ TTTTTTGAATTCGCTTATTCATGTTCGAATC 3′ and O582_5′ TTTTTTGGATCCGGTACCCTTATCGTCGTCATCCTTGTAATCCATTGCTGCTCTTTTAGCTTTGC) and yeast genomic DNA as template, and which contains the promoter of *RPS28B* followed by the coding sequence for the FLAG tag, was cloned between the *Eco*RI and *Bam*HI sites producing YEplac195-pRPS28B (request number K349). The *RPS0A* open reading frame lacking the intron was subcloned using *Bam*HI and *Pst*I from YCplac111-pGAL-RPS0A (request number K251, [33]) into K349 to result in vector YEp-pRPS28B-FLAG-RPS0A (request number K421). YEp-pRPS28B-FLAG-RPS0A-ΔCTT (request number K514) was obtained by inserting a PCR amplicon, produced with oligos O490 and O848_5′ TTACTGCAGTTAGATGGACCATGGTTGA 3′ and yeast genomic DNA as template, into the *Bam*HI and *Pst*I sites of K349. Sequencing analysis of K514 revealed a neutral C45T conversion.

Biochemical methods

GST pull-down assays with GST fusions and *in vitro*-synthesized [^{35}S]-labeled polypeptides were conducted as follows. Individual GST-fusion proteins were expressed in *E. coli*, immobilized on glutathione-Sepharose beads and incubated with 10 µl of [^{35}S]-labeled potential binding partners at 4°C for 2 h. The beads were washed 3 times with 1 ml of phosphate-buffered saline and bound proteins separated by SDS-PAGE. Gels were first stained with Gelcode Blue Stain Reagent (Pierce) and then subjected to autoradiography. Polysome profile analysis, 2% HCHO cross-linking, WCE preparation and fractionation of extracts for analysis of pre-initiation complexes were carried out as described by [38].

40S-binding assay

40S ribosomal subunits were purified as described previously [39]. GST-pull down assays with purified 40S subunits were performed according to [20,34] with minor modifications. Briefly, the glutathione-Sepharose beads adsorbed with wt GST-a/TIF32-NTD fusion proteins were firstly preincubated with 2 µg/ml total yeast tRNA (Sigma) in the binding buffer B (20 mM HEPES [pH 7.5], 2.5 mM $MgCl_2$, 100 mM KCl, 0.1 mM EDTA, and 2 mM DTT) to prevent unspecific binding. After several washing steps with the buffer B, the beads were incubated with purified ribosomal 40S subunits at the final concentration of 0.4 µM in the buffer B supplemented with 0.75% dry milk for 30 min at 22°C. After three washes with the buffer B, the resulting complexes were subjected to SDS-PAGE electrophoresis followed by immunoblotting with anti-ASC1 and anti-RPS22 antibodies.

FLAG tag co-immunoprecipitation pull-down

FLAG tag co-immunoprecipitation pull-down was performed according to [28] with minor modifications. Transformants of the H2880 wt strain overexpressing either wt or C-terminally truncated RPS0A-FLAG were grown in SD medium at 30°C to an OD_{600} of ~1, cooled down to 4°C and disrupted by FastPrep-24 (MP Biomedicals) with glass beads in the buffer A200 (200 mM KCl, 20 mM Tris [pH 8], 5 mM $Mg(CH_3C00)_2$, 1 mM DTT, 1 mM PMSF, Complete EDTA-free protease inhibitor cocktail tablet [Roche]). Extracts were clarified by two consecutive centrifugations at 14,000 rpm for 5 and 10 min at 4°C. Triton X-100 was added to the supernatants to 0.2%. The resulting WCEs (300 mg) in a final volume of 250 µl were incubated with 100 µl of anti-FLAG M2 affinity matrix (Sigma) for 60 min at 4°C in A200T (buffer A200, 0.2% Triton X-100). Subsequently, the beads were washed five times with 2 ml of A200 and once with 10 ml of A200T. Co-immunoprecipitated proteins were eluted from the affinity matrix by boiling the samples in the SDS-PAGE loading buffer, loaded on the gel and analyzed by Western blotting.

Preparation of antibodies against RPS0A

The GST-RPS0A fusion protein encoded by pGEX-RPS0A was expressed in *E. coli* and purified from the WCE by incubation with Glutathione-Sepharose 4B beads (Pharmacia). The isolated protein was resolved by SDS-PAGE (4–20% gels), excised from the gel, and washed with 1× PBS. Rabbits were injected with the purified protein and serum containing polyclonal antibodies against RPS0A was obtained commercially by Apronex (Prague, the Czech Republic).

Supporting Information

Figure S1 Growth cessation caused by the RPS0A-depletion under non-permissive conditions is fully reversible by high copy expression of the wt RPS0A allele expressed form its endogenous promoter. Strain YID16 (*rps0aΔ rps0bΔ* YEpMET-RPS0A-U) bearing the *RPPS0A* WT allele under control of *MET3* promoter was further transformed by YEpRPS0A-L (bearing the wt *RPS0A* allele under control of its own promoter) and the resulting transformant was spotted in four serial 10-fold dilutions on SD medium +/− methionine and incubated at 30°C for 2.5 days.
(PDF)

Acknowledgments

We are thankful to Béla Szamecz for help with cloning, to the members of the Valášek and Krásný laboratories for helpful suggestions, and to Olga Krydová for technical and administrative assistance.

Author Contributions

Conceived and designed the experiments: LV PM. Performed the experiments: TK ID SG VM VV LC AN. Analyzed the data: TK ID SG PM LV. Wrote the paper: LV.

References

1. Valášek LS (2012) 'Ribozoomin' – Translation Initiation from the Perspective of the Ribosome-bound Eukaryotic Initiation Factors (eIFs). Curr Protein Pept Sci: in press.
2. Koromilas AE, Lazaris-Karatzas A, Sonenberg N (1992) mRNAs containing extensive secondary structure in their 5′ non-coding region translate efficiently in cells overexpressing initiation factor eIF-4E. EMBO J 11: 4153–4158.

3. Pestova TV, Kolupaeva VG (2002) The roles of individual eukaryotic translation initiation factors in ribosomal scanning and initiation codon selection. Genes Dev 16: 2906–2922.
4. Jivotovskaya A, Valášek L, Hinnebusch AG, Nielsen KH (2006) Eukaryotic translation initiation factor 3 (eIF3) and eIF2 can promote mRNA binding to 40S subunits independently of eIF4G in yeast. Mol Cell Biol 26: 1355–1372.
5. Mitchell SF, Walker SE, Algire MA, Park E-H, Hinnebusch AG, et al. (2010) The 5′-7-Methylguanosine Cap on Eukaryotic mRNAs Serves Both to Stimulate Canonical Translation Initiation and to Block an Alternative Pathway. Mol Cell 39: 950–962.
6. Cuchalová L, Kouba T, Herrmannová A, Danyi I, Chiu W-l, et al. (2010) The RNA Recognition Motif of Eukaryotic Translation Initiation Factor 3g (eIF3g) Is Required for Resumption of Scanning of Postermination Ribosomes for Reinitiation on GCN4 and Together with eIF3i Stimulates Linear Scanning. Mol Cell Biol 30: 4671–4686.
7. Nielsen KH, Szamecz B, Valasek LJ, A., Shin BS, Hinnebusch AG (2004) Functions of eIF3 downstream of 48S assembly impact AUG recognition and GCN4 translational control. EMBO J 23: 1166–1177.
8. Valášek L, Nielsen KH, Zhang F, Fekete CA, Hinnebusch AG (2004) Interactions of Eukaryotic Translation Initiation Factor 3 (eIF3) Subunit NIP1/c with eIF1 and eIF5 Promote Preinitiation Complex Assembly and Regulate Start Codon Selection. Mol Cell Biol 24: 9437–9455.
9. Nielsen KH, Valášek L, Sykes C, Jivotovskaya A, Hinnebusch AG (2006) Interaction of the RNP1 motif in PRT1 with HCR1 promotes 40S binding of eukaryotic initiation factor 3 in yeast. Mol Cell Biol 26: 2984–2998.
10. ElAntak L, Wagner S, Herrmannová A, Karásková M, Rutkai E, et al. (2010) The indispensable N-terminal half of eIF3j co-operates with its structurally conserved binding partner eIF3b-RRM and eIF1A in stringent AUG selection. J Mol Biol 396: 1097–1116.
11. Chiu W-L, Wagner S, Herrmannová A, Burela L, Zhang F, et al. (2010) The C-Terminal Region of Eukaryotic Translation Initiation Factor 3a (eIF3a) Promotes mRNA Recruitment, Scanning, and, Together with eIF3j and the eIF3b RNA Recognition Motif, Selection of AUG Start Codons. Mol Cell Biol 30: 4415–4434.
12. Herrmannová A, Daujotyte D, Yang JC, Cuchalová L, Gorrec F, et al. (2012) Structural analysis of an eIF3 subcomplex reveals conserved interactions required for a stable and proper translation pre-Initiation complex assembly. Nucleic Acids Res 40: 2294–2311.
13. Asano K, Clayton J, Shalev A, Hinnebusch AG (2000) A multifactor complex of eukaryotic initiation factors eIF1, eIF2, eIF3, eIF5, and initiator $tRNA^{Met}$ is an important translation initiation intermediate in vivo. Genes Dev 14: 2534–2546.
14. Sokabe M, Fraser CS, Hershey JWB (2011) The human translation initiation multi-factor complex promotes methionyl-tRNAi binding to the 40S ribosomal subunit. Nucleic Acids Research 40: 905–913.
15. Dennis MD, Person MD, Browning KS (2009) Phosphorylation of Plant Translation Initiation Factors by CK2 Enhances the in Vitro Interaction of Multifactor Complex Components. J Biol Chem 284: 20615–20628.
16. Valášek L, Nielsen KH, Hinnebusch AG (2002) Direct eIF2-eIF3 contact in the multifactor complex is important for translation initiation in vivo. EMBO J 21: 5886–5898.
17. Yamamoto Y, Singh CR, Marintchev A, Hall NS, Hannig EM, et al. (2005) The eukaryotic initiation factor (eIF) 5 HEAT domain mediates multifactor assembly and scanning with distinct interfaces to eIF1, eIF2, eIF3, and eIF4G. Proc Natl Acad Sci U S A 102: 16164–16169.
18. Valášek L, Mathew A, Shin BS, Nielsen KH, Szamecz B, et al. (2003) The Yeast eIF3 Subunits TIF32/a and NIP1/c and eIF5 Make Critical Connections with the 40S Ribosome in vivo. Genes Dev 17: 786–799.
19. Rabl J, Leibundgut M, Ataide SF, Haag A, Ban N (2011) Crystal Structure of the Eukaryotic 40S Ribosomal Subunit in Complex with Initiation Factor 1. Science 331: 730–736.
20. Kouba T, Rutkai E, Karasková M, Valášek LS (2012) The eIF3c/NIP1 PCI domain interacts with RNA and RACK1/ASC1 and promotes assembly of the pre-initiation complexes. Nucleic Acids Research 40: 2683–2699.
21. Szamecz B, Rutkai E, Cuchalova L, Munzarova V, Herrmannova A, et al. (2008) eIF3a cooperates with sequences 5′ of uORF1 to promote resumption of scanning by post-termination ribosomes for reinitiation on GCN4 mRNA. Genes Dev 22: 2414–2425.
22. Spahn CM, Beckmann R, Eswar N, Penczek PA, Sali A, et al. (2001) Structure of the 80S ribosome from Saccharomyces cerevisiae - tRNA ribosome and subunit-subunit interactions. Cell 107: 373–386.
23. Ford CL, Randal-Whitis L, Ellis SR (1999) Yeast proteins related to the p40/laminin receptor precursor are required for 20S ribosomal RNA processing and the maturation of 40S ribosomal subunits. Cancer Res 59: 704–710.
24. Demianova M, Formosa TG, Ellis SR (1996) Yeast proteins related to the p40/laminin receptor precursor are essential components of the 40 S ribosomal subunit. J Biol Chem 271: 11383–11391.
25. Ben-Shem A, Jenner L, Yusupova G, Yusupov M (2010) Crystal Structure of the Eukaryotic Ribosome. Science 330: 1203–1209.
26. Valášek L, Szamecz B, Hinnebusch AG, Nielsen KH (2007) In vivo stabilization of preinitiation complexes by formaldehyde cross-linking. Methods Enzymol 429: 163–183.
27. Soudet J, Gelugne J-P, Belhabich-Baumas K, Caizergues-Ferrer M, Mougin A (2010) Immature small ribosomal subunits can engage in translation initiation in Saccharomyces cerevisiae. EMBO J 29: 80–92.
28. Ferreira-Cerca S, Poll G, Kuhn H, Neueder A, Jakob S, et al. (2007) Analysis of the in vivo assembly pathway of eukaryotic 40S ribosomal proteins. Mol Cell 28: 446–457.
29. Fraser CS, Berry KE, Hershey JW, Doudna JA (2007) 3j is located in the decoding center of the human 40S ribosomal subunit. Mol Cell 26: 811–819.
30. Valášek L, Phan L, Schoenfeld LW, Valášková V, Hinnebusch AG (2001) Related eIF3 subunits TIF32 and HCR1 interact with an RNA recoginition motif in PRT1 required for eIF3 integrity and ribosome binding. EMBO J 20: 891–904.
31. Lumsden T, Bentley AA, Beutler W, Ghosh A, Galkin O, et al. (2010) Yeast strains with N-terminally truncated ribosomal protein S5: implications for the evolution, structure and function of the Rps5/Rps7 proteins. Nucleic Acids Research 38: 1261–1272.
32. Munzarová V, Pánek J, Gunišová S, Dányi I, Szamecz B, et al. (2011) Translation Reinitiation Relies on the Interaction between eIF3a/TIF32 and Progressively Folded cis-Acting mRNA Elements Preceding Short uORFs. PLoS Genet 7: e1002137.
33. Ferreira-Cerca S, Pöll G, Gleizes P-E, Tschochner H, Milkereit P (2005) Roles of Eukaryotic Ribosomal Proteins in Maturation and Transport of Pre-18S rRNA and Ribosome Function. Molecular Cell 20: 263–275.
34. Nemoto N, Singh CR, Udagawa T, Wang S, Thorson E, et al. (2010) Yeast 18S rRNA is directly involved in the ribosomal response to stringent AUG selection during translation initiation. Journal of Biological Chemistry: in press.
35. Voth WP, Jiang YW, Stillman DJ (2003) New 'marker swap' plasmids for converting selectable markers on budding yeast gene disruptions and plasmids. Yeast 20: 985–993.
36. Gietz RD, Sugino A (1988) New yeast-Escherichia coli shuttle vectors constructed with in vitro mutagenized yeast genes lacking six-base pair restriction sites. Gene 74: 527–534.
37. Smith DB, Johnson KS (1988) Single-step purification of polypeptides expressed in Escherichia coli as fusions with glutathione S-transferase. Gene 67: 31–40.
38. Nielsen KH, Valášek L (2007) In vivo deletion analysis of the architecture of a multi-protein complex of translation initiation factors. Methods Enzymol 431: 15–32.
39. Acker MG, Kolitz SE, Mitchell SF, Nanda JS, Lorsch JR, et al. (2007) Reconstitution of Yeast Translation Initiation. Methods in Enzymology: Academic Press. pp. 111–145.
40. Taylor DJ, Devkota B, Huang AD, Topf M, Narayanan E, et al. (2009) Comprehensive Molecular Structure of the Eukaryotic Ribosome. Structure 17: 1591–1604.

SUPPLEMENTARY DATA

MATERIALS AND METHODS

Plasmid constructions and site-directed mutagenesis

Table S1 contains brief descriptions of all plasmids employed in this study.

YCpNIP1-Myc-L was constructed by insertion of the SalI-BamHI-digested PCR product amplified from YCpNIP1-His-L (7) using primers TK46 and TK51 back into SalI-BamHI-digested YCpNIP1-His-L. Analogously, YCpNIP1-Δ60, 80, 100, 120 and Δ180-Myc-L were all constructed by insertion of the SalI-BamHI-digested PCR products amplified from YCpNIP1-His-L by using TK46 in combination with primers PS1, TK52, TK53, PS2, and PS3, respectively.

To construct six consecutive 10-Ala c/NIP1 substitutions in plasmids YCpNIP1-693A702-Myc-L to YCpNIP1-743A752-Myc-L, the following two pairs of primers were used for separate PCR amplifications with YCpNIP1-Myc-L as a template: (i) TK46 in combination with TK56, TK58, TK60, TK62, TK64, and TK66, respectively, and (ii) TK74 in combination with TK55, TK57, TK59, TK61, TK63, and TK65, respectively. The corresponding PCR products thus obtained were used in a 1:1 ratio as templates for a second PCR amplification with primers TK46 and TK74. The resulting PCR products were digested with SalI-BamHI and ligated with SalI-BamHI-cleaved YCpNIP1-Myc-L.

YEpNIP1-743A752-Myc-L and YEpNIP1-723A732-Myc-L were constructed by insertion of the BamHI-XbaI fragments of YCpNIP1-743A752-Myc-L and YCpNIP1-723A732-Myc-L, respectively, into BamHI-XbaI-digested YEpNIP1-His-L (7).

pGEX-c/NIP1-571-812 and pGEX-c/NIP1-701-812 expression plasmids were constructed by insertion of the corresponding BamHI-XhoI-digested PCR products amplified from YCpNIP1-His-L using the primer TK1 in combination with primers TK2 and TK3, respectively, into BamHI-XhoI-digested pGEX-5X-3 (Pharmacia). Analogously, pGEX-c/nip1-743A752 and pGEX-c/nip1-723A732 plasmids were constructed by insertion of the corresponding BamHI-XhoI-digested PCR products amplified from YCpNIP1-743A752-Myc-L and YCpNIP1-723A732-Myc-L, respectively, using primers TK2 and TK1.

YCpMJ-MET-NIP1-W was constructed by inserting the 2618-bp BamHI-HindIII fragment from pGAD-NIP1 (16) into YCplac22MET-W (a kind gift of Kim Nasmyth) digested by BamHI-HindIII.

To construct pRSASC1-intron-less-U carrying the *ASC1* gene without an intron, the following two pairs of primers were used for separate PCR amplifications with pRSASC1-U (28) as a template: (i) AJ2 and TK30 and (ii) TK31 and TK45. The PCR products thus obtained were used in a 1:1 ratio as templates for a third PCR amplification with primers AJ2 and TK45. The resulting PCR products were digested with BamHI-XbaI and ligated with BamHI-XbaI-cleaved pRS416 (28).

pFL45s which removes the *SNR24* coding sequence was created by cutting pFL45s/ACTU24 (32) with BamHI and self-ligating the isolated vector fragment.

To construct pGADT7-ASC1-exon1 and pGADT7-ASC1-exon2, the following two pairs of primers were used for separate PCR amplifications with pRSASC1-U as a template: (i) TK4 and TK5 and (ii) TK94 and TK5. The resulting PCR products were digested with BamHI-XhoI and ligated with BamHI-XhoI-cleaved pGADT7 (Clontech).

Two-Hybrid analysis

Two-hybrid analysis of protein-protein interactions between the c/NIP1-CTD and all 33 small subunit ribosomal proteins (RPSs) was conducted using the Matchmaker Two-Hybrid System 3 (Clontech) according to the vendor's instructions using strain AH109. Constructions of all two-hybrid plasmids in the vectors pGADT7 (activation domain hybrid vector) and pGBKT7 (DNA-binding domain hybrid vector) were carried out as follows. The two-hybrid plasmid pGBKT7 RPS1 to RPS32 were used from our previous study (16). The coding sequence of *ASC1* was PCR amplified from a 2.13-kb BamHI-XbaI fragment containing the entire *ASC1* gene locus inserted into pRSASC1-U using primers TK4 and TK5. The obtained PCR product was cleaved with BamHI-SalI and inserted into BamHI-SalI-digested pGBKT7 producing pGBKT7-RPS33/ASC1. To construct pGAD-c/NIP1-571-812 and pGAD-c/NIP1-701-812, the coding sequences of c/NIP1 corresponding to residues 571 to 812 and 701 to 812 were PCR amplified using two pairs of primers in TK1, TK2 and TK1, TK3, respectively, and YCpNIP1-His-L as a template. The PCR product thus obtained was cleaved with BamHI-XhoI and inserted into BamHI-XhoI-digested pGADT7.

Construction of yeast strains

To create HMJ08, H2880 (8) was first transformed with YCpNIP1-His-L to cover for the deletion of *NIP1* that was made in the next step by introducing the SacI-SphI fragment carrying the *nip1Δ::hisG-URA3-hisG* integration cassette from pLV10 (6). The Uracil auxotrophy was regained by growing the cells on SD plates containing 5-fluoro-orotic acid (5-FOA). The resulting strain was subsequently transformed with YCpNIP1-His-U and the Leucine auxotrophy was regained by growing the cells in liquid media containing Leucine and selecting for those that lost the YCpNIP1-His-L plasmid on SD +/- Leucine plates producing HMJ08.

HMJ06 was generated by introducing YCpMJ-MET-NIP1-W into HKN06 (6). The original pNIP1^{+} (*NIP1 URA3*) plasmid was evicted on SD plates containing 5-FOA.

To construct TK01 and ED43 with the chromosomal deletion of *ASC1*, HMJ08 and YBS47 (3), respectively, were introduced with the *asc1Δ::KanMX3* disruption cassette and Geneticin G418 resistant colonies were selected on YPD media containing G418. The *ASC1* disruption was verified by Western blotting. The *asc1Δ::KanMX3* disruption cassette was obtained by PCR form the genomic DNA of AL150 (28) using primers TK32 and TK35.

To produce TK149, TK150 and TK494, HMJ08 was transformed with YCpNIP1-Myc-L, YCpNIP1-743A752-Myc-L and YCpNIP1-Δ60, respectively, and the resident YCpNIP1-His-U plasmid was evicted on SD plates containing 5-FOA.

To generate TK145 and TK142, del'32a9A (3) was first transformed with pRS-a/tif32-box6-His-L and pRS-a/tif32-R731I-His-L (14), respectively, and the original pRSTIF32-His-U (*TIF32 URA3*) plasmid was evicted on SD plates containing 5-FOA. The resulting strains were then transformed to Ura+ with the integrative *GCN2* plasmid pHQ835 (kindly provided by Hongfang Qiu) digested with *Sna*BI. Ura- segregants were obtained by selecting for growth on medium containing 5-FOA, and the resulting TK145 and TK142 were tested for the presence of integrated *GCN2* by testing growth on medium containing 3-aminotriazole (3-AT).

YER27, with the chromosomal deletion of *ASC1*, was made by introducing del'32a9A (3) first with the *asc1Δ::KanMX3* disruption cassette as described above, and subsequently with pFL45s/ACTU24.

Yeast biochemical methods

GST pull-down assays with GST fusions and in vitro-synthesized ^{35}S-labeled polypeptides were conducted as follows. Individual GST-fusion proteins were expressed in *E. coli* (see below), immobilized on glutathione-Sepharose beads and incubated with 10 μl of ^{35}S-labeled potential binding partners at 4 °C for 2 h in binding buffer A (20 mM HEPES [pH 7.5], 75mM KCl, 0,1 mM $MgCl_2$, 0.05% IPEGAL, 1mM DTT, 0.1% milk). The ^{35}S-labeled proteins were synthetized using TNT Quick Coupled Transcription/Translation RRL kit (Promega), according to the manufacturer's instructions. The beads were washed 3 times with 1 ml of phosphate-buffered saline and bound proteins separated by SDS-PAGE. Gels were first stained with Gelcode Blue Stain Reagent (Pierce) and then subjected to autoradiography.

GST-fusion proteins were produced and purified as follows. Transformants of *E. coli* strain BL21-CodonPlus (DE3)-RIL (Stratagene) expressing GST-c/NIP1 fusion proteins were induced at OD_{600} ~ 0.5 for 2.5 h with 1 mM IPTG, harvested and washed once with ice-cold PBS. Following resuspension of the cell pellet from 500 ml culture in 20 mL of lysis buffer L (PBS [pH7.4], 10% glycerol, 2 μg/mL Aprotinin, 2 μg/mL Leupeptin, 2 μg/mL Pepstatin, Complete protease inhibitor cocktail tablets [EDTA-free, Roche diagnostics]), the cells were lysed by sonication on ice. Triton X-100 was added to the resulting cell lysates to final concentration of 1%. The lysate were subsequently clarified by centrifugation at 10,000 g for 10-20 min and incubated with 400 μl of 50% slurry of glutathione-Sepharose 4B beads equilibrated in PBS by gentle rocking for 30 min at 4 °C. The protein-bound beads were then washed three times with 5 ml of PBS.

WCE preparations, polysome profile analysis, 2% HCHO-cross-linking and fractionation of WCEs by high velocity sedimentation followed by Western blot analysis were all carried out as described by (41).

β-galactosidase assays were conducted as described previously (62).

REFERENCES

7. Valášek, L., Nielsen, K.H. and Hinnebusch, A.G. (2002) Direct eIF2-eIF3 contact in the multifactor complex is important for translation initiation in vivo. *EMBO J*, **21**, 5886-5898.
16. Valášek, L., Mathew, A., Shin, B.S., Nielsen, K.H., Szamecz, B. and Hinnebusch, A.G. (2003) The Yeast eIF3 Subunits TIF32/a and NIP1/c and eIF5 Make Critical Connections with the 40S Ribosome in vivo. *Genes Dev*, **17**, 786-799.
28. Gerbasi, V.R., Weaver, C.M., Hill, S., Friedman, D.B. and Link, A.J. (2004) Yeast Asc1p and Mammalian RACK1 Are Functionally Orthologous Core 40S Ribosomal Proteins That Repress Gene Expression. *Molecular and Cellular Biology*, **24**, 8276-8287.
32. Kiss-Laszlo, Z., Henry, Y., Bachellerie, J.P., Caizergues-Ferrer, M. and Kiss, T. (1996) Site-specific ribose methylation of preribosomal RNA: a novel function for small nucleolar RNAs. *Cell*, **85**, 1077-1088.

8. Nielsen, K.H., Szamecz, B., Valasek, L.J., A., Shin, B.S. and Hinnebusch, A.G. (2004) Functions of eIF3 downstream of 48S assembly impact AUG recognition and GCN4 translational control. *EMBO J.*, **23**, 1166-1177.
6. Valášek, L., Nielsen, K.H., Zhang, F., Fekete, C.A. and Hinnebusch, A.G. (2004) Interactions of Eukaryotic Translation Initiation Factor 3 (eIF3) Subunit NIP1/c with eIF1 and eIF5 Promote Preinitiation Complex Assembly and Regulate Start Codon Selection. *Mol. Cell. Biol.*, **24**, 9437-9455.
3. Szamecz, B., Rutkai, E., Cuchalova, L., Munzarova, V., Herrmannova, A., Nielsen, K.H., Burela, L., Hinnebusch, A.G. and Valášek, L. (2008) eIF3a cooperates with sequences 5' of uORF1 to promote resumption of scanning by post-termination ribosomes for reinitiation on GCN4 mRNA. *Genes Dev*, **22**, 2414-2425.
14. Chiu, W.-L., Wagner, S., Herrmannova, A., Burela, L., Zhang, F., Saini, A.K., Valasek, L. and Hinnebusch, A.G. (2010) The C-Terminal Region of Eukaryotic Translation Initiation Factor 3a (eIF3a) Promotes mRNA Recruitment, Scanning, and, Together with eIF3j and the eIF3b RNA Recognition Motif, Selection of AUG Start Codons. *Mol Cell Biol*, **30**, 4415-4434.
41. Valášek, L., Szamecz, B., Hinnebusch, A.G. and Nielsen, K.H. (2007) In Vivo Stabilization of Preinitiation Complexes by Formaldehyde Cross-Linking. *Methods Enzymol.*, **429**, 163-183.
40. Guex, N. and Peitsch, M.C. (1997) SWISS-MODEL and the Swiss-PdbViewer: an environment for comparative protein modeling. *Electrophoresis*, **18**, 2714-2723.
56. Larkin, M.A., Blackshields, G., Brown, N.P., Chenna, R., McGettigan, P.A., McWilliam, H., Valentin, F., Wallace, I.M., Wilm, A., Lopez, R. *et al.* (2007) Clustal W and Clustal X version 2.0. *Bioinformatics*, **23**, 2947-2948.
9. Nielsen, K.H., Valášek, L., Sykes, C., Jivotovskaya, A. and Hinnebusch, A.G. (2006) Interaction of the RNP1 motif in PRT1 with HCR1 promotes 40S binding of eukaryotic initiation factor 3 in yeast. *Mol Cell Biol*, **26**, 2984-2998.
57. Algire, M.A., Maag, D., Savio, P., Acker, M.G., Tarun, S.Z., Jr., Sachs, A.B., Asano, K., Nielsen, K.H., Olsen, D.S., Phan, L. *et al.* (2002) Development and characterization of a reconstituted yeast translation initiation system. *Rna*, **8**, 382-397.
58. Gietz, R.D. and Sugino, A. (1988) New yeast-Escherichia coli shuttle vectors constructed with in vitro mutagenized yeast genes lacking six-base pair restriction sites. *Gene*, **74**, 527-534.
32. Kiss-László, Z., Henry, Y., Bachellerie, J.-P., Caizergues-Ferrer, M. and Kiss, T. (1996) Site-Specific Ribose Methylation of Preribosomal RNA: A Novel Function for Small Nucleolar RNAs. *Cell*, **85**, 1077-1088.
16. Elantak, L., Wagner, S., Herrmannová, A., Karásková, M., Rutkai, E., Lukavsky, P.J. and Valášek, L. (2010) The indispensable N-terminal half of eIF3j co-operates with its structurally conserved binding partner eIF3b-RRM and eIF1A in stringent AUG selection. *J Mol Biol.*, **396**, 1097-1116.
12. Valášek, L., Hašek, J., Nielsen, K.H. and Hinnebusch, A.G. (2001) Dual function of eIF3j/Hcr1p in processing 20 S Pre-rRNA and translation initiation. *J Biol Chem*, **276**, 43351-43360.

60. Asano, K., Vornlocher, H.-P., Richter-Cook, N.J., Merrick, W.C., Hinnebusch, A.G. and Hershey, J.W.B. (1997) Structure of cDNAs encoding human eukaryotic initiation factor 3 subunits: possible roles in RNA binding and macromolecular assembly. *J Biol Chem*, **272**, 27042-27052.
61. Asano, K., Krishnamoorthy, T., Phan, L., Pavitt, G.D. and Hinnebusch, A.G. (1999) Conserved bipartite motifs in yeast eIF5 and eIF2Bε, GTPase-activating and GDP-GTP exchange factors in translation initiation, mediate binding to their common substrate eIF2. *EMBO J*, **18**, 1673-1688.
62. Mueller, P.P. and Hinnebusch, A.G. (1986) Multiple upstream AUG codons mediate translational control of *GCN4*. *Cell*, **45**, 201-207.

FIGURE LEGENDS

Figure S1. (**A**) Structural alignment of the 3D threading model of the c/NIP1-PCI (residues 650-812 in green) with the crystal structure of the PCI of *A. thaliana* CSN7 (yellow) and with the NMR solution structure of the C-terminal winged helix subdomain from the *Mus. musculus* COP9 subunit SGN4 (blue) computed by Swiss-PDBViewer 4.0.1. (40) The alignment of the area of WH subdomains is magnified. The c/NIP1-PCI α-helices 1, 1', 2 and 3 as well as the extra N-terminal α-helices of CSN7 (designated N1 and N2) are indicated. (**B**) Electrostatic potential of the solvent-accessible surface of the c/NIP1-CTD rendered on the molecular surface of its 3D threading model. A gradient of blue to red shows positive to negative charge, respectively, as calculated using Swiss-PDBViewer 4.0.1. (40) tool for analysis of Poisson-Boltzmann electrostatic potential. Positions of *nip1-723A732* and *nip1-743A752* are marked by magenta and sky blue, respectively (left cartoon), a position of helix α7 is shown in red (right cartoon).

Figure S2. (**A**) Western blot analysis of WCEs from the wt *NIP1* and mutant *nip1-743A752* and *nip1-Δ60* strains grown at 37 °C using anti-c/NIP1 (lanes 1 and 2) or anti-Myc (lanes 3 and 4) antibodies. Anti-GCD11 antibodies raised against the γ subunit of eIF2 were used as a loading control. (**B**) To test the expression of the lethal *nip1-723A732* allele, we constructed a derivative of a HMJ06 strain, in which the Myc-tagged c/nip1-723A732 mutant protein was overexpressed from a high copy plasmid on top of the wt His-tagged c/NIP1. The viable *nip1-743A752* mutant allele was used as a control. (**C**) GST fusions of two segments of the c/NIP1-CTD (residues 701-812 [lane 3] or 571-812 [lane 4]) and two 10-ala substitutions 743A752 (lane 5) and 723A732 (lane 6) inserted into the 571-812 fusion, or GST alone (lane 2) were tested for binding to the ^{35}S-labeled fragment of ASC1 corresponding to its exon1. Lane 1 (IN) contains 10% of the input amount.

Figure S3. Amino acid sequence alignment of the c/NIP1-CTD with other species. The amino acid sequence of c/NIP1-CTD from *Saccharomyces cerevisiae* (accession number NP_014040.1) is aligned with its *Zygosaccharomyces rouxii* homolog (accession number XP_002495716.1), *Lachancea thermotolerans* homolog (accession number XP_002552208.1), *Ashbya gossypii* homolog (accession number NP_986323.1), *Schizosaccharomyces pombe* homolog (accession number P_593828.2), *Mus musculus* homolog (accession number NP_666312.1), *Homo*

sapiens homolog (accession number NP_003743.1), *Xenopus laevis* homolog (accession number NP_001129648.1), *Drosophila melanogaster* homolog (accession number NP_611242.1) and *Caenorhabditis elegans* homolog (accession number NP_492638.1). The alignment was conducted with ClustalX version 2.0.12 (56). Identical and similar residues are color coded, a bar diagram shown below indicates the quality of the alignment by plotting a conservation score for each column of the alignment; the higher the bar, the better conservation of a particular column. Numbering refers to the amino acid sequence of *S. cerevisiae* c/NIP1. Mutated regions in *nip1-723A732* and *nip1-743A752* are boxed and marked by magenta and sky blue, respectively.

Table S1 Yeast strains used in this study.

Strain	Genotype	Source or reference
AH109	*MATa trp1-901 leu2-3, -112 ura3-52 his3-200 gal4Δ gal80Δ*	Clontech
H2880	*MATa trp1 leu2-3,-112 ura3-52*	(8)
HMJ08	*MATa, trp1 leu2-3,-112 ura3-52 nip1Δ* YCpNIP1-His-U (*NIP1-His URA3*)	This study
TK149	*MATa trp1 leu2-3,-112 ura3-52, nip1Δ* YCpNIP1-Myc-L (*NIP1-Myc LEU2*)	This study
TK150	*MATa trp1 leu2-3,-112 ura3-52 nip1Δ* YCpNIP1-743A752-Myc-L (*nip1-743A752-Myc LEU2*)	This study
TK494	*MATa trp1 leu2-3,-112 ura3-52 nip1Δ* YCpNIP1-Δ60-Myc-L (*nip1-Δ60-Myc LEU2*)	This study
TK01	*MATa trp1 leu2-3,-112 ura3-52 nip1Δ asc1Δ::KanMX3* (YCpNIP1-His-U) (*NIP1-His URA3*)	This study
HKN06	*MATa trp1 leu2-3,112 ura3-52 gcn2Δ nip1Δ (NIP1 URA3)*	(8)
HMJ06	*MATa trp1 leu2-3,-112 ura3-52 nip1Δ gcn2Δ* YCpMJ-Met-NIP1-W (*MET3-NIP1 TRP1*)	This study
ED43	*MATa trp1 leu2-3,-112 ura3-52 tif32Δ gcn2Δ asc1Δ::KanMX3 URA3::GCN2 ura3* pRSTIF32-His-L (*TIF32-His LEU2*)	This study
del'32a9A	*MATa trp1 leu2-3,-112 ura3-52 tif32Δ gcn2Δ* pRSTIF32-His-U (*TIF32-His URA3*)	(3)

YBS47	*MATa trp1 leu2-3,-112 ura3-52 tif32Δ gcn2Δ URA3::GCN2 ura3* pRSTIF32-His-L (*TIF32-His LEU2*)	(3)
YBS53	*MATa trp1 leu2-3,-112 ura3-52 tif32Δ gcn2Δ URA3::GCN2 ura3* pRStif32-Δ8-His-L (*tif32-Δ8-His LEU2*)	(3)
TK145	*MATa trp1 leu2-3,-112 ura3-52 tif32Δ gcn2Δ URA3::GCN2 ura3* pRStif32-Box6-His-L (*tif32-box6-His LEU2*)	This study
TK142	*MATa trp1 leu2-3,-112 ura3-52 tif32Δ gcn2Δ URA3::GCN2 ura3* pRStif32-R731I-His-L (*tif32-R731I-His LEU2)*	This study
AL150	*MATa/MAT@ his3Δ1/his3Δ1 leu2Δ0/leu2Δ0 met15Δ0/MET15 LYS2/lys2Δ0 ura3Δ0/ura3Δ0 asc1Δ::KanMX3/ asc1Δ::KanMX3*	(28)
H428	*MATa leu2-3,-112 ura3-52 hcr1Δ*	(9)
YER27	*MATa trp1 leu2-3,-112 ura3-52 tif32Δ gcn2Δ asc1Δ::KanMX3* pRSTIF32-His-U *(TIF32-HIS, URA3)* pFL45s/ACTU24 (*SNR24, TRP1*)	This study
H503	*MATa leu2-3 112 his4-539 trp1 ura3-52 cup1::LEU2/PGK1pG/MFA2pG*	(57)

Table S2 Plasmids used in this study.

Plasmid	Description	Source or reference
YCplac111	single copy cloning vector, *LEU2*	(58)
YEplac181	high copy cloning vector, *LEU2*	(58)
YCplac22MET-W	single copy cloning vector with conditional *MET3* promoter, *TRP1* plasmid from YCplac22	K. Nasmyth
YCpNIP1-His-U	single copy *NIP1-His*, *URA3* plasmid from YCplac33	(7)
YEpNIP1-His-U	high copy *NIP1-His*, *URA3* plasmid from YEplac195	(7)
YEpNIP1-His-L	high copy *NIP1-His*, *URA3* plasmid from YEplac181	(7)
YEpNIP1-ΔB´-His-U	high copy *nip1-ΔB'-His* [1-570]*, URA3*plasmid from YEplac195	(7)
YCpNIP1-His-L	single copy *NIP1-His*, *LEU2* plasmid from YCplac111	(7)
YCpMJ-MET-NIP1-W	single copy *NIP1* under *MET3* promoter, *TRP1* plasmid from YCplac22	This study
YCpNIP1-Myc-L	single copy *NIP1-Myc*, *LEU2* plasmid from YCplac111	This study
YCpNIP1-Δ60 to Δ180-MYC-L	single copy *NIP1-Myc* truncated by 60, 80, 100, 120 or 180 amino acid residues, *LEU2* plasmid from YCplac11	This study
YCpNIP1-693A702 to YCpNIP1-743A752-Myc-L	single copy *NIP1-Myc* containing 10 Ala substitutions between amino acid residues 693 and 752, *LEU2* plasmid from YCplac111	This study

YEpNIP1-743A752-Myc-L	high copy *NIP1-Myc* containing 10 Ala substitutions between aa 743 and 752, *LEU2* plasmid from YCplac181	This study
YEpNIP1-723A732-Myc-L	high copy *NIP1-Myc* containing 10 Ala substitutions between aa 723 and 732, *LEU2* plasmid from YCplac181	This study
pRS416	low copy cloning vector, *URA3*	(28)
pRSASC1-U	low copy *ASC1*, *URA3* plasmid from pRS416	(28)
pRSASC1-intron-less-U	low copy *ASC1* lacking its intron, *URA3* plasmid from pRS416	This study
pFL45S	high copy cloning vector, *TRP1*	This study
pFL45s/ACTU24	high copy *SNR24*, *TRP1* plasmid from pFL45s	(32)
pRSTIF32-His L	low copy *TIF32-His*, *LEU2* plasmid from pRS315	(7)
pRStif32-Δ8-His-L	low copy *tif32-Δ8-His* [200-964], *LEU2* plasmid from pRS315	(7)
pRS-a/tif32-box6-His-L	low copy *tif32-box6-His*, *LEU2* plasmid from pRS315	(14)
pRS-a/tif32-R731I-His-L	low copy *tif32-R731I-His*, *LEU2* plasmid from pRS315	(14)
YEpLVHCR1-L	high copy *HCR1*, *LEU2* plasmid from YEplac181	(16)
pT7-18S rRNA	full length 18S rDNA under T7 promoter	(12)
pT7-25S rRNA	full length 25S rDNA under T7 promoter	(16)

pT7-18S rRNA-I	domain I of 18S rRNA [24-612] under T7 promoter	(16)
pT7-18S rRNA-II	domain II of 18S rRNA [613-1148] under T7 promoter	(16)
pT7-18S rRNA-III	domain III of 18S rRNA [1148-1798] under T7 promoter	(16)
pKA18	β-globin mRNA under SP6 promoter	(60)
pGEX-5X-3	cloning vector for GST fusions	Pharmacia
pGEX- c/NIP1-571-812	GST-c/NIP1 [571-812] fusion, from pGEX-5X-3	This study
pGEX- c/NIP1-701-812	GST-c/NIP1 [701-812] fusion, from pGEX-5X-3	This study
pGEX-c/nip1-743A752	GST-c/nip1-743A752 fusion, from pGEX-5X-3	This study
pGEX-c/nip1-723A732	GST-c/nip1-723A732 fusion, from pGEX-5X-3	This study
pGBKT7	cloning vector for GAL4 DNA-binding domain fusion, *TRP1*	Clontech
pGADT7	cloning vector for GAL4 activation domain fusion, *LEU2*	Clontech
pGADT7-ASC1-exon1	*ASC1*-exon1 under T7 promoter cloned into pGADT7, *LEU2*	This study
pGADT7-ASC1-exon2	*ASC1*-exon2 under T7 promoter cloned into pGADT7, *LEU2*	This study
pGAD-NIP1	*NIP1* under T7 promoter cloned into pGADT7, *LEU2*	(16)
pGAD-c/NIP1-571-812	*NIP1-571-812* under T7 promoter cloned into pGADT7, *LEU2*	This study
pGAD-c/NIP1-701-812	*NIP1-701-812* under T7 promoter cloned into pGADT7, *LEU2*	This study

p1780-IMT	high-copy *SUI2, SUI3, GCD11, IMT4*, *URA3* plasmid from YEp24	(61)
p180 (YCp50–GCN4–lacZ)	low copy *URA3* vector containing wild-type *GCN4* leader	(62)

Table S3 List of oligonucleotides used in this study.

Oligonucleotide	Sequence (5' to 3')
TK1	CCCCGTCGACTCGAGACGACGATTTGATGG
TK2	CCCCGGATCCTCGATTCATCCCTACAA
TK3	CCCCGGATCCCTTTATTACCAAACATG
TK4	CCCCGGATCCAAATGGCATCTAACGAA
TK5	CCCCGTCGACTCGAGTTAGTTAGCAGTCAT
TK30	GCTTGGAACTTAAACCAATTCCAAA
TK31	TTTGGAATTGGTTTAAGTTCCAAGCCTTAACCATTTTGTCGTTACCGGCA
TK32	GCCATCTGTAGCCTTATGACTATGT
TK35	ACTGAATTTAATGAACTCCTTGCAG
TK45	ACACAGGAAACAGCTATGAC
AJ2	GATTCACTATAGGGCGAATTGG
TK46	AGACCAGCTCGATTCTGC
TK51	CCCCGGATCCTCACAGGTCCTCCTCTGAGATCAGCTTCTGCTCACGACGATTTGATGGTGGG
PS1	CCCCGGATCCTCACAGGTCCTCCTCTGAGATCAGCTTCTGCTCCACCTTATTTTCTGGAAGATC

PS2	CCCCGGATCCTCACAGGTCCTCCTCTGAGATCAGCTTCTGCTCGTATTTAACAGAGTCTCTCC
PS3	CCCCGGATCCTCACAGGTCCTCCTCTGAGATCAGCTTCTGCTCTGGAATTTCGATCAATAAGG
TK52	CCCCGGATCCTCACAGGTCCTCCTCTGAGATCAGCTTCTGCTCGAACCTCTTGAAAGAAAAGA
TK53	CCCCGGATCCTCACAGGTCCTCCTCTGAGATCAGCTTCTGCTCACTATTCAACACCGTTTCCA
TK55	TCTGTTGCTAAACTAGCCGAAGCAGCTGCTGCAGCAGCAGCAGCAGCAGCAGAAGTTTTGCAATC TGTTATC
TK56	TTCGGCTAGTTTAGCAACAGA
TK57	TTTTCTTTCAAGAGGTTCTATGCAGCTGCTGCAGCAGCAGCAGCAGCAGCATTATTTGATCTTCCA GAAAAT
TK58	ATAGAACCTCTTGAAAGAAAA
TK59	GTACAAGTTGAATCTTTGAAGGCAGCTGCTGCAGCAGCAGCAGCAGCAGCATCAAGTTTTTCTGT TGCTAAA
TK60	CTTCAAAGATTCAACTTGTAC
TK61	GAAACGGTGTTGAATAGTTTAGCAGCTGCTGCAGCAGCAGCAGCAGCAGCAACTTATTTCTTTTCT TTCAAG
TK62	TAAACTATTCAACACCGTTTC
TK63	ATAAAATCTTGGGCTTTATTAGCAGCTGCTGCAGCAGCAGCAGCAGCAGCAACGGAAAGAGTACA AGTTGAA
TK64	TAATAAAGCCCAAGATTTTAT
TK65	TGGAGAGACTCTGTTAAATACGCAGCTGCTGCAGCAGCAGCAGCAGCAGCACCAAACATGGAAA

	CGGTGTTG
TK66	GTATTTAACAGAGTCTCTCCA
TK74	TTCTTCGGATCCTCACAGGTCCTC
TK94	CCCCGGATCCAAGCTTGGAACTTAAAC

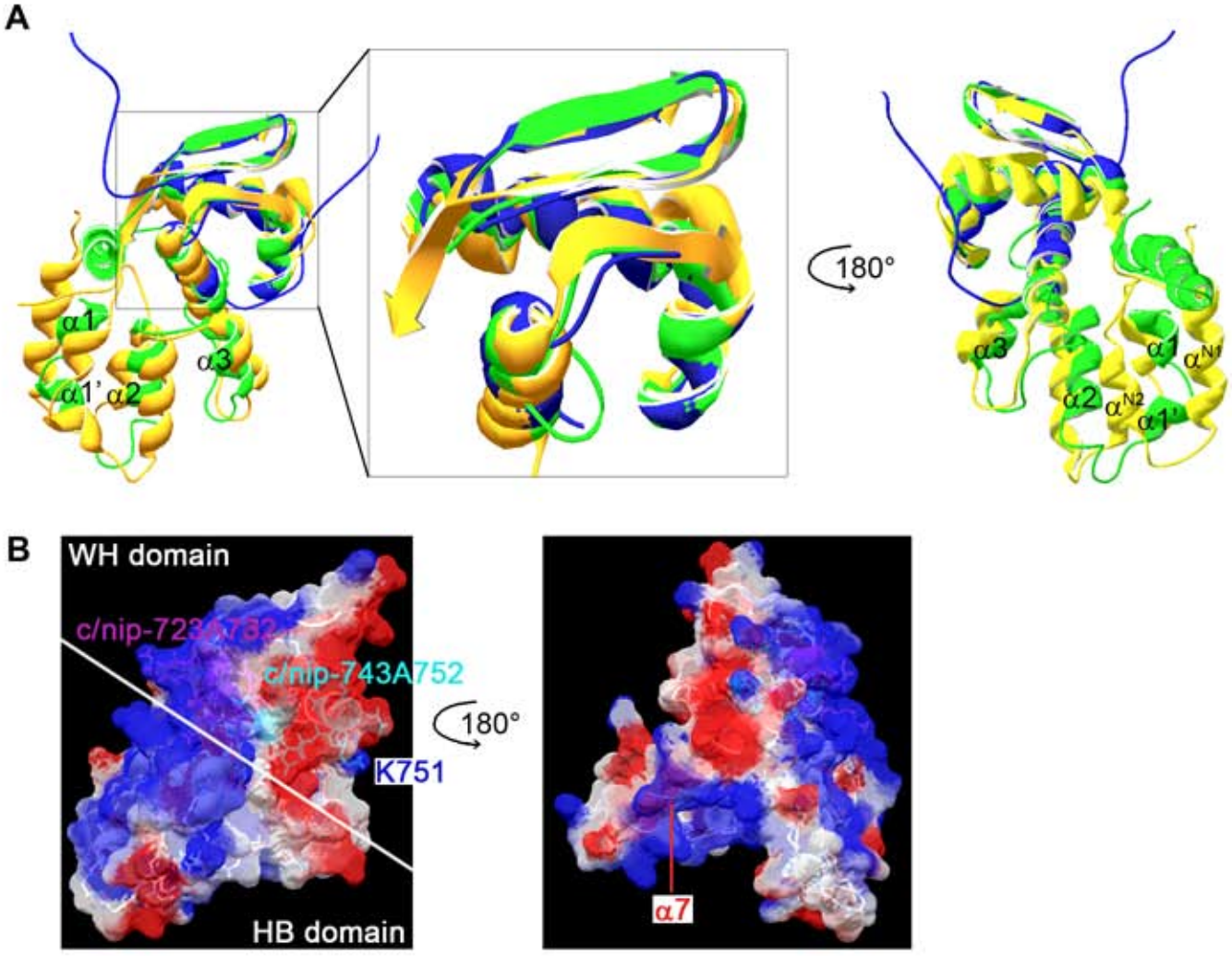
A
α1
α3
α1' α2
180°
α3
α1
α^N1
α2
α^N2
α1'
B
WH domain
c/nip-723A732
c/nip-743A752
K751
HB domain
180°
α7

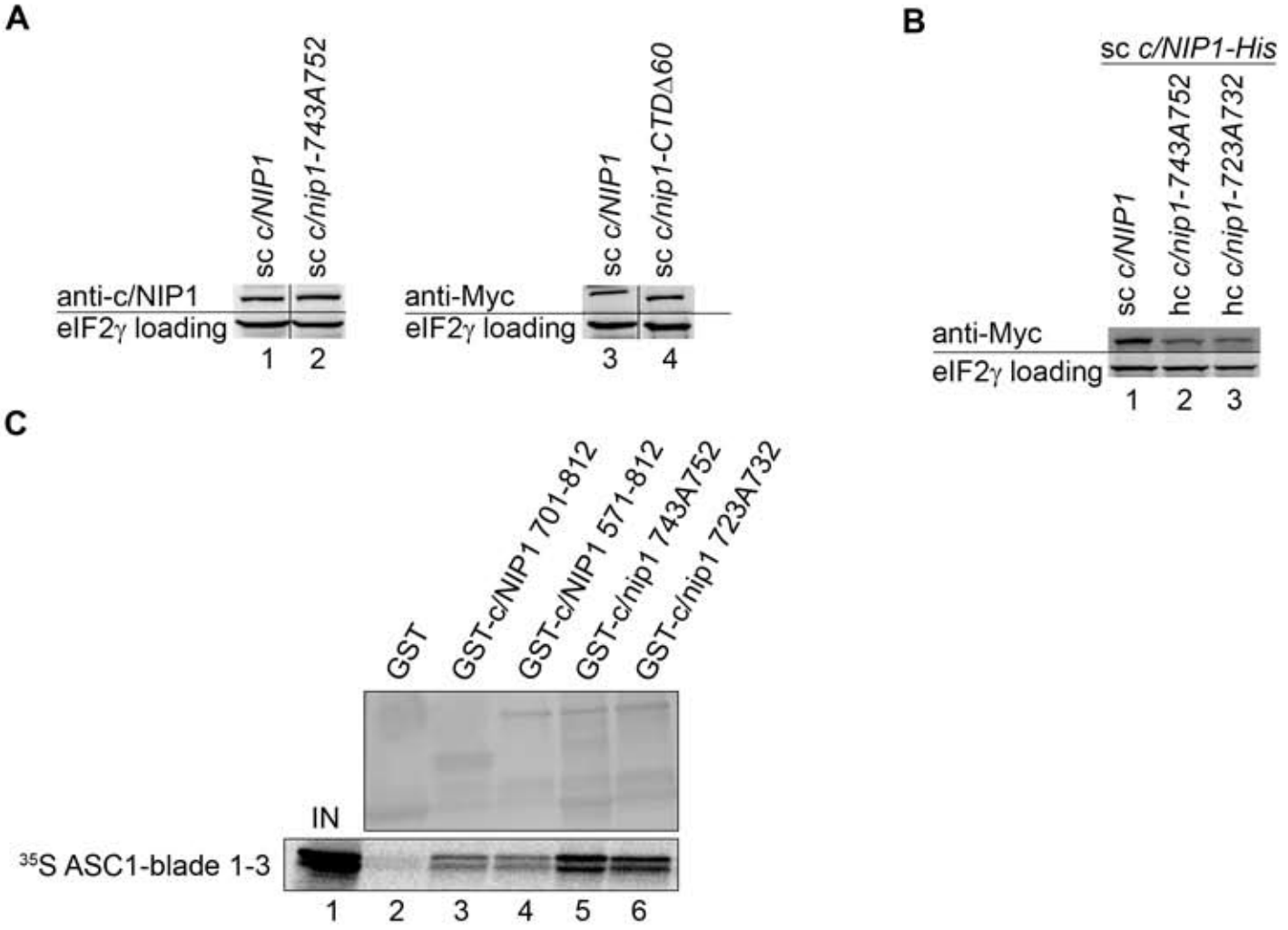
A
sc c/NIP1
sc c/nip1-743A752
anti-c/NIP1
eIF2γ loading
1 2
sc c/NIP1
sc c/nip1-CTDΔ60
anti-Myc
eIF2γ loading
3 4
B
sc c/NIP1-His
sc c/NIP1
hc c/nip1-743A752
hc c/nip1-723A732
anti-Myc
eIF2γ loading
1 2 3
C
GST
GST-c/NIP1 701-812
GST-c/NIP1 571-812
GST-c/nip1 743A752
GST-c/nip1 723A732
IN
35S ASC1-blade 1-3
1 2 3 4 5 6

A

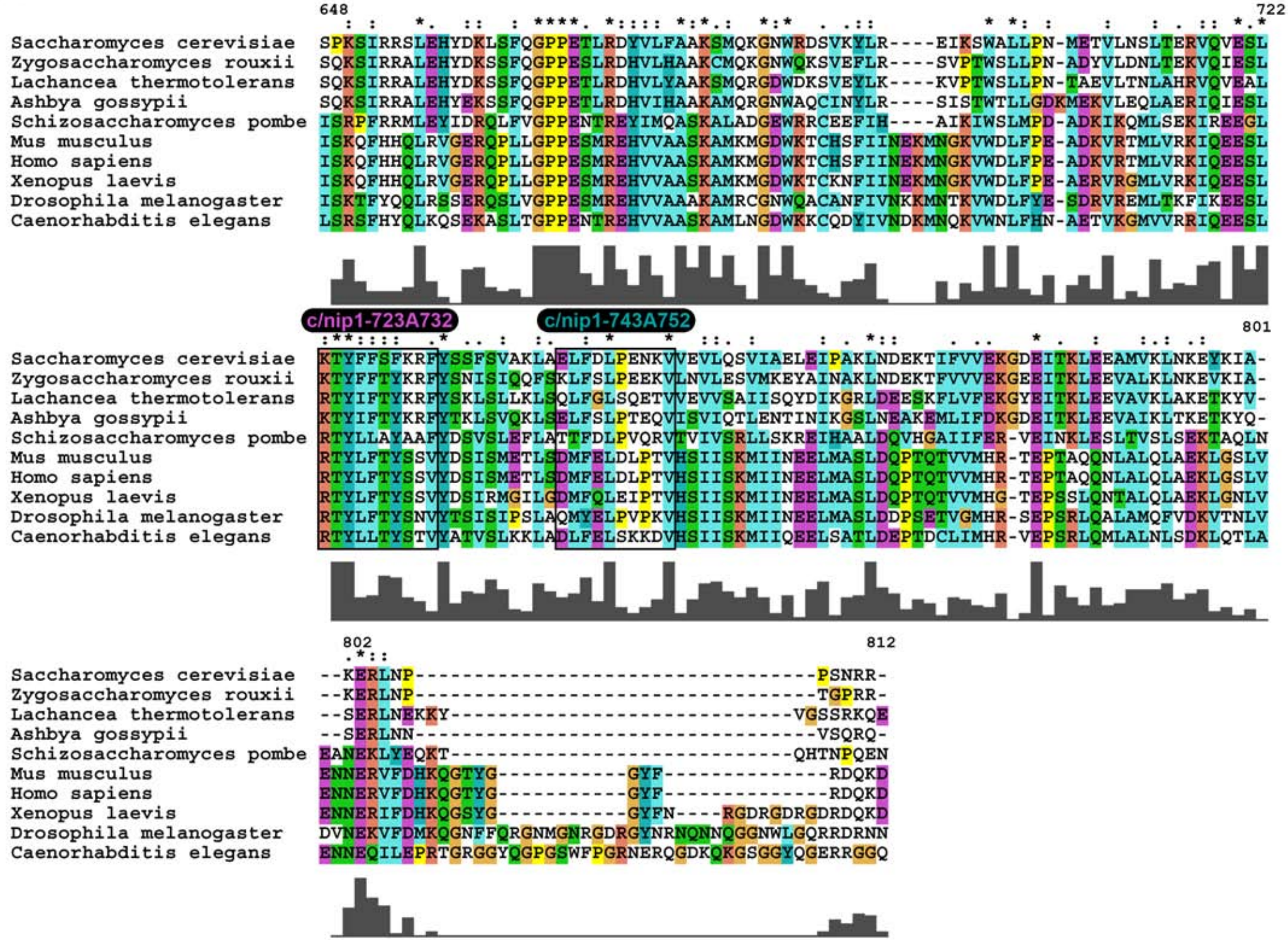
648
722
Saccharomyces cerevisiae
Zygosaccharomyces rouxii
Lachancea thermotolerans
Ashbya gossypii
Schizosaccharomyces pombe
Mus musculus
Homo sapiens
Xenopus laevis
Drosophila melanogaster
Caenorhabditis elegans
c/nip1-723A732
c/nip1-743A752
801
802
812

Translation in Yeast Cells Begins and Ends with Translation Initiation Factor 3 (eIF3)

Lucie Cuchalová and Petra Beznosková, Christopher J. Shoemaker, Stanislava Gunišová, Tobias von der Haar, and Leoš Shivaya Valášek

Under the review in PLoS Biol.

It is becoming increasingly apparent that factors involved in regulating various steps of gene expression may have multiple functions and that this multitasking may integrate transcription, mRNA export, translation and mRNA decay into a delicately regulated higher-order process that promptly responds to immediate needs of the cell in a complex manner. For example, translation initiation factor eIF3 links translation initiation to transcription, to mRNA export and to the NMD pathway.

Here we show for the first time that the bona fide translation initiation factor eIF3 also links translation initiation with translation termination in vivo. Our genetic as well as biochemical data clearly show that: 1) various eIF3 mutants either increase or decrease the fidelity of termination efficiency ("the stop codon read-through phenotype") and show genetic interactions with the mutant release factors; 2) the ability of ABCE1/RLI1 to stimulate termination, as shown recently, depends on the intact 4Fe-4S clusters that it contains as well as on its intact ATP-ase activity; 3) the j/HCR1 subunit of eIF3 genetically and physically interacts with ABCE1/RLI1, and increased dosage of RLI1 suppresses all termination defects of the HCR1 deletion strain; 4) eRF1 directly interacts with i/TIF34 and g/TIF35 subunits of eIF3 and both eRFs as well as ABCE1/RLI1 and eIF3 can be found in a ribosome- and RNA-free complexes in vivo; 5) a loss of non-essential j/HCR1 from cells prevents eRF3 from stable binding to terminating polysomes and, conversely, several eRF3 and eRF1 mutants prevent j/HCR1 association with the latter. Based on these and other results of ours and several recent studies, we propose that eIF3 forms a molecular bridge between initiation and termination phases of translation, suggesting that they mutually communicate and can be co-ordinated by external stimuli.

PLOS Biology

Translation in Yeast Cells Begins and Ends with Translation Initiation Factor 3 (eIF3)

--Manuscript Draft--

Manuscript Number:	
Full Title:	Translation in Yeast Cells Begins and Ends with Translation Initiation Factor 3 (eIF3)
Short Title:	eIF3 promotes termination of translation
Article Type:	Research Article
Keywords:	translation initiation; translation termination; eIF3; eIF3j/HCR1; eRF1; eRF3; ABCE1/RLI1; read-through
Corresponding Author:	Leos Shivaya Valasek, Ph.D. Institute of Microbiology ASCR Prague 4, CZECH REPUBLIC
Corresponding Author Secondary Information:	
Corresponding Author's Institution:	Institute of Microbiology ASCR
Corresponding Author's Secondary Institution:	
First Author:	Lucie Cuchalova
First Author Secondary Information:	
Order of Authors:	Lucie Cuchalova
	Petra Beznoskova
	Christopher J Shoemaker
	Stanislava Gunisova
	Tobias von der Haar
	Leos Shivaya Valasek, Ph.D.
Order of Authors Secondary Information:	
Abstract:	Translation is divided into initiation, elongation, termination and ribosome recycling. Earlier work implicated several eukaryotic initiation factors (eIFs) in ribosomal recycling in vitro. Here, we identify and define a role for eIF3 in the stop codon selection process in vivo. Mutations in core eIF3 subunits reduce observed rates of stop codon read-through, whereas deletion of the eIF3j/HCR1 subunit increases read-through and accumulates eRF3 in polyribosomes. Remarkably, eIF3 occurs in ribosome- and RNA-free complexes with release and recycling factors eRF1, eRF3, and ABCE1/RLI1, and eIF3 mutants genetically interact with mutant eRFs. When overexpressed, ABCE1/RLI1 fully suppresses slow growth and increased read-through defects of hcr1Δ, correcting an impaired ability of eRF3 to dissociate from post-termination complexes upon stop codon recognition to clear the way for its own binding. This work uncovers active roles of initiation factor eIF3 in translation termination, defining a communication bridge between initiation and termination/recycling phases of protein synthesis.
Suggested Reviewers:	Alan Hinnebusch NICHD/NIH alanh@mail.nih.gov expert in the field
	David Bedwell University of Alabama at Birmingham dbedwell@uab.edu expert in the field
	Nahum Sonenberg

	McGill University, Montreal, Canada nahum.sonenberg@mcgill.ca expert in the field
	Tatyana Pestova SUNY Downstate Medical Center, Brooklyn, New York, USA tatyana.pestova@downstate.edu expert in the field
	Thomas Preiss The John Curtin School of Medical Research , The Australian National University thomas.preiss@anu.edu.au expert in the field
	Thomas Dever NICHD/NIH Thomas.Dever@nih.gov expert in the field
	Jon Lorsch Johns Hopkins University School of Medicine, MD jlorsch@jhmi.edu expert in the field
	Jean-Pierre Rousset IGM, Univ Paris & CNRS, Orsay, France jean-pierre.rousset@igmors.u-psud.fr expert in the field
	Ian Brierley University of Cambridge, Cambridge, UK ib103@mole.bio.cam.ac.uk expert in the field
Opposed Reviewers:	John WB Hershey UC Davis Cancer Center potential conflict of interest
	Jennifer Doudna University of California, Berkeley potential conflict of interest
	Christopher Fraser UC Davis Cancer Center potential conflict of interest

January 3, 2013

LABORATORY OF REGULATION
OF GENE EXPRESSION

Dear editor,

We are pleased to submit our manuscript "**Translation in Yeast Cells Begins and Ends with Translation Initiation Factor 3 (eIF3)**" for publication in *PLoS Biology*.

It is becoming increasingly apparent that factors involved in regulating various steps of gene expression may have multiple functions and that this multitasking may integrate transcription, mRNA export, translation and mRNA decay into a delicately regulated higher-order process that promptly responds to immediate needs of the cell in a complex manner. For example, translation initiation factor eIF3 links translation initiation to transcription (Harel-Sharvit et al., Cell, 2010), to mRNA export (Bolger et al., Cell, 2008) and to the NMD pathway (Isken et al., Cell, 2008).

Here we show for the first time that the *bona fide* translation initiation factor eIF3 also links translation initiation with translation termination *in vivo*. In particular, eIF3 occurs together with eRFs 1 and 3 and the ribosomal recycling factor ABCE1/RLI1 in a ribosome- and RNA-free complex. Various mutants of core eIF3 subunits, but not of other initiation factors, decrease stop codon read-through in living cells and show synthetic phenotypes with mutant release factors eRF1 and 3. These and other results suggest that eIF3 modulates the precision of the stop codon recognition by eRF1 in order to fine tune the termination process.

Conversely, deletion of *hcr1* encoding the eIF3j subunit of eIF3 increases stop codon read through and results in accumulation of eRF3 in heavy polysomes. Based on these and other findings we proposed a model that upon stop codon recognition and subsequent GTP hydrolysis, j/HCR1 promotes eRF3·GDP ejection from the post-TCs to allow binding of its interacting partner ABCE1/RLI1 and polypeptide release. Finally, increased dosage of ABCE1/RLI1 substitutes for the j/HCR1 roles in termination (but not in initiation) and in enabling efficient cell growth. This strongly implies that the j/HCR1 function in termination is more critical for optimal cell proliferation than its function in translation initiation. Since eIF3 was, based on *in vitro* experiments, previously implicated in promoting also the very final step of translation – ribosomal recycling – by an unknown mechanism (Pisarev et al., Cell, 2007; Pisarev et al., Mol Cell, 2010), we further propose that eIF3 is one of the very few

factors that connects various processes of mRNA life and integrates them into the ultimate translational output. Taken into account that the translation pathway is highly conserved among low and high eukaryotes, it is highly likely that also this connecting role of eIF3 is conserved.

We hope that the editors of *PLoS Biology* and the reviewers will concur that these findings constitute a significant conceptual advance of our understanding of the translation process, and as such are of interest to the broad readership of *PLoS Biology*. We thank you for consideration of our work for publication in your journal.

Sincerely,

Leoš Shivaya Valášek
Laboratory of Regulation of Gene Expression
Institute of Microbiology ASCR
Prague, the Czech Republic

Videnska 1083 *tel. +420 241 062 288* *e-mail: valasekl@biomed.cas.cz*
142 20 Praha 4 *mobil +420 724 731 661* *http://www.biomed.cas.cz/mbu/lrge*
the Czech Republic *fax +420 241 062 665*

Translation in Yeast Cells Begins and Ends with Translation Initiation Factor 3 (eIF3)

Lucie Cuchalová,[1,4] Petra Beznosková,[1,4] Christopher J. Shoemaker,[2] Stanislava Gunišová,[1] Tobias von der Haar,[3] and Leoš Shivaya Valášek[1]*

[1]Laboratory of Regulation of Gene Expression, Institute of Microbiology ASCR, Videnska 1083, 142 20, Prague, the Czech Republic

[2]Howard Hughes Medical Institute, Johns Hopkins University School of Medicine, Baltimore, Maryland, USA

[3]School of Biosciences, University of Kent, Kent CT2 7NJ, UK

[4]These authors contributed equally to this work

*Correspondence: valasekl@biomed.cas.cz

Tel: +420 241 062 288

Fax: +420 241 062 665

Abstract

Translation is divided into initiation, elongation, termination and ribosome recycling. Earlier work implicated several eukaryotic initiation factors (eIFs) in ribosomal recycling *in vitro*. Here, we identify and define a role for eIF3 in the stop codon selection process *in vivo*. Mutations in core eIF3 subunits reduce observed rates of stop codon read-through, whereas deletion of the eIF3j/HCR1 subunit increases read-through and accumulates eRF3 in polyribosomes. Remarkably, eIF3 occurs in ribosome- and RNA-free complexes with release and recycling factors eRF1, eRF3, and ABCE1/RLI1, and eIF3 mutants genetically interact with mutant eRFs. When overexpressed, ABCE1/RLI1 fully suppresses slow growth and increased read-through defects of *hcr1Δ,* correcting an impaired ability of eRF3 to dissociate from post-termination complexes upon stop codon recognition to clear the way for its own binding. This work uncovers active roles of initiation factor eIF3 in translation termination, defining a communication bridge between initiation and termination/recycling phases of protein synthesis.

Introduction

Protein synthesis or mRNA translation is a complex and highly conserved process that can be separated into initiation, elongation, termination and ribosome recycling phases. Although these four phases are distinct in time, there is a longstanding notion for some form of communication among them. Notably, several initiation factors and related proteins have been proposed to function in more than one phase. These include ABCE1/RLI1 and GLE1, which are believed to promote both the initiation and termination phases by a mechanism that remains to be elucidated [1-3], and the *bona fide* translation initiation factor eIF3, which has been recently suggested to promote the recycling phase, at least in a mammalian *in vitro* reconstituted system [4,5].

The beginning of a translational cycle involves a series of steps that culminate in the assembly of the 80S initiation complex (IC) on the AUG start codon (reviewed in [6]). These steps include 1) Met-tRNA$_i^{Met}$ recruitment to the 40S subunit to form the 43S pre-initiation complex (PIC), 2) mRNA recruitment to the 43S PIC to form the 48S PIC, 3) scanning of the 48S PIC to the first recognized start codon, and 4) joining of the 60 subunit to commit thus formed 80S IC for the elongation phase. The translation initiation factor eIF3, which in yeast consists of five essential core subunits (eIF3a/TIF32, b/PRT1, c/NIP1, g/TIF35, and i/TIF34) and one transiently associated, non-essential subunit (j/HCR1), is actively involved in regulation of the first three of these steps [6]. In the PIC assembly steps, the action of eIF3 is further stimulated by one of its interacting partners, the ATP-binding cassette protein ABCE1/RLI1, by an unknown mechanism [1]. In contrast to most eIFs, eIF3 interacts with the solvent-

exposed side of the small ribosomal subunit [6] and as such, it is thought to remain bound at this position during the first elongation cycles [7,8].

The end of a translational cycle involves another series of steps that culminate in the release of a newly synthesized polypeptide from the translating ribosome (the termination phase), and in the dissolution of the ribosome:tRNA:mRNA complex (the recycling phase). Termination begins when a stop codon enters the ribosomal A-site, forming a pre-termination complex (pre-TC) [9]. In eukaryotes, all three stop codons are decoded by the eukaryotic release factor 1 (eRF1). According to recent models [10,11], eRF1 enters the ribosomal A-site in complex with a second release factor, eRF3, in its GTP bound form. Recognition of a stop codon triggers GTPase activity of eRF3, which leads to its dissociation from the complex in its GDP bound form. eRF1 is then free to activate the ribosomal peptidyl transferase centre (PTC), which hydrolyses the bond between the P-site tRNA and the nascent polypeptide. Importantly, these steps are promoted by RLI1 in an ATP-independent manner; i.e. by the same factor that also stimulates eIF3 functions in the initiation phase. Molecular details of this RLI1 role in termination are not known, nevertheless, the proposed active role of RLI1 in stop codon recognition is consistent with observations that conditional downregulation of RLI1 protein levels increases stop codon read-through in yeast [2]. Based on the most recent structural model, RLI1 binds to the same site on the terminating ribosome as eRF3 (thus their binding is mutually exclusive), and its 4Fe-4S domain interacts with the C-terminal domain of eRF1 to push the conserved GGQ motif in the middle domain of eRF1 to the PTC next to the acceptor stem of the P-site tRNA to trigger polypeptide release [11].

Recycling of eRF1-associated post-termination complexes (post-TCs) is also mediated by ABCE1/RLI1, this time, however, in an ATP-dependent manner [5,10]. It

was hypothesized that RLI1, upon binding and hydrolysing ATP, switches its conformation into a closed state, and the mechanochemical work generated by this switch splits post-TCs into free 60S subunits and deacylated tRNA- and mRNA-bound 40S subunits (40S-post-TC) [11]. Finally, Pisarev et al. showed that the release of tRNA and mRNA from the 40S-post-TCs is *in vitro* ensured by the *bona fide* initiation factors eIF1, eIF1A and eIF3 [4,5]. eIF3, and in particular its j subunit (HCR1 in yeast), were suggested to play the key role in mRNA dissociation.

Since the implication of eIF3 in the recycling process was deduced only from experiments carried out with 11-codon long model mRNA in mammalian *in vitro* reconstituted systems, we decided to investigate whether or not eIF3 also plays a direct role in translation termination and/or ribosomal recycling in the living cell. Here we show that the five core eIF3 subunits and one non-core eIF3j/HCR1 control translation termination and stop codon read-through in yeast. Core and non-core subunits both cooperate with the eRFs and RLI1 in doing so, although they regulate translation termination in the opposite manner. Involvement of the *bona fide* translation initiation factor eIF3 in termination strongly supports the idea that there is a highly coordinated communication between individual translational phases.

Results

Mutations in eIF3 Subunits Affect Stop Codon Read-Through

eIF3 and the eIF3-core-associated factors j/HCR1 and RLI1 play a role in ribosome recycling – at least *in vitro* [4,5], while only RLI1 is to date known to somehow promote also the preceding translation termination step [2]. In order to address whether eIF3 itself is likewise functionally involved in translation termination, we

measured the frequency of stop codon read-through in a battery of eIF3 mutants using an established dual-luciferase reporter assay [12]. The reporter system is similar to the one which was also used to demonstrate increased stop codon read-through upon conditional down-regulation of RLI1 [2]. The [psi$^-$] strain background used in these initial experiments contains an UGA suppressor tRNA in the genome leading to unusually high basal UGA read-through levels of 3-4%, which is however ideal for studying stop-codon read-through effects. Importantly, however, as we show below, the results we obtained are independent of the presence of this suppressor tRNA.

The eIF3 mutants that were chosen for read-through analysis were previously shown to affect multiple initiation steps from 43 PIC assembly (due to reduced 40S-binding affinity of eIF3) to scanning for AUG recognition (with wild-type 40S-binding affinity of eIF3); summarized in [6]. Surprisingly, the majority of mutations in the core eIF3 subunits that we tested showed a significant reduction in stop-codon read-through (Figure 1) that thus could not be simply attributed to the reduced eIF3 association with ribosomes. In contrast, deletion of the non-essential *HCR1* gene encoding eIF3j resulted in significantly increased stop-codon read-through (Figure 1), similar to that reported for RLI1 down-regulation [2].

In order to confirm this unexpected result and to explore whether the observed effect on translation termination was specific to eIF3 or common to all other members of the Multifactor complex (MFC; composed of eIF1, eIF2, eIF3 and eIF5) and their closely co-operating factor eIF1A, we used partial depletion alleles (DaMP alleles) for these essential factors from the genome-wide DaMP collection [13]. DaMP alleles contain a selectable marker cassette inserted into the 3'-UTR of a gene, leading to

destabilization of the respective mRNA *via* the nonsense mediated decay pathway (NMD).

By their nature, DaMP alleles show varying degrees of depletion for different genes, and data obtained with DaMP alleles have to be interpreted with this in mind. Since the depleted genes are all essential, loss of the corresponding gene product below a critical level will affect growth, and demonstration of reduced growth for an individual strain can thus be taken as a reliable indicator for depletion below a critical threshold. In contrast, an absence of growth phenotypes cannot be unambiguously interpreted, as depletion of the gene product may have occurred but may have remained above a level where fitness is detectably affected.

When we compared growth rates of the MFC DaMP alleles to the corresponding wild type (wt) strain, we observed that all non-eIF3 MFC factors but only one of the eIF3 strains (*TIF35*) showed a growth phenotype indicative of significant depletion (Figure S1). When we proceeded to assess stop codon read-through in these strains, we observed that the one eIF3 strain for which the growth assay indicated significant depletion also showed significantly reduced stop codon read-through. In addition, the *NIP1* depletion strain also showed significantly reduced stop-codon read-through, which may be caused by depletion of the gene product to a level that does not yet affect growth rates. In contrast, none of the depletion alleles for the non-eIF3 MFC component showed a reduction in read-through, although several (eIF1A and the two eIF2 subunits tested) showed significant increases in stop codon read-through. While the mechanism behind the increased read-through in the eIF1A and eIF2 alleles is yet to be explored, these observations demonstrate that i) reductions in eIF3 activity reliably lead to reductions in stop-codon read-through levels, whether this reduction is caused by point mutations or other gene ablation

alleles, and ii) that this effect is specific to core eIF3 subunits, whereas other MFC components and j/HCR1 display either none or the opposite phenotype.

Mutants in eIF3 subunits interact genetically with termination factor mutants

To obtain further supporting evidence implicating eIF3 in regulation of the termination process, we analyzed genetic interactions between mutants in two eIF3 subunits and both release factors. The temperature sensitive eRF mutants we used are all known to cause termination defects including stop codon read-through strong enough to suppress the *ade1-14* nonsense allele [14]. They include a *sup35*^{N536T} mutant located in a region near the C-terminus of eRF3 that disrupts termination by an unknown mechanism, a *sup45*^{M48I} mutant that interferes with stop codon decoding [15], and a *sup45*^{Y410S} mutant that directly disrupts the eRF1–eRF3 interaction [16].

We initially combined three selected mutations in the a/TIF32 subunit of eIF3 reducing the stop codon read-through in otherwise wt cells (Figure 1) with the *sup35*^{N536T} and *sup45*^{Y410S} mutants. When combined, the double mutants show a stop codon read-through frequency that is clearly reduced compared to either release factor mutant (Figure 2A), demonstrating that the *TIF32* mutations partially rescue the read-through phenotype of the latter. In contrast, when we investigated slow growth (Slg$^-$) and temperature sensitive (Ts$^-$) phenotypes, we observed synthetic exacerbation of these phenotypes (Figure 2B). This demonstrates that i) the release factors and the core eIF3 complex have antagonistic functions in the same stage of the termination phase, and losses in their functions can thus partially compensate for each other in terms of the stop codon read-through efficiency; and ii) that the degree of stop codon read-through *per se* is not the major source of the fitness defects in these strains. This latter notion is consistent with earlier quantitative trait analyses,

which showed that the termination defects are unlinked from growth defects in many eRF1 mutants [17]. Hence, synthetic exacerbation of growth could be explained by proposing that besides the stop codon recognition step (which is assessed in the dual luciferase assay), also other aspects of termination are impaired in the eRF and eIF3 mutants, which, in combination with the initiation defects of eIF3 mutants, reduce the growth rate as a compound effect.

Next we combined the *hcr1Δ* mutant with the three release factor mutants. Whereas *sup45*^{M48I} (eRF1) and *sup35*^{N536T} (eRF3) mutants showed no synthetic effect in the background of the *hcr1* deletion (Figure S2), the *sup45*^{Y410S} mutation displayed complex interactions with the *hcr1* deletion. At the permissive temperature, the effect of the two mutations on read-through was additive (Figure 2D, 30°C; compare open and grey bars with the black one), as was the effect on growth (Figure 2C). At the semi-permissive temperature of 34°C, where the eRF1:eRF3 interaction is more severely disrupted by the eRF1 mutation (Akhmaloka et al 2008) – as evidenced by its increased termination defect (Figure 2D; compare grey bars between 30 and 34°C), *hcr1Δ* did not additively increase the *sup45*^{Y410S} read-through (Figure 2D, 34°C; black vs. grey bars). Moreover, the *sup45*^{Y410S} mutation also completely eliminated the negative impact of *hcr1Δ* on growth rates at this temperature (Figure 2C). This epistasis effect indicates that the *hcr1* deletion may affect the same termination step that is impaired in the eRF1 mutant, namely the eRF1:eRF3 interaction.

Overexpression of ABCE1/RLI1 Fully Suppresses the Growth and Read-Through but Not the Initiation Defects of the *hcr1* (eIF3j) Deletion Strain

As mentioned above, recent reports suggested that the ABCE1/RLI1 protein critically promotes both translation termination and ribosomal recycling [2,5,10,18]. Moreover, RLI1 was also implicated in biogenesis and transport of pre-ribosomes from the nucleolus [19] and in stimulating translation initiation by promoting assembly of 43S PICs together with eIF3 [1]. The striking resemblance of the latter effects with the previously reported functions of j/HCR1 [19-23] plus the fact that RLI1 directly interacts with j/HCR1 *via* its ABC2 domain [2] prompted us to test a potential functional redundancy between these two proteins.

Strikingly, we found that overexpression of RLI1 fully suppressed the slow growth defect of an *hcr1Δ* strain (Figure 3A). Moreover, high copy (hc) *RLI1* also fully suppressed the increased read-through phenotype of this strain (Figure 3B). By way of control, we overexpressed elongation factor eEF3 (encoded by *YEF3*) as an independent ABC cassette-containing protein engaged in translation, which had no effect on the growth or read-through phenotypes of the *hcr1Δ* strain (Figure S3A and B).

Importantly, no hc suppression was observed when either the formation of the N-terminal 4Fe-4S clusters of RLI1 or the ATP binding by its ABC cassettes were compromised (Figure 3B and data not shown). The integrity of the crucial N-terminal region of RLI1 as well as its intact ATPase activity are therefore critically required for a functional replacement of j/HCR1. In the opposite arrangement, hc *HCR1* suppressed neither the slow growth nor the increased read-through phenotype of the *Tet::RLI1* conditional depletion strain (Figure S4). It is noteworthy that in agreement with earlier results [2,10,18], the intact N-terminal 4Fe-4S clusters and the ability of RLI1 to bind and hydrolyze ATP were absolutely essential for restoration of the read-through defect in the *Tet::RLI1* cells (Figure S4).

In order to find out if j/HCR1 acts independently of eIF3 in the termination process, we examined the read-through phenotype of several *HCR1* mutations known to eliminate binding of full length j/HCR1 to eIF3 [22,23]. As shown in Figure 3B, no effect was observed implying that the j/HCR1 function in termination does not require its physical association with eIF3.

One of the major initiation phenotypes of *hcr1Δ* is a leaky scanning defect (a decreased ability to recognize AUG as the translational start site resulting in increased scanning past it), which can be suppressed by hc eIF1A [22]. As can be seen in Figure 3B neither hc eIF1A nor eIF1 suppressed the read-though defect of *hcr1Δ*. Similarly, hc RLI1 did not suppress the leaky scanning defect of *hcr1Δ* (Figure S5). Hence, these findings clearly suggest that the *hcr1Δ* defects in initiation and termination are mutually separable and that RLI1 cannot replace j/HCR1 in all of its functions. Importantly, however, since hc eIF1A suppressed the *hcr1Δ* growth defect only partially [22], as opposed to the full suppression by hc *RLI1* (Figure 3A), we propose that the major contributor to the *hcr1Δ* slow growth phenotype is not a defect in initiation, as previously believed, but a defect related to translation termination.

Complexes Containing eIF3, ABCE1/RLI1 and both eRFs, Free of Ribosomes and RNA, Occur *in vivo*

If eIF3 is indeed implicated in translation termination, it should be possible to detect a complex between eIF3 and the release factors *in vivo*. We therefore carried out a series of *in vivo* pull down experiments using Myc-tagged RLI1, or TAP-tagged j/HCR1, a/TIF32 or eRF3 as baits. As shown in Figure 4A, Myc-tagged RLI1 specifically pulled down selected eIF3 subunits, including j/HCR1, as shown before [1]. In addition and in contrast to the latter study, we also observed significant co-

precipitation of both release factors. The TAP-tagged j/HCR1 repeatedly co-purified with the other eIF3 subunits, as expected, but also with significant amounts of RLI1, eRF1 and eRF3 (Figure 4B; eRF1 is indicated by an asterisk). To stabilize presumably only transient interactions between eIF3 and termination/recycling factors, this and the following TAP-tag experiments were performed after modest (1 %) pre-treatment of growing cells with formaldehyde as described in [24]. (Importantly, similar although less pronounced results were also obtained without this pre-treatment [data not shown]). eRF3 also co-precipitated with TAP-tagged a/TIF32, and, importantly, TAP-tagged eRF3 reproducibly brought down small but significant amounts of core eIF3 subunits (Figure 4C and D; note that the mobility of a/TIF32 and eRF3 vary between Input and Elution lanes due to a TEV protease-mediated cleavage of the TAP tag). We also tested the TAP-tagged eRF1 strain, however, no proteins were recovered – not even the TAP-eRF1 by itself – indicating that this particular fusion allele is not functional. Importantly, the yield of neither of these experiments was affected by RNAse treatment (data not shown) and no ribosomes were present in the purified complexes (see RPS0A strips in panels A – D) strongly suggesting that the ribosome- and RNA-free complexes of eIF3, eRF1, eRF3 and RLI1 do exist in the cytoplasm. More specifically, these experiments show that eIF3 contacts all critical termination players discussed in this study, though we cannot conclude whether all these factors occur in one single super-complex, or whether we are pulling down their partial subcomplexes.

To further strengthen these observations, we tested protein-protein interactions between eIF3 subunits and both eRFs and their individual domains. As shown in Figure S6, the N-terminal and Middle (N-M) domains of eRF1 but not the middle and C-terminal (M-C) domains specifically interacted with GST-g/TIF35 and to

a smaller extent also with GST-i/TIF34. The N domain of eRF1 carries determinants of the stop codon recognition; the M domain contains the conserved GGQ motif required for peptide release; and the C domain interacts with eRF3. Hence we propose that eIF3 and eRF1 are in direct contact *via* two small eIF3 subunits and the NTD of eRF1; for more details please see Supplemental Results.

Deletion of *hcr1* Results in Accumulation of the Polysome-associated eRF3, and the *sup45*^{Y410S} Mutant Prevents Stable Association of eRF3 and j/HCR1 with Polyribosomes

In order to examine if and how the network of interactions between translation initiation and termination factors affects their functions, we investigated the distribution of selected translation factors in wt cells and cells mutated for either of the factors under study using formaldehyde cross-linking of living cells followed by high velocity sedimentation of whole cell extracts (WCE) in sucrose density gradients [24].

Figure 5A and D shows a typical distribution of the selected proteins across all gradient fractions obtained from wt WCEs and divided into several separable groups: “Top” (fractions 1-4), “40S” (5-6), “60S” (7-8) and “80S+polysomes” (9-18). (The *hcr1Δ* strain expressing the *HCR1* gene from a hc plasmid that we purposely used here shows an identical distribution profile to the wt strain with an intact chromosomal copy of *HCR1* [data not shown]). For technical reasons, several fractions from individual groups were pooled together to fit all samples on a single SDS-PAGE gel. Whereas eRF3 is clearly enriched in the polysome-containing fractions and practically lacking in the Top fractions, eRF1 is more or less evenly distributed across the entire gradient, and RLI1 predominantly sediments in the Top fractions and

partially also in the 40S-containing fractions. Importantly, all strains that we worked with in this study are [psi$^-$] and hence the observed sedimentation of eRF3 into heavy fractions cannot be attributed to Sup35 aggregation. To our surprise, eIF3 represented by two of its subunits (a/TIF32 and j/HCR1) shows a robust enrichment in polysomal fractions, similar to eRF3. In contrast, eIF5, which is known to tightly interact with eIF3 during translation initiation, occurs mainly in the Top and 40S fractions. These findings are critical because they strongly suggest that the majority of the polysomal eIF3 signal derives from eIF3 molecules bound to 80S couples in polysomes (most probably terminating) and not from those bound to 40S subunits initiating on polysomal mRNAs. To our knowledge, this is the first case where the distribution of initiation factors was examined beyond the 40S-containing fractions in such a sensitive experimental set-up.

Deletion of *hcr1* reduced the amount of “initiating” eIF3 and eIF5 in the 40S fractions, as observed before [21], and had no effect on distribution of eRF1 and RLI1. However, it led to a marked accumulation of eRF3 in polysomes with a commensurate reduction in lighter fractions (Figure 5B and D). We interpret the polysomal accumulation of eRF3 as an increased number of post-TCs bound by eRF3 in a less-productive manner; perhaps with a decreased dissociation rate. Most importantly, overexpression of RLI1, which suppresses both the read-through and Slg$^-$ phenotypes of *hcr1Δ* (Figure 3), significantly suppressed this effect and partially restored the eRF3 distribution in polysomes to wt (Figure 5C and D). The fact that the 40S-binding by the “initiating” eIF3 and eIF5 was not restored underscores a specificity of the RLI1 suppressor effect on the j/HCR1 role in termination versus initiation. Together these data suggest that j/HCR1 may promote the release of eRF3·GDP from the post-TCs upon stop codon recognition and GTP hydrolysis on

eRF3, which serves as a prerequisite for the subsequent binding of RLI1. Inability to complete this step may lead to a reduced stop codon recognition resulting in an increased read-through, which was observed. Hence the suppression effect of RLI1 on the molecular level could be explained by proposing that increased dosage of RLI1 forces dissociation of eRF3·GDP from the post-TCs by mass action and thus eliminates a need for j/HCR1.

We next analyzed changes in polysomal distributions of factors of interest in the *sup45*^{Y410S} mutant, which shows epistatic interaction with *hcr1Δ* at semi-permissive temperature (Figure 2C and D). The *sup45*^{Y410S} mutant markedly redistributed eRF3 from the polysomal towards the Top fractions when compared to wt (Figure 6A - C), consistent with the fact that it disrupts the eRF1–eRF3 interaction [16]. A similar change was also observed for j/HCR1 but not for a/TIF32 and RLI1. Hence these results are consistent with the proposed role for j/HCR1 in promoting the eRF3·GDP ejection from the post-TCs.

Discussion

It is becoming increasingly apparent that factors involved in regulating various steps of gene expression may have multiple functions and that this multitasking may integrate transcription, mRNA export, translation and mRNA decay into a delicately regulated higher-order process. For example, translation initiation factor eIF3 links translation initiation to transcription [25], to mRNA export [3] and to the NMD pathway [26,27]. Here we show for the first time that eIF3 critically connects initiation of translation with its termination. In particular, eIF3 occurs together with eRFs 1 and 3 and the ribosomal recycling factor RLI1 in a ribosome- and RNA-free complex *in vivo*. Various mutants of core eIF3 subunits, but not of other initiation factors, decreases

stop codon read-through in living cells and show synthetic phenotypes with mutant release factors eRF1 and 3. Conversely, deletion of *hcr1* increases stop codon read-through and results in accumulation of eRF3 in heavy polysomes. Finally, increased dosage of RLI1 substitutes for the j/HCR1 roles in termination (but not in initiation) and in enabling efficient cell growth, implying that the j/HCR1 function in termination is more critical for optimal cell proliferation than its function in translation initiation. Since eIF3 was, based on *in vitro* experiments, previously implicated in promoting also the very final step of translation – ribosomal recycling [4], we propose that eIF3 is one of the very few factors that connects various processes of mRNA life and integrates them into the ultimate translational output. Taking into account that the translation pathway is highly conserved among low and high eukaryotes, it is highly likely that this connecting role of eIF3 is also conserved.

eIF3 modulates the precision of the stop codon recognition by eRF1

The fact that we could detect a complex between eIF3, RLI1 and eRFs free of RNA and ribosomes (Figure 4) and that two small eIF3 subunits i/TIF34 and g/TIF35 directly interacted with the N and N-M domains of eRF1 (Figure S6) suggests that at least eIF3 and eRFs come to the pre-TC in a pre-formed complex. The alternative that they are ejected from post-TCs as a holocomplex upon completion of termination is highly unlikely considering that i) eRF3 must be ejected prior to RLI1 binding [10] and ii) that eIF3 is supposed to participate in the late steps of ribosomal recycling that should be devoid of eRF1 and RLI1 [4,5]. The last scenario would be that eIF3 stays present on the elongating ribosome throughout the entire elongation cycle and promotes recruitment of eRF1·eRF3·GTP to the pre-TCs; there is, however, indirect evidence contradicting this possibility [8].

Our data show that eIF3 mutants specifically decrease stop codon read-through in otherwise wt cells (Figure 1 and Figure S1) and that *TIF32* mutations partially compensate for the increased read-through in eRF mutants (Figure 2A). This clearly suggests that wt eIF3 modulates the precision of the stop codon recognition by eRF1 in order to fine tune the termination process (Figure 7). During stop codon decoding, eRF1 was proposed to sit in the ribosomal A-site with a part of its N-domain contacting small ribosomal protein RPS3 and helix (h) 18 of 18S rRNA [28]. Strikingly, g/TIF35 also interacts with RPS3, in addition to RPS20 [29], and as both g/TIF35 and i/TIF34 are tightly bound to the extreme C-terminus of b/PRT1 [30], i/TIF34 is expected to occur nearby g/TIF35. Moreover, the C-terminal domain of a/TIF32 interacts with h16-18 of 18S rRNA [31]. Taylor and colleagues further proposed that one of the conformational changes induced by eRF1–eRF3–GMPPNP binding to pre-TCs involves a movement of h16 of 18S rRNA and the N-terminal domain (NTD) of RPS3 toward each other, which results in the establishment of a new head–body connection on the solvent side of the 40S subunit and a constriction of the mRNA entrance. Hence, it is easily conceivable that eRF1 and eIF3 preserve and subsequently rearrange their mutual contacts in the termination complexes upon their formation. These contacts could for example impair proper orientation of eRF1 in the spatially restricted A-site, thus providing a rational explanation for the antagonistic effect of eIF3 on translation termination. For interpretation of these data, it must be kept in mind that the reporter constructs we use essentially measure stop codon read-through on a premature termination codon. At present, we do not know whether the antagonistic influence of eIF3 on stop-codon read-through is restricted to such sites, or whether it also affects termination on stop codons located nearer to the poly(A) tail. However, our observation that the *sup45*^{Y410S} mutant, which affects stop

codon selection by disrupting the eRF1–eRF3 interaction, reduced the polysome-associated amounts of eRF3 and j/HCR1 (Figure 6) indicates that a delay or imperfection in the decoding of natural stop codons disrupts this "initiation-termination" complex, most probably to enable resumption of elongation. Investigation of the precise molecular mechanism of the eIF3 action in termination is a subject of the follow-up study that is extensively worked on in our laboratories.

j/HCR1 promotes eRF3·GDP ejection from the post-TCs to allow RLI1 binding

In contrast to mutations in core eIF3 subunits, deletion of *hcr1* did not decrease but increased the stop codon read-through (Figure 1). The fact that mutations disrupting the j/HCR1 contact with eIF3 had no effect on read-through clearly suggests that the j/HCR1 role in termination is independent of its association with eIF3. Indeed, j/HCR1 is only loosely associated with the core eIF3 complex [20] and was shown to interact with both sides of the 40S mRNA entry channel on its own [22,32]. Our striking findings that *hcr1Δ* results in accumulation of eRF3 in higher polysomal fractions (Figure 5) and that *sup45*^{Y410S} (breaking the eRF1–eRF3 interaction) conversely prevents j/HCR1 association with heavy polysomes (Figure 6) led to the model presented in Figure 7. We propose that following stop codon recognition and subsequent GTP hydrolysis on eRF3, j/HCR1 promotes eRF3·GDP ejection from the post-TCs to allow binding of its interacting partner RLI1 [2] and polypeptide release. In support, eRF1 was shown to associate more firmly with post-TCs in the presence of eRF3 [5], which led the authors to propose that after GTP hydrolysis, eRF3 might not dissociate entirely from ribosomal complexes on its own and its release thus might require a stimulus by an additional factor; in our opinion by the j/HCR1 protein. Based on the cryo-EM structures of DOM34:HBS1 (release factor-like proteins

closely related in sequence and structure to eRF1:eRF3) on the yeast ribosome showing that the N-terminus of HBS1 extends away from the body of the protein and contacts the mRNA entry site, it was proposed that the N-terminus of eRF3 also occurs in the A-site area [11]. Hence j/HCR1 could directly act upon this eRF3 domain to trigger the release of this factor in its GDP form from eRF1-bound post-TCs. In support, the N-terminal extension of *S. pombe* eRF3 was proposed to regulate eRF1 binding to eRF3 in a competitive manner [33]. Interestingly, both the N-terminus of eRF3 as well as the j/HCR1 protein as a whole are non-essential [33,34], suggesting that they might act simply by shifting the equilibrium towards the loss of affinity between the eRF1 and eRF3·GDP binary complex. If true, the loss-of-function of both of them could be overcome by redundant mechanisms with slower reaction rates. In agreement, hc *RLI1* fully suppressed the read-through effect of *hcr1Δ* in the manner dependent on its intact 4Fe-4S and ABC domains (Figure 3B). We propose that in the *hcr1Δ* cells RLI1 makes its way to its binding site in the post-TCs, which is identical to that of eRF3, by replacing eRF3·GDP through mass action.

The model proposed in Figure 7 also explains the behavior of the genetic interactions observed for the *hcr1* deletion. Failure to eject eRF3·GDP can perceivably have two consequences. First, if peptidyl hydrolysis by eRF1 fails to be induced because RLI1 cannot bind to it, the eRF1·eRF3·GDP complex can dissociate from the ribosomal A-site, thus necessitating a renewed round of tRNA sampling with an ensuing risk of stop codon decoding by a near-cognate or suppressor tRNA. This is consistent with the increased stop codon read-through we observe experimentally in *hcr1* deletion strains. Second, if peptidyl hydrolysis does take place (*in vitro*, eRF1 clearly has some release factor activity also in the absence of RLI1 [9], a stalled ribosome complex would be formed in which eRF1 was still bound to eRF3, and in

which RLI1 was thus not free to initiate the recycling step. Such stalled complexes would impede ribosome flow on the affected mRNA, reduce corresponding gene expression levels and potentially necessitate degradation by one of the surveillance pathways. If this occurred frequently, it would give rise to fitness defects, as we observe for *hcr1* deletion strains. This is also consistent with the fact that deletion of *hcr1* produces unexpectedly mild polysomal run-off with respect to its growth defect [35]. However, in the presence of eRF1 mutations, which accelerate spontaneous dissociation of eRF3·GDP from eRF1, timely RLI1 binding to eRF1 would be re-enabled even in the absence of HCR1. This would explain why the *sup45*^{Y410S} mutation, but not *sup45*^{M48I} and *sup35*^{N536T} mutations, eliminated the negative impact of *hcr1Δ* on growth rates at the semipermissive temperature.

To further support our model, we wished to employ a recently established *in vitro* reconstituted yeast translation system, which has been used previously to monitor both the peptide release and ribosome recycling steps of the translation cycle [10]. j/HCR1 did not have an appreciable effect on either of these activities *in vitro* (data not shown). This is probably not that surprising given the fact that based on our model we would rather expect to see an effect of j/HCR1 on GTP hydrolysis by eRF3 and/or its subsequent release from post-TCs. However, since the former two assays are the only *in vitro* assays available to us at the moment, further efforts will be necessary to fully characterize the role of j/HCR1 in termination/recycling reactions biochemically.

Upon completion of the termination-specific reactions, eIF3, j/HCR1 and RLI1 further participate in the ribosomal recycling steps, as proposed by [5], and it is conceivable that all these factors remain bound to the small 40S subunit to promote the next round of initiation (Figure 7). Alternatively, the pre-occupation of the

40S·mRNA complex by the “initiation factors” that would not be recycled could ensure reinitiation on the same mRNA molecule as proposed by the mRNA closed-loop model [36]. An *in vivo* experimental evidence implicating eIF3 and other eIFs in the recycling steps is, however, still lacking.

General Conclusions

Taken together, we argue that strict mechanistic separation of translation into its individual, mutually independent phases should be reconsidered in the light of “multitasking” of eIF3, j/HCR1, RLI1 and most likely also eIF1 and eIF1A, for which evidence is presented here and elsewhere. Collectively, these findings suggest that changes in one phase of translation, evoked for example *via* cell signaling pathways, are promptly communicated to and coordinated with changes in the other phases to maintain cellular homeostasis of all ongoing processes. Without a doubt there is much to be learned about how all four phases of translation come together in one balanced system that rapidly and accurately responds to different needs of the cell exposed to constantly changing environmental conditions.

Materials and Methods

Yeast Strains and Plasmids and Various Biochemical Techniques

Detailed description of the read-through assay, polysomal gradient analysis, co-immunoprecipitations and affinity tag pull downs, and the lists and descriptions of plasmids and yeast strains used throughout this study (summarized in Tables S1 – 3) can be found in the Supplemental Information.

Acknowledgments

We are grateful to Rachel Green, Matthias Hentze and Mick F. Tuite for critical reading of the manuscript. We would like to thank Mick F. Tuite and Nadja Koloteva-Levine (University of Kent, UK) for sharing an unpublished SUP35-TAP strain, and David Bedwell, Susan Liebman, Alan G. Hinnebusch, and Terry Kinzi for strains and plasmids.

Financial Disclosure

This research was supported for the most part by The Wellcome Trust Grant 090812/Z/09/Z, and partly also by the Howard Hughes Medical Institute and the Centrum of Excellence Grant (P305/12/G034) awarded by the Czech Science Foundation (all to L.S.V.); and by Wellcome Trust Grant 075438 (to T.v.d.H.). The funders had no role in study design, data collection and analysis, decision to publish, or preparation of the manuscript.

References

1. Dong J, Lai R, Nielsen K, Fekete CA, Qiu H, et al. (2004) The essential ATP-binding cassette protein RLI1 functions in translation by promoting preinitiation complex assembly. J Biol Chem 279: 42157-42168.
2. Khoshnevis S, Gross T, Rotte C, Baierlein C, Ficner R, et al. (2010) The iron-sulphur protein RNase L inhibitor functions in translation termination. EMBO Rep 11: 214-219.

3. Bolger TA, Folkmann AW, Tran EJ, Wente SR (2008) The mRNA export factor Gle1 and inositol hexakisphosphate regulate distinct stages of translation. Cell 134: 624-633.

4. Pisarev AV, Hellen CUT, Pestova TV (2007) Recycling of Eukaryotic Posttermination Ribosomal Complexes. Cell 131: 286–299.

5. Pisarev AV, Skabkin MA, Pisareva VP, Skabkina OV, Rakotondrafara AM, et al. (2010) The Role of ABCE1 in Eukaryotic Posttermination Ribosomal Recycling. Mol Cell 37: 196-210.

6. Valášek LS (2012) 'Ribozoomin' – Translation Initiation from the Perspective of the Ribosome-bound Eukaryotic Initiation Factors (eIFs). Curr Protein Pept Sci 13: 305-330.

7. Pöyry TA, Kaminski A, Jackson RJ (2004) What determines whether mammalian ribosomes resume scanning after translation of a short upstream open reading frame? Genes Dev 18: 62-75.

8. Szamecz B, Rutkai E, Cuchalova L, Munzarova V, Herrmannova A, et al. (2008) eIF3a cooperates with sequences 5' of uORF1 to promote resumption of scanning by post-termination ribosomes for reinitiation on GCN4 mRNA. Genes Dev 22: 2414-2425.

9. Alkalaeva EZ, Pisarev AV, Frolova LY, Kisselev LL, Pestova TV (2006) In vitro reconstitution of eukaryotic translation reveals cooperativity between release factors eRF1 and eRF3. Cell 125: 1125-1136.

10. Shoemaker CJ, Green R (2011) Kinetic analysis reveals the ordered coupling of translation termination and ribosome recycling in yeast. Proc Natl Acad Sci U S A 108: E1392-1398.

11. Becker T, Franckenberg S, Wickles S, Shoemaker CJ, Anger AM, et al. (2012) Structural basis of highly conserved ribosome recycling in eukaryotes and archaea. Nature 482: 501-506.

12. Keeling KM, Lanier J, Du M, Salas-Marco J, Gao L, et al. (2004) Leaky termination at premature stop codons antagonizes nonsense-mediated mRNA decay in S. cerevisiae. RNA 10: 691-703.

13. Schuldiner M, Collins SR, Thompson NJ, Denic V, Bhamidipati A, et al. (2005) Exploration of the function and organization of the yeast early secretory pathway through an epistatic miniarray profile. Cell 123: 507-519.

14. Bradley ME, Bagriantsev S, Vishveshwara N, Liebman SW (2003) Guanidine reduces stop codon read-through caused by missense mutations in SUP35 or SUP45. Yeast 20: 625-632.

15. Bertram G, Bell HA, Ritchie DW, Fullerton G, Stansfield I (2000) Terminating eukaryote translation: domain 1 of release factor eRF1 functions in stop codon recognition. Rna 6: 1236-1247.

16. Akhmaloka, Susilowati PE, Subandi, Madayanti F (2008) Mutation at tyrosine in AMLRY (GILRY like) motif of yeast eRF1 on nonsense codons suppression and binding affinity to eRF3. Int J Biol Sci 4: 87-95.

17. Merritt GH, Naemi WR, Mugnier P, Webb HM, Tuite MF, et al. (2010) Decoding accuracy in eRF1 mutants and its correlation with pleiotropic quantitative traits in yeast. Nucleic Acids Res 38: 5479-5492.

18. Barthelme D, Dinkelaker S, Albers SV, Londei P, Ermler U, et al. (2011) Ribosome recycling depends on a mechanistic link between the FeS cluster domain and a conformational switch of the twin-ATPase ABCE1. Proc Natl Acad Sci U S A 108: 3228-3233.

19. Yarunin A, Panse VG, Petfalski E, Dez C, Tollervey D, et al. (2005) Functional link between ribosome formation and biogenesis of ironsulfur proteins. EMBO J 24: 580–588.

20. Valášek L, Phan L, Schoenfeld LW, Valášková V, Hinnebusch AG (2001) Related eIF3 subunits TIF32 and HCR1 interact with an RNA recoginition motif in PRT1 required for eIF3 integrity and ribosome binding. EMBO J 20: 891-904.

21. Nielsen KH, Valášek L, Sykes C, Jivotovskaya A, Hinnebusch AG (2006) Interaction of the RNP1 motif in PRT1 with HCR1 promotes 40S binding of eukaryotic initiation factor 3 in yeast. Mol Cell Biol 26: 2984-2998.

22. ElAntak L, Wagner S, Herrmannová A, Karásková M, Rutkai E, et al. (2010) The indispensable N-terminal half of eIF3j co-operates with its structurally conserved binding partner eIF3b-RRM and eIF1A in stringent AUG selection. J Mol Biol 396: 1097-1116.

23. Chiu W-L, Wagner S, Herrmannová A, Burela L, Zhang F, et al. (2010) The C-Terminal Region of Eukaryotic Translation Initiation Factor 3a (eIF3a) Promotes mRNA Recruitment, Scanning, and, Together with eIF3j and the eIF3b RNA Recognition Motif, Selection of AUG Start Codons. Mol Cell Biol 30: 4415-4434.

24. Valášek L, Szamecz B, Hinnebusch AG, Nielsen KH (2007) In vivo stabilization of preinitiation complexes by formaldehyde cross-linking. Methods Enzymol 429: 163-183.

25. Harel-Sharvit L, Eldad N, Haimovich G, Barkai O, Duek L, et al. (2010) RNA polymerase II subunits link transcription and mRNA decay to translation. Cell 143: 552-563.

26. Isken O, Kim YK, Hosoda N, Mayeur GL, Hershey JWB, et al. (2008) Upf1 Phosphorylation Triggers Translational Repression during Nonsense-Mediated mRNA Decay. Cell 133: 314–327.

27. Sha Z, Brill LM, Cabrera R, Kleifeld O, Scheliga JS, et al. (2009) The eIF3 interactome reveals the translasome, a supercomplex linking protein synthesis and degradation machineries. Mol Cell 36: 141-152.

28. Taylor D, Unbehaun A, Li W, Das S, Lei J, et al. (2012) Cryo-EM structure of the mammalian eukaryotic release factor eRF1-eRF3-associated termination complex. Proc Natl Acad Sci U S A 109: 18413-18418.

29. Cuchalová L, Kouba T, Herrmannová A, Danyi I, Chiu W-l, et al. (2010) The RNA Recognition Motif of Eukaryotic Translation Initiation Factor 3g (eIF3g) Is Required for Resumption of Scanning of Posttermination Ribosomes for Reinitiation on GCN4 and Together with eIF3i Stimulates Linear Scanning. Mol Cell Biol 30: 4671-4686.

30. Herrmannová A, Daujotyte D, Yang JC, Cuchalová L, Gorrec F, et al. (2012) Structural analysis of an eIF3 subcomplex reveals conserved interactions required for a stable and proper translation pre-Initiation complex assembly. Nucleic Acids Res 40: 2294-2311.

31. Valášek L, Mathew A, Shin BS, Nielsen KH, Szamecz B, et al. (2003) The Yeast eIF3 Subunits TIF32/a and NIP1/c and eIF5 Make Critical Connections with the 40S Ribosome in vivo. Genes Dev 17: 786-799.

32. Fraser CS, Berry KE, Hershey JW, Doudna JA (2007) 3j is located in the decoding center of the human 40S ribosomal subunit. Mol Cell 26: 811-819.

33. Kong C, Ito K, Walsh MA, Wada M, Liu Y, et al. (2004) Crystal structure and functional analysis of the eukaryotic class II release factor eRF3 from S. pombe. Mol Cell 14: 233-245.

34. Valášek L, Hašek J, Trachsel H, Imre EM, Ruis H (1999) The *Saccharomyces cerevisiae HCRI* gene encoding a homologue of the p35 subunit of human translation eukaryotic initiation factor 3 (eIF3) is a high copy suppressor of a temperature-sensitive mutation in the Rpg1p subunit of yeast eIF3. J Biol Chem 274: 27567-27572.

35. Valášek L, Hašek J, Nielsen KH, Hinnebusch AG (2001) Dual function of eIF3j/Hcr1p in processing 20 S Pre-rRNA and translation initiation. J Biol Chem 276: 43351-43360.

36. Tarun SZ, Sachs AB (1996) Association of the yeast poly(A) tail binding protein with translation initiation factor eIF-4G. EMBO J 15: 7168-7177.

Figure Legends

Figure 1. Mutations Reducing the Activity of Translation Initiation Factor eIF3 Affect Stop Codon Read-through.

Stop codon read-through was measured using dual luciferase reporter constructs as described in the main text. Plasmid-born mutant alleles of genes encoding eIF3 subunits were introduced into their respective shuffling strains, which are derived from a common strain background (for details please see Extended Experimental Procedures). The wt strain background has unusually high levels of UGA read-through, due to the presence of an opal (UGA) suppressor tRNA in the genome. For each independently derived shuffling strain, read-through is shown for pairs of strains

shuffled with wt or the indicated mutant alleles of the gene in question. For the non-essential j/HCR1 subunit, the H3675 *hcr1Δ* strain is shown. All investigated mutants showed significant ($p<0.05$) reductions in the level of stop codon read-through, with the exception of *tif35*^{TKMQ}, which showed no significant difference, and *Δhcr1* which showed strong and significant increase in stop codon read-through.

Figure 2. eIF3 Mutants Genetically Interact with Release Factor Mutants.

(A - B) Combining the selected *TIF32* mutants with *sup35*^{N536T} and *sup45*^{Y410S} (A) reduces their read-through defects and (B) produces synthetic growth phenotypes. The wt and mutant alleles of *TIF32* were introduced into *tif32Δ*, *sup35*^{N536T} *tif32Δ*, and *sup45*^{Y410S} *tif32Δ* strains, respectively, by plasmid shuffling. (A) The resulting double mutant strains were grown in SD and processed for the stop codon read-through as described in Figure 1 (the read-through values of both single eRF mutants were set to 100%), or (B) spotted in four serial 10-fold dilutions on SD medium and incubated at indicated temperatures for 4 days. ND; not determined due to severe growth deficiency.

(C - D) The *sup45*^{Y410S} mutation eliminates the negative impact of *hcr1Δ* on (C) growth rates and (D) read-through. The *hcr1Δ* strain was crossed with the *sup45*^{Y410S} mutant strain and the resulting double mutant was transformed with sc *SUP45*, hc *HCR1*, or empty vector (EV), respectively, and (C) subjected to a growth spot assay at indicated temperatures for 2 or 3 days or (D) processed for stop codon read-through as described in Figure 1 (the read-through values of *hcr1Δ* were set to 100%).

Figure 3. Increased Gene Dosage of ABCE/RLI1 Suppresses the Slow Growth and Read-through Defects of *hcr1Δ*.

(A) The *hcr1Δ* strain was transformed with either empty vector (EV), hc *HCR1* or hc *RLI1*. The resulting transformants were subjected to a growth spot assay at 30°C for 2 days.

(B) The *hcr1Δ* strain was transformed with hc vectors carrying either wt or mutant *HCR1* and *RLI1* alleles, and *SUI1* (eIF1) and *TIF11* (eIF1A). The resulting transformants were grown in SD and processed for the stop codon read-through as described in Figure 1. Thus obtained values were normalized to the value obtained with the *hcr1Δ* strain transformed with wt *HCR1*, which was set to 100%.

Figure 4. Complexes Containing eIF3, ABCE1/RLI1 and both eRFs, Free of Ribosomes and RNA, Occur *in vivo.*

(A) WCEs were prepared from YDH353 bearing chromosomal Myc-tagged *RLI1* and immunoprecipitated with or without anti-Myc antibodies. The immune complexes were subjected to Western analysis. In, 5% of input; E, 100% of the elution fraction; W, 5% of the supernatant fraction. Also note that anti-RLI1 and -eRF1 antibodies were raised for the purpose of this study.

(B) WCEs were prepared from HCHO-treated (1%) cells bearing wt (H2879) or TAP-tagged (H553) chromosomal alleles of *HCR1* and incubated with IgG Sepharose 6 Fast Flow beads. The immune complexes were eluted by boiling in the SDS buffer and subjected to Western analysis. In, 1.5% of input; E, 50% of the elution fraction; W, 1.5% of the supernatant fraction. eRF1 is indicated by an asterisk below the immunoglobulins.

(C) WCEs from HCHO-treated cells (1%) cells bearing wt (H2879) or TAP-tagged (H555) chromosomal alleles of *TIF32* were processed as in panel B except that the immune complexes were eluted by the TEV protease cleavage. In, 1.5% of input; E, 100% of the elution fraction; W, 1.5% of the supernatant fraction.

(D) WCEs from HCHO-treated cells (1%) cells bearing wt (74D-694) or TAP-tagged (H517) chromosomal alleles of *SUP35* were processed as in panel C.

Figure 5. Deletion of *hcr1* Results in Accumulation of the Polysome-associated eRF3.

(A - C) The *hcr1Δ* strain (H3675) was transformed with either hc *HCR1* (A), empty vector (B), or hc *RLI1* (C), and the resulting transformants were grown in SD medium at 30˚C to an OD_{600} of ~ 1 and cross-linked with 0.5% HCHO prior to harvesting. WCEs were prepared, separated on a 5%-45% sucrose gradient by centrifugation at 39,000 rpm for 2.5 h and subjected to Western blot analysis. Several fractions corresponding to the Top, 40S, 60S, and 80S plus polysomal species were pooled, as indicated. Asterisk indicates a non-specific band.

(D) Distributions of the selected factors across the polysomal gradients shown in panels A – C. Amounts of each individual factor in the pooled fractions from three independent experiments were quantified by fluorescence imaging, combined, and the percentage representation of the signal corresponding to the Top (1-3 and 4), 40S (5-6), 60S (7-8), and 80S plus polysomal fractions (9 through 18) was calculated and plotted.

Figure 6. The *sup45*^{Y410S} Mutation Prevents Stable Association of eRF3 and j/HCR1 with Polyribosomes.

(A - B) The *sup45*^{Y410S} mutant and its corresponding wt strain were subjected to HCHO cross-linking (0.5%) and polysomal gradient analysis as described in Figure 5A.

(C) Amounts of each individual factor in the pooled fractions from three independent experiments were quantified by fluorescence imaging, combined, and the percentage representation of the signal corresponding to the Top (1 – 3), 40S (4-5), 60S (6-7), and 80S plus polysomal fractions (8-11) was calculated and plotted.

Figure 7. Model of eIF3 Involvement in Yeast Translation Termination.

Upon the stop codon entry into the ribosomal A-site the pre-TC forms, composed of the canonical release factors eRF1 and eRF3·GTP and eIF3. eRFs and eIF3 may associate with the pre-TC as a pre-formed unit or alone. Theoretically it is also possible that eIF3 dynamically associates and dissociates during the entire elongation phase. In the pre-TC, eIF3 interacts with the N domain of eRF1, *via* its two small i/TI34 and g/TIF35 subunits, and modulates its stop codon recognition activity during the proofreading step. Upon stop codon recognition the GTP molecule on eRF3 is hydrolyzed. Subsequently, j/HCR1 promotes eRF3·GDP ejection to allow the ABCE1/RLI1·ATP recruitment to begin the accommodation phase of termination – the eRF1 GGQ motif is pushed to the peptidyl-transferase center (PTC) – during which j/HCR1 interacts with ABCE1/RLI1. Subsequently, both factors together with the eIF3 core participate in ribosomal recycling to enable and promote initiation of the next translational cycle.

Supporting Information

Figure S1. DaMP Alleles of Various 43S PIC-associated Initiation Factors Display Distinct Effects on Efficiency of the Stop Codon Read-through.

Figure S2. The *sup45*^{Y410S} but not the Other Mutations in eRFs 1 and 3 Eliminate the Negative Impact of *hcr1Δ* on Growth Rates.

Figure S3. Increased Gene Dosage of eEF3 Does Not Suppress the Slow Growth and Read-through Defects of *hcr1Δ.*

Figure S4. Increased Gene Dosage of *HCR1* Does Not Suppress the Slow Growth and Read-through Defects of the *Tet::RLI1* strain; Intact ATP-Binding Cassettes and the Fe-S Cluster of RLI1 are Indispensable for its Role in Ensuring the Stop Codon Selection Accuracy.

Figure S5. Increased Gene Dosage of ABCE1/RLI1 Does Not Suppress the Leaky Scanning Defect of *hcr1Δ*.

Figure S6. i/TIF34 and g/TIF35 Directly Interact with the N and M domains of eRF1.

Text S1. Supporting Results, Materials and Methods, and References.

Table S1. Yeast strains used in this study.

Table S2. Plasmids used in this study.

Table S3. Primers used in this study.

Figure 1
Click here to download high resolution image

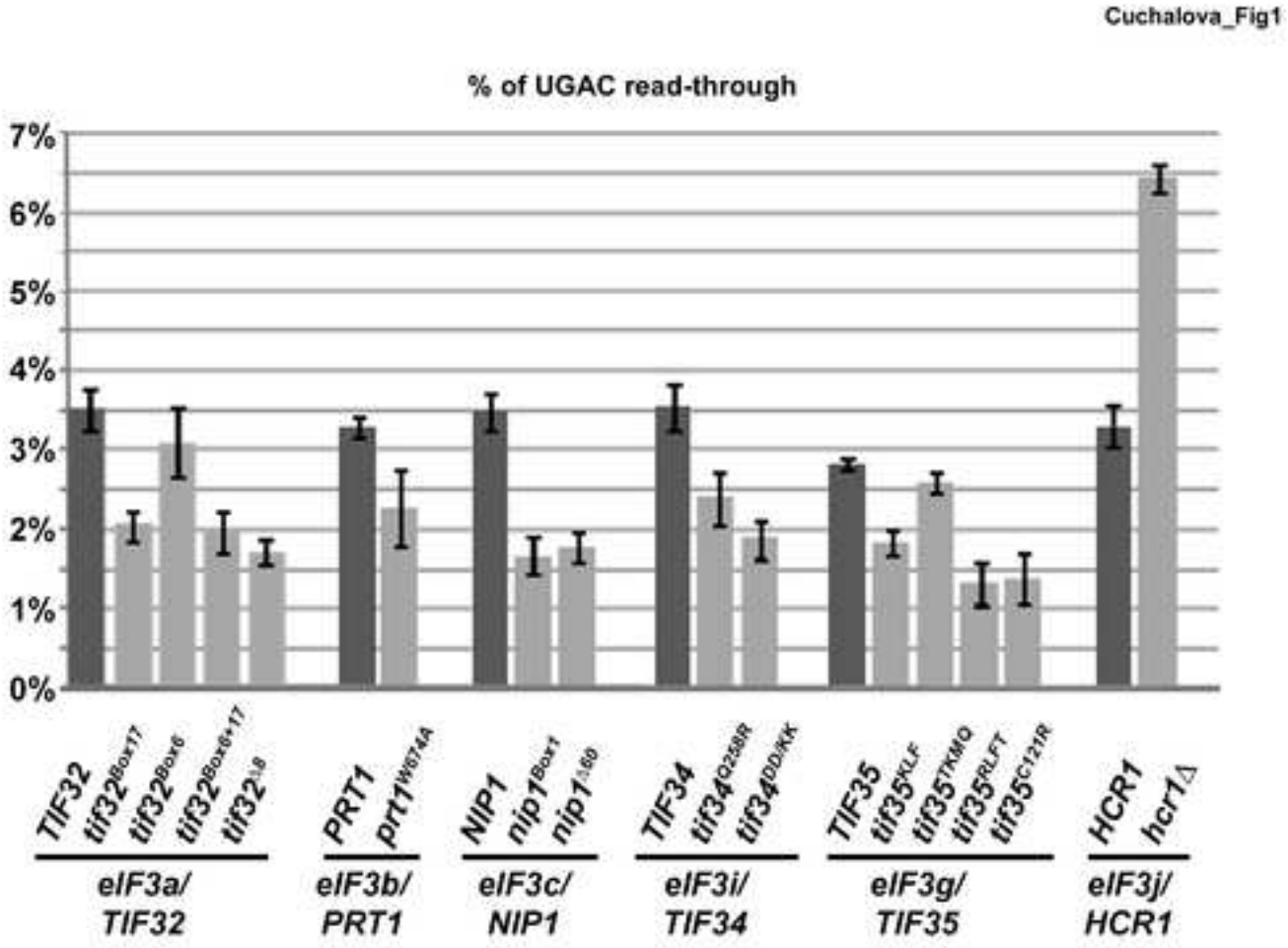

Figure 2
Click here to download high resolution image

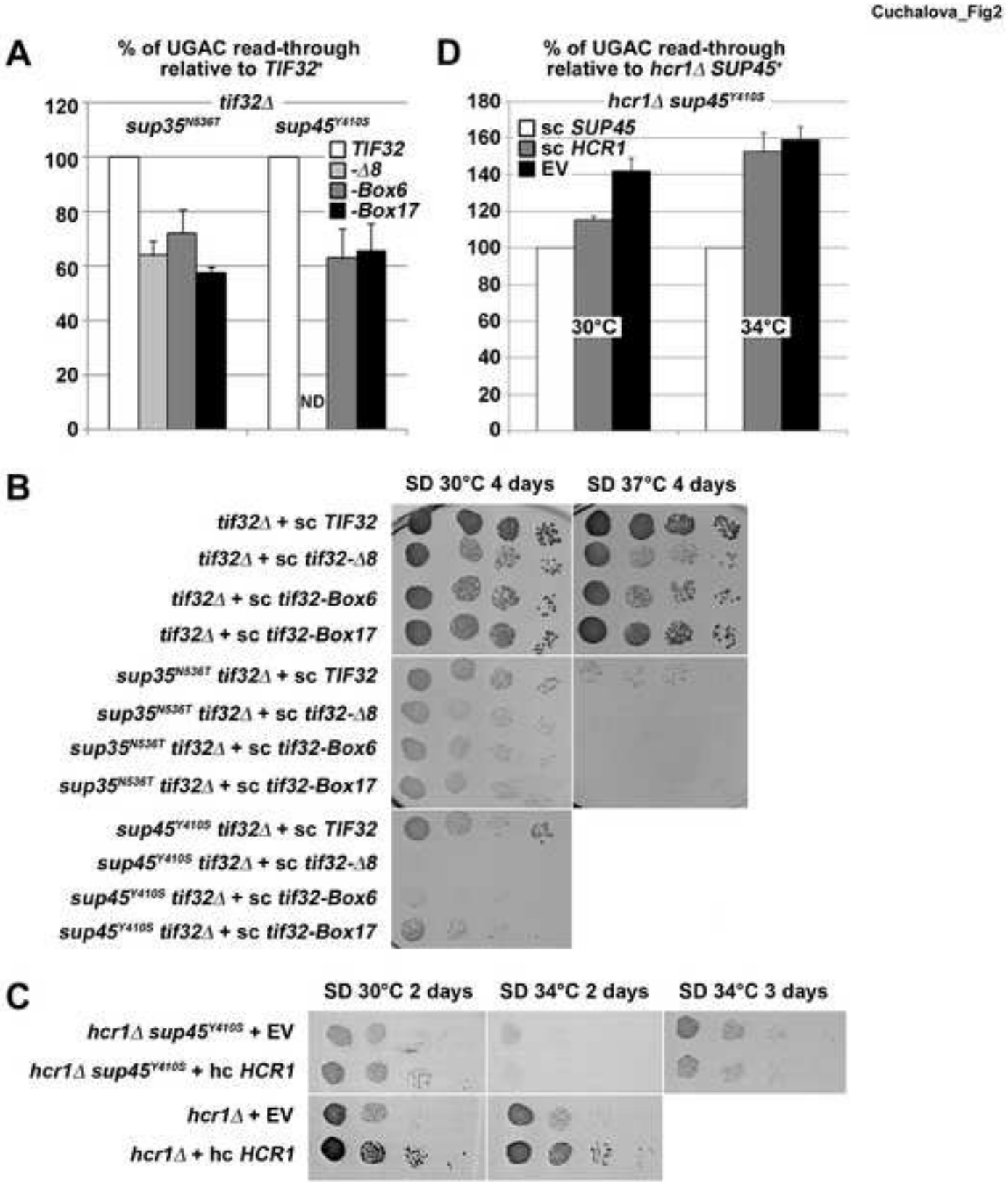

Figure 3
Click here to download high resolution image

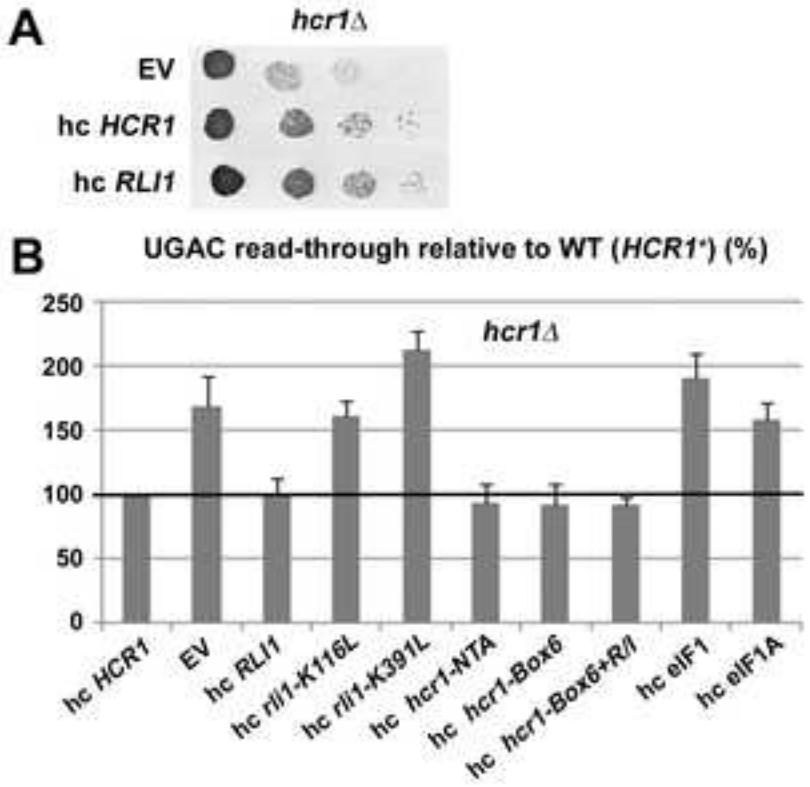

Figure 4
Click here to download high resolution image

Cuchalova_Fig4

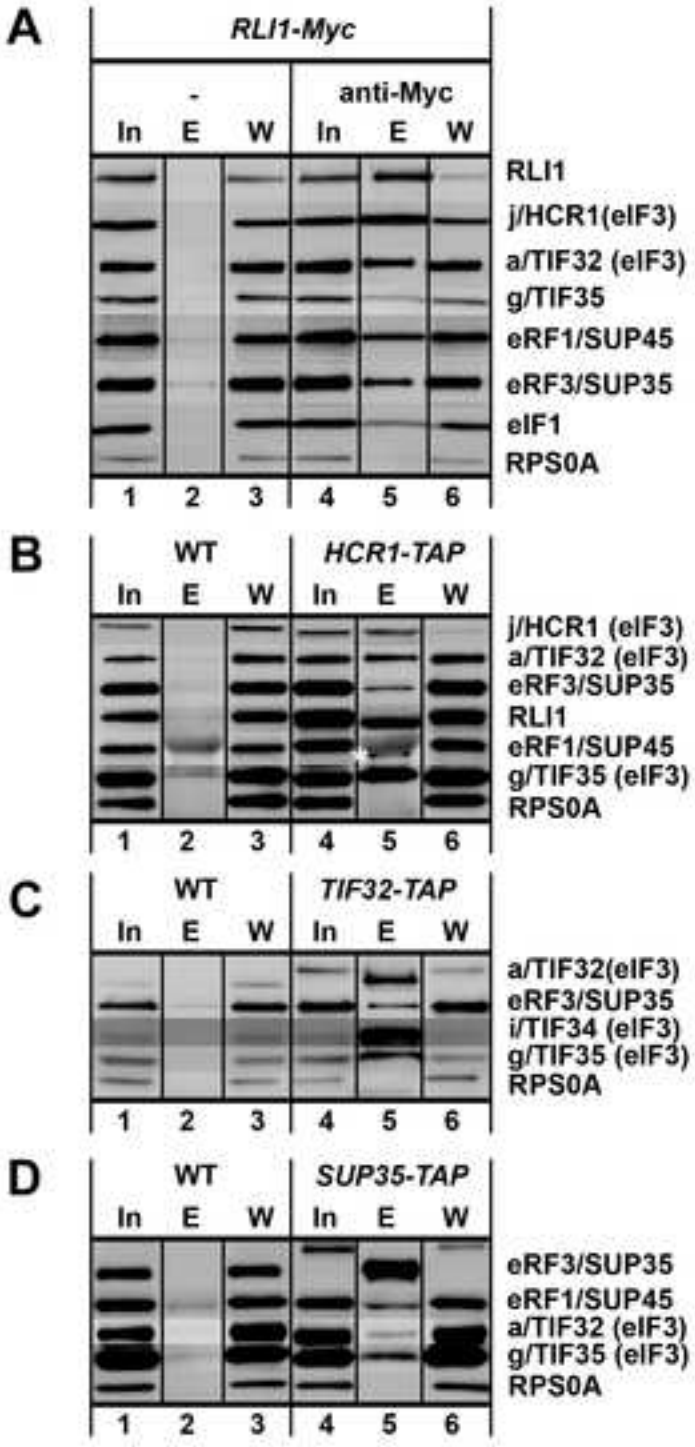

Figure 5
Click here to download high resolution image

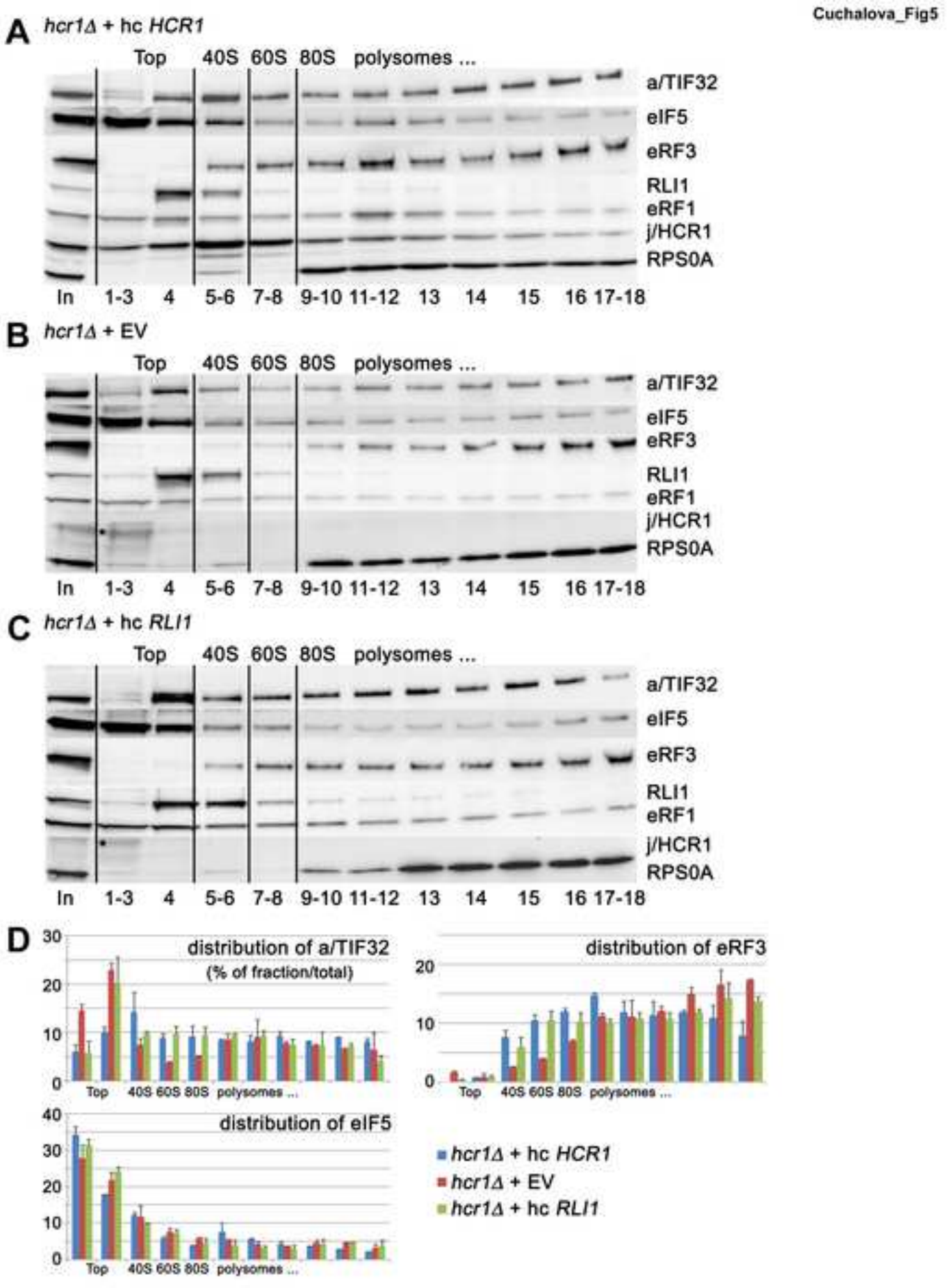

Figure 6
Click here to download high resolution image

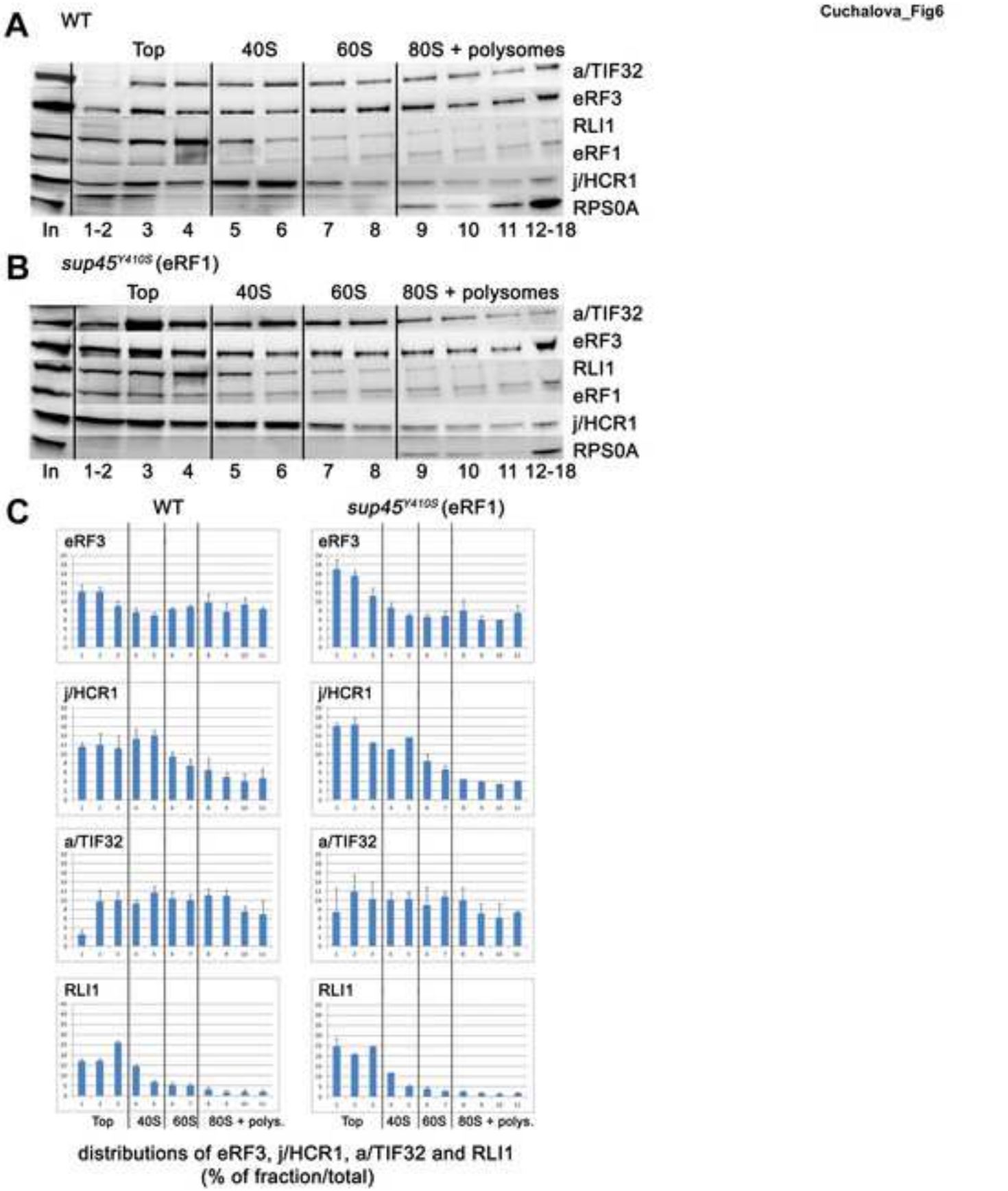

Figure 7
Click here to download Figure: Cuchalova II Fig.7.eps

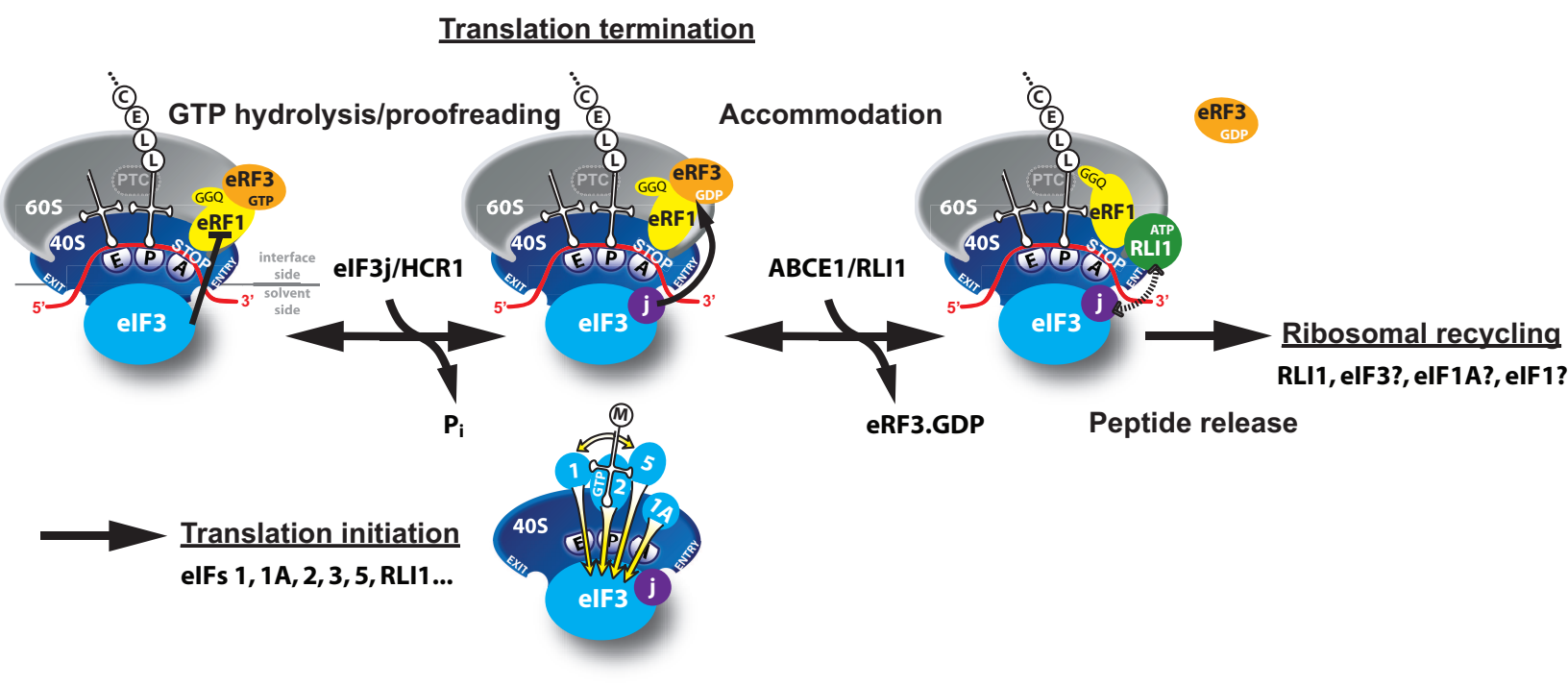

Striking Image

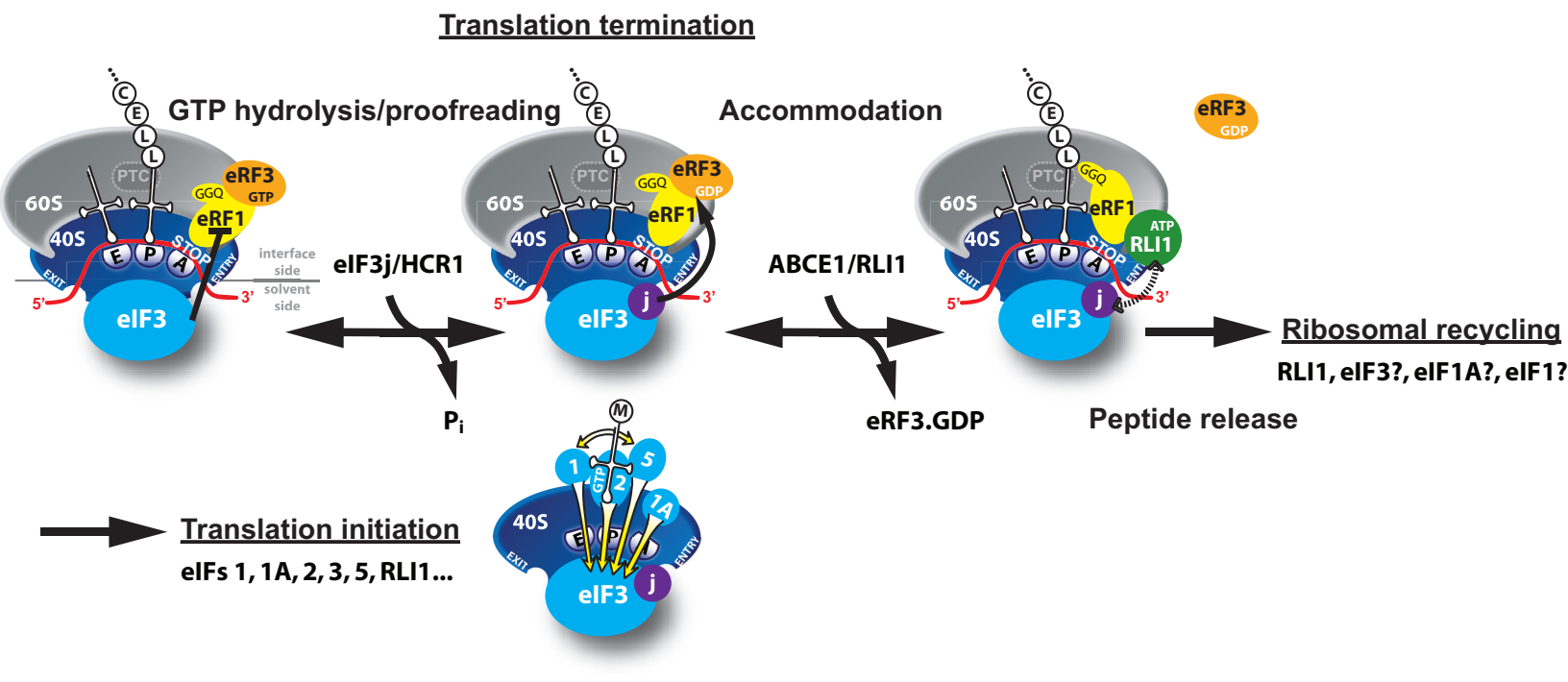

SUPPORTING INFORMATION

SUPPORTING RESULTS

The N-M Domains of eRF1 Directly Interacts with Two Small eIF3 Subunits i/TIF34 and g/TIF35 *in vitro*.

The fact that mutations in all six eIF3 subunits affect fidelity of the termination process prompted us to test protein-protein interactions between eIF3 subunits and both eRFs. We fused individual eIF3 subunits to a GST moiety and used these fusions in pull-down assays with *in vitro* synthesized, radiolabeled, well defined domains of eRF1 and eRF3. As shown in Supplementary Figure S6, the N-terminal and Middle (N-M) domains but not the middle and C-terminal (M-C) domains of eRF1 specifically interacted with GST-g/TIF35 and GST-i/TIF34, in contrast to GST-j/HCR1 and a negative control of the GST protein. (The N domain of eRF1 carries determinants of the stop codon recognition; the M domain contains the conserved GGQ motif required for peptide release; and the C domain interacts with eRF3.) Interestingly, DOM34/Pelota, the release-like factor closely related in sequence and structure to eRF1, also binds eIF3g in human cell lines [1], albeit in this case *via* Pelota's C-terminal domain. No interactions between eIF3 subunits and eRF3 were observed. Hence we propose that eIF3 and eRF1 are in direct contact *via* two small eIF3 subunits and the NTD of eRF1, which requires further support from the M domain to get fully engaged in these interactions.

SUPPORTING FIGURES

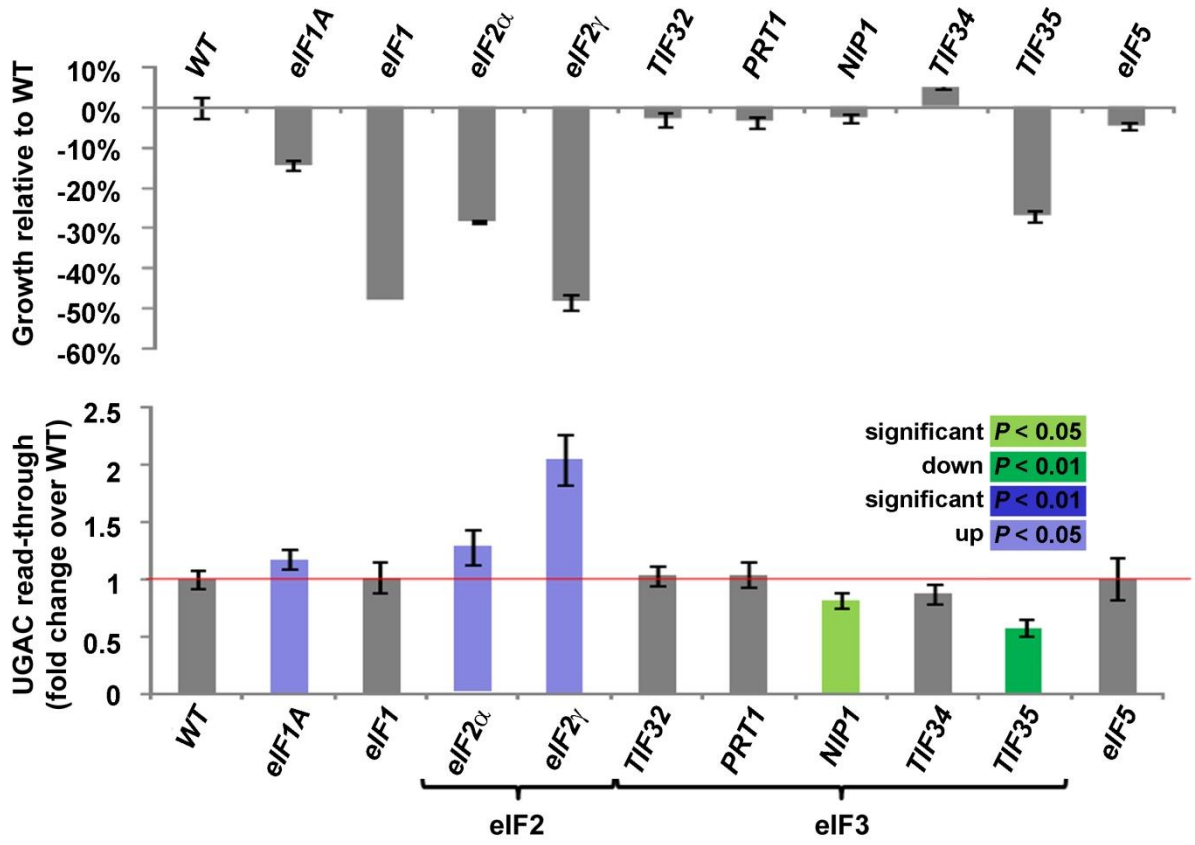

Figure S1. DaMP Alleles of Various 43S PIC-associated Initiation Factors Display Distinct Effects on Efficiency of the Stop Codon Read-through.
Yeast strains containing kanMX4 cassettes integrated into their 3'-UTRs (so-called DaMP alleles) were recovered from the genome-wide collection for these alleles [2]. We were able to recover alleles for all 43S PIC-associated eIFs with the exception of eIF2β, for which no allele was present in the collection.

In order to aid interpretation of results, and to assess the efficiency of depletion of the gene in question, we initially measured growth rates of the respective strains (top panel). Since all of the factors studied here are essential, we expected a reduction in growth rate upon significant depletion of any of these factors. We then proceeded to measure stop codon read-through in these strains, using dual luciferase reporters as described in the main text.

Of the eIF3 subunits tested, only g/TIF35 is sufficiently depleted to cause a significant growth defect, and this strain shows a significant reduction in stop codon read-through. Moreover, the c/NIP1 DaMP allele also shows a significant reduction in stop codon read-through, even though this protein is not sufficiently depleted to produce a significant growth defect. Together, these results confirm those presented for other eIF3 alleles in the main text.

In contrast to the eIF3 subunits, other 43S PIC-associated translation initiation factors do not reduce stop codon read-through upon depletion. Conversely, both eIF2 subunits tested and eIF1A increased read-through when depleted. This demonstrates that the role of eIF3 in translation termination is specific to this factor.

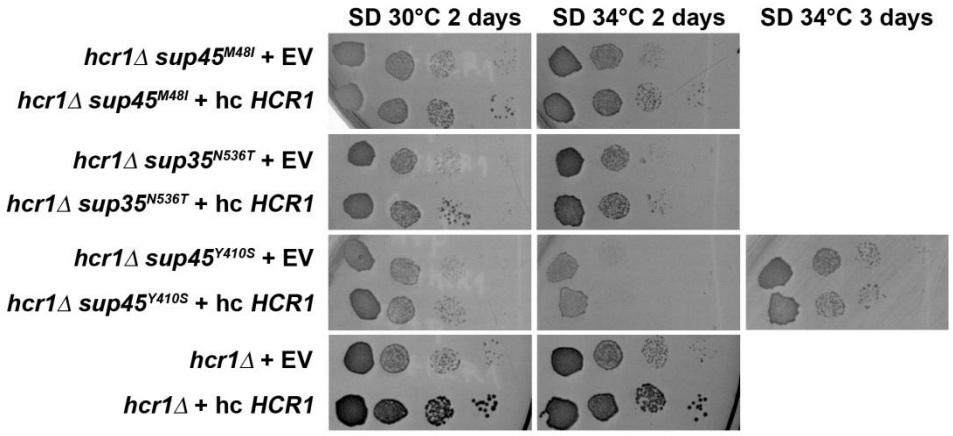

Figure S2. The *sup45*^{Y410S} but not the Other Mutations in eRFs 1 and 3 Eliminate the Negative Impact of *hcr1Δ* on Growth Rates.
The *hcr1Δ* strain was crossed with the indicated *sup45* and *sup35* mutant strains and the resulting double mutants (PBH104, PBH103 and PBH105) were transformed with either empty vector (EV) or hc vector containing *HCR1* and together with the corresponding *hcr1Δ SUP35 SUP45* "wt" strain (YLVH13) spotted in four serial 10-fold dilutions on SD medium and incubated at indicated temperatures for 2 or 3 days.

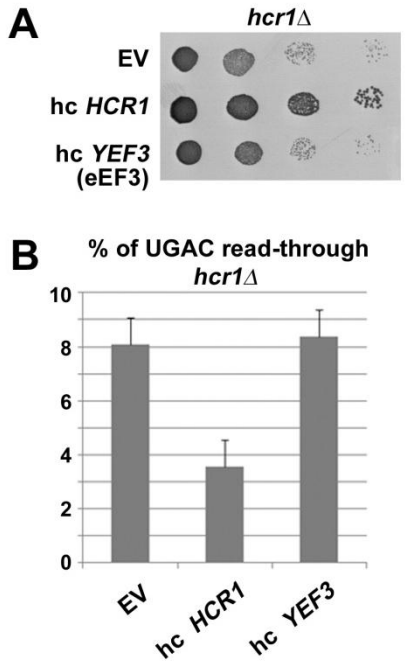

Figure S3. Increased Gene Dosage of eEF3 Does Not Suppress the Slow Growth and Read-through Defects of *hcr1Δ.*

(A) The *hcr1Δ* strain (H3675) was transformed with either empty vector, high copy (hc) *HCR1* or hc *YEF3* (eEF3), the resulting transformants were spotted in four serial 10-fold dilutions on SD medium and incubated at 30°C for 2 days. Unlike RLI1, eEF3 (which is also an ABC cassette-containing protein) does not suppress the growth defect of an *hcr1* deletion strain.

(B) The strains from panel A were grown in SD and processed for the stop codon read-through measurements as described in Figure 1.

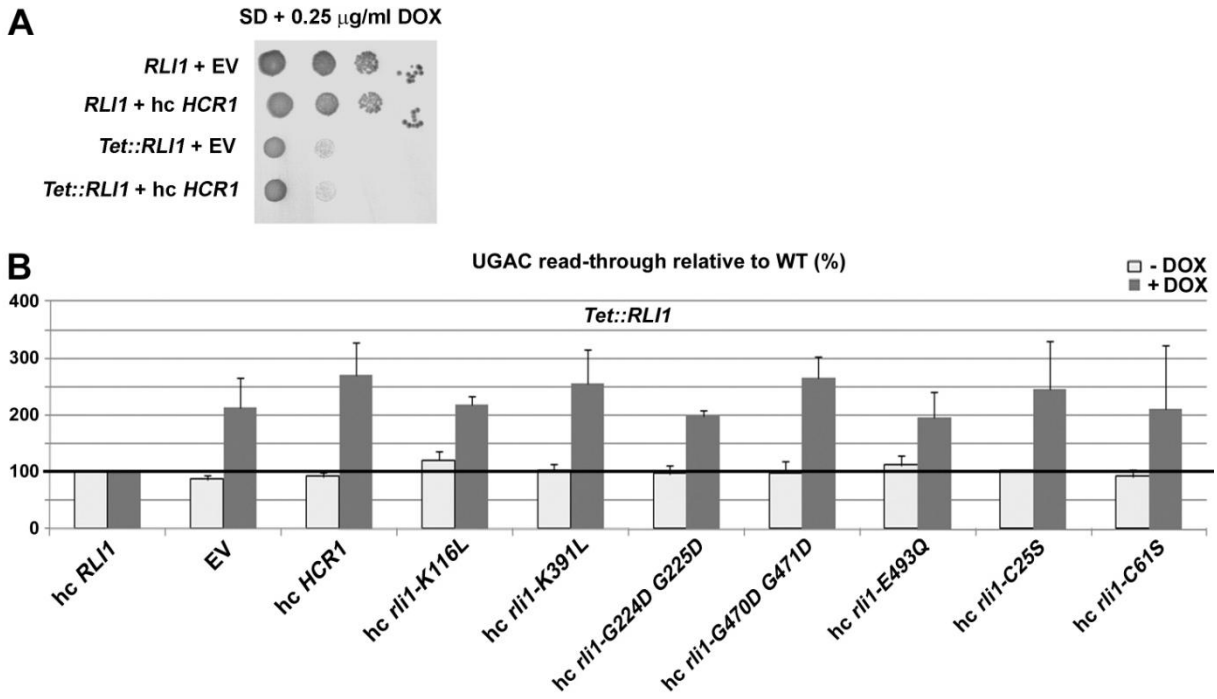

Figure S4. Increased Gene Dosage of *HCR1* Does Not Suppress the Slow Growth and Read-through Defects of the *Tet::RLI1* strain; Intact ATP-Binding Cassettes and the Fe-S Cluster of RLI1 are Indispensable for its Role in Ensuring the Stop Codon Selection Accuracy.

(A) The *Tet::RLI1* (Tet-RLI1) and the corresponding wt strain (W303) were transformed with either empty vector or hc *HCR1,* and the resulting transformants were spotted in four serial 10-fold dilutions on SD medium supplemented with 0.25 μg/ml of doxycycline and incubated at 30°C for 2 days.

(B) The *Tet::RLI1* (Tet-RLI1) strain was transformed with hc vectors carrying wt or mutant *RLI1* alleles, or empty vector or hc *HCR1*. The resulting transformants were grown in SD supplemented with 1 μg/ml of doxycycline (DOX) and processed for the stop codon read-through measurements as described in Figure 1. Obtained values were normalized to the value obtained with the *Tet::RLI1* strain transformed with wt *RLI1*, which was set to 100%.

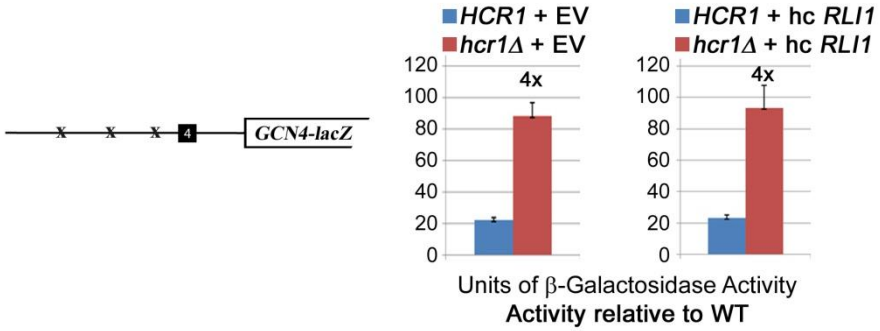

Figure S5. Increased Gene Dosage of ABCE1/RLI1 Does Not Suppress the Leaky Scanning Defect of *hcr1Δ*.

The *HCR1*$^+$ (H2879) and *hcr1Δ* (H3675) strains were first transformed with either empty vector or hc *RLI1* and subsequently with the *GCN4-lacZ* reporter plasmid plig102-3. The resulting double transformants were grown in SD medium at 30°C to an OD_{600} of ~ 1. The β-galactosidase activities were measured in the WCEs and expressed in units of nmol of o-nitrophenyl-b-D-galactopyranoside hydrolyzed per min per mg of protein. The plots show mean values and standard deviations obtained from at least 3 independent measurements with three independent transformants. The fold-difference between the *hcr1Δ* versus *HCR1*$^+$ strains with or without hc *RLI1* is indicated.

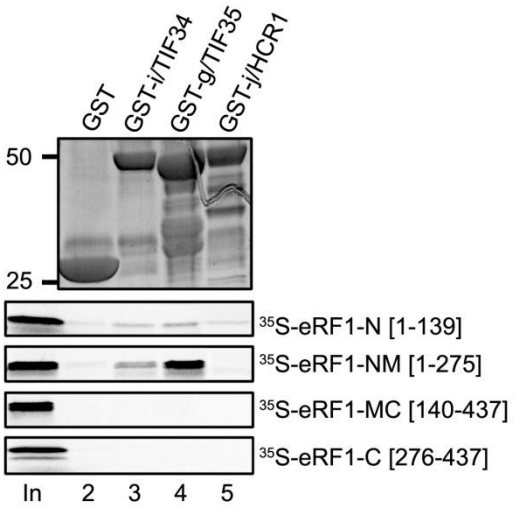

Figure S6. i/TIF34 and g/TIF35 Directly Interact with the N and M domains of eRF1.
Full-length i/TIF34 (lane 3), g/TIF35 (lane 4), and j/HCR1 (lane 5) fused to GST, and GST alone (lane 2), were tested for binding to ^{35}S-labeled individual domains of eRF1; 10% of input amounts added to each reaction is shown in lane 1 (In).

SUPPORTING TABLES

Table S1. Yeast strains used in this study.

Strain	Genotype	Source or reference
del'32a9A[a]	*MAT*a *leu2-3, -112 ura3-52 trp1Δ gcn2Δ a/tif32Δ* (sc *TIF32, URA3*)	[3]
YAH06[a]	*MATa leu2-3,112 ura3-52 trp1Δ prt1::hisG GCN2* (hc *PRT1 URA3*)	[4]
HMJ08[a]	*MATa, trp1 leu2-3,-112 ura3-52 nip1Δ* (sc *NIP1-His URA3*)	[5]
H450[a]	*MAT*a *leu2-3,-112 ura3-52::GCN2 trp1Δ tif34Δ* (hc *TIF34 URA3)*)	[6]
H464[a]	*MAT*a *leu2-3,-112 ura3-52::GCN2 trp1Δ tif35Δ* (hc *TIF35 URA3*)	[6]
PBH103	*MATα ade1-14 trp1-289 his3-Δ200 leu2-3,112 ura3-52 sup35-N536T hcr1Δ::LEU2*	this study
PBH104	*MATα ade1-14 trp1-289 his3-Δ200 leu2-3,112 ura3-52 sup45-M48I hcr1Δ::LEU2*	this study
PBH105	*MATa ade1-14 trp1-289 his3-Δ200 leu2-3,112 ura3-52 sup45-Y410S hcr1Δ::LEU2*	this study
YLVH13[b]	*MATα hcr1Δ::LEU2 ade2-1 trp1-1 can1-100 leu2-3 leu2-112 his3-11 his3-15 ura3*	[7]
L2334[c]	*MAT*a *ade1-14 trp1-289 his3-Δ200 leu2-3,112 ura3-52 sup35-N536T*	[8]
L2327[c]	*MAT*a *ade1-14 trp1-289 his3-Δ200 leu2-3,112 ura3-52 sup45-M48I*	[8]
L2521[c]	*MAT*a *ade1-14 trp1-289 his3-Δ200 leu2-3,112 ura3-52 sup45-Y410S*	[8]
74D-694[c]	*MAT*a *ade1-14 trp1-289 his3-Δ200 leu2-3,112 ura3-52*	[9]
PBH106	*MATα trp1-289 his3-Δ200 leu2-3,112 ura3-52 sup45-Y410S a/tif32Δ* (sc *TIF32, URA3*)	this study
PBH107	*MATα ade1-14 trp1-289 his3-Δ200 leu2-3,112 ura3-52 sup35-N536T a/tif32Δ* (sc *TIF32, URA3*)	this study
del'32a9B[a]	*MATα leu2-3, -112 ura3-52 trp1Δ gcn2Δ a/tif32Δ* (sc *TIF32, URA3*)	[3]
YDH353	*MATa his3Δ1 leu2Δ0 ura3Δ0 met15Δ0 RLI1-MYC::HIS3*	[10]
H553[d]	*MATa his3Δ1 leu2Δ0 met15Δ0 ura3Δ0 HCR1-TAP*	Thermo Scientific
H555[d]	*MATa his3Δ1 leu2Δ0 met15Δ0 ura3Δ0 TIF32-TAP*	Thermo Scientific
H517[c]	*MATa ade1-14 trp1-289 his3-Δ200 leu2-3,112 ura3-52 SUP35::TAP-HIS3*	this study
H3675[a]	*MATa PRT1 leu2-3, 112 ura3-52 hcr1Δ*	[11]
H2879[a]	*MATa PRT1 leu2-3, 112 ura3-52*	[12]
W303 [b]	*MATa ade2 can1-100 his3-11 his3-15*	A. Hopper

	leu2-3 leu2-112 trp1-1 ura3-1	
Tet-RLI1[b]	*MATα ade2 can1-100 his3-11 his3-15 leu2-3 leu2-112 trp1-1 ura3-1 Tet::RLI1*	[13]

[a-d] Identical superscripts denote isogenic strain backgrounds.

Table S2. Plasmids used in this study.

Plasmid	Description	Source of reference
pTH477	high copy PGK-Renilla-Firefly R/T cassette (stop codon of Renilla is UGA-C; for read-through measurements) in *URA3* plasmid from YEplac195	[14]
pTH460	high copy PGK-Renilla-Firefly R/T cassette (stop codon of Renilla is replaced with CAA-C [coding triplet]; for control read-through measurements) in *URA3* plasmid from YEplac195	[14]
YEp-R/T-UGAC-L	high copy PGK-Renilla-Firefly R/T cassette (stop codon of Renilla is UGA-C; for read-through measurements) in *LEU2* plasmid from YEplac181	this study
YEp-R/T-CAAC-L	high copy PGK-Renilla-Firefly R/T cassette (stop codon of Renilla is replaced with CAA-C [coding triplet]; for control read-through measurements) in *LEU2* plasmid from YEplac181	this study
YCp-a/TIF32-His-L	single copy wt *TIF32-His* in *LEU2* plasmid from YCplac111	[15]
YCp-a/tif32-Box17-His	single copy *tif32-Box17-His* in *LEU2* plasmid from YCplac111	[15]
YCp-a/tif32-Box6-His	single copy *tif32-Box6-His* in *LEU2* plasmid from YCplac111	[15]
YCp-a/tif32-Box6+17-His	single copy *tif32-Box6+17-His* in *LEU2* plasmid from YCplac111	[15]
YCp-a/tif32-Δ8-His-L	single copy *tif32-Δ8-His* in *LEU2* plasmid from YCplac111	this study
pRS-b/PRT1-HisXS	low copy wt *PRT1* in *LEU2* plasmid from pRS315	[4]
pRS-b/PRT1-W674A-His	low copy *prt1-W674A* in *LEU2* plasmid from pRS315	[4]
YCpNIP1-Myc-L	single copy wt *NIP1-Myc* in *LEU2* plasmid from YCplac111	[5]
YCpNIP1-743A752(box1)	single copy *NIP1-Myc* containing 10 Ala substitutions between amino acid residues 743 and 752, in *LEU2* plasmid from YCplac111	[5]
YCpNIP1-Δ60-MYC-L	single copy *NIP1-Myc* truncated by 60 amino acid residues, in *LEU2* plasmid from YCplac111	[5]
YCp-i/TIF34-HA	single copy wt *TIF34-HA* in *LEU2* plasmid from YCplac111	[6]

YCpL-i/tif34-HA-3 (Q258R)	single copy *tif34-HA-Q258R* in *LEU2* plasmid from YCplac111	[6]
YCp-i/TIF34-D207K-D224K-HA	single copy *TIF34-HA* containing D207K and D224K mutations in *LEU2* plasmid from YCplac111	[16]
YCp22-g/TIF35-screen	single copy wt *TIF35-His* in *TRP1* plasmid from YCplac22	[6]
YCp22-g/TIF35-KLF	single copy *TIF35-KLF-His* in*TRP1* plasmid from YCplac22	[6]
YCp22-g/TIF35-TKMQ	single copy *TIF35-TKMQ-His* in *TRP1* plasmid from YCplac22	this study
YCp22-g/TIF35-RLFT	single copy *TIF35-RLFT-His* in *TRP1* plasmid from YCplac22	this study
YCp22-g/TIF35-C121R	single copy *TIF35-C121R-His* in *TRP1* plasmid from YCplac22	this study
YEplac181	high copy cloning vector, *LEU2*	[17]
YEplac195	high copy cloning vector, *URA3*	[17]
YEpLVHCR1	high copy wt *HCR1* in *LEU2* plasmid from YEplac181	[7]
YEp-j/HCR1-DS-U	high copy *j/HCR1* coding region flanked by *Bam*HI and *Nco*I sites, respectively, in *URA* plasmid from YEplac195	[4]
YEp-RLI1-L	high copy wt *RLI1* in *LEU2* plasmid from YEplac181	this study
YEp-j/hcr1-NTD	high copy *hcr1-NTD* in *LEU2* plasmid from YEplac181	[4]
YEp-j/hcr1-CTD	high copy *hcr1-CTD* in *LEU2* plasmid from YEplac181	[4]
YEp-j/hcr1-NTA1	high copy *hcr1-NTA1* in *LEU2* plasmid from YEplac181	[4]
YEp-j/hcr1-box6	high copy *hcr1-Box6* in *LEU2* plasmid from YEplac181	[18]
YEp-j/hcr1-box6-R215I	high copy *hcr1-Box6-R215I* in *LEU2* plasmid from YEplac181	[18]
PDH177	single copy wt *RLI1* in *URA3* plasmid from YCplac33	[10]
YEp-rli1-K116L-L	high copy *rli1-K116L* in *LEU2* plasmid from YEplac181	this study
YEp-RLI1-ndeI-L	high copy wt *RLI1* in *LEU2* plasmid from YEplac181	this study
YEp-rli1-K391L-L	high copy *rli1-K391L* in *LEU2* plasmid from YEplac181	this study
YEp-rli1-G224D,G225D-L	high copy *rli1-G224D,G225D* in *LEU2* plasmid from YEplac181	this study
YEp-rli1-G470D,G471D-L	high copy *rli1-G470D,G471D* in *LEU2* plasmid from YEplac181	this study
YEp-rli1-E493Q-L	high copy *rli1-E493Q* in *LEU2* plasmid from YEplac181	this study

PDH184	single copy P_{GAL}-UBI-M-FH-rli1-G224D,G225D plasmid from YCplac111	[10]
PDH185	single copy P_{GAL}-UBI-M-FH-rli1-G470D,G471D plasmid from YCplac111	[10]
PDH202	low copy *rli1-E493Q-myc$_5$* plasmid from pRS315	[10]
YEp-rli1-C25S-L	high copy *rli1-C25S* in *LEU2* plasmid from YEplac181	this study
YEp-rli1-C61S-L	high copy *rli1-C61S* in *LEU2* plasmid from YEplac181	this study
YEpSUI1-U	high copy *SUI1* in *LEU2* plasmid from YEplac181	this study
pDSO166	high copy *TIF11* in *LEU2* plasmid from YEplac181	[19]
pGEX-5X-3	cloning vector for GST fusions	[20]
pGEX- g/TIF34	GST-g/Tif34 fusion plasmid from pGEX-4T-1	[21]
pGEX- g/TIF35	GST-g/Tif35 fusion plasmid from pGEX-5X-3	[21]
pGEX-j/HCR1	GST-j/HCR1 fusion plasmid from pGEX-5X-3	[22]
pTH338	T7 promoter plasmid containing a full length SUP45 gene	this study
pTH339	T7 promoter plasmid containing the SUP45 N-domain	this study
pTH340	T7 promoter plasmid containing the SUP45 N- and M-domains	this study
pTH341	T7 promoter plasmid containing the SUP45 M- and C-domains	this study
pTH342	T7 promoter plasmid containing the SUP45 C-domain	this study
TKB668	high copy *YEF3* in *URA3* plasmid from YEPlac195	a gift of T. Kinzy
pGEX-RLI1	GST-RLI1 fusion plasmid from pGEX-5X-3	this study
pGEX-SUP45	GST-SUP45 fusion plasmid from pGEX-6P-1	a gift of A. Hinnebusch
plig102-3	Low copy *URA3* vector with *GCN4* leader point mutations containing uORF4 only at its original position in front of the *GCN4-lacZ* coding region	[23]
YCplac22	single copy cloning vector, *TRP1*	[17]
YCp22-SUP45-W	single copy wt *SUP45* in *TRP1* plasmid from YCplac22	this study

Table S3. Primers used in this study.

Primer name	Primer sequence (5´to 3´)
SG-TIF32D8bamHI	GCGGATCCATATGAGATTAGCTGAAATG
BS-TIF32D8nheI-R	GGGGCTAGCGGGTCCCTGCCCCCCTTGGCCAATC
TIF35 NdeI	TAACGACCATATGACCATGAA
MM2r 3gTLKVr	ACACATATCATCACGTTCTCT
y3gTKMQ (RNP2)	GACTCTAGAGAACGTGATGATATGTGTgctTTGgcaATTgctgcaGTTAATGAAAATGCCGATGAAAATAGT
y3g XhoIr	GTGCATCTCGAGCTAATGATG
MM1r	TGATTTACCTGTTTCTTTGT
y3gRLFT (RNP1)	GTTAGAAACAAAGAAACAGGTAAATCAgcaGGTgcaGCCgcaGTTgcaTTTTCGAGCGAAGAAGTTGCCGAACAA
PB-RLI1ndeI	AATAACATATGAGTGATAAAAACAGTCGT
PB-RLI1-K116LaccI-R	AATAAGTAGACAGACCAATACCGTTGGTACCGAC
PB-RLI1accI-R	CAAGGCGGTAGACTTAC
PB-RLI1ncoI	GCAAATACCATGGATAG
PB-RLI1ndeI-R	ACGACTGTTTTTATCACTCATATGGGTCTGTCGTGTTTTCTTAAG
PB-RLI1-K391L-R	AGACCGGTACCGTTTTCACCCAT
PB-RLI1-K391L	ATGGGTGAAAACGGTACCGGTCTGACCACTTTGATCAAATTACTA
PB-RLI1termXbaI-R	GGCGTATATCTAGAAATAAACAACC
PB-RLI1xbaI-R	AATAATCTAGATTAAATACCGGTGTTATCCAA
PB-RLI1-C25S	CTAAACGTTCGTGTCCCG
PB-RLI1-C25S-R	CGGGACACGAACGTTTAGACTCTTGACGACACTTTTTTGG
PB-RLI1-C61S	CCGTTAAGAAATGTCCATTTG
PB-RLI1-C61S-R	CAAATGGACATTTCTTAACGGAAATACCACAACCAATAC
Sup45_D1f	CGGGCCATGGAGATGGATAACGAGGTTGAAAAAAA
Sup45_D3r	CGGGCCTGCAGTTAAATGAAATCATAGTCGGAT
Sup45_D1r	CGGGCCTGCAGTTATTGAAGCAATTCCGAAAGAAC
Sup45_D2r	CGGGCCTGCAGTTAATTGGCCAACGCTTCGGC
Sup45_D2f	CGGGCCATGGAGGCTGACGACAAGTTCGGT
Sup45_D3r	CGGGCCTGCAGTTAAATGAAATCATAGTCGGAT
Sup45_D3f	CGGGCCATGGAGGTCAAGTATGTTCAAGAAAAGA
PB-RLI1smaI	AATAACCCGGGTCATGAGTGATAAAAACAGTCGT
PB-RLI1xhoI-R	AATAACTCGAGTTAAATACCGGTGTTATCCAA
PB-SUP45SphI	AATAAGCATGCGCTACATCATTTCCCCCAATAGC
PB-SUP45SacI-R	AATAAGAGCTCCGAGGCTTTTGAAGAGAAACTCTCC

SUPPORTING MATERIALS AND METHODS

Construction of Yeast Strains and Plasmids

List of all strains used throughout this study can be found in Supplementary Table 1.

To generate *TIF32*$^{+}$, *tif32*^{Box17}, *tif32*^{Box6}, *tif32*$^{Box6+17}$ and *tif32*$^{\Delta 8}$ mutant strains (all showing in Figure 1), del'32a9A was transformed with YCp-a/TIF32-His-L, YCp-a/tif32-Box17-His, YCp-a/tif32-Box6-His , YCp-a/tif32-Box6+17-His, and YCp-a/tif32-Δ8-His-L, respectively, and the resident *URA3*-based plasmid carrying wt *TIF32* was evicted on 5-FOA-containing medium.

To generate *PRT1*$^{+}$ and *prt1*^{W647A} mutant strains (Figure 1), YAH06 was transformed with pRS-b/PRT1-HisXS and pRS-b/PRT1-W674A-His, respectively, and the resident *URA3*-based plasmid carrying wt *PRT1* was evicted on 5-FOA-containing medium.

To generate *NIP1*$^{+}$, *nip1*^{Box1} and *nip1*$^{\Delta 60}$ mutant strains (Figure 1), HMJ08 was transformed with YCpNIP1-Myc-L, YCpNIP1-743A752(box1) and YCpNIP1-Δ60-MYC-L, respectively, and the resident *URA3*-based plasmid carrying wt *NIP1* was evicted on 5-FOA-containing medium.

To generate *TIF34*$^{+}$, *tif34*^{Q258R} and *tif34*$^{DD/KK}$ mutant strains (Figure 1), H450 was transformed with YCp-i/TIF34-HA, YCpL-i/tif34-HA-3 (Q258R) and YCp-i/TIF34-D207K-D224K-HA, respectively, and the resident *URA3*-based plasmid carrying wt *TIF34* was evicted on 5-FOA-containing medium.

To generate *TIF35*$^{+}$, *tif35*^{KLF}, *tif35*^{TKMQ}, *tif35*^{RLFT} and *tif35*^{C121R} mutant strains (Figure 1), H464 was transformed with YCp22-g/TIF35-screen, YCp22-g/tif35-KLF, YCp22-g/tif35-TKMQ, YCp22-g/tif35-RLFT and YCp22-g/tif35-C121R, respectively, and the resident *URA3*-based plasmid carrying wt *TIF35* was evicted on 5-FOA-containing medium.

Strains PBH103 [*hcr1Δ sup35*^{N536T}], PBH104 [*hcr1Δ sup45*^{M48I}], and PBH105 [*hcr1Δ sup45*^{Y410S}] were all generated by a genetic cross of YLVH13 with L2334, L2337, and L2521, respectively, selecting for a haploid ascospore showing the Ts^{-} phenotype and being prototrophic for leucine.

PBH106 [*tif32Δ sup45*^{Y410S}] and PBH107 [*tif32Δ sup35*^{N536T}] were generated by a genetic cross of del'32a9B with L2521 and L2334, respectively, selecting for a haploid ascospore showing the Ts^{-} phenotype and being unable to lose the resident *URA3*-based cover plasmid.

TAP-tagging at the chromosomal locus of SUP35 was performed in strain 74D-694 as described [24] producing H517.

List of all plasmids and PCR primers used throughout this study can be found in Supplementary Tables 2 and 3, respectively.

YEp-R/T-UGAC-L and YEp-R/T-CAAC-L were constructed by inserting the 4567-bp *Alw*NI-*Nsi*I fragment from pTH477 and pTH460, respectively, into YEplac181 digested by AlwNI-NsiI.

YCp-a/tif32-Δ8-His-L was made by inserting the *Bam*HI-*Xba*I digested PCR product obtained with primers SG-TIF32D8bamHI and BS-TIF32D8nheI-R using pRS-eIF3a-Δ8-His-L as a template into *Bam*HI-*Xba*I digested YCp-a/TIF32-His-L.

YCp22-g/TIF35-TKMQ was generated by fusion PCR. The following pairs of primers were used for separate PCR amplifications using YCp22-g/TIF35-screen as template: (1) TIF35 NdeI – MM2r 3gTLKVr; and (2) y3gTKMQ (RNP2) – y3g XhoIr. The PCR products thus obtained were used in a 1:1 ratio as templates for the third PCR amplification using primers y3g XhoIr and TIF35 NdeI. The resulting PCR

product was digested with *Nde*I and *Xho*I and ligated with *Nde*I-XhoI-cleaved YCp22-g/TIF35-screen.

YCp22-g/TIF35-RLFT was generated by fusion PCR. The following pairs of primers were used for separate PCR amplifications using YCp22-g/TIF35-screen as template: (1) TIF35 NdeI – MM1r; and (2) y3gRLFT (RNP1) – y3g XhoIr. The PCR products thus obtained were used in a 1:1 ratio as templates for the third PCR amplification using primers y3g XhoIr and TIF35 NdeI. The resulting PCR product was digested with *Nde*I and *Xho*I and ligated with *Nde*I-XhoI-cleaved YCp22-g/TIF35-screen.

YCp22-g/TIF35-C121R was obtained by random mutagenesis of the template plasmid YCp22-g/TIF35-screen with help of XL1-Red Competent Cells (Stratagene).

YEp-RLI1-L was constructed by inserting the 2887-bp *Spe*I-*Pst*I fragment from PDH177 into YEplac181 digested with *Xba*I-*Pst*I.

YEp-rli1-K116L-L was made by inserting the *Nde*I-*Acc*I digested PCR product obtained with primers PB-RLI1ndeI and PB-RLI1-K116LaccI-R using YEp-RLI1-L as the template into *Nde*I-*Acc*I digested YEp-RLI1-ndeI-L. To create YEp-RLI1-ndeI-L, fusion PCR was employed. The following pairs of primers were used for separate PCR amplifications using YEp-RLI1-L as template: (1) PB-RLI1ndeI – PB-RLI1accI-R; and (2) PB-RLI1ncoI – PB-RLI1ndeI-R. The PCR products thus obtained were used in a 1:1 ratio as templates for the third PCR amplification using primers PB-RLI1ncoI and PB-RLI1accI-R. The resulting PCR product was digested with *Nco*I and *Acc*I and ligated with *Nco*I-*Acc*I-cleaved YEp-RLI1-L.

YEp-rli1-K391L-L was generated by fusion PCR. The following pairs of primers were used for separate PCR amplifications using YEp-RLI1-ndeI-L as template: (1) PB-RLI1ndeI – PB-RLI1-K391L-R; and (2) PB-RLI1-K391L – PB-RLI1termXbaI-R. The PCR products thus obtained were used in a 1:1 ratio as templates for the third PCR amplification using primers PB-RLI1ndeI and PB-RLI1termXbaI-R. The resulting PCR product was digested with *Nde*I and *Xba*I and ligated with *Nde*I-*Xba*I-cleaved YEp-RLI1-ndeI-L.

YEp-rli1-G224D,G225D-L, YEp-rli1-G470D,G471D-L, and YEp-rli1-E493Q-L were made by inserting the *Nde*I-*Xba*I digested PCR product obtained with primers PB-RLI1ndeI and PB-RLI1xbaI-R using PDH184, PDH185, and PDH202 as templates, respectively, into *Nde*I-*Xba*I digested YEp-RLI1-ndeI-L.

YEp-rli1-C25S-L was generated by fusion PCR. The following pairs of primers were used for separate PCR amplifications using YEp-RLI1-ndeI-L as template: (1) PB-RLI1ndeI – PB-RLI1-C25S-R; and (2) PB-RLI1-C25S – PB-RLI1accI-R. The PCR products thus obtained were used in a 1:1 ratio as templates for the third PCR amplification using primers PB-RLI1ndeI and PB-RLI1accI-R. The resulting PCR product was digested with *Nde*I and *Acc*I and ligated with *Nde*I-*Acc*I-cleaved YEp-RLI1-ndeI-L.

YEp-rli1-C61S-L was generated by fusion PCR. The following pairs of primers were used for separate PCR amplifications using YEp-RLI1-ndeI-L as template: (1) PB-RLI1ndeI – PB-RLI1-C61S-R; and (2) PB-RLI1-C61S – PB-RLI1accI-R. The PCR products thus obtained were used in a 1:1 ratio as templates for the third PCR amplification using primers PB-RLI1ndeI and PB-RLI1accI-R. The resulting PCR product was digested with *Nde*I and *Acc*I and ligated with *Nde*I-*Acc*I-cleaved YEp-RLI1-ndeI-L.

To generate YEpSUI1-L, a *Sac*I-*Hind*III fragment from YEpSUI1-U [25] was ligated into *Sac*I-*Hind*III-cleaved YEplac181 [17].

Plasmids used for the generation of *in vitro*-translated eRF1 fragments (pTH339-342) were generated as follows. Fragments of the *SUP45* gene were generated by PCR using yeast genomic DNA as template. The primers used were Sup45_D1f and Sup45_D3r (for eRF1(fl)); Sup45_D1f and Sup45_D1r (for eRF1-N); Sup45_D1f and Sup45_D2r (for eRF1-NM); Sup45_d2f and Sup45_D3r (for eRF1-MC); and Sup45_D3f and Sup45_D3r (for eRF1-C). All primers added *Nco*I and *Not*I sites at the 5'- and 3'-ends of the PCR products, respectively, and also introduced translation start- and stop codons where required. The DNA fragments were then cloned into the yeast two-hybrid binding domain vector pGBK-T7 (Clontech Europe, France), which also contains a T7 transcription start site upstream of the gene's start codon, using *NcoI* and *NotI* sites.

pGEX-RLI1 expression plasmid was constructed by insertion of the corresponding *Sma*I-*Xho*I-digested PCR product amplified from YEp-RLI1-L using the primers PB-RLI1smaI and PB-RLI1xhoI-R into *Sma*I-*Xho*I-digested pGEX-5X-3 [17].

YCp22-SUP45-W was made by inserting the *Sph*I-*Sac*I-digested PCR product (2033 bp-long) obtained from genomic DNA using primers PB-SUP45SphI and PB-SUP45SacI-R into the *Sph*I-*Sac*I-cut YCplac22.

Read-through assays

Stop codon read-through assays were performed using a bicistronic reporter construct consisting of a *Renilla* luciferase gene followed by an in-frame firefly luciferase gene. Separating the two genes is either a tetranucleotide termination signal (e.g., UGA C) [plasmids pTH477 (*URA3*) or YEp-R/T-UGAC-L (*LEU2*)] or, for control purposes, a similar sequence containing a sense codon (e.g., CAA C) [plasmids pTH460 (*URA3*) or YEp-R/T-CAAC-L (*LEU2*)]. It is noteworthy that this system avoids possible artifacts associated with changes in the efficiency of translation initiation associated with the function of the NMD machinery [26], because both the *Renilla* and firefly enzymes initiate translation from the same AUG codon. For further details, see [14]. Microtitre-plate based dual luciferase assays and analyses of the resulting data were as described [27]. Samples were processed in quintuplicate, and each experiment was repeated at three times.

Co-immunoprecipitation and Affinity Tag Pull Downs

Yeast whole cell extracts (WCEs) were prepared as described previously [28] except that buffer A (30 mM HEPES (pH 8.8), 20 mM KAc, 3 mM magnesium acetate,1 mM dithiothreitol, 1% Nonidet P-40 supplemented with Complete Protease Inhibitor Mix tablets (ROCHE), and protease inhibitors 1µg/ml aprotinin, 1µg/ml leupeptin, 1µg/ml pepstatin and 100 µM phenylmethylsulfonyl fluoride (PMSF)) was used for lysis of the cells, and cell lysates were centrifuged at 3,000 r.p.m. for 10 min at 4 °C. The co-immunoprecipitation analysis was performed as described elsewhere ([29]), using 500 µg of the total protein and 1 µl of mouse anti Myc-Tag IgG (CELL SIGNALING TECHNOLOGY).

Yeast cells expressing the TAP-tagged genes of interest were grown in YPD medium at 30°C to an OD_{600} of ~1 and treated with 1% HCHO prior to harvesting for 60 mins. The WCEs was prepared as described above using buffer B (50 mM Tris-HCl (pH 7.6), 150 mM NaCl, 0.05% Tween 20) with all protease inhibitors in the presence or absence of 0.1 mg/ml RNase A. Samples containing 1 mg of total protein in a final volume of 600 µl were incubated for 2 h at 4°C with 50 µl of 1:1 slurry of IgG Sepharose 6 Fast Flow beads in buffer B. Samples were centrifuged briefly and the

supernatants were removed. The collected beads were then washed five times with 1 ml of ice cold buffer B, and incubated either with TEV protease (INVITROGEN) for 30 min at 30°C followed by boiling in the SDS-loading buffer for 5 min at 95°C, or directly boiled the SDS-loading buffer. Corresponding aliquots of input, eluate and wash (supernatant) were analyzed by SDS-PAGE followed by immunoblotting.

Polysomal Gradient Analysis

The 0.5% formaldehyde (HCHO) cross-linking followed by WCE preparation and fractionation of extracts for analysis of translational complexes were carried out as described previously [30] with the following exceptions. Cycloheximide was added at a concentration of 0.05 mg/ml 5 minutes before the HCHO treatment, after which the cells were broken by FastPrep Instrument (MP Biomedicals) at the intensite level of 5 in two 20 second cycles. The resulting WCEs was separated on 5-45% the sucrose gradients.

Other Yeast Biochemical Methods

GST pull-down experiments with GST fusions and *in vitro*-synthesized [^{35}S]-labeled polypeptides (see Supplementary Table 2 for vector descriptions) were conducted as follows. Individual GST-fusion proteins were expressed in *E. coli*, immobilized on glutathione-Sepharose beads and incubated with 10 μl of ^{35}S-labeled potential binding partners at 4°C for 2 h. The beads were washed 3 times with 1 ml of phosphate-buffered saline, and bound proteins were separated by SDS-PAGE. Gels were first stained with Gelcode Blue Stain Reagent (Pierce) and then subjected to autoradiography. β-galactosidase assays were conducted as described previously [31].

Preparation of Antibodies Against RLI1 and SUP45.

The GST-RLI1 and GST-SUP45 fusion proteins encoded by pGEX-RLI1, pGEX-SUP45, respectively, were expressed in *E. coli* and purified from the WCE by incubation with Glutathione-Sepharose 4B beads (Pharmacia). The isolated proteins were resolved by SDS-PAGE (4-20% gels), excised from the gel, and washed with 1x PBS. Rabbits were injected with the purified protein and sera containing polyclonal antibodies against RLI1, SUP45, respectively, were obtained commercially by Apronex (Prague, the Czech Republic).

SUPPORTING REFERENCES

1. Burnicka-Turek O, Kata A, Buyandelger B, Ebermann L, Kramann N, et al. (2010) Pelota interacts with HAX1, EIF3G and SRPX and the resulting protein complexes are associated with the actin cytoskeleton. BMC Cell Biol 11: 28.
2. Schuldiner M, Collins SR, Thompson NJ, Denic V, Bhamidipati A, et al. (2005) Exploration of the function and organization of the yeast early secretory pathway through an epistatic miniarray profile. Cell 123: 507-519.
3. Szamecz B, Rutkai E, Cuchalova L, Munzarova V, Herrmannova A, et al. (2008) eIF3a cooperates with sequences 5' of uORF1 to promote resumption of scanning by post-termination ribosomes for reinitiation on GCN4 mRNA. Genes Dev 22: 2414-2425.
4. ElAntak L, Wagner S, Herrmannová A, Karásková M, Rutkai E, et al. (2010) The indispensable N-terminal half of eIF3j co-operates with its structurally

conserved binding partner eIF3b-RRM and eIF1A in stringent AUG selection. J Mol Biol 396: 1097-1116.
5. Kouba T, Rutkai E, Karasková M, Valášek LS (2012) The eIF3c/NIP1 PCI domain interacts with RNA and RACK1/ASC1 and promotes assembly of the pre-initiation complexes. Nucleic Acids Research 40: 2683-2699.
6. Cuchalová L, Kouba T, Herrmannová A, Danyi I, Chiu W-l, et al. (2010) The RNA Recognition Motif of Eukaryotic Translation Initiation Factor 3g (eIF3g) Is Required for Resumption of Scanning of Posttermination Ribosomes for Reinitiation on GCN4 and Together with eIF3i Stimulates Linear Scanning. Mol Cell Biol 30: 4671-4686.
7. Valášek L, Hašek J, Trachsel H, Imre EM, Ruis H (1999) The *Saccharomyces cerevisiae HCRI* gene encoding a homologue of the p35 subunit of human translation eukaryotic initiation factor 3 (eIF3) is a high copy suppressor of a temperature-sensitive mutation in the Rpg1p subunit of yeast eIF3. J Biol Chem 274: 27567-27572.
8. Bradley ME, Bagriantsev S, Vishveshwara N, Liebman SW (2003) Guanidine reduces stop codon read-through caused by missense mutations in SUP35 or SUP45. Yeast 20: 625-632.
9. Chernoff YO, Derkach IL, Inge-Vechtomov SG (1993) Multicopy SUP35 gene induces de-novo appearance of psi-like factors in the yeast Saccharomyces cerevisiae. Curr Genet 24: 268-270.
10. Dong J, Lai R, Nielsen K, Fekete CA, Qiu H, et al. (2004) The essential ATP-binding cassette protein RLI1 functions in translation by promoting preinitiation complex assembly. J Biol Chem 279: 42157-42168.
11. Nielsen KH, Valášek L, Sykes C, Jivotovskaya A, Hinnebusch AG (2006) Interaction of the RNP1 motif in PRT1 with HCR1 promotes 40S binding of eukaryotic initiation factor 3 in yeast. Mol Cell Biol 26: 2984-2998.
12. Nielsen KH, Szamecz B, Valasek LJ, A., Shin BS, Hinnebusch AG (2004) Functions of eIF3 downstream of 48S assembly impact AUG recognition and GCN4 translational control. EMBO J 23: 1166-1177.
13. Kispal G, Sipos K, Lange H, Fekete Z, Bedekovics T, et al. (2005) Biogenesis of cytosolic ribosomes requires the essential iron-sulphur protein Rli1p and mitochondria. EMBO J 24: 589-598.
14. Keeling KM, Lanier J, Du M, Salas-Marco J, Gao L, et al. (2004) Leaky termination at premature stop codons antagonizes nonsense-mediated mRNA decay in S. cerevisiae. RNA 10: 691-703.
15. Munzarová V, Pánek J, Gunišová S, Dányi I, Szamecz B, et al. (2011) Translation Reinitiation Relies on the Interaction between eIF3a/TIF32 and Progressively Folded cis-Acting mRNA Elements Preceding Short uORFs. PLoS Genet 7: e1002137.
16. Herrmannová A, Daujotyte D, Yang JC, Cuchalová L, Gorrec F, et al. (2012) Structural analysis of an eIF3 subcomplex reveals conserved interactions required for a stable and proper translation pre-Initiation complex assembly. Nucleic Acids Res 40: 2294-2311.
17. Gietz RD, Sugino A (1988) New yeast-Escherichia coli shuttle vectors constructed with in vitro mutagenized yeast genes lacking six-base pair restriction sites. Gene 74: 527-534.
18. Chiu W-L, Wagner S, Herrmannová A, Burela L, Zhang F, et al. (2010) The C-Terminal Region of Eukaryotic Translation Initiation Factor 3a (eIF3a) Promotes mRNA Recruitment, Scanning, and, Together with eIF3j and the

eIF3b RNA Recognition Motif, Selection of AUG Start Codons. Mol Cell Biol 30: 4415-4434.
19. Olsen DS, Savner EM, Mathew A, Zhang F, Krishnamoorthy T, et al. (2003) Domains of eIF1A that mediate binding to eIF2, eIF3 and eIF5B and promote ternary complex recruitment *in vivo*. EMBO J 22: 193-204.
20. Smith DB, Johnson KS (1988) Single-step purification of polypeptides expressed in Escherichia coli as fusions with glutathione S-transferase. Gene 67: 31-40.
21. Asano K, Phan L, Anderson J, Hinnebusch AG (1998) Complex formation by all five homologues of mammalian translation initiation factor 3 subunits from yeast *Saccharomyces cerevisiae*. J Biol Chem 273: 18573-18585.
22. Valášek L, Phan L, Schoenfeld LW, Valášková V, Hinnebusch AG (2001) Related eIF3 subunits TIF32 and HCR1 interact with an RNA recoginition motif in PRT1 required for eIF3 integrity and ribosome binding. EMBO J 20: 891-904.
23. Grant CM, Miller PF, Hinnebusch AG (1994) Requirements for intercistronic distance and level of eIF-2 activity in reinitiation on GCN4 mRNA varies with the downstream cistron. Mol Cell Biol 14: 2616-2628.
24. Puig O, Caspary F, Rigaut G, Rutz B, Bouveret E, et al. (2001) The Tandem Affinity Purification (TAP) method: a general procedure of protein complex purification. Methods 24: 218-229.
25. Valášek L, Nielsen KH, Zhang F, Fekete CA, Hinnebusch AG (2004) Interactions of Eukaryotic Translation Initiation Factor 3 (eIF3) Subunit NIP1/c with eIF1 and eIF5 Promote Preinitiation Complex Assembly and Regulate Start Codon Selection. Mol Cell Biol 24: 9437-9455.
26. Muhlrad D, Parker R (1999) Recognition of yeast mRNAs as "nonsense containing" leads to both inhibition of mRNA translation and mRNA degradation: implications for the control of mRNA decapping. Mol Biol Cell 10: 3971-3978.
27. Merritt GH, Naemi WR, Mugnier P, Webb HM, Tuite MF, et al. (2010) Decoding accuracy in eRF1 mutants and its correlation with pleiotropic quantitative traits in yeast. Nucleic Acids Res 38: 5479-5492.
28. Nielsen KH, Valášek L (2007) In vivo deletion analysis of the architecture of a multi-protein complex of translation initiation factors. Methods Enzymol 431: 15-32.
29. Valášek L, Trachsel H, Hašek J, Ruis H (1998) Rpg1, the *Saccharomyces cerevisiae* homologue of the largest subunit of mammlian translation initiation factor 3, is required for translational activity. J Biol Chem 273: 21253-21260.
30. Valášek L, Szamecz B, Hinnebusch AG, Nielsen KH (2007) In vivo stabilization of preinitiation complexes by formaldehyde cross-linking. Methods Enzymol 429: 163-183.
31. Grant CM, Hinnebusch AG (1994) Effect of sequence context at stop codons on efficiency of reinitiation in *GCN4* translational control. Mol Cell Biol 14: 606-618.

Discussion

Mapping the eIF3 binding site on the 40S ribosome

Previous studies of yeast Saccharomyces cerevisiae eIF3 demonstrated that it plays a stimulatory role in nearly all steps of the canonical translation initiation pathway. The multiprotein eIF3 complex, together with eIFs 1, 1A, and 5, promotes recruitment of the Met-$tRNA_i^{Met}$/eIF2/GTP ternary complex (TC) to the small ribosomal subunit (40S), producing the 43S preinitiation complex (PIC). eIFs 1, 3, and 5 and the TC occur in a preformed unit called the multifactor complex (MFC) and we and others previously demonstrated that there is a substantial cooperation among the eIFs assembled in the MFC in their binding to the 40S as well as their ribosome-associated functions in scanning and AUG recognition (Valášek, Mathew et al. 2003; Nielsen, Szamecz et al. 2004; Chiu, Wagner et al. 2010; Cuchalová, Kouba et al. 2010; ElAntak, Wagner et al. 2010; Herrmannová, Daujotyte et al. 2012)

Systematic effort was devoted to mapping the binding site of eIF3 on the 40S. We earlier identified several important domains of eIF3 subunits and eIF5 mediating interaction of the MFC with the 40S that allowed us to predict certain aspects of the organization of the 43S PIC (Valášek, Mathew et al. 2003). Importantly, the findings that the a/TIF32-CTD interacts with helices 16–18 of 18S rRNA (Valášek, Mathew et al. 2003) and RPS2 and RPS3 (Chiu, Wagner et al. 2010), all of which occurs near the mRNA entry channel (Chiu, Wagner et al. 2010), and that a/TIF32-NTD binds to ribosomal proteins RPS0A and RPS10A *in vitro* (Valášek, Mathew et al. 2003) suggested that yeast eIF3 associates with the solvent-exposed side of the 40S, as proposed by others for mammalian eIF3 (Srivastava, Verschoor et al. 1992; Siridechadilok, Fraser et al. 2005). The latter suggestion was later supported by our finding that the partial deletion of the RPS0A-binding domain of eIF3a impairs translation initiation and reduces binding of eIF3 and associated eIFs to native preinitiation complexes *in vivo* (Szamecz, Rutkai et al. 2008). Since it also reduced 40S association of the TC and eIF5, we concluded that eIF3 stimulates 40S-binding also of other MFC components. Subsequently, other points of contacts between eIF3 and the 40S subunit that have been mapped such as those between (i) the j/HCR1-CTD and RPS2 and RPS23 (Chiu, Wagner et al. 2010), the C-

terminal proteasome component (PCI) domain of c/NIP1 and RACK1/ASC1/RPS33 and probably also 18S rRNA segments of the solvent-exposed head region (Kouba, Rutkai et al. 2012). Finally, in my work presented here we showed that g/TIF35 interacts with the 40S beak proteins RPS20 and mainly with RPS3 (Cuchalová, Kouba et al. 2010), which is one of the main components of the conformational change upon scanning arrest which is characterized by dissolution of the contact between RPS3 and helix 16 of 18S rRNA and reformation of the helix18–helix34-RPS3 connection designated as the latch at the mRNA entry channel (Passmore, Schmeing et al. 2007). Besides the aforementioned interaction of the c/NIP1-PCI with RACK1/ ASC1 and 18S rRNA that was characterized by mutational analysis of both binding partners (Kouba, Rutkai et al. 2012), our very recent work, belonging to the Ph.D. thesis, also concluded characterization of the aforementioned intermolecular bridge spanning between the RPS0A and the a/TIF32-NTD by showing that deletion of the C-terminal tail (CTT) of RPS0A fails to anchor the MFC to the small ribosomal subunit, as would be predicted (Kouba, Danyi et al. 2012). Based on all these interactions we concluded that at least the NTD of a/TIF32 and the PCI domain in the c/NIP1-CTD form important intermolecular bridges between eIF3 and the 40S via its RPS0A and ASC1 protein constituents, and modified our original model of the eIF3 position on the 40S subunit.

Fig. 3

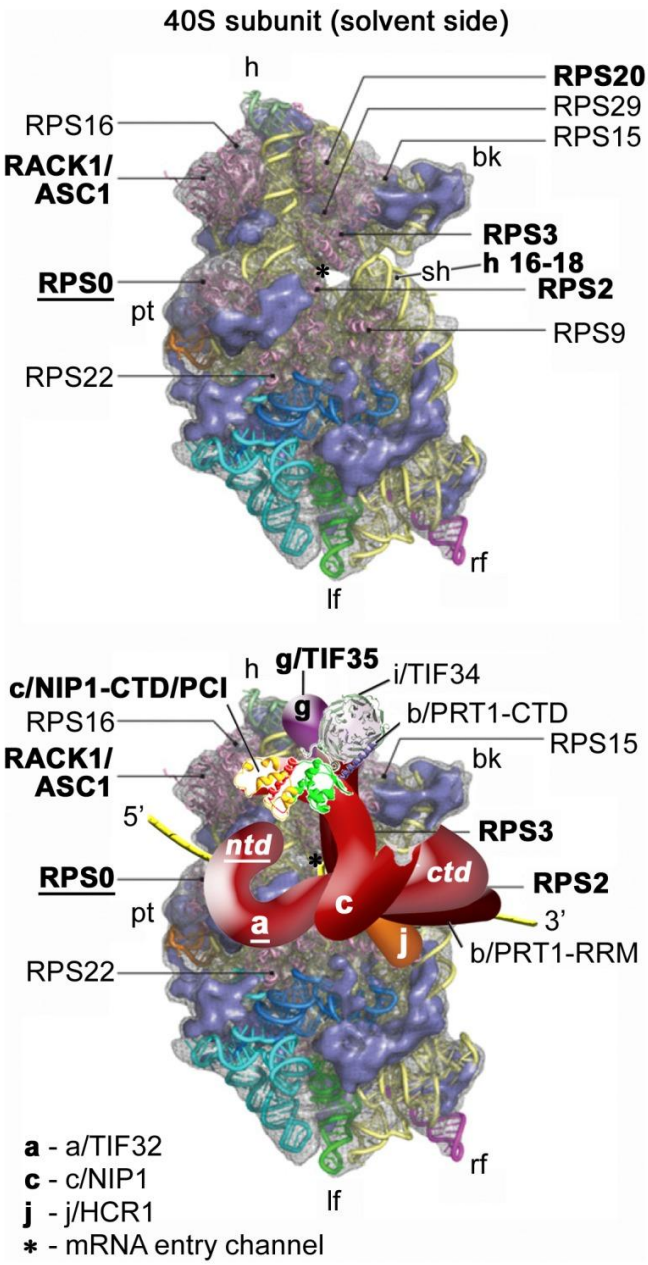

Model of the hypothetical location of eIF3 on the *S. cerevisiae* small ribosomal subunit (Kouba, Danyi et al. 2012).

Characterization of the two smallest core subunits of eIF3 and their roles in translation

In other series of articles, we focused on functional characterization of two small subunits of eIF3, g/TIF35 and i/TIF34, the cellular roles of which have remained highly elusive even though these subunits are essential for the viability of yeast cells (Naranda, Kainuma et al. 1997; Humphrey and Enoch 1998; Hanachi, Hershey et al. 1999). Even more, detailed biochemical analysis carried out with purified eIF3 subcomplexes identified that the trimeric complex of a/ TIF32, b/PRT1 and c/NIP1 promoted TC and mRNA recruitment to the 40S subunit and even stimulated translation in vitro on a model mRNA as efficiently as the wild-type (wt) five subunit complex (Phan, Schoenfeld et al. 2001). Hence given the aforementioned fact that i/TIF34 and g/TIF35 subunits are otherwise essential for cell proliferation and their individual depletions result in a typical polysome run-off (Naranda, Kainuma et al. 1997), their cellular roles were for long time fairly mysterious.

Yeast i/TIF34 is composed of seven WD40 repeats assembled into a propeller ring and has been shown to interact with the NTD of g/TIF35 and the extreme CTD of b/PRT1 (Asano, Phan et al. 1998; Valášek, Nielsen et al. 2002). The functionally important yet nonessential C-terminal domain of g/TIF35 is formed by the canonical RRM previously shown to possess nonspecific RNA-binding activity (Hanachi, Hershey et al. 1999). We tested the g/TIF35 and i/TIF34 mutants for specific phenotypes indicating impairment of translational control of *GCN4* expression (Hinnebusch 2005). This mechanism has been extensively used in the past as a valuable genetic tool for dissecting the contributions of individual eIFs to translation initiation (Szamecz, Rutkai et al. 2008; Cuchalová, Kouba et al. 2010; Valášek 2012). We found that substitutions of conserved residues of the RRM of g/TIF35 in g/TIF35-KLF significantly reduced processivity of scanning through a stable stem-loop structure inserted into the uORF-less *GCN4* mRNA leader; this prevented a large proportion of scanning PICs from reaching the coding region. We also demonstrated that the single point mutation Q258R, mapping to the WD40 repeat 6 of i/Tif34, markedly impairs the rate of scanning of the 40S ribosomes that translate *GCN4*'s uORF1 and resume scanning downstream. Besides the fact that both subunits stimulate linear scanning, they genetically interact with several scanning-promoting initiation factors (Cuchalová, Kouba et al. 2010).

Scanning consists of two linked processes: unwinding of secondary structures in the 5' UTR and ribosomal movement along it. In a simplified *in vitro* system with model, unstructured mRNA, the eIF3-containing 43S PICs can scan through its unstructured 5´ UTRs without factors associated with RNA unwinding and are thus intrinsically capable of movement along mRNA (Pestova and Kolupaeva 2002). Omission of eIF1A substantially reduces this ability and lack of eIF1 almost abrogates it, indicating that movement of the 43S complexes requires at minimum the open/scanning-conducive conformation induced by the synergistic actions of eIF1 and eIF1A (Passmore, Schmeing et al. 2007). In contrast, scanning along 5´ UTRs containing even weak secondary structures requires ATP and eIF4A, eIF4G, and eIF4B (Pestova and Kolupaeva 2002). However, the mechanism by which these factors assist scanning remains unknown for years.

Furthermore, we reported the 2.2A ˚ resolution crystal structure of the i/TIF34 subunit in complex with the minimal CTD of b/PRT1 (654–700), the boundaries of which we defined by solution NMR spectroscopy (Fig 4.) (Herrmannová, Daujotyte et al. 2012). Mutating the conserved residues mediating the b/PRT1—i/TIF34 contact resulted in lethality or severe growth phenotypes owing to the loss of the i/TIF34-g/TIF35 mini-module from the rest of eIF3 and from pre-initiation complexes (PICs). Since binding of the remaining a/TIF32-b/PRT1-c/NIP1 subcomplex and eIF5 was also unexpectedly destabilized, aberrant PICs containing eIFs 2 and 1 accumulated and dramatically increased leaky scanning over the AUG start codon in the manner suppressible by overexpression of g/TIF35 and eIF1. Hence we proposed that stable association of the i/TIF34–g/TIF35 mini-module with the rest of eIF3 via b/PRT1 significantly stabilizes binding of eIF3 and eIF5 to the nascent pre-initiation complexes in vivo and ensure fidelity of scanning (Herrmannová, Daujotyte et al. 2012).

To summarize the observed findings about i/TIF34 and TIF35: (i) both are essential, (ii) according to previous reports, neither yeast i/TIF34 and g/TIF35 nor mammalian eIF3g appears to be required for assembly of the 48S PIC, which includes sequential recruitment of the TC and mRNA to the 40S subunit (Phan, Schoenfeld et al. 2001; Masutani, Sonenberg et al. 2007), (iii) stable association of the i/Tif34–g/Tif35 stabilizes binding of eIF3 and eIF5 to the nascent pre-initiation complexes in vivo (Herrmannová, Daujotyte et al. 2012), (iv) both two subunits are involved in promoting the rate and processivity of scanning in living cells (Cuchalová, Kouba et al. 2010), (v) g/TIF35 specifically interacts with RPS3 and RPS20

located near the ribosomal mRNA entry channel (Cuchalová, Kouba et al. 2010), (vi) the RRM of g/TIF35, along with the a/TIF32-NTD, plays role in stabilizing uORF1 post-termination 40S ribosomes on *GCN4* mRNA and/or in promoting resumption of scanning for REI downstream (Cuchalová, Kouba et al. 2010) (discussed below), (vii) we have observed an interaction between these two small eIF3 subunits with the N and N-M domains of release factor eRF1(discussed below) (Cuchalova and Beznoskova et al. under the review). The essential character of both small eIF3 subunits might explained by suggesting that the loss of their stimulatory effects on scanning predominantly compromises translation of a subset of critical mRNAs encoding tightly regulated genes, such as those involved in cell cycle regulation, signal transduction, etc. - mRNAs which often have long 5´-UTRs rich in secondary structures (van der Velden and Thomas 1999; Kozak 2005). This proposal is consistent with earlier observations showing that (i) specific mutations in i/TIF34 or overexpression of its fission yeast homolog Sum1 deregulates progression through the cell cycle and affects mating and the osmotic stress response (Verlhac, Chen et al. 1997; Humphrey and Enoch 1998), and (ii) overexpression of human eIF3i, often observed in carcinomas, resulted in cell size increase, proliferation enhancement, cell cycle progression, and anchorage-independent growth (Ahlemann, Zeidler et al. 2006) etc..

Fig.4

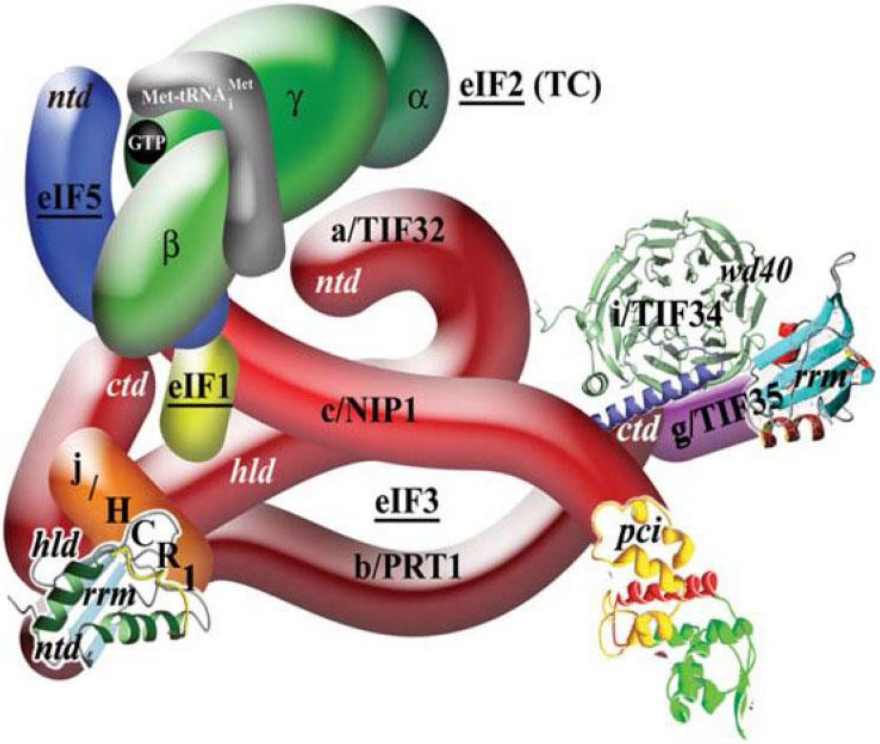

3D model of eIF3 and its associated eIFs in the MFC (Herrmannová, Daujotyte et al. 2012)

eIF3 is critical for resumption of scanning by post-termination ribosomes

Reinitiation is a gene-specific translational control mechanism characterized by the ability of some short upstream uORFs to retain post-termination 40S subunits on mRNA. In order to reinitiate translation on the downstream main ORF, a ribosome has to stay bound to mRNA after it has terminated short uORF translation. It was proposed that REI might be depended on the post-termination interaction between eIF4G and the 40S ribosomal subunit, reinitiation was observed when the mRNA was translated in a system containing all the initiation factors, but not in an eIF4G-depleted system (Pöyry, Kaminski et al. 2004). Interestingly, this interaction is in mammalian PICs bridged by eIF3 (Korneeva, Lamphear et al. 2000), most probably via the e subunit of eIF3, which is absent from yeast (Hinnebusch 2006; LeFebvre, Korneeva et al. 2006). Accordingly, yeast eIF3 and eIF4G make only indirect interactions bridged by eIF5 and eIF1 (Hinnebusch 2006). Nevertheless, interestingly, it seems that eIF3 and eIF4G stay as the only factors bound to the 40S subunit after the

formation of the active 80S complex and may even remain bound for several elongation cycles (Szamecz, Rutkai et al. 2008). As aforementioned, both mammalian and yeast eIF3 are believed to bind primarily to the solvent-exposed side of the 40S, which would not impose any restrains on their prolonged staying with the 40S subunit already joined by the large 60S subunit. Together, these facts provoked an idea that eIF3, together with eIF4G, could be a possible key player in reinitiation. To examine that, we employed the translational control mechanism of *GCN4* expression, which has been extensively used in the past as a valuable genetic tool for dissecting the contributions of individual eIFs to translation initiation (Hinnebusch 2005; Szamecz, Rutkai et al. 2008; Chiu, Wagner et al. 2010; Cuchalová, Kouba et al. 2010; ElAntak, Wagner et al. 2010).

In two studies that I co-authored, we revealed that eIF3 is indeed critical for resumption of scanning by post-termination ribosome, which is a vital prerequisite for efficient REI. In detail, we detected a genetic interaction between the partial deletion of the RPS0A-binding site in the a/TIF32-NTD (Δ8) and mutations in sequences 5´ of uORF1, wherein the deleterious effect of a/TIF32-Δ8 on REI is blunted or even eliminated by these 5' UTR mutations. Genetic epistasis interactions between mutations in the identified stimulatory sequences upstream of uORF1 and a/TIF32-Δ8 strongly indicated that eIF3a interacts with these REI-enhancing sequences that we named a/TIF32-NTD-responsive site (eIF3a-RS). We proposed that establishment of the interaction between a/TIF32-NTD and the specific eIF3a-RS 5' of uORF1 at or near the mRNA exit channel of the post-termination 40S subunit stabilizes its association with mRNA and promotes the resumption of scanning for efficient REI at the downstream ORF. In support of this, the immediately following region still within the NTD of a/TIF32 interacts with the small ribosomal protein RPS0A, as aforementioned, which is positioned near the mRNA exit pore on the solvent side of the small subunit, where the uORF1's 5' enhancer occurs, already out of the mRNA binding channel, on the post-termination 40S ribosome (Szamecz, Rutkai et al. 2008). My colleagues from our laboratory further extended these studies by identification of four particularly critical nucleotide sequence and/or structural motifs, which they named REI-promoting elements (RPEs) (Munzarová, Pánek et al. 2011). Two of them were shown to operate in the a/TIF32-NTD dependent manner. Similarly, systematic alanine substitutions of consecutive blocks of 10 residues throughout the a/TIF32-NTD revealed three particularly critical REI motifs (amino

acids 51-60, 71-80 and 161-170), which most probably directly interact with the very two RPEs. Together these findings led to a model in which wild-type eIF3 remains at least transiently associated with the translating 80S ribosome via RPS0A and other mutual contacts with the solvent-exposed side of the 40S subunit, and if it does not drop off prior to termination, the extreme NTD of a/TIF32 interacts with the 5' enhancer to permit ribosomal recycling of only the large 60S subunit, while aiding to preserve the small subunit on the GCN4 mRNA (Munzarová, Pánek et al. 2011).

In the second study that I co-authored as the first author, g/TIF35-KLF (substitutions of conserved residues of the RRM) were shown to provoke a strong Gcn$^-$ phenotype owing to the inability of post-termination 40S subunits at the *GCN4*'s uORF1 to resume scanning for reinitiation downstream. We conclude that besides a/TIF32, g/TIF35 also most likely promotes REI. Hence, this fact is further supported by another aforementioned observation that it interacts with the 40S beak proteins RPS20 and mainly with RPS3. Detailed genetic analysis revealed, however, that the g/TIF35-RRM and the a/TIF32-NTD ensure efficient resumption of scanning by different molecular mechanisms (Cuchalová, Kouba et al. 2010). In fact, since both a/TIF32-NTD and g/TIF35-RRM seem to occupy different positions on the back of the 40S, it is not really surprising that the nature of their involvement in the initial REI phase is mechanistically different, at least to a certain extent. In general support of our major conclusion that eIF3 is critical for efficient REI in yeast, also mammalian eIF3 was identified as the key factor required for REI after translation of a long ORF2 that overlaps the beginning of a downstream ORF3 on polycistronic subgenomic mRNA of feline calicivirus. Analogously, the authors found that REI on ORF3 is enhanced by an 87-nt element at the 3' end of ORF2 that functions at least partly as a binding site for eIF3 (Pöyry, Kaminski et al. 2007).

eIF3 critically connects initiation of translation with its termination

In contrast to the intense focus on elucidating the molecular mechanism of translation initiation going back almost 40 years, termination and, especially, post-termination events in eukaryotic mRNA translation, such as ribosomal recycling, have been relatively neglected until quite recently. It is becoming increasingly apparent that factors involved in regulating

various steps of gene expression may have multiple functions and that this multitasking may integrate transcription, mRNA export, translation and mRNA decay into a delicately regulated higher-order process. For example, translation initiation factor eIF3 links translation initiation to transcription (Harel-Sharvit, Eldad et al. 2010), to mRNA export (Bolger, Folkmann et al. 2008) and to the NMD pathway (Isken, Kim et al. 2008; Sha, Brill et al. 2009). In addition, eIF3, together with eIFs 1 and 1A, has been also implicated in ribosomal recycling. Since the implication of eIF3 in the recycling process was, however, deduced only from experiments carried out with 11-codon long model mRNA in mammalian *in vitro* reconstituted systems, we decided to investigate whether or not eIF3 also plays a direct role in translation termination and/or ribosomal recycling in the living cell. In our article, currently under review in PLOS Biology, where I am as one of the first two co-authors, we showed for the first time that besides initiation, eIF3 also promotes translation termination. In detail, we demonstrated that eIF3 occurs together with eRFs 1 and 3 and the ribosomal recycling factor RLI1 in a ribosome- and RNA-free complex in vivo. Various mutants of core eIF3 subunits, but not of other initiation factors, decreased stop codon read-through in living cells (actually, decreased stop codon read-through is a novel phenotype, never ever observed before) and showed synthetic phenotypes with mutant release factors eRF1 and 3. Conversely, deletion of the non-essential j/HCR1 subunit of eIF3 increased stop codon read-through and resulted in accumulation of eRF3 in heavy polysomes. Finally, increased dosage of RLI1 was shown to substitute for the j/HCR1 roles in termination (but not in initiation) and in enabling efficient cell growth, as it fully suppressed both the read-through as well as slow growth phenotypes of the *hcr1Δ* strain, implying that the j/HCR1 function in termination is more critical for optimal cell proliferation than its function in translation initiation (Cuchalova and Beznoskova et al. under the review).

The fact that we could detect a complex between eIF3, RLI1 and both eRFs free of RNA and ribosomes, and that two small eIF3 subunits i/TIF34 and g/TIF35 directly interacted with the N and N-M domains of eRF1 as mentioned above, suggests that at least eIF3 and eRFs come to the pre-TC in a pre-formed complex (Cuchalova and Beznoskova et al. under the review). The alternative that they are ejected from post-TCs as a holocomplex upon completion of termination is highly unlikely considering that i) eRF3 must be ejected prior to RLI1 binding (Shoemaker and Green 2011), and ii) that eIF3 is supposed to participate in the

late steps of ribosomal recycling that should be devoid of eRF1 and RLI1 (Pisarev, Hellen et al. 2007; Pisarev, Skabkin et al. 2010). The last scenario would be that eIF3 stays present on the elongating ribosome throughout the entire elongation cycle and promotes recruitment of eRF1·eRF3·GTP to the pre-TCs; there is, however, indirect evidence contradicting this possibility (Szamecz, Rutkai et al. 2008).

During stop codon decoding, eRF1 was proposed to sit in the ribosomal A-site with a part of its N domain contacting small ribosomal protein RPS3 and helix (h) 18 of 18S rRNA (Taylor, Unbehaun et al. 2012). Strikingly, g/TIF35 also interacts with RPS3, in addition to RPS20 (Cuchalová, Kouba et al. 2010), and as both g/TIF35 and i/TIF34 are tightly bound to the extreme C-terminus of b/PRT1 (Herrmannová, Daujotyte et al. 2012) , i/TIF34 is expected to occur nearby g/TIF35. Moreover, the C-terminal domain of a/TIF32 interacts with h16-18 of 18S rRNA (Valášek, Mathew et al. 2003). Taylor and colleagues further proposed that one of the conformational changes induced by eRF1–eRF3–GMPPNP binding to pre-TCs involves a movement of h16 of 18S rRNA and the N-terminal domain (NTD) of RPS3 toward each other, which results in the establishment of a new head–body connection on the solvent side of the 40S subunit and a constriction of the mRNA entrance. Hence, it is easily conceivable that eRF1 and eIF3 preserve and subsequently rearrange their mutual contacts in the termination complexes upon their formation. These contacts could for example impair proper orientation of eRF1 in the spatially restricted A-site, thus providing a rational explanation for the antagonistic effect of eIF3 on translation termination (eRF1 and 3 mutants increase, whereas eIF3 mutants decrease the read-through phenotype.

Based on all of these findings, we proposed the following model (Fig. 5). Upon the stop codon entry into the ribosomal A-site the pre-TC forms, composed of the canonical release factors eRF1 and eRF3·GTP and eIF3. eRFs and eIF3 may associate with the pre-TC as a pre-formed unit or alone. Theoretically it is also possible that eIF3 dynamically associates and dissociates during the entire elongation phase. In the pre-TC, eIF3 interacts with the N domain of eRF1, *via* its two small i/TI34 and g/TIF35 subunits, and modulates its stop codon recognition activity during the proofreading step. Upon stop codon recognition the GTP molecule on eRF3 is hydrolyzed. Subsequently, j/HCR1 promotes eRF3·GDP ejection to allow the ABCE1/RLI1·ATP recruitment to begin the accommodation phase of termination –

the eRF1 GGQ motif is pushed to the peptidyl-transferase center (PTC) – during which j/HCR1 interacts with ABCE1/RLI1.

Since eIF3 was, based on *in vitro* experiments, previously implicated in promoting also the very final step of translation – ribosomal recycling (Pisarev, Hellen et al. 2007), as mentioned above, we propose that eIF3 is one of the very few factors that connects various processes of mRNA life and integrates them into the ultimate translational output. We also argue that strict mechanistic separation of translation into its individual, mutually independent phases should be reconsidered in the light of "multitasking" of eIF3, j/HCR1, RLI1 and most likely also eIF1 and eIF1A. Collectively, these findings suggest that changes in one phase of translation, evoked for example via cell signaling pathways, are promptly communicated to and coordinated with changes in the other phases to maintain cellular homeostasis of all ongoing processes. Without a doubt there is much to be learned about how all four phases of translation come together in one balanced system that rapidly and accurately responds to different needs of the cell exposed to constantly changing environmental conditions.

Fig. 5

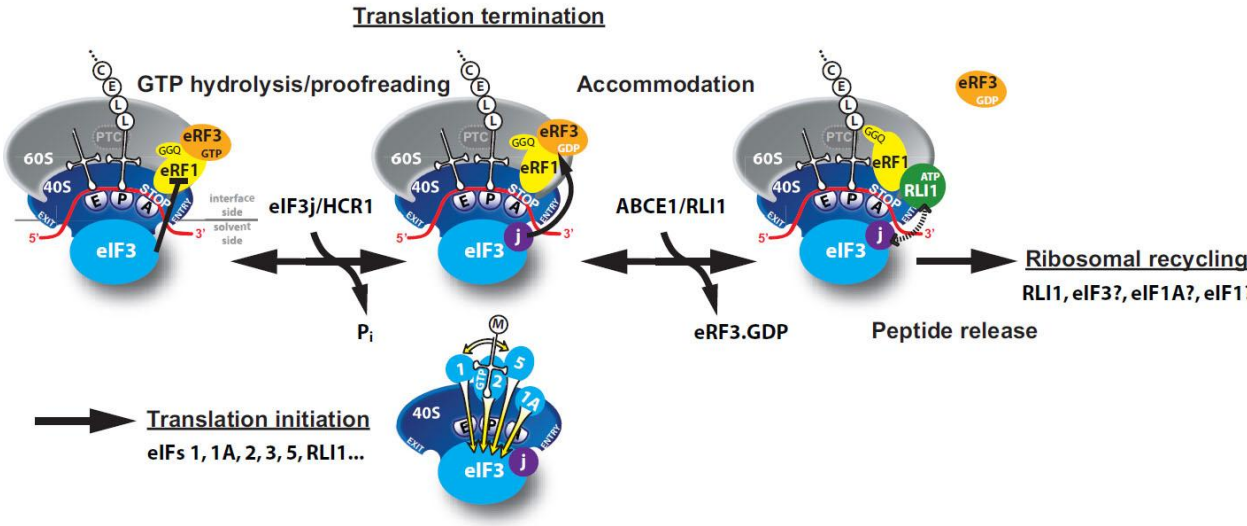

Model of eIF3 Involvement in Yeast Translation termination

General conclusions:

We demonstrated biochemical and genetic mapping of yeast eIF3 binding site on the small ribosomal subunit that enabled us to model the organization of the eIF3-40S complex.

We focused on functional characterization of two small essential subunits of eIF3, g/TIF35 and i/TIF34, and provide the first insights into their functional contributions to general translation initiation as well as to translational control of GCN4 expression. Furthermore, we reported crystal structure of i/TIF34 subunit in complex with the minimal CTD of b/PRT1.

We revealed that a/TIF32-NTD and g/TIF35-RRM, are needed critical for resumption of scanning by post-termination ribosome, which is a vital prerequisite for efficient reinitiation. Finally, we identified and define the role of eIF3 in termination and our findings suggest that changes in one phase of translation are promptly communicated to and coordinated with changes in the other phases to maintain cellular homeostasis of all ongoing processes.

References

Ahlemann, M., R. Zeidler, et al. (2006). "Carcinoma-associated eIF3i overexpression facilitates mTOR-dependent growth transformation." Molecular Carcinogenesis 45(12): 957-967.

Algire, M. A., D. Maag, et al. (2005). "Pi release from eIF2, not GTP hydrolysis, is the step controlled by start-site selection during eukaryotic translation initiation." Mol Cell 20: 251-62.

Asano, K., L. Phan, et al. (1998). "Complex formation by all five homologues of mammalian translation initiation factor 3 subunits from yeast Saccharomyces cerevisiae." J Biol Chem 273: 18573-18585.

Becker, T., S. Franckenberg, et al. (2012). "Structural basis of highly conserved ribosome recycling in eukaryotes and archaea." Nature 482(7386): 501-6.

Bolger, T. A., A. W. Folkmann, et al. (2008). "The mRNA export factor Gle1 and inositol hexakisphosphate regulate distinct stages of translation." Cell 134(4): 624-33.

Calvo, S. E., D. J. Pagliarini, et al. (2009). "Upstream open reading frames cause widespread reduction of protein expression and are polymorphic among humans." PNAS 106: 7507-7512.

Cheung, Y. N., D. Maag, et al. (2007). "Dissociation of eIF1 from the 40S ribosomal subunit is a key step in start codon selection in vivo." Genes Dev 21: 1217-30.

Chiu, W.-L., S. Wagner, et al. (2010). "The C-Terminal Region of Eukaryotic Translation Initiation Factor 3a (eIF3a) Promotes mRNA Recruitment, Scanning, and, Together with eIF3j and the eIF3b RNA Recognition Motif, Selection of AUG Start Codons." Mol Cell Biol 30(18): 4415-34.

Cuchalová, L., T. Kouba, et al. (2010). "The RNA Recognition Motif of Eukaryotic Translation Initiation Factor 3g (eIF3g) Is Required for Resumption of Scanning of Posttermination Ribosomes for Reinitiation on GCN4 and Together with eIF3i Stimulates Linear Scanning." Mol Cell Biol 30(19): 4671-4686.

Dong, J., R. Lai, et al. (2004). "The essential ATP-binding cassette protein RLI1 functions in translation by promoting preinitiation complex assembly." J Biol Chem 279(40): 42157-68.

ElAntak, L., S. Wagner, et al. (2010). "The indispensable N-terminal half of eIF3j co-operates with its structurally conserved binding partner eIF3b-RRM and eIF1A in stringent AUG selection." J Mol Biol. 396: 1097-1116.

Gao, N., A. V. Zavialov, et al. (2007). "Specific Interaction between EF-G and RRF and Its Implication for GTP-Dependent Ribosome Splitting into Subunits." Journal of Molecular Biology 374(5): 1345-1358.

Grant, C. M. and A. G. Hinnebusch (1994). "Effect of sequence context at stop codons on efficiency of reinitiation in GCN4 translational control." Mol Cell Biol 14: 606-618.

Grant, C. M., P. F. Miller, et al. (1994). "Requirements for intercistronic distance and level of eIF-2 activity in reinitiation on GCN4 mRNA varies with the downstream cistron." Mol Cell Biol 14: 2616-2628.

Grant, C. M., P. F. Miller, et al. (1995). "Sequences 5' of the first upstream open reading frame in GCN4 mRNA are required for efficient translational reinitiation." Nuc Acids Res 23: 3980-3988.

Hanachi, P., J. W. B. Hershey, et al. (1999). "Characterization of the p33 subunit of eukaryotic translation initiation factor-3 from Saccharomyces cerevisiae." J Biol Chem 274: 8546-8553.

Harel-Sharvit, L., N. Eldad, et al. (2010). "RNA polymerase II subunits link transcription and mRNA decay to translation." Cell 143(4): 552-63.

Herrmannová, A., D. Daujotyte, et al. (2012). "Structural analysis of an eIF3 subcomplex reveals conserved interactions required for a stable and proper translation pre-Initiation complex assembly." Nucleic Acids Res. 40(5): 2294-311.

Hinnebusch, A. G. (2005). "Translational regulation of GCN4 and the general amino acid control of yeast." Annu Rev Microbiol. 59: 407-50.

Hinnebusch, A. G. (2006). "eIF3: a versatile scaffold for translation initiation complexes." Trends Biochem Sci. 31: 553-562.

Hinnebusch, A. G. (2011). "Molecular Mechanism of Scanning and Start Codon Selection in Eukaryotes." Microbiology and Molecular Biology Reviews 75(3): 434-467.

Hinnebusch, A. G., T. E. Dever, et al. (2007). Mechanism of translation initiation in the yeast Saccharomyces cerevisiae. Translational Control in biology and medicine. N. Sonenberg, M. Mathews and J. W. B. Hershey. Cold Spring Harbor, NY., Cold Spring Harbor Laboratory Press: 225-268.

Humphrey, T. and T. Enoch (1998). "Sum1, a highly conserved WD-repeat protein, suppresses S-M checkpoint mutants and inhibits the osmotic stress cell cycle response in fission yeast." Genetics 148: 1731-1742.

Isken, O., Y. K. Kim, et al. (2008). "Upf1 Phosphorylation Triggers Translational Repression during Nonsense-Mediated mRNA Decay." Cell 133: 314–327.

Jackson, R. J., C. U. Hellen, et al. (2012). "Termination and post-termination events in eukaryotic translation." Adv Protein Chem Struct Biol 86: 45-93.

Jackson, R. J., C. U. T. Hellen, et al. (2010). "The mechanism of eukaryotic translation initiation and principles of its regulation." Nat Rev Mol Cell Biol 11(2): 113-127.

Khoshnevis, S., T. Gross, et al. (2010). "The iron-sulphur protein RNase L inhibitor functions in translation termination." EMBO Rep 11(3): 214-219.

Klaholz, B. P. (2011). "Molecular recognition and catalysis in translation termination complexes." Trends in Biochemical Sciences 36(5): 282-292.

Komar, A. A., B. Mazumder, et al. "A new framework for understanding IRES-mediated translation." Gene 502(2): 75-86.

Kong, C., K. Ito, et al. (2004). "Crystal Structure and Functional Analysis of the Eukaryotic Class II Release Factor eRF3 from S. pombe." Molecular Cell 14(2): 233-245.

Korneeva, N. L., B. J. Lamphear, et al. (2000). "Mutually cooperative binding of eukaryotic translation initiation factor (eIF) 3 and eIF4A to human eIF4G-1." J Biol Chem 275: 41369-41376.

Kouba, T., I. Danyi, et al. (2012). "Small Ribosomal Protein RPS0 Stimulates Translation Initiation by Mediating 40S-binding of eIF3 via its Direct Contact with the eIF3a/TIF32 Subunit." PLoS One: in press.

Kouba, T., E. Rutkai, et al. (2012). "The eIF3c/NIP1 PCI domain interacts with RNA and RACK1/ASC1 and promotes assembly of the pre-initiation complexes." Nucleic Acids Research 40(6): 2683-99.

Kozak, M. (1986). "Point mutations define a sequence flanking the AUG initiator codon that modulates translation by eukaryotic ribosomes." Cell 44: 283-292.

Kozak, M. (1987). "Effects of intercistronic length on the efficiency of reinitiation by eucaryotic ribosomes." Mol Cell Biol 7: 3438-3445.

Kozak, M. (2001). "Constraints on reinitiation of translation in mammals." Nucleic Acids Res. 29: 5226-32.

Kozak, M. (2005). "Regulation of translation via mRNA structure in prokaryotes and eukaryotes." Gene 361: 13-37.

Kozak, M. and A. J. Shatkin (1978). "Migration of 40S ribosomal subunit on messenger RNA in the presence of edeine." J Biol Chem 253: 6568-6577.

Lee, J. H., T. V. Pestova, et al. (2002). "Initiation factor eIF5B catalyzes second GTP-dependent step in eukaryotic translation initiation." Proc Natl Acad Sci U S A 99(26): 16689-16694.

LeFebvre, A. K., N. L. Korneeva, et al. (2006). "Translation initiation factor eIF4G-1 binds to eIF3 through the eIF3e subunit." J Biol Chem 281: 22917-32.

Luukkonen, B. G., W. Tan, et al. (1995). "Efficiency of reinitiation of translation on human immunodeficiency virus type 1 mRNAs is determined by the length of the upstream open reading frame and by intercistronic distance." Journal of virology 69(7): 4086-4094.

Masutani, M., N. Sonenberg, et al. (2007). "Reconstitution reveals the functional core of mammalian eIF3." EMBO J. 26: 3373-83.

Mokrejs, M., T. Masek, et al. (2010). "IRESite- a tool for the examination of viral and cellular internal ribosome entry sites." Nucleic Acids Research 38(suppl 1): D131-D136.

Munzarová, V., J. Pánek, et al. (2011). "Translation Reinitiation Relies on the Interaction between eIF3a/TIF32 and Progressively Folded cis-Acting mRNA Elements Preceding Short uORFs." PLoS Genet 7(7): e1002137.

Naranda, T., M. Kainuma, et al. (1997). "The 39-kilodalton subunit of eukaryotic translation initiation factor 3 is essential for the complex's integrity and for cell viability in Saccharomyces cerevisiae." Mol Cell Biol 17: 145-153.

Nielsen, K. H., B. Szamecz, et al. (2004). "Functions of eIF3 downstream of 48S assembly impact AUG recognition and GCN4 translational control." EMBO J. 23: 1166-77.

Passmore, L. A., T. M. Schmeing, et al. (2007). "The eukaryotic translation initiation factors eIF1 and eIF1A induce an open conformation of the 40S ribosome." Mol Cell 26: 41-50.

Pestova, T. V. and V. G. Kolupaeva (2002). "The roles of individual eukaryotic translation initiation factors in ribosomal scanning and initiation codon selection." Genes Dev 16(22): 2906-2922.

Pestova, T. V., I. B. Lomakin, et al. (2000). "The joining of ribosomal subunits in eukaryotes requires eIF5B." Nature 403: 332-335.

Pestova, T. V., J. R. Lorsch, et al. (2007). The mechanism of translation initiation in eukaryotes. Translational Control in biology and medicine. N. Sonenberg, M. Mathews and J. W. B. Hershey. Cold Spring Harbor, NY., Cold Spring Harbor Laboratory Press: 87-128.

Phan, L., L. W. Schoenfeld, et al. (2001). "A subcomplex of three eIF3 subunits binds eIF1 and eIF5 and stimulates ribosome binding of mRNA and tRNAiMet." EMBO J 20: 2954-2965.

Pisarev, A. V., C. U. T. Hellen, et al. (2007). "Recycling of Eukaryotic Posttermination Ribosomal Complexes." Cell 131: 286–299.

Pisarev, A. V., M. A. Skabkin, et al. (2010). "The Role of ABCE1 in Eukaryotic Posttermination Ribosomal Recycling." Mol Cell 37(2): 196-210.

Pöyry, T. A., A. Kaminski, et al. (2007). "The mechanism of an exceptional case of reinitiation after translation of a long ORF reveals why such events do not generally occur in mammalian mRNA translation." Genes Dev. 21: 3149-62.

Pöyry, T. A., A. Kaminski, et al. (2004). "What determines whether mammalian ribosomes resume scanning after translation of a short upstream open reading frame?" Genes Dev. 18: 62-75.

Sha, Z., L. M. Brill, et al. (2009). "The eIF3 interactome reveals the translasome, a supercomplex linking protein synthesis and degradation machineries." Mol Cell 36(1): 141-52.

Shoemaker, C. J. and R. Green (2011). "Kinetic analysis reveals the ordered coupling of translation termination and ribosome recycling in yeast." Proc Natl Acad Sci U S A 108(51): E1392-8.

Siridechadilok, B., C. S. Fraser, et al. (2005). "Structural roles for human translation factor eIF3 in initiation of protein synthesis." Science 310: 1513-5.

Srivastava, S., A. Verschoor, et al. (1992). "Eukaryotic initiation factor 3 does not prevent association through physical blockage of the ribosomal subunit-subunit interface." J Mol Biol 220: 301-304.

Szamecz, B., E. Rutkai, et al. (2008). "eIF3a cooperates with sequences 5' of uORF1 to promote resumption of scanning by post-termination ribosomes for reinitiation on GCN4 mRNA." Genes Dev 22(17): 2414-2425.

Taylor, D., A. Unbehaun, et al. (2012). "Cryo-EM structure of the mammalian eukaryotic release factor eRF1-eRF3-associated termination complex." Proceedings of the National Academy of Sciences of the United States of America 109(45): 18413-18418.

Valášek, L., A. Mathew, et al. (2003). "The Yeast eIF3 Subunits TIF32/a and NIP1/c and eIF5 Make Critical Connections with the 40S Ribosome in vivo." Genes Dev 17: 786-799.

Valášek, L., K. H. Nielsen, et al. (2002). "Direct eIF2-eIF3 contact in the multifactor complex is important for translation initiation in vivo." EMBO J 21: 5886-5898.

Valášek, L. S. (2012). "'Ribozoomin' – Translation Initiation from the Perspective of the Ribosome-bound Eukaryotic Initiation Factors (eIFs)." Curr Protein Pept Sci.: in press.

van der Velden, A. W. and A. A. M. Thomas (1999). "The role of the 5' untranslated region of an mRNA in translation regulation during development." The International Journal of Biochemistry & Cell Biology 31(1): 87-106.

Vattem, K. M. and R. C. Wek (2004). "Reinitiation involving upstream ORFs regulates ATF4 mRNA translation in mammalian cells." Proc Natl Acad Sci U S A. 101: 11269-74.

Verlhac, M.-H., R.-H. Chen, et al. (1997). "Identification of partners of TIF34, a component of the yeast eIF3 complex, required for cell proliferation and translation initiation." EMBO J 16: 6812-6822.

Vilela, C., B. Linz, et al. (1998). "The yeast transcription factor genes YAP1 and YAP2 are subject to differential control at the levels of both translation and mRNA stability." Nucleic Acids Res. 26: 1150-9.

Yamamoto, Y., C. R. Singh, et al. (2005). "The eukaryotic initiation factor (eIF) 5 HEAT domain mediates multifactor assembly and scanning with distinct interfaces to eIF1, eIF2, eIF3, and eIF4G." Proc Natl Acad Sci U S A. 102: 16164-9.

Zavialov, A. V., V. V. Hauryliuk, et al. (2005). "Splitting of the Posttermination Ribosome into Subunits by the Concerted Action of RRF and EF-G." Molecular Cell 18(6): 675-686.

Zhou, D., L. R. Pallam, et al. (2008). "Phosphorylation of eIF2 directs ATF5 translational control in response to diverse stress conditions." J Biol Chem 283: 7064-73.